Droplet-Based Microfluidics for Continuous Chemical Sensing and Quantitative High-Throughput Separations

SAMMER-UL HASSAN

University of Southampton

Faculty of Engineering and the Environment

Engineering Sciences

Thesis for the degree of Doctor of Philosophy

July 2016

ABSTRACT

By translating bioanalytical testing from the laboratory into the clinic or at home, point-of-care (POC) diagnostics enables timely diagnosis, monitoring, and treatment of patients. Fundamental to the development of POC diagnostics has been the use of microfluidics, which offers small sample volume consumption and can combine multiple sample-processing steps into a single device. However, microfluidics has provided a limited throughput due to the multiple microvalve switching of samples, slow mixing, sample dispersion and band-broadening in microfluidic channels which result in decreasing the temporal resolution of the system. Droplet-based microfluidics has emerged as an alternative technique to manipulate and analyse sample droplets in a high-throughput format. Samples are compartmentalized in nanolitre sized droplets which eliminate dispersion or band-broadening and hence increase the temporal resolution of the system.

The development of high-throughput, quantitative and rapid microfluidic-based separations has been a long-sought goal for applications in proteomics, genomics, biomarker discovery and clinical diagnostics. Using droplet-interfaced microchip electrophoresis (MCE) techniques, a novel parallel MCE platform, based on the concept of Slipchip and a newly developed 'Gelchip' has been presented in this Thesis. The platform consisted of two "slipping" plastic plates, with droplet wells on one plate and separation channels with preloaded/cured gel on the other. A single relative slipping of the plates enabled generation and then injection of multiple droplets in parallel into the separation channels, allowing to analyse sample droplets in parallel and in a high-throughput format.

As proof-of-concept applications, the separation of 30 sub-nanolitre sample droplets containing fluorescent dyes was performed. Theoretical plates were calculated to be 7560/s at a distance of 3.5 cm. We further determined the effect of droplet sizes on the separation efficiency and found that theoretical plates were higher (2220/s) for smallest droplets (320 picolitres) and lower (1480/s) for largest droplets (1750 picolitres) at a distance of 8 mm. For the quantitative determination of fluorescent molecules, the change in peak areas of different concentrations of the fluorescent molecule (Fluorescein-isothiocyanate) was found to be linear with a small error of 3.6% RSD. Furthermore, separation of DNA step ladder at a distance of 1.3 cm was also achieved with theoretical plates of 79800/s which is one order of magnitude higher than our previously reported droplet-interfaced platform (Niu *et al*. 2013). To facilitate 'non-microfluidic users', new protocols were also developed to pre-cure separation gels (e.g. agarose and polyacrylamide) in open channels forming a 'Gelchip' that can be prepared in batch and used off-the-shelf.

Droplet-based microfluidics is ideally suited to continuous biochemical analysis, requiring small sample volumes and offering a high temporal resolution. Many biochemical assays are based on enzymatic reactions, the kinetics of which can be obtained by probing droplets at multiple points over time. Real-time and continuous chemical monitoring of traumatic brain injury (TBI) or liver transplant in intensive care unit (ICU) could be life-saving and protect from further damage to the tissue. Current systems to monitor these patients are bulky and are placed at a distance from the patient (typically 30-40 cm) which introduces sample dispersion and limits the temporal resolution of the system.

A droplet-based portable continuous chemical sensing device capable of generating droplets-on-demand and analysing glucose or lactate from near patient has been developed. The primary task of the project was to calibrate the performance of the device by generating droplets by a novel screw-driven pump, calibrating droplet sizes and detecting different droplet concentrations in an absorbance based flow cell.

To measure the reactions in droplets calorimetrically, a miniaturised 7-detector flow cell to analyse enzyme kinetics, with an example application of continuous glucose assay in droplets has been developed. Reaction rates and Michaelis-Menten kinetics were quantified for each individual droplet, and unknown glucose concentrations were accurately determined (errors < 5%) with the lowest quantified concentration of 0.5 mM. Droplets can be probed continuously giving short sample-to-result time (~30 s) measurement. In contrast to previous reports of multipoint droplet analysis (all of which used bulky microscope-based setups) the flow cell presented here has a small footprint (45 by 10 by 15 mm) and uses low-powered, low-cost components, making it ideally suited for use in field-deployable devices.

The flow cell was further upgraded via fabrication of precise micromilling of the cartridge and successfully applied for detection of glucose and lactate droplets (lowest quantified concentrations of 0.175 mM and 0.1 mM respectively) for clinical applications. Another significant development of the optical flow cell is dual light paths for accurately quantifying the size and velocity of the continuously flowing droplets, as well as quantifying the composition of the droplet. The flow cell was capable of measuring droplet lengths with errors of < 5%. With all these features, a fully functional optical flow cell is built that can be readily used in wearable/portable microfluidic devices.

ACKNOWLEDGEMENTS

First and foremost I would like to express my gratitude to my supervisor Dr. Xize Niu for his expert advice, encouragement and support throughout my research project, without which, the production of this work would have been impossible. I would also like to thank Xize for helping with experiments, preparation of manuscripts, Matlab codes for separation platform and data analysis.

I would also like to express my gratitude and thanks to the following people:

- Dr. Xunli Zhang from Bioengineering group for his supervision and supportive advice throughout my project. I would like to thank members of Xunli's group for their help.
- Prof. Hywel Morgan from Centre for Hybrid Biodevices (CHB) for his encouragement and advice in continuing my project. I would like to thank members of Hywel's group for their help.
- Dr. Peter Glynne-Jones and his group for the use of microscopes and other lab equipment.
- Dr. Dario Carugo for useful suggestions and providing help with Matlab learning.
- Dr. Adrian Nightingale for support, courage and constructive discussions to perform experiments. A special thanks goes for helping with writing publications, providing Arduino and Matlab codes for data loading, droplet analysis, and Michaelis-Menten kinetics, and LabVIEW programs for real-time plotting of droplet signal.
- Gareth Evans, Yu Zhang, C L Leong (Agnes) and other past and present members of our group for support and useful discussions and at some occasions help with experimental setups.
- Sandrine Willaime-Morawek from University Hospital Southampton and Shellie Long from Wickham Laboratories Ltd for discussions and providing samples of snap-25.
- Jun-jun Lee for help on COMSOL Simulation.
- My parents, family and friends especially my spiritual instructor Syed Ansir Sibtain Naqvi for his unconditional love and support throughout my life.

RESEARCH ACTIVITIES AND ACHIEVEMENTS

List of Publications

Part of this work has been or will be reported in the following publications or conference presentations:

Conference Presentations

1. **Sammer-ul Hassan**, Adrian M. Nightingale, Yu Zhang, Gareth Evans, Martyn G. Boutelle, Xize Niu, Wearable Droplet-Based Microfluidic Sensor Device for Continuous Sampling and Real-Time Analysis, microtas, Accepted for **Oral presentation**, 2016, Dublin.

2. Adrian M. Nightingale, Gareth W. H. Evans, **Sammer-ul Hassan**, Byung-Jae Kim and Xize Niu, Generation of droplet sequences with pre-specified compositions using a "hardcoded" peristaltic micropump, microtas, Accepted for **Poster presentation**, 2016, Dublin.

3. Gareth W. H. Evans, Adrian M. Nightingale, **Sammer-ul Hassan**, Byung-Jae Kim and Xize Niu, Robust droplet generation and sampling with micro-peristaltic pump and antiphase pulsed flows, microtas, Accepted for **Poster presentation**, 2016, Dublin.

4. **Sammer-ul Hassan**, Adrian M. Nightingale, Xize Niu, Continuous measurement of enzymatic kinetics in droplet flow for point-of-care monitoring, **Poster presentation** delivered at Microfluidics Congress, 2015, London

5. **Sammer-ul Hassan**, Yu Zhang, Adrian M. Nightingale, Geraldine F. Clough, David Voegeli, Martin G Boutelle, Xize Niu, Wearable droplet microfluidic device for continuous sampling and real-time analysis, **Poster presentation** delivered at Sensors in Medicine, 2015, London

6. **Sammer-ul Hassan,** Hywel Morgan, Xunli Zhang, Xize Niu, Droplet Interfaced Parallel and Quantitative Microfluidic-based Separations, **Oral presentation** delivered at Microfluidics Awayday, 2014, Southampton, UK

7. **Sammer-ul Hassan**, Xize Niu, Droplet Interfaced Quantitative and High Throughput Microfluidic Separations, **Poster presentation** delivered at The Postgraduate Conference in Engineering Sciences, 2014, Southampton, UK

8. **Sammer-ul Hassan**, Hywel Morgan, Xunli Zhang, Xize Niu, Droplet Interfaced Parallel and Quantitative Microfluidic Separations, p. 133, 2014, **Poster presentation** delivered at EMBL Microfluidics, Heidelberg, Germany

9. Yu Zhang, **Sammer-ul Hassan**, Geraldine F. Clough, David Voegeli, Martin G Boutelle, Xize Niu, Lab-on-an-organ: A Droplet-Based Portable Continuous Chemical Sensor, p. 49, 2014, **Poster presentation** delivered at EMBL Microfluidics, Heidelberg, Germany

10. **Sammer-ul Hassan**, Hywel Morgan, Xunli Zhang, Xize Niu, Droplet Interfaced Parallel and Quantitative Microfluidic-based Separations, **Oral presentation** delivered at The Postgraduate Conference in Engineering Sciences, 2013, Southampton, UK

Peer Reviewed Publications

1. **Sammer-ul Hassan**, Xize Niu, Micromilling as an emerging platform for droplet-based Point-of-care Diagnostic Applications, ***Micromachines***, Invited article, under preparation.

2. **Sammer-ul Hassan**, Adrian M. Nightingale, Xize Niu, An optical flow cell for measuring the size, velocity and composition of flowing droplets, ***Micromachines***, under preparation.

3. **Sammer-ul Hassan**, Xize Niu, Recent advances in droplet-based compartmentalisation of biomolecules for microchip electrophoresis and potential applications, ***Lab Chip***, Invited review article, under preparation.

4. Adrian M. Nightingale, Gareth W. H. Evans, **Sammer-ul Hassan**, Byung-Jae Kim, Xize Niu, Pulsed flows for robust and easily tunable droplet generation, ***Nature Communications***, under preparation.

5. **Sammer-ul Hassan**, Adrian M. Nightingale, Xize Niu, Continuous measurement of enzymatic kinetics in droplet flow for point-of-care monitoring, ***Analyst***, 2016, 141, 3266-3273.

6. **Sammer-ul Hassan**, Droplet-Based Microfluidics as a Potential Platform for Point-of-Care Diagnostics. ***Austin J Biosens & Bioelectron,*** 2015, 1, 1013 (*Editorial View*).

7. **Sammer-ul Hassan**, Hywel Morgan, Xunli Zhang, Xize Niu, Droplet Interfaced Parallel and Quantitative Microfluidic-based Separations, ***Anal. Chem***, 2015, 87, 3895−3901.

Awards and Grants

1. **NERC, UK Grant,** Droplet microfluidic based chemical sensors for rapid measurement of nutrients in water, £174K, 2016 Sammer-ul Hassan (Named Scientist), Xize Niu (Principal Investigator), Hywel Morgan and Matt C Mowlem (Co-Investigators)

2. **ICURe – HEFCE and Innovate UK,** Innovation to Commercialisation Programme, £50K, 2015 Sammer-ul Hassan (Entrepreneurial Team Lead), Xize Niu (Principal Investigator)

3. **Best Poster Award,** Sensors in Medicine, London, UK 2015

4. **Best Oral Presentation Award**, Microfluidics Awayday, Centre for Hybrid Biodevices (CHB), Southampton, UK 2014

5. **Best Oral Presentation Award**, Postgraduate Conference in Engineering Sciences, Southampton, UK 2013

Patent Applications

Sammer-ul Hassan, Xize, Niu, Methods and Apparatus for Introducing a Sample into a Separation Channel for Electrophoresis, ***Patent***, 4 Nov 2015, ***GB 2525633.***

DECLARATION OF AUTHORSHIP

I, Sammer-ul Hassan, declare that this thesis and the work presented in it are my own and has been generated by me as the result of my own original research.

Droplet-Based Microfluidics for Continuous Chemical Sensors and Quantitative High-Throughput Separations

I confirm that:

1. This work was done wholly or mainly while in candidature for a research degree at this University;

2. Where any part of this thesis has previously been submitted for a degree or any other qualification at this University or any other institution, this has been clearly stated;

3. Where I have consulted the published work of others, this is always clearly attributed;

4. Where I have quoted from the work of others, the source is always given. With the exception of such quotations, this thesis is entirely my own work;

5. I have acknowledged all main sources of help;

6. Where the thesis is based on work done by myself jointly with others, I have made clear exactly what was done by others and what I have contributed myself;

Signed: ....

Date: ....

TABLE OF CONTENTS

LIST OF FIGURES

Chapter 1 Introduction and Motivations

This Chapter introduces microfluidics and droplet-based microfluidics for point-of-care diagnostics and outlines the aims and objectives of the current work.

1.1 Introduction

Microfluidics has been a key technology for over two decades to study and manipulate fluids in microstructures. It has the potential to provide smart microdevices which can change how the modern biology, chemical synthesis, and point-of-care diagnostics are performed [1]. Microfluidics offers many advantages including minute quantities of samples and reagents, compact ability, low cost, rapid, high resolution and sensitive analyses. Droplet-based microfluidics has emerged as a powerful tool, and the technique can encapsulate chemical and biological samples in discrete droplets and has generated a diverse array of applications including biochemical reactions, chemical synthesis, drug delivery, and point-of-care diagnostics [2]–[4].

1.2 Droplet-Based Microfluidics as an Emerging Technology for High-Throughput Electrophoretic Separations

Electrophoresis is an analytical technique which has been applied to resolve complex mixtures containing DNA, proteins and other chemical or biological species. Since its discovery in the 1930s by Arne [5], traditional slab gel electrophoresis has been widely used till today. Meanwhile, new separation techniques based on electrophoresis continue to be developed in the 21st century especially in life sciences. Capillary electrophoresis (CE) can provide higher separation resolution and automated operation. Thus it has been widely used to characterise proteins and peptides [6], biopharmaceutical drugs [7], nucleic acids [8] and the genome [9]. The development of microfabrication techniques has led to the further miniaturisation of electrophoresis known as microchip electrophoresis (MCE), which offers particular advantages including ultra-small volume sample consumption, integration with other ‘lab-chip’ processes or functions such as extraction, purification, washing, mixing and sample concentration [10]. As a result, MCE has been used in a variety of applications, e.g. to analyse biomolecules in blood [11], saliva [12], tear [13], dialysate [14], and islets [15].

The majority of MCE technologies have used one of the two standard sample injection methods, i.e. electrokinetic or hydrostatic injection. In the former, the sample is mobilized electrophoretically, and a fraction of the sample is dispensed into the separation channel that forms a cross junction with the sample loading channels [16], [17]. This mode of sample injection may introduce bias as different analytes have different electrophoretic mobilities. Therefore, the injected sample may not reflect the concentration and composition of the original sample [9]. The second method, hydrostatic sample injection technique has many difficulties, e.g. in controlling the flow in the small microchannels, and has limited throughput [18]. To analyse samples in parallel, microfluidic chips have been fabricated that consist of arrays of channels. These chips have been used for high-throughput electrophoretic separation of nucleic acids [19], [20], proteins [21], [22] and for immunoassays [15]. However, multiplexing MCE requires multiple electrodes switching patterns, with electronic control and high running costs. This has significantly hindered further applications of MCE with only limited commercial success [23].

Droplet-based microfluidics enables manipulation and analysis of sample droplets in a high-throughput format [24]–[27]. Sub-nanolitre sample droplets can be generated in a microfluidic chip or collected from a bioreactor, an upstream separation column, or sampled from the tissue environment [28]–[30]. These discrete sample droplets can be further analysed by electrophoresis by injecting them into a separation channel [31], [32]. Such droplet-interfaced systems have been shown to be effective for sample injection and offer many other advantages including ultra-small volume consumption, no sample waste, quantitative analysis without bias, simple device setup and no electric field switching. Such systems could reintroduce MCE as a powerful analytical tool to resolve complex mixtures within microdroplets [14], [32].

From the above discussion, it is suggested that multiplexing of MCE is essential for high-throughput biological assays and droplet-interfaced injection method is a new approach to achieving this goal. Therefore, the general aim of this project is to develop a simple and robust sample injection method for high-throughput MCE and further miniaturise the device to be used for POC diagnostics. The specific objectives of the project are to combine the concepts of Slipchip and MCE, develop a novel device that can load entire volume of the sample droplets into separation gel/medium and achieve parallel droplet-interfaced separations, quantify biomolecules such as DNA, proteins and biomarkers in sample droplets, and facilitate ‘non-microfluidic users’ by developing protocols to pre-cure separation gels (e.g. agarose and polyacrylamide) in open channels forming a ‘Gelchip’ that can be prepared in batch and used off-the-shelf.

1.3 Droplet-Based Microfluidics as a Potential Platform for Continuous and Real-Time Point-of-Care (POC) Monitoring

POC diagnostics enables diagnosis and monitoring of patients from the clinic or home and requires miniaturization of laboratory techniques. Microfluidics has played a key role in the development of POC diagnostics. It offers small sample volume consumption and can combine multiple sample-processing steps into a single device [33]. Consequently, microfluidic POC devices have been developed and commercialised for numerous procedures, including a range of assays and tests for quantification of various small molecules, protein biomarkers, nucleic acids and even cells [34].

Thus far POC research has almost exclusively focussed on diagnostic devices – machines that can analyse a specimen to give a single standalone reading. Much less attention has been given to POC monitoring – in which the concentration of fast-changing biomarkers (such as metabolites) are continuously measured to provide a continuous readout in much the same way that heart-rate is reported in critical care. In addition to an up-to-date measurement, POC monitoring also provides clinicians with information on the trend and rate of biomarker change over a continuous period, such that they can make more informed decisions. Previous studies on real-time online monitoring of glucose levels in TBI [35] and diabetes [36] patients have shown that continuous and rapid monitoring of key analytes could play critical roles in clinical decision-making.

Currently, research into POC monitoring has exclusively utilised electrochemical sensors – either inserted under the skin [37] or by inline measurement of microdialysate [35], [38], [39]. Using this method several different analytes (including glucose [35], lactate [40], pyruvate [41], glutamate [42] and potassium [35], [40]) have been accurately monitored in vivo. Recently, Gao and co-workers developed a non-invasive wearable sensor to measure glucose, lactate, potassium and sodium in the perspiration of cycling and running human subjects [43]. Importantly electrochemical sensors can suffer from surface fouling and signal drift, which leads to short measurement time or errors over time [44]–[47]. In droplet-based detections, it adds an extra challenge to wet the electrodes due to the presence of thin oil layer in between droplets and electrodes. Droplets can be wetted on the surface of the electrode but the wetting can lead to contamination of the sample between the droplets [48]. Thus, there is a need to develop POC monitoring based on robust analytical methods that can go long periods without recalibration.

Colorimetry is well-suited for POC testing, having been successfully applied to accurate quantitative analysis in continuous microfluidics [49]–[51] and with multiple assays already developed for many metabolites and other important biomarkers [52]. Although sensitive, these devices rely on intensive microvalve control to switch between samples and cleaning reagents and can suffer from slow mixing, often requiring specialised channel geometries to enhance mixing out of laminar diffusion. Critically, fluidic samples experience dispersion in the channel and signal smearing. Taylor dispersion and band broadening, caused by the parabolic flow profile in microchannels, limits the throughput of the microfluidic device and hence decreases the temporal resolution of the system.

For POC monitoring, droplet-based microfluidics has recently emerged as an alternative approach - encapsulating biomolecules and performing biochemical assays in nanolitre or picolitre-sized droplets [53]. Analytes of interest are compartmentalized into droplet plugs, eliminating dispersion or band-broadening of the sample and hence increasing the temporal resolution of the system. Thus, in droplet-based microfluidics, each droplet acts as a separate microreactor and multiple of them can be analysed in a single device in high-throughput [54]. For example, Lyu *et al.* [55]

compartmentalized bacteria and single cells in picolitre droplets for high-throughput diagnosis and quantification of Tuberculosis (TB). Kiss *et al*. [56] developed a droplet-based polymerized chain reaction (PCR) platform to encapsulate PCR reagents and fluorescent probes and achieved high-throughput quantification and amplification of genome sequencing. Additionally, Srinivasan *et al*. [57] demonstrated the droplet-based platform to perform colorimetric enzymatic glucose assay on real samples (serum, plasma, urine, and saliva) and quantified bioassays for clinical diagnostics.

Consequently, droplet-Based microfluidics can provide high-throughput analyses with high temporal resolution and continuous detection of fast changing biomarkers. Thus, the broad aims of the project are to develop portable chemical sampling device for continuous and real-time monitoring of metabolic species from critically injured or diabetes patients. The particular objectives of the project include the development of optical flow cell for measuring the size, velocity and composition of flowing droplets, development of multi-detector flow cell for continuous measurement of enzyme kinetics, optimisation of colorimetric assays for metabolites such as glucose and lactate, and monitoring metabolite levels from microdialysate in droplet flow.

1.4 Thesis Structure

The thesis is structured into two literature review chapters, four research chapters, and one conclusion chapter. Four core research chapters are as follows, briefly:

Chapter 4 focuses on droplet-interfaced MCE. It enlists all the experimental details and results with discussions and is based on the on-chip droplet generation without using any pumps. Chapter 5 describes the development of miniaturised flow cells with single and multiple optical detectors for measuring the absorbance and enzyme kinetics of flowing droplets using peristaltic and syringe pumps. Chapter 7 presents an optical flow cell with dual light paths for real-time monitoring of droplet sizes and velocities. The above mentioned work has been completely done by myself from designs, fabrications and experimental results. Any sources of external contributions are listed in the acknowledgements section. Chapter 6 presents a portable continuous chemical sampling device for real-time monitoring of metabolic species including glucose and lactate. This work has been done as a group project and using screw-driven pump (Developed by Dr Niu’s group). Mainly, droplet calibrations and enzymatic assays are developed and all the listed experiments are done by myself. Chapter 8 concludes all the work and discusses possible future directions for current work.

Chapter 2 Droplet-Based Microfluidics

This Chapter reviews droplet-based microfluidics, describes the common droplet generation techniques and highlights key studies on the effect of surfactants on droplet stability, manipulation of droplets including droplet mixing, merging, detection, and reactions in droplets.

2.1 Introduction

Miniaturization of microfluidic devices has become practical with the development of microfabrication technologies, with the significant advantages in miniaturizing chemical and biological assays, such as reduced amounts of samples and reagents, cost-effectiveness, robustness and sensitive assays [1]. In general, these systems are developed to provide high-throughput, parallel, and automated analytical analyses.

Continuous microfluidics normally involves single phase flow in microchannels, although traditionally liquids with macromolecules, microparticles or cells are also categorised in continuous microfluidics. Due to the small Reynolds number (0.01-100), $Re= UL\rho/\mu$, the flow is laminar in microfluidic devices, where U, L, ρ and μ stand for velocity of the flow, diameter of the capillary, density and viscosity of fluid flow respectively [58]. Continuous microfluidics devices have been developed to scale down the amount of reagents from millilitres or microliters to nanolitres and study chemical reactions or synthesize materials in a short interval of time. However, there are a number of disadvantages associated with continuous microfluidics such as slow and weak mixing in microchannels (only diffusion causes mixing alongside the fluid flow), Taylor dispersion of the analytes and sample loss or contamination of biomolecules on the surface of the channel walls (Fig. 2.1). Parabolic velocity profile of two miscible fluids (Fig. 2.1a) shows that the velocity of fluidic flow is zero on the surface of the channel walls (due to non-slippery boundary conditions) and the highest in the middle of the microchannel. This effect introduces Taylor dispersion that leads to spreading of sample and signal smearing along the microchannel [53], [58].

In contrast, droplet-based microfluidics encapsulates biomolecules or analytes of interest into discrete droplets and perform analysis with these ‘digital’ units [48]. As shown in Fig. 2.1b, nanolitre to femtolitre sized discrete droplets are generated in a microchannel by pinching off continuous aqueous stream with an immiscible carrier phase, which is usually oil. Mixing in droplets is faster as compared to continuous microflows because of fluidic circulations inside the droplets [59]. Analytes of interest are compartmentalized into droplet plugs, and the carrier phase prevents the sample from contact with the surface wall and hence, eliminates sample loss on the channel surfaces. Carrier phase also prevents leakage of the molecules and cross-contamination between droplets. Thus, in droplet-based microfluidics, each droplet acts as a separate microreactor and multiple of them (as many as millions) can be transported and analysed in a single device [49], whereas in continuous microfluidics, it requires separate microchannel for each sample or complicated fluidic controls to clean the channels between samples, because of contamination and dilution problems.

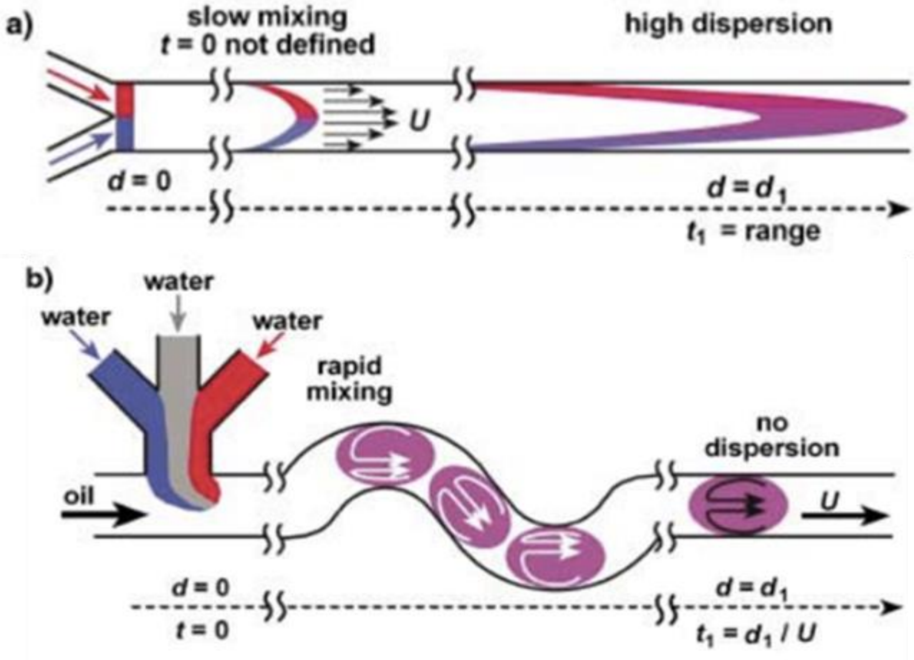

Figure 2.1 Flow profile of continuous and droplet-based microfluidics a) Flow profile is parabolic, and the reagents have variable velocities in the microchannel thus fluid velocity is higher in the middle of the channel and minimum at the channel walls which introduces dispersion along the microchannel, b) The reagents encapsulated in droplets mix thoroughly via recirculating flows, have no dispersion, and the mixing is robust [53].

2.2 Droplet Generation

Droplets are generally formed with two different techniques known as T-junction [60] and flow focussing [61] illustrated in Fig. 2.2. In T-junction technique, dispersed phase flow intersects perpendicularly with the carrier phase flow as shown in Fig. 2.2Aa. The tip of the dispersed phase enters the carrier phase as the flow continues and elongates along the channel due to the interfacial tension and shear stress present at the interface. Finally, the interfacial tension increases and breaks the dispersed phase into a droplet stream.

Droplets can be generated with different sizes and frequencies by altering the physical parameters namely flow rates, ratio of the carrier and dispersed phases flow rates, viscosity of aqueous phase [62], microchannel dimensions [63], and interfacial tension [64]. Ismagilov’s group [27] is among the first to demonstrate that droplets can also be generated with multiple aqueous phase streams and oil carrier phase to initiate reactions inside droplet plugs (Fig. 2.2Ba). Reactions can also be initiated by injecting gas as carrier phase. In the latter case, aqueous slugs (water in gas plugs are known as slugs) are separated by gas bubbles where reaction happens as shown in Fig. 2.2Bb.

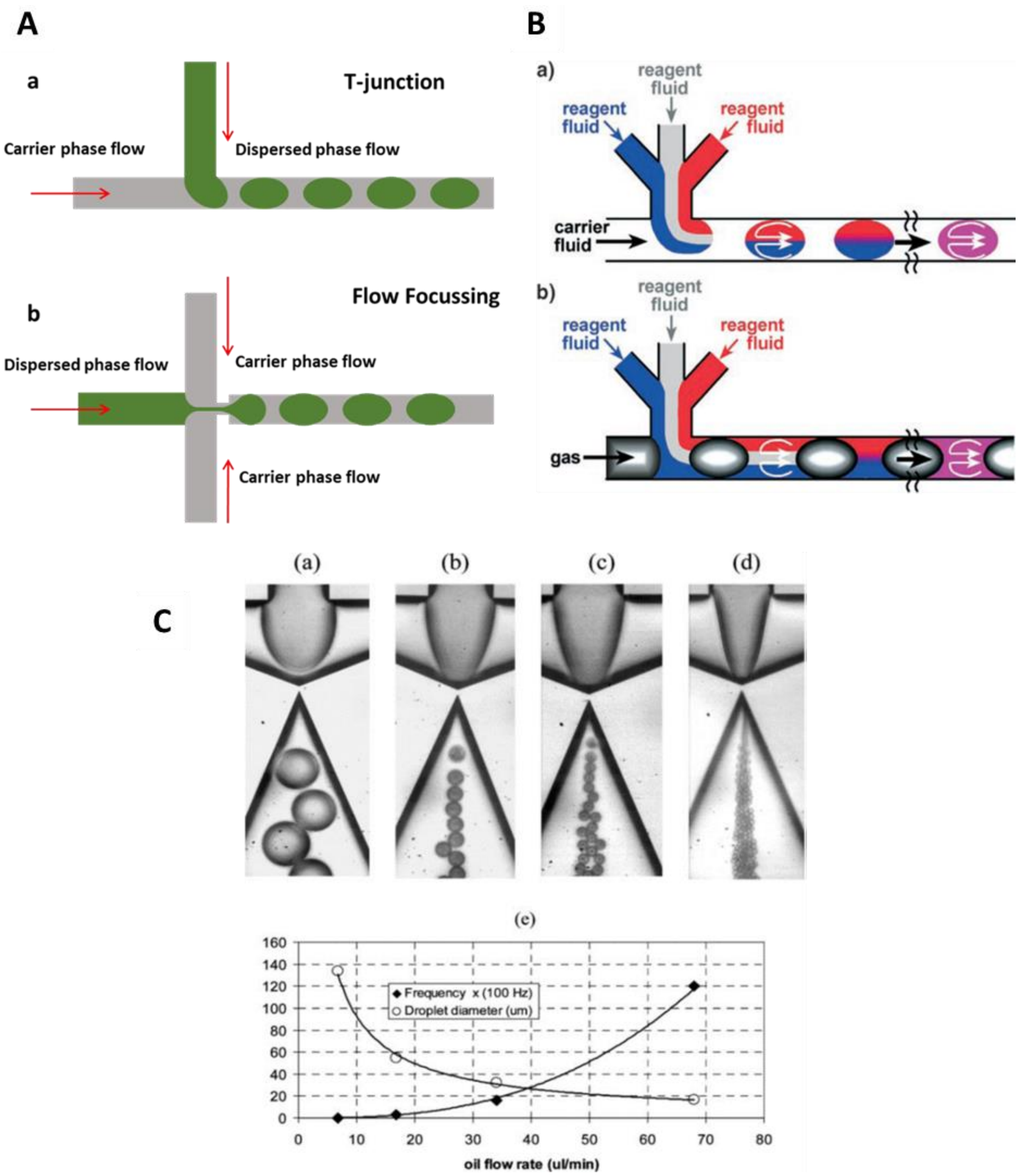

Figure 2.2 A) Illustration of droplet generation by a) T junction, b) Flow focusing. B) Reactions in droplets a) Aqueous plugs in carrier phase oil, b) Aqueous slugs in carrier phase gas [62]. C) Droplet generation in flow focussing device showing images of a-d) Increase in flow rate decreases droplet sizes, e) Plot of the change in droplet size versus oil rate which shows an increase in frequency with an increase in flow rate [61].

Another droplet generation technique is flow focusing, in which two opposite carrier phase streams intersect through a narrow opening with the centrally dispersed phase stream as illustrated in Fig. 2.2Ab. As the dispersed phase passes through the intersection, it elongates due to the increased shear stress and interfacial tension and finally, the dispersed phase breaks into droplets. In this configuration, the shear stress and interfacial tension is symmetrical from both sides of the carrier phase and thus form more stable droplets. Levent *et al.* [61] fabricated a nozzle like an orifice with extreme shear stress as shown in Fig. 2.2C. The authors generated very uniform droplets and controlled the size of droplets by changing carrier phase flow rates i.e. droplet size decreased with increase in oil flow rate (Fig. 2.2Ca-d). It shows that the frequency of droplet generation also increases with increase in oil flow rate (Fig. 2.2Ce). Note that flow focusing and T-junction technique work on the similar principle utilising shear stress and interfacial tension. Therefore, droplet generation is determined/affected by the same set of physical parameters.

Except the flow rate and ratio mentioned above, surfactants, viscosity of the liquids and hydrophobic and hydrophilic nature of the channel surfaces also affect the droplet generation and their stability in microchannels. The dynamics of droplet formation are determined by capillary number (Ca) which is defined as $\eta v/\gamma$, where η is the viscosity of dispersed phase, v is velocity of the carrier phase and γ is interfacial tension between carrier and dispersed phases. Ca is primarily used to compare strength of viscous and interfacial tension in a multiphase microfluidic system. During droplet generation, the shear force at the oil-water interface causes the elongation of the droplet and the interfacial tension causes the contraction of the surface area, with the result that, droplet generation occurs.

Both water-in-oil and oil-in-water droplets can be produced by injecting oil or water as a carrier phase. In any case, the carrier phase should have lower interfacial tension (wet) with channel walls as compared to dispersed phase. In water-in-oil droplet systems, usually fluorocarbons such as FC-40 are used as carrier phase fluids. FC-40 is an inert oil because of the extremely stable bond between carbon and fluorine atoms. Moreover, fluorocarbons have weak intermolecular forces, high density, and low surface tension which make them suitable to be used as a carrier fluid. In addition, surfactants are also added in the carrier phase to adjust surface tension or prevent droplet coalescence after generation.

2.2.1 Surfactants in Continuous Phase

Surfactants are a class of compounds known as amphiphilic molecules [65] consisting of hydrophobic and hydrophilic groups on each end which drive the molecule towards the interface between water and oil layers as shown in Fig. 2.3A. In droplet-based microfluidics, surfactants are added in the carrier phase which lowers the interfacial tension between the carrier phase and continuous phase and helps stabilize the droplet generation. Moreover, surfactant makes a layer on the liquid/liquid interface which prevents coalescence of the droplets or leakage of molecules from the droplets [66]. Daniel *et al*. [67] synthesized twelve different surfactants and tested the stability of droplets in microfluidic systems. The hydrophobic tails were perfluoropolyether (PTFE) and perfluoroalkyl (PFA) alkyl groups and hydrophilic ends comprised of carbohydrate, crown ether, and hexaethylene. Interfacial tension was measured by pendant drop technique, and it was found that surfactant with hexaethylene hydrophilic groups had the smallest interfacial tension (<5 mN/m) and hence, a most satisfactory surfactant for stabilizing droplets. The structures of these surfactants are shown in Fig. 2.3B. On the molecule, hydrophilic heads have highly electronegative hydroxyl groups which make a strong interaction with an aqueous phase at the interface and decrease the interfacial tension.

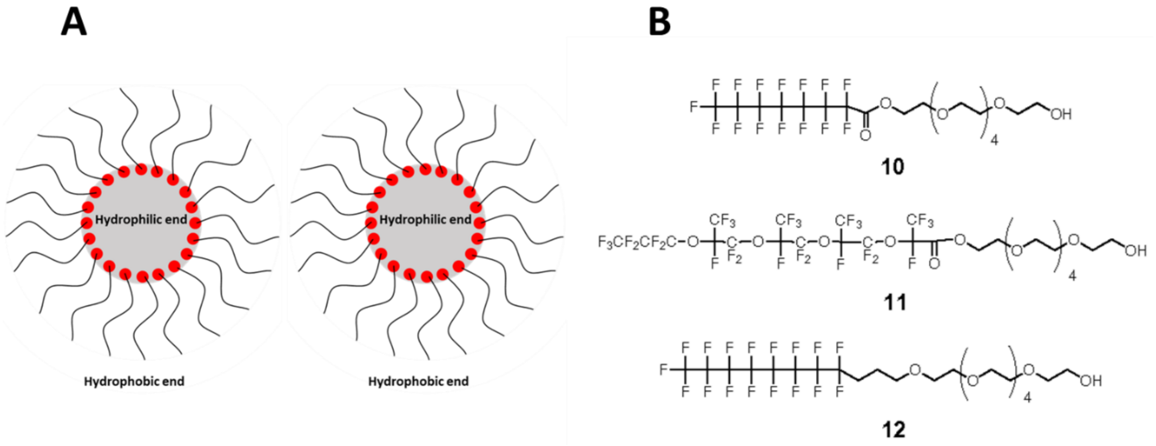

Figure 2.3 Surfactants for water-in-oil emulsions A) Schematic of surfactant layer on droplet interface. The surfactant molecules have hydrophilic heads and hydrophobic tails. The head has hydroxyl groups which decrease the interfacial tension at the droplet interface, B) Hexaethylene glycol hydrophilic head group surfactants and hydrophobic tails 10, 12 PFA and 11 PTFE. The hexaethylene glycol hydrophilic group proved to have lowest interfacial tension (<5 mN/m) and most suitable for water-in-oil droplets [67].

2.2.2 Droplet Generation in Slipchips

Apart from the aforementioned sequential droplet generation with T-junction or flow focusing, there are parallel droplet generation techniques, for example, Slipchip first developed by Ismagilov’s group [68]. Slipchip is a simple device consisting of two plates with microwells fabricated on each surface of the plates. The wells can be filled with different reagents and upon sliding one layer relative to the other, droplets can be generated in parallel or fused to initiate chemical reactions. The Slipchip is ideal for integrating multiple sample handling steps into a single chip enabling critical processes for droplet-based microfluidics, for example, parallel droplet generation, and manipulation, or sample washing steps [69], [70].

Fig. 2.4 shows the schematic of the working principle of the Slipchip [68]. A Slipchip platform has two plates with fabricated wells on one plate and ducts on another plate as shown in Fig. 2.4a. Reagents are loaded onto the wells of the bottom plate, and both the plates are joined together in a way that the wells and ducts link each other and form a continuous channel (Fig. 2.4b). Samples are loaded onto the continuous channel as illustrated in Fig. 2.4c-d. The ducts and the wells are disconnected by sliding the plates relative to each other which generate droplets into the wells on the top plate. The droplets are further slipped to react with the reagents into the wells of the bottom plate (Fig. 2.4e). This slipping mechanism can be performed many times to merge the droplets with the other reagents and so on (Fig. 2.4f). The oil is used in between two plates to remove air bubbles and wet the surface of the plates. It also serves as a lubricating layer in between the plates to ease the sliding.

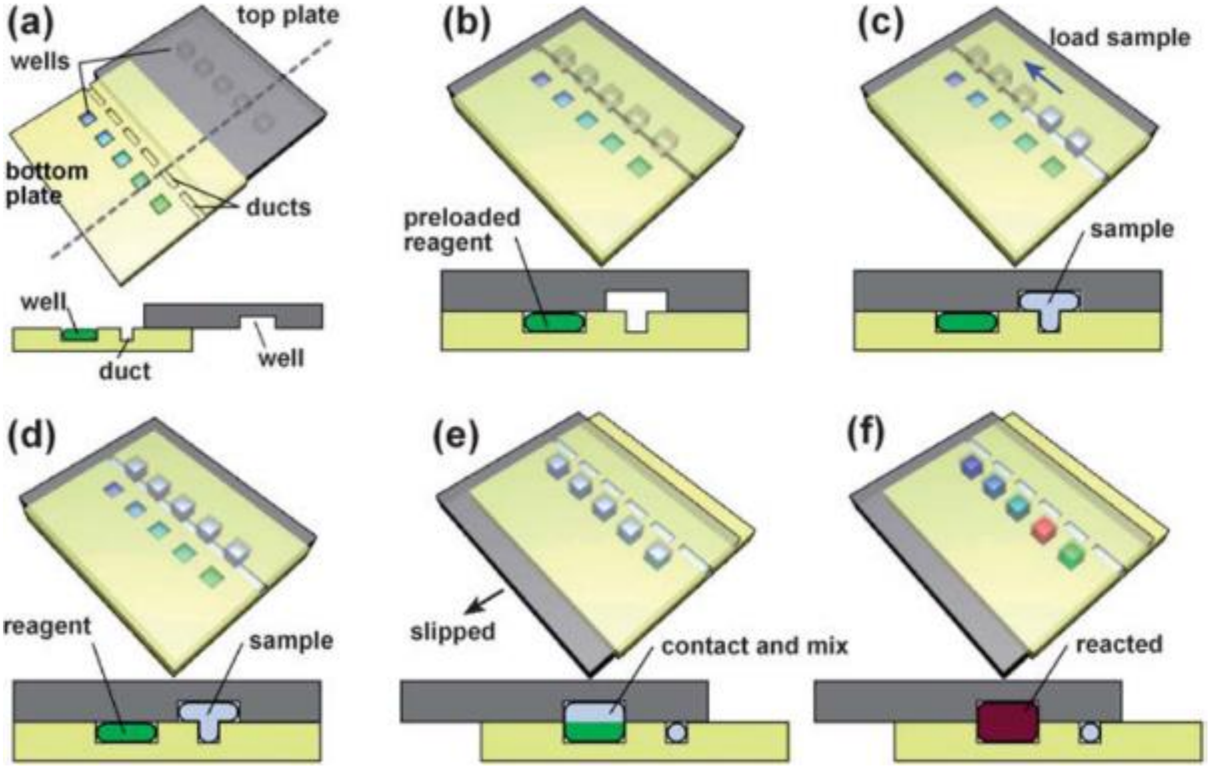

Figure 2.4 Schematic of the working principle of the Slipchip a-f) Illustrates different operational stages of the Slipchip [68].

Microfluidic channels in Slipchip are controlled by positioning the wells and ducts on two separate plates. Hence, these two plates are not bonded to each other, unlike other bonded microchips. For this reason, the sample can leak out from the wells if the pressure on the two plates is not enough or non-uniform and hence, can contaminate the sample. The platform offers the ability to perform parallel and multiple processes on a single microchip. High-throughput bead-based heterogeneous immunoassay on Slipchip has been carried out for 48 samples in parallel [70]. Ismagilov’s group performed many operations using Slipchips in a high throughput format [69], [71]–[75] and the Slipchip format can be a step forward in parallelization of biochemical assays [76]. Niu *et al.* [77] and later Shujun *et al.* [70] demonstrated that this Slipchip format has the potential to be used for separation science, e.g. for segmenting separated samples after isoelectric focusing (IEF) into microdroplets to avoid any sample remixing during post-separation sample collection.

2.3 Mixing inside Droplets

Mixing inside microfluidic channels between two co-flowing continuous streams of liquids is very weak and slow because of the dominance of laminar flows in continuous microfluidics [53], [59]. The molecules mix via diffusion along the flow streams in the microchannels and require longer times to mix thoroughly even though the microchannel dimensions are small. To be able to study the chemical kinetics and essential biological reactions, fast mixing in microfluidic systems is required. Mixing in droplets is enhanced by circulating flow and chaotic advection. For a droplet plug flowing in a channel, circulation flows are produced by shear for the droplets touching the solid channel walls. In a straight channel, the opposite sides in a droplet remain unmixed [59], however, this symmetry can easily be broken up and chaotic advection induced by flowing the droplets via bends and turns geometries in the microfluidic channels as shown in Fig. 2.5a. These geometries introduce stretching and folding of the fluid halves inside the droplets and advance mixing [53]. Serpentine microchannels are designed to bring in chaotic advection and uniform mixing inside the droplets after few turns [78]. Sharp bends can also be used to reorient the droplets and to promote mixing as shown in Fig. 2.5b-c, however, sharp bends increase the chance of further breakup of droplets where the surface of droplet experience the strongest shear force.

Mixing in such serpentine channels is very efficient, and the extent of mixing can be easily quantified with the length of the channels [2]. It’s reported in one of the studies [78] that only 0.72 ms of time is needed for a uniform mixing in a droplet (to measure kinetics of Ribonuclease A), this kind of fast passive mixing (without active actuators) in droplets is in strike contrast with the continuous microflows where mixing is relatively slow, making droplets an ideal tools for the study of fast reactions like nanoparticle synthesis.

There are other geometries studied to promote mixing in droplet such as coalescence geometry in which droplets are mixed perpendicularly [79], protrusion in the serpentine channels for mixing viscous biological reagents such as Bovine serum albumin (BSA) [80], serpentine geometry to decrease distance between the droplet and channel wall which increases chaotic advection [81].

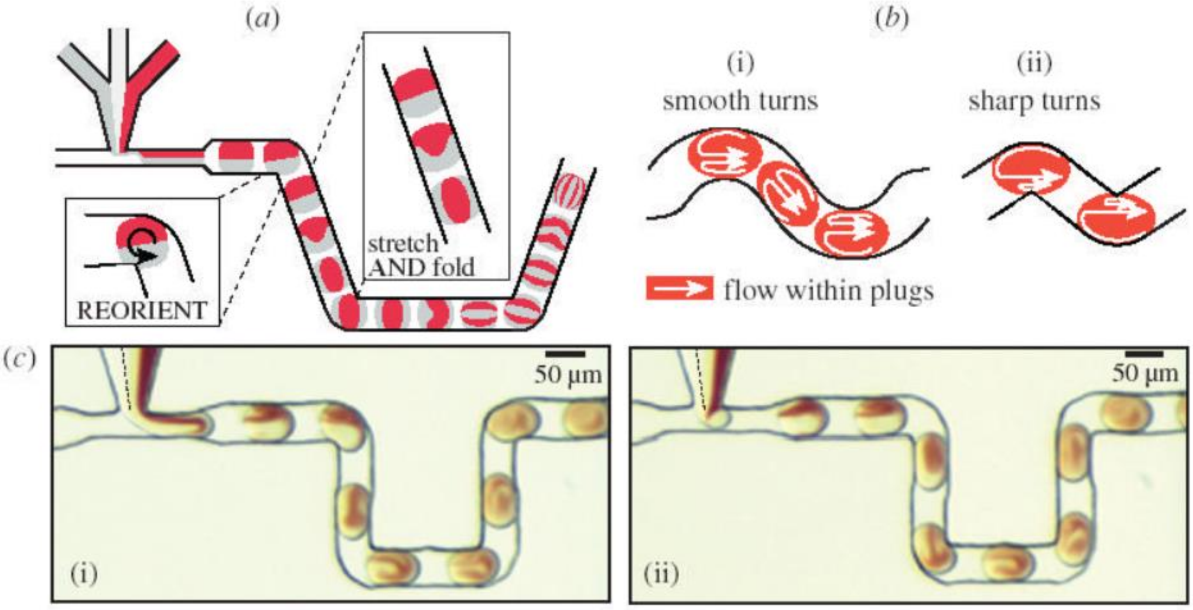

Figure 2.5 Schematic of mixing patterns in droplets a) Serpentine channels for stretching and folding of two layers inside droplets. Turns in microchannels reorientate mixing layers, b) Mixing through smooth and sharp turn via recirculating flow, c) Experimental results showing mixing patterns inside droplets [78].

2.4 Droplet Merging

Droplet merging is an important unit of function for the study of chemical/biological reactions, synthesis of nanoparticles/biomolecules and their kinetics in a controlled manner. Compartmentalization of specific reagents allows merging reagents when the reaction conditions are available. For the fusion to start, the droplet interfaces need to come in contact with each other with a thin layer between them. When the pressure increases on the thin film between the droplets, then the imbalance in interfacial tension will break this thin layer merging two droplets into a single one as shown in Fig 2.6A(a-f). Fig. 2.6A indicates that this type of geometry allows the drainage of the carrier phase and decreases the droplet flow rate in the wider channel [82], [83]. The droplets are again directed into the narrow channel where the pressure increases due to increase in flow rate, and hence, the droplets coalesce. However, this approach is less useful because multiple droplets can merge inside microchannels and requires extremely precise control of flow rates and droplet sizes.

Pillar array structures have also been designed to merge droplets in a selective manner by Niu *et al.* [84]. The droplet merging is achieved by injecting the droplet in a pillar based chamber where it slows down and waits for the other droplet to come into the chamber. The pillars are fabricated at a distance smaller than the droplet size. Therefore, the continuous phase is drained, and the droplet slows down or even be trapped. The second droplet approaches the pillar and merges with the first droplet because of the pressure generated by the flow as shown in Fig. 2.6B. The electric field can also be applied to facilitate droplet merging especially when surfactant is mixed in the oil to stabilize the droplets. As shown in Fig. 2.6C, [85] a pair of electrodes were built at the bottom of the chamber. The pillars help to drain the oil, slow down the droplet and bring both droplets in contact with each other. Upon application of electric field via built-in electrodes in the chamber, the thin oil film between the droplet breaks and the second droplet merges with the first droplet. This type of geometry can be very useful for the selective merging of chemical and biological reagents. Droplet fission [86] and droplet sorting [87] are other droplet manipulation techniques which are beyond the scope of this report. This chapter will further review reactions in droplets, various detection techniques for droplets and their applications.

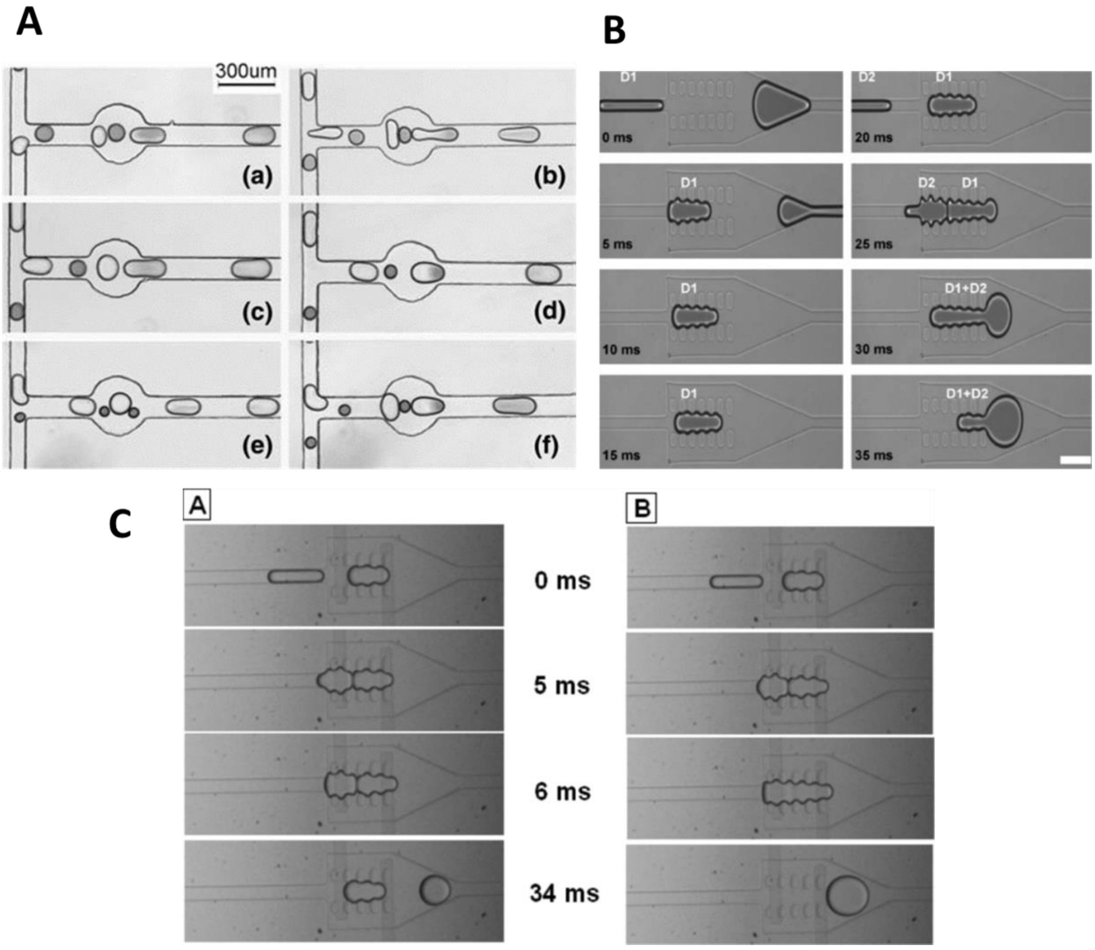

Figure 2.6 Droplet merging inside microfluidic channels A) a-f) Droplet merging in open and narrow channel structure [83], B) Droplet merging in pillar based chamber in 35 seconds without surfactant [84], C) Droplet trapping in a surfactant stabilised chamber and droplet passage without merging (A), Droplet merging in a surfactant stabilised chamber with the application of an electric field (B) [85].

2.5 Reactions in Droplets

Reactions in droplets offer robust mixing, shorter distances between molecules for diffusion, fast mass, and heat transfer, reduced hazardous material exposure and requirement of small quantities of precious and expensive reagents [2]. Reactions such as gene expression analysis, drug discovery require high-throughput parallel reactions to be performed at the same time, and droplet-based microfluidics fulfils this requirement by fabricating parallel microchannels with inexpensive fabrication techniques such as soft lithography or plastic micromachining. Multiple reactions can be performed within droplets by changing reaction conditions such as temperature, concentration or catalysts. Diffusion occurs in microchannels before reaction products are detected which can be overcomed by segmenting into droplets. Droplets can also be stored for long times in microchannels without evaporation of the reagents and transported whenever required for detections or further reactions. For the reactions to be performed in microchannels, conditions such as controlled reagent addition, mixing and reaction times, and analysis must be similar to the macroscale reactions. High-throughput reactions also require accurate indexing of the droplets and analysis in a shorter time [27].

Reagents are injected into the droplets via droplet generation at the interface (Fig. 2.1) or merging droplets in the microchannels (Fig. 2.6). Multiple reagent droplets can be stored in a capillary or tubing to serve as cartridge and used as per demand. These droplets can have different reagent concentrations or even different reagents and can be directed into the microchannel and allowed to react with the sample as shown in Fig. 2.7A. Droplets of 15 nanolitre volume with different reagents were formed in an array and reacted with target sample in T-junction device. These reagent cartridges can be stored for months and used as plug and play devices [27], [88]. Song *et al.* [89] generated sample blood droplets and injected controlled volumes of calcium chloride to study the clotting effect. Droplets were formed in Teflon coated microchannel, and calcium chloride was injected from the hydrophilic channel as shown in Fig. 2.7B. The fluorogenic substrate was used to assess the reaction via fluorescence microscopy for thrombin formation, and bright field microscope was used to analyse fibrin clots inside droplets. In contrast, bromination reaction has also been studied inside droplets to explore the effect of organic phase on swelling of the polymeric devices [90]. A colourless solution of styrene and orange solution of bromine was added to the droplet, and the colour change was observed. As shown in Fig. 2.7C, the droplet becomes faded as the reaction proceeds towards the formation of colourless product. Ahmed *et al.* [91] performed hydrolysis reaction inside droplets and increased the product yield by changing flow rates. Segmented flow at 50 ^{o}C under microwave irradiation produced higher amounts of product as compared to the bulk reaction inside beaker (Fig. 2.7C).

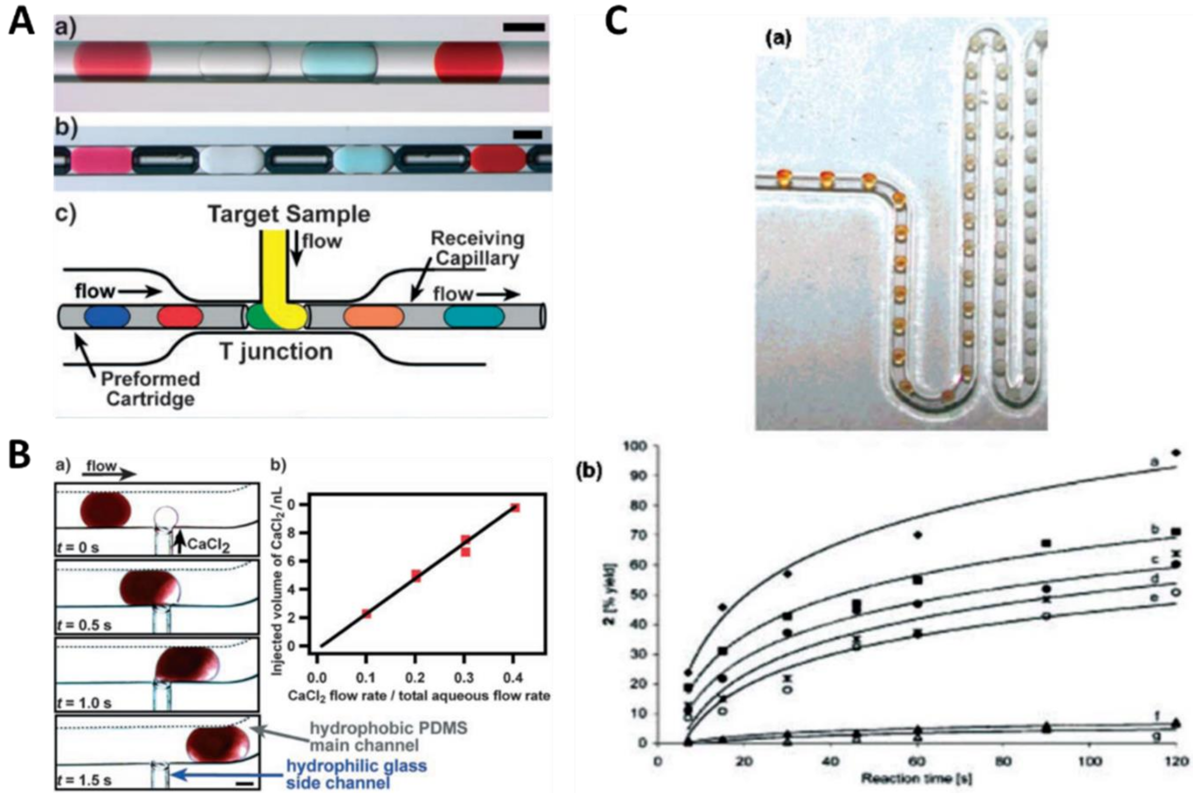

Figure 2.7 Reactions inside droplets A) Droplet storage in a tubing or cartridge [27], [88], B) Consistent merging of $CaCl_2$ from glass capillary to a droplet within 1.5 s. The graph shows injected $CaCl_2$ volume with change in the ratio between $CaCl_2$ flow rate and aqueous flow rate [89], C) Bromination reaction with styrene inside droplets. Along the channel, droplet colour fades with continuous product formation. The graph shows hydrolysis of p-nitrophenyl acetate at different flow rates [90], [91].

2.6 Droplet Detection Techniques

Qualitative and quantitative analysis of droplet contents is an essential requirement for the development of droplet-based systems. Bright field microscopy, fluorescence microscopy, absorption spectroscopy and analytical methods such as MCE, immunoassay and Mass spectrometry (MS) are the most common droplet detection techniques used in microfluidic labs around the world and are briefly discussed below.

2.6.1 Bright Field Microscopy

Physical and biological behaviours of droplets, chemical reactions inside droplets, droplet generation, and manipulation functions are widely studied by imaging techniques [27], [78], [83], [86], [87]. These processes are very fast, and bright field microscopy equipped with a high-speed camera is used for studying dynamics inside droplets. Reactions with colour formation are easily detected by microscopes such as the reaction of Fe^{3+} with SCN^- [92]. Droplets of KCN and ferric solution were generated as water-in-oil emulsions and directed towards a trap where electric field was applied to merge these droplets. The thin film between the droplets takes about 100 µs to break completely, and the reaction starts as shown in Fig. 2.8A. Bright field microscope attached to the high-speed camera was used to study the kinetics of the reaction which completed in 1166 ms (Fig. 2.8A).

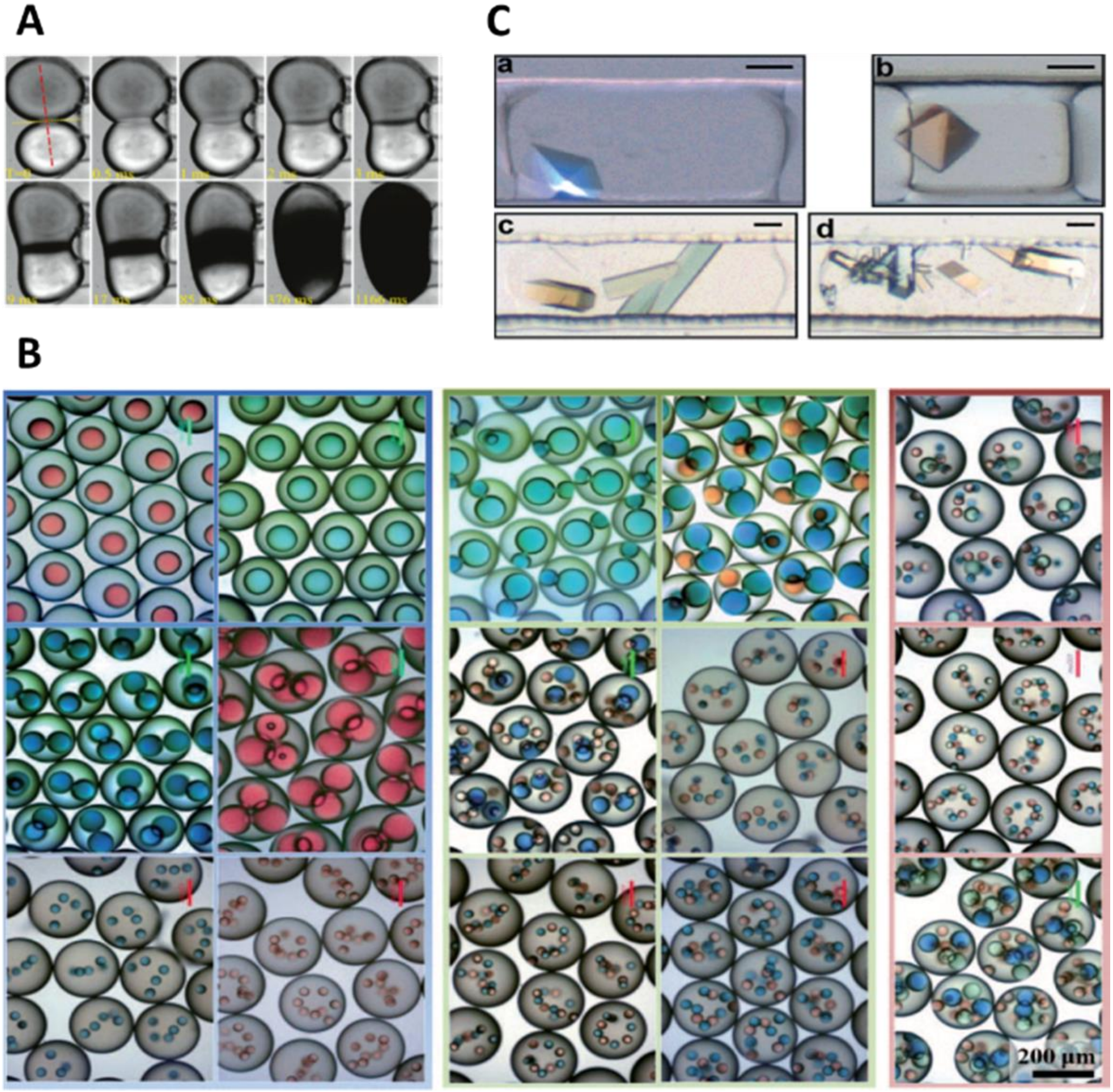

Figure 2.8 Applications of bright field microscopy, A) Electrocoalescence of droplets of KCN (lighter) and Fe (darker) to study reaction kinetics. The reaction completes in 1166 ms, and the colour is observed under high-speed camera [27], B) Encoded droplets in microspheres, First and second column show single colour coded droplets, third and fourth column show two colour coded droplets and fifth column show three colour coded droplets [93], C) Protein crystallization under polarized light [94].

Kim *et al*. [93] generated double emulsions with colour coded droplets and solidified using UV polymerization. These transparent microspheres were coded with single, double and triple colours and optically identified as shown in Fig. 2.8B. This type of coding can be very useful to perform multiple chemical and biological analyses such as multiplex immunoassays for immobilising target biomolecules on the surfaces of microspheres. Bright field microscopy can also be useful for heterogeneous reactions such as protein crystallization in droplets [94], [95], such as Fig. 2.8C shows that droplets formed of protein, precipitants, and additives in microchannels can be screened under a microscope to find out the optimal conditions for protein crystallization. The colour difference of proteins makes it easy to be distinguished from reagents when the protein crystals precipitate out in the droplets (Fig. 2.8C). Bright field microscopy also allows for the study of kinetics for nucleation of protein crystals within droplets [96].

2.6.2 Fluorescence Microscopy

Fluorescence microscopy is a powerful technique to quantify very low concentrations of biomolecules in droplets, and its sensitivity can be very high with excellent light sources and optics. Fluorescence is based on excitation and emission of light from the molecule [97]. Most of the proteins, nucleic acids, antibodies and other biomolecules require derivatization with fluorescent dyes. Derivatization has been successfully applied to biomolecules using fluorescein isothiocyanate (FITC) [98], naphthalene-2,3-dicarboxyaldehyde (NDA) [99], nano-orange [100] etc. The fluorescence efficiency of derivatization dyes is measured by quantum yield (Φ) which is known as the ratio of a number of photons emitted to the number of photons absorbed. Extinction coefficient (ε) also determine the fluorescent efficiency and measures how strongly the molecule absorbs the photons. For example FITC, a strong fluorescent molecule has an extinction coefficient of 76,000 $M^{-1}cm^{-1}$ and quantum yield of 0.93 [101].

The emitted photons from the molecule are captured by detectors known as sensors. The sensors are of three types briefly: 1) a photomultiplier tube (PMT). It works in two stages. Firstly, the electrons are produced when photons absorb on the cathode. Secondly, the dynodes (electron multipliers) present in between the cathode and anode, multiply the electrons exponentially while they reach the anode [102]; 2) avalanche photodiode (APD) that works on the principle of generating electron-hole pairs [103] and 3) charge-coupled device (CCD). CCD is a versatile detection method as it allows the position of the light to be measured as well as intensity. The images can be recorded and analysed by imaging software [104].

Fig. 2.9A shows an example of studying single cell kinetics with a fluorescence microscope and an optical trapping and pulsed laser [105]. A single cell is trapped by using Nd: YAG2 laser at a wavelength of 1064 nm and moved to the oil-water interface. Once the cells are confined inside droplets, a laser at a wavelength of 355 (Nd: YAG1) is used to lyse the cell with a pulse of 5 ns duration. The enzyme activity is immediately measured from the changes of fluorescence intensity inside the droplets with an Ar^+ laser at a wavelength of 488 nm. At 0 s, no fluorescence signal is present because of the intracellular enzyme β-galactosidase was separated by the cell wall from FDG. After laser pulse had induced lysis, enzyme catalysed the production of fluorescein which was observed by a high fluorescence signal as shown in Fig. 2.9B.

Another example shows that surface properties of the droplet can be studied by detecting protein adsorption on the surface as shown in fig. 2.9C. Protein adsorption was controlled with the addition of surfactants miscible in carrier phase, and Alexafluor-fibrinogen compound was detected under the fluorescent microscope [106]. This example shows that the adsorption of protein on channel surfaces can be prevented by encapsulation of droplets, and non-specific protein adsorption can be quantified and/or controlled via fluorescent microscopy. In a study from Ismagilov's group [107], chemical kinetics of ribonuclease A (RNase A) were measured in milliseconds time within the droplet-based system. Fluorescent intensity at different points along the channels was measured to access enzyme activity as shown in Fig. 2.9D.

Laser-induced fluorescence (LIF) is the most common technique used for analytical detections and offers best signal to noise ratio among the other optical detection methods [108], [109]. LIF can be employed for high-throughput screening and single molecule detection in droplets [110]. For example, droplet-based system has been used previously to detect fluorescence-labelled single DNA molecules by LIF. Droplets were squeezed at detection window to increase detection efficiency of the LIF systems [111]. Confocal based LIF detection is the most sensitive technique and provides on-chip detection of the biomolecules with a very low LOD in the range of picomolar concentrations [112], [113]. However, due to the complexity and intricate structure of the LIF setups, it is very difficult to be miniaturized for portable applications.

Light Emitting Diode-Induced fluorescence (LED-IF) is an alternative method to miniaturize detectors for lab-on-a-chip systems. LED-IFs offer reasonable sensitivity and perform much better when combined with optical fibres [114]. LED-IF systems can be very compact and cheap. An array of LEDs can be integrated for multiple sample detections. LEDs are available in single wavelengths and therefore, the sensitivity can be increased by matching the maximum absorption wavelength with test samples. For instance, Boutonnet *et al*. [115] used LEDs with matching maximum absorbance of fluorescent dyes and achieved 6 times lower LODs as compared to the conventional LIF detections.

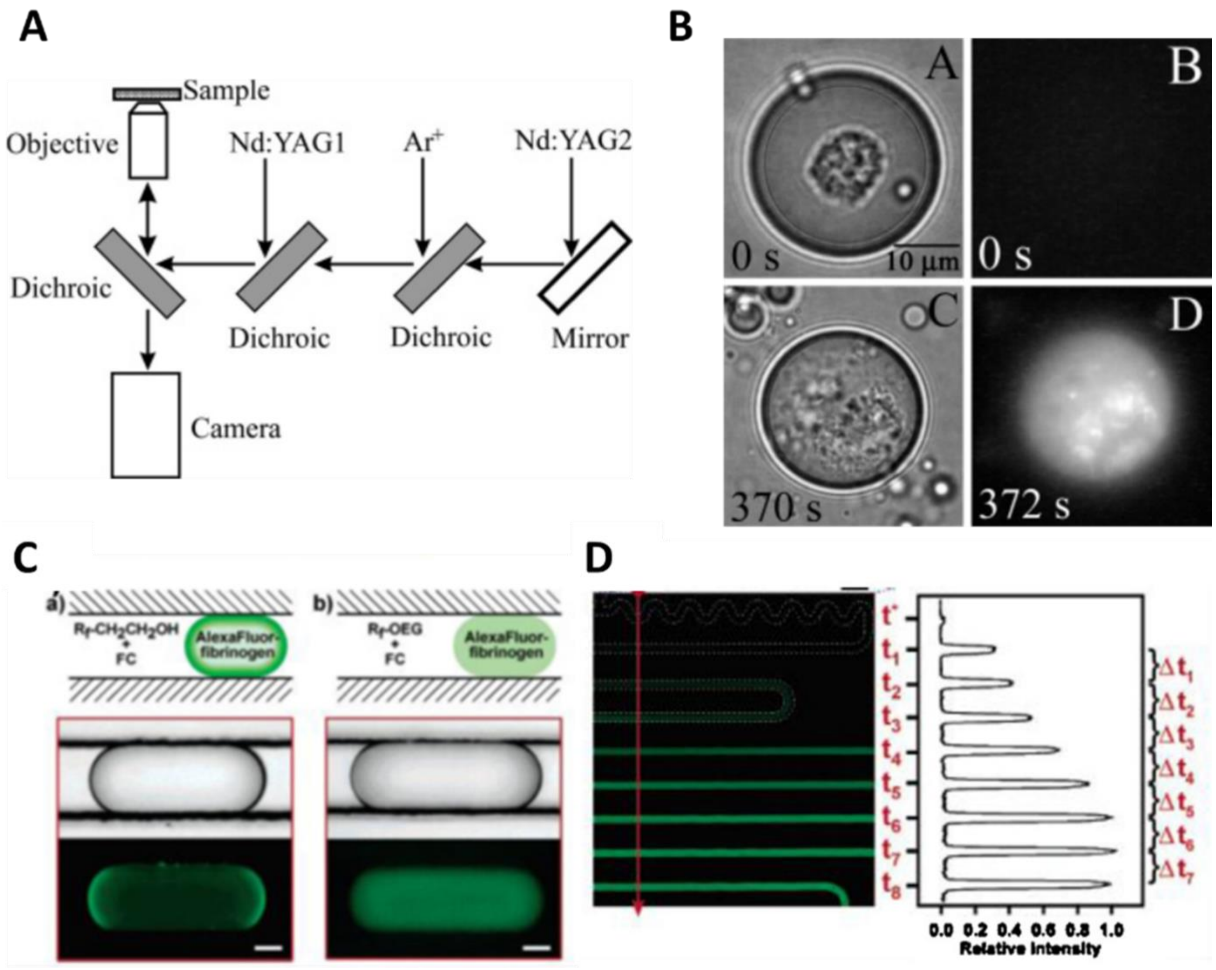

Figure 2.9 Fluorescence microscopy a) Optical setup for single cell enzyme analysis, b) Enzyme activity after laser pulse induced lysis [105], c) Protein adsorption on droplet surface [106], d) Study of millisecond kinetics inside droplet [107].

2.6.3 Analytical Methods

Apart from imaging techniques, the composition of droplets can also be quantified using analytical techniques such as MCE (discussed later in Chapter 3), absorption spectroscopy (see Chapter 5), immunoassays and Mass Spectrometry (MS).

Immunoassay is a widely used technique to detect and quantify proteins based on the reactivity of antibody with specific proteins. Immunoassays in droplets have been performed to quantify the specific biomarkers. Guo *et al*. [116] showed the generation of droplet libraries for high-throughput immunoassay in droplets (Fig. 2.10A). Droplets are generated in parallel from individual vials and are labelled with different colours to separate them from the others as shown in Fig. 2.10Aa. Fig. 2.10Ab illustrates the reinjection of single cell to each droplet for incubation and studying antimicrobial activity. This method of droplet injection allows the high-throughput screening of droplets for suitable antimicrobial drugs.

Magnetic bead-based immunoassays using droplets have also been developed, and a typical droplet-based immunoassay on a digital platform works in different steps as shown in Fig. 2.10B [117]. Firstly, droplets of sample and reagents (containing capture antibodies with magnetic beads and secondary antibodies) are dispensed on the platform. The droplets are then merged, mixed and incubated for a specific time. Those droplets containing antibody-antigen complex are immobilized by a magnet, washed and split to remove unbound species. Finally, the detection is achieved by the addition of reagents as shown in Fig. 2.10B.

Slipchip has also been applied for immunoassays [118] such as insulin immuno-enzymatic assay in 48 parallel droplets, as shown in a schematic in Fig. 2.10C. Droplets containing immunoassay reagents were generated in a Slipchip (section 2.2.2), merged with the sample to initiate the antibody-antigen reaction. The droplets were then washed in multiple steps to remove unbound material, before merging with substrate to read the signal.

Mass Spectrometry is another powerful technique to identify molecules based on their mass-to-charge ratios. Droplet-based chips have been integrated with electrospray ionization-mass spectrometry (ESI-MS) detection. Zhu *et al*. [119] integrated droplet generation, droplet extraction and ESI emission on a single chip as shown Fig. 2.11A. The authors used the hydrophilic tongue to extract the sample droplet while the oil flowed to the waste reservoir. In another study done by Kennedy's group [120], a simple ESI-MS method was developed by directly injecting droplets into the commercially available ESI emitter and eliminated the need for extraction as shown in Fig. 2.11B. The droplets were loaded in a cartridge segmented with oil and gas and were analysed without dilution of the sample. Therefore, low concentration analytes can be analysed. This method of droplet injection can detect the complex mixtures of reagents, and also be combined with other analytical techniques such as electrophoresis or high performance liquid chromatography (HPLC) to enhance the capability of droplet-based systems.

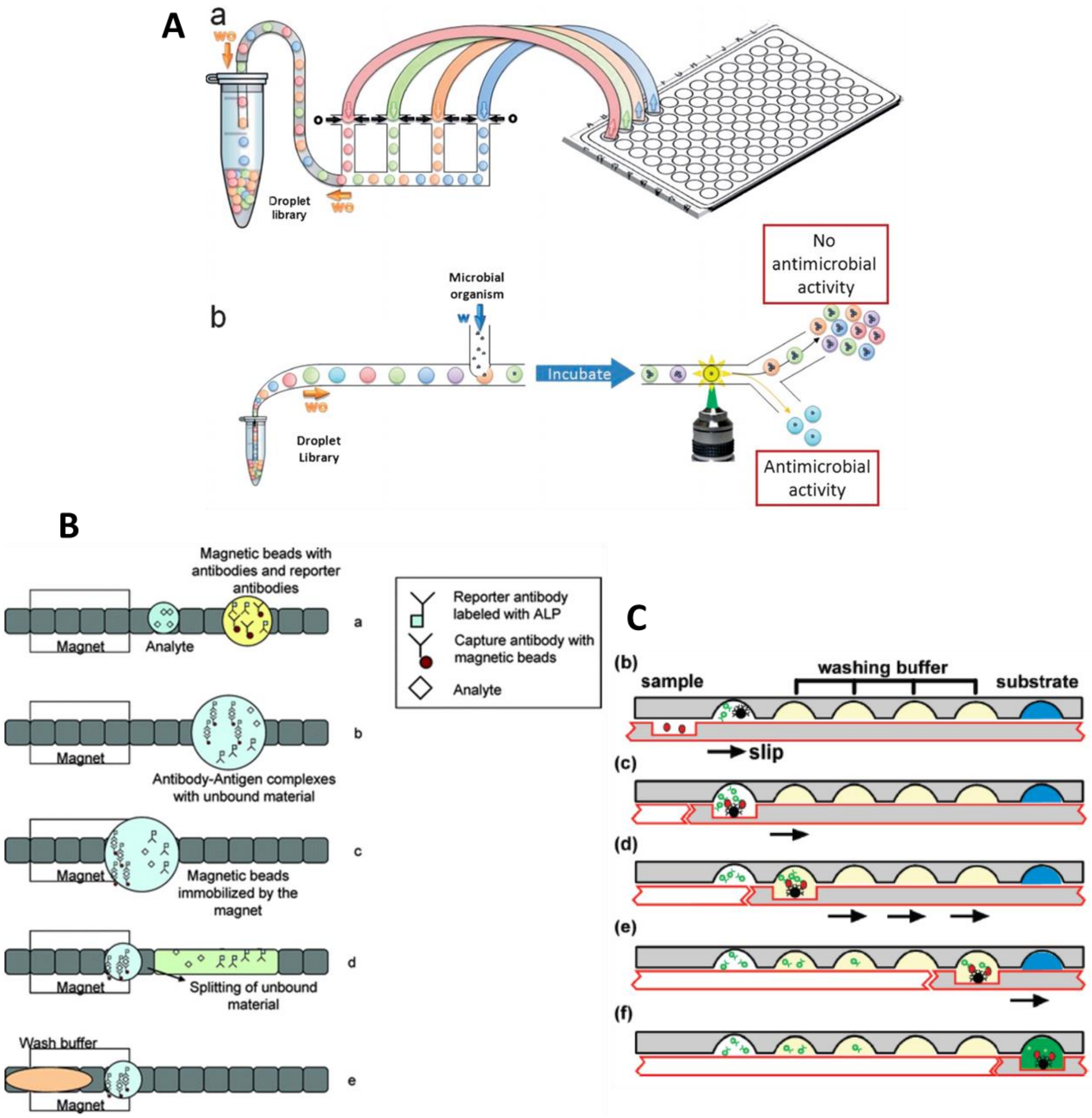

Figure 2.10 Immunoassay in Droplets A) Schematic of the droplet generation for immunoassay in parallel, reinjection and incubation with single cells for antimicrobial activity [116], B) Schematic of the droplet-based immunoassay on digital platform showing dispensing of sample and reagent droplets, merging, washing and splitting of assay droplets [117], C) Slipchip based immunoassay illustrating generation of reagent and sample droplets, merging, multiple washing and merging with substrate to read the signal [118].

Research efforts have also been devoted to study the contents of droplets by Matrix-Assisted Laser Desorption Ionization Mass Spectrometry (MALDI-MS). For example, Fiona *et al*. [121] developed a method to generate droplets containing separated biomolecules from high performance liquid chromatography (nano-HPLC) column. The droplets were deposited onto the MALDI-MS plate for further MS analysis. The authors used an oleophilic film to remove the oil before the deposition. This method achieved 50% enhancement of the performance when compared with conventional nano-LC MALDI-MS using the digests of BSA and Cytochrome C, due to the in situ encapsulation of the separated eluent from nano-LC column. The platform has the potential to be interfaced with other analytical techniques such as MCE or solid phase extraction.

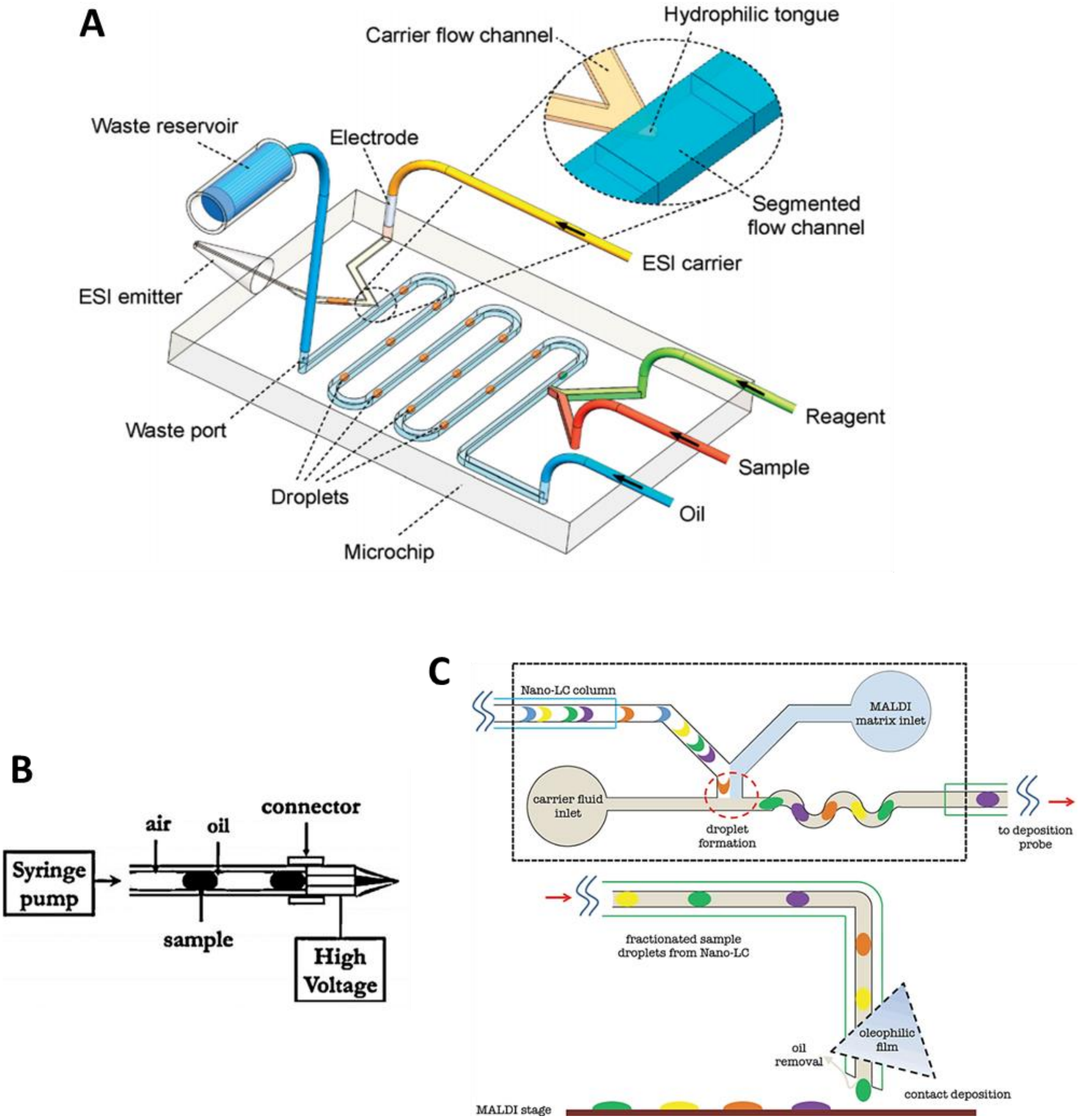

Figure 2.11 Interfacing droplet-based microchips with mass spectrometry (MS) A) 3D schematic of the droplet based device showing droplet generation, extraction and sample injection into the mass spectrometer by ESI emitter [119], B) Schematic of the simple device showing direct injection of droplets into the commercially used ESI emitter [120], and C) Schematic of the droplet-interface with Matrix-Assisted Laser Desorption Ionization Mass Spectrometry (MADLI-MS) by generating droplets from the upstream of nano-high performance liquid chromatography (nano-HPLC), removing the oil with oleophilic film and depositing sample droplets onto the MALDI plate [121].

2.7 Conclusions

This chapter reviewed the droplet generation and manipulation techniques along with the effect of surfactants on the stability of droplets, reactions in droplets, and droplet detection techniques. In summary, droplet-based microfluidics offers robust mixing inside droplets reducing the reaction time, eliminates Taylor dispersion, band-broadening and contamination usually encountered in continuous microfluidics. This chapter mainly discussed bench top techniques and paves the way for the development of droplet-based portable devices benefitting from the high-throughput nature of the droplet-based microfluidics. All of the important parameters reviewed in this chapter have been taken into account when building microfluidic-based devices (Chapter 4-7) in the current study.

Chapter 3 Microchip Electrophoresis (MCE)

The first part of the Chapter introduces the concepts of microchip electrophoresis (MCE) and describes different modes of MCE separation including microchip capillary zone electrophoresis, microchip gel electrophoresis, microchip western blotting, and microchip isoelectric focusing. Furthermore, this Chapter highlights the recent developments in droplet-interfaced sample injection into the separation channel.

3.1 Introduction

Electrophoresis is a powerful analytical technique to separate and analyse biological samples such as separation and detection of nucleic acid fragments (DNA, RNA) and cell proteins, immuno-separation of biomarkers and enzymes, etc. Traditional slab gel electrophoresis (SGE) and capillary electrophoresis (CE) are among the most common forms of electrophoresis and have been widely used in biochemistry laboratories. However, the requirement of higher voltages (300 V/cm) and longer capillaries (40 cm) [122], [123] makes the CE system difficult to be used for portable POC devices. With the advancement of microfabrication technologies, electrophoresis has been miniaturised to achieve on-chip electrophoretic separations known as microchip electrophoresis (MCE). MCE offers many advantages over conventional electrophoresis techniques such as integration of different separation functions onto the chip, consumption of small amounts of sample and reagents, faster analyses and efficient separations, etc. [124]. A few additional functions such as sample preparation, washing, and incubation with antibodies and derivatization with dyes can be integrated on a single stamp size microchip, MCE has the potential to be adapted for portable POC and clinical diagnostics devices. This chapter reviews basic principles and recent advances in the development of MCE.

3.2 Principles of Microchip Electrophoresis

The working principle of MCE is based on the mobility of charged molecules due to the electrostatic force acting on them under the presence of an electric field [125]. Electrophoretic movement of charged molecules is determined by the type of charge on the molecules and electric field strength. For example, negatively charged molecules travel towards positive electrode, and vice versa. The electrophoretic velocity (ν_{ep}) and electrophoretic mobility (μ_{ep}) of the charged molecule are described by the equations given below (Eq. 1-4) [126]

$$\nu_{ep} = \frac{E.q}{f} \tag{1}$$

$$\nu_{ep} = \mu_{ep}.E \tag{2}$$

$$\nu_{ep} = L_D/t \tag{3}$$

$$\mu_{ep} = \mathrm{L}_D/(t.\frac{V}{L}) \tag{4}$$

Where E is an electric field applied (units: Volts/cm), q is the net charge on the molecule (units: Coulombs), f is the frictional coefficient (units: Joule.s/m) which is a friction against the electrophoretic mobility of the molecule, V is the voltage applied (units: Joule/Coulomb), L is the total length of the separation channel (units: cm), L_D (units: cm) and t (units: s) is the length and time a molecule travels to reach the detection point [127]. Eqs. 1-4 show that ν_{ep} (cm/s) of the molecule is proportional to the applied voltage and net charge on the molecule (q) but is inversely related to the f of the molecule. Other factors such as temperature, structure of the molecule, separation medium concentration, and porosity also affect the electrophoretic velocity of the molecule [128].

Electroosmotic flow (EOF) in the capillary or channel can also affect the movement of charged molecules. MCE chips are usually made of fused silica with silanol groups present at the surface of the channel. At pH above 3, silanol groups are deprotonated in the buffer solution and form a negatively charged layer on the surface. The ionised silanol groups on the wall attract the oppositely charged ions from the buffer solution and as a result of this, a double layer is formed on the channel wall also known as a stern double layer. This layer results in zeta potential (ζ) which is defined as the electrokinetic potential at any given point in the double layer [129]. The value of zeta potential (ζ) decreases with increasing distance from the surface of the capillary wall. When an electric field is applied, the positively charged ions in the double layer of the wall are dragged towards the cathode which produces bulk movement in the capillary towards cathode [126], and therefore, EOF is formed, which is usually measured with electroosmotic mobility μ_{eo}.

Proteins and nucleic acids are negatively charged typically at pH above 7 and travel towards the anode. Therefore, EOF must be controlled to develop MCE systems for separation of such molecules. EOF can be suppressed by coating separation channels dynamically or permanently [130]. Polymer materials such as polymethyl methacrylate (PMMA) have lower surface charged groups and hence, have lower EOF values [131]. The commonly used aqueous solutions cannot completely wet the hydrophobic surface of the separation channels. Thus different coatings have been applied to control EOF such as amine-terminated PMMA surface [132], sol-gel treatment [133], evaporation coating [134] and polyelectrolyte multilayers [135].

Fig. 3.1 shows a typical MCE chip. [17]. The separation chip consists of two channels i.e. sample loading channel and separation channel. Firstly, the channels are filled with buffer solution, and the sample is electrophoretically driven in the sample loading channel in the presence of an electric field as shown in Fig. 3.1. This step is known as sample loading step. Secondly, a sample plug from the intersection of the cross channel is injected into the separation channel under an electric field.

This step is known as sample dispensing. Separation occurs as the sample moves along the channel and separates into small bands [16]. Finally, the sample enters the detection point where the electropherograms are recorded (Fig. 3.1).

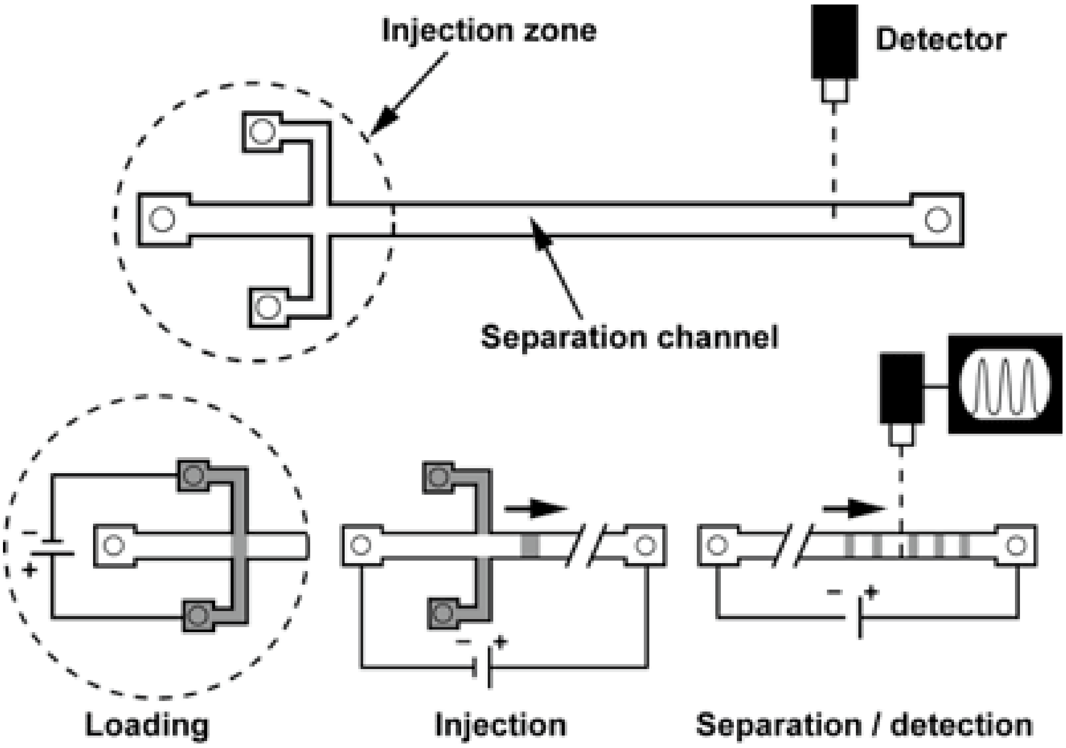

Figure 3.1 Schematic of the cross-chip illustrating steps of sample loading, injection to separation channel, separation and detection. Sample is loaded into the cross-channel and electrophoretically drives towards sample waste reservoir. Sample is then injected into the separation channel at channel intersection upon application of electric field. The sample is resolved into its components in separation channel and detected in the detection region [136].

Separation efficiency is quantified by two main factors known as separation resolution (R) and number of theoretical plates (N) [129], [137]. R measures how well the molecules are separated along the separation medium. R is defined as the ratio of the time difference between two peaks ($t_2 - t_1$) to the sum of the peak half widths ($\sigma_1 + \sigma_2$) at the base (Eq. 5) as shown in Fig. 3.2.

$$R = \frac{t_2 - t_1}{2(\sigma_1 + \sigma_2)} \qquad (5)$$

The number of theoretical plates, an indicator of maximum separation efficiency of a separation column/channel as given in Eq. 6

$$N = 5.54 \left[\frac{t_r}{\sigma}\right]^2 \qquad (6)$$

Where σ is the width of the peak at half of the height (expressed in terms of time) and t_r is the retention time.

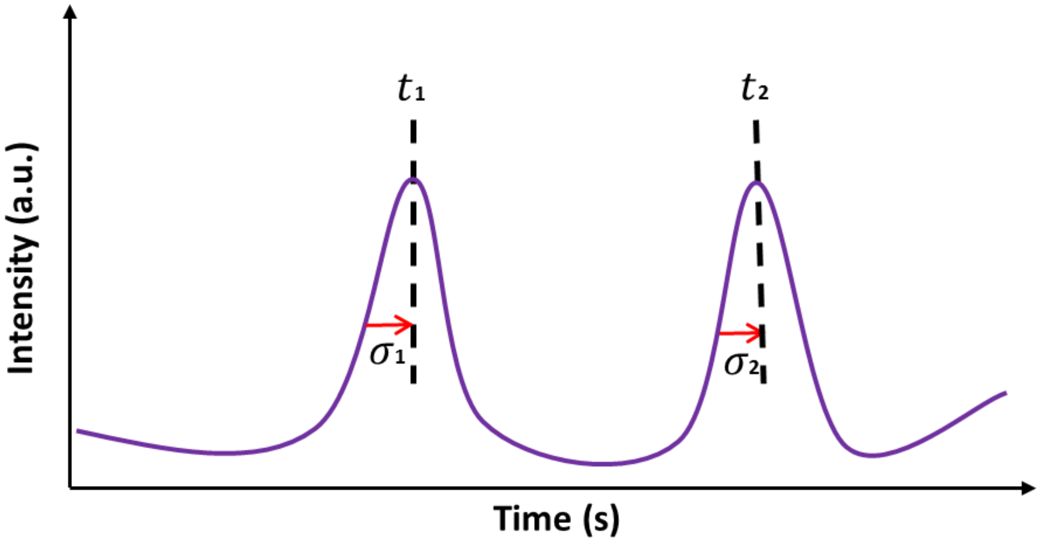

Figure 3.2 Schematic of the electropherogram for calculation of separation resolution (R) and number of theoretical plates (N).

3.3 Applications of Microchip Electrophoresis

Microchip Electrophoresis (MCE) has been a key technology to study proteomics, DNA sequencing, antibody-antigen immuno-separations and POC diagnostics [138]. Different modes of MCE along with highly advanced applications are discussed in this section.

3.3.1 Microchip Capillary Zone Electrophoresis (Microchip CZE)

Microchip capillary zone electrophoresis (Microchip CZE) is the simplest form of electrophoresis. The separation is carried out on the basis of the difference in charge and size of molecules in the solution. From its earlier development CZE was used for separation of amino acids [139] and proteins [140] to its use for proteomics coupled with mass spectrometry [141], environmental studies [142] and biomolecules [143]. In recent developments, human serum proteins were separated in borate buffer and labelled with 2-Toluidinonaphthalene-6-sulfonate after electrophoresis in Microchip CZE [144]. Xia *et al.* [145] improved the power of Micro CZE by introducing the pressure-driven backflow in the separation and achieved the 8-fold higher resolution of a mixture of amino acids. Furthermore, Jacobson's group [146] improved the microchip CZE separation performance at higher temperatures by applying higher voltages in the separation channel.

Fanggui *et al.* [147] fabricated a microchip to quantify the carcinoembryonic antibody-antigen reaction for the detection of cancer disease in blood serum samples. Carcinoembryonic antigen (CEA) standards and serum samples from patients were incubated first with primary antibody (Ab_1) and secondly with the fluorescently labelled secondary antibody (Ab_2*). The reacted antibody, and antigen samples consisted of Ab_2*, Ab_1-Ab_2* and Ab_1-Ab_2*-CEA which were separated on MCE and quantified. In another study, serial immunoassays [15] within 10s have been performed on a microchip for the detection of insulin secretion from pancreatic islets. Islets chambers were fabricated on the microchip and all steps like washing, reaction with labelling antibody and insulin secretion, etc. were integrated on the chip.

3.3.2 Microchip Gel Electrophoresis

MCE has been widely used as a robust and reliable method for protein separations. High-resolution MCE separations can be achieved because of the smaller channel lengths and shorter separation times. Two types of gels are used to separate biomolecules such as sieving gels and agarose/polyacrylamide gels.

Hydrophilic polymers such as polyethylene oxide (PEO), linear polyacrylamide, polyvinyl alcohol (PVA), hexamethylcellulose and hexaethylcellulose, etc. are filled in the microchannels and serve as the sieving matrix for microchip capillary gel electrophoresis (microchip CGE). Different concentrations of polymers are prepared by dissolving polymers in separation buffers, and the viscosity and porosity are controlled by varying the concentrations and molecular weights of the polymer chain. Microchip sodium dodecyl sulphate CGE (SDS-CGE) has been favoured in the biopharmaceutical industry for protein separations because of the ability to quantify proteins. As an alternative to sodium dodecyl sulphate polyacrylamide gel electrophoresis (SDS-PAGE), it can provide more reproducible results (low %RSD values) [23], [148]. Microchip CGE has been applied for protein separations such as Root *et al*. [149] separated mixture of proteins on the cross-chip by using different concentrations of sieving matrices and a different surfactant called acid-labile surfactant which is suitable for downstream applications such as mass spectrometry (MS). Two-dimensional separation of proteins in plastic microchips has also been reported previously [150] in which micellar electrokinetic chromatography (MEKC) was coupled with Microchip SDS-CGE to separate proteins ranging from 38 to 110 kDa. Zheng *et al.* [151] made a device with four capillary array channels and showed the consistent migration times and analyte intensities from channels to channels and from each different runs using sieving matrices (PEO gel).

Agarose gels are very popular in separating large molecular weight nucleic acid fragments because of the large pore sizes and non-reactivity towards DNA molecules [152]. Nucleic acid fragments are detected by intercalating dyes into the DNA base pairs, and the most used ones are Ethidium Bromide and Syber Green [129]. Agarose gels are chemically inert to nucleic acids, can be stored for later visualisation, are non-toxic, easy to cast and quick to run but are expensive and cannot achieve separation of small biomolecules such as proteins (below 200 KDa) because the pore size of agarose gel is larger than the size of the smaller proteins [152].

Acrylamide is a monomer and forms polyacrylamide gel when acrylamide molecules are polymerized with cross-linkers such as bis-acrylamide by a free radical mechanism. The reaction is initiated using ammonium persulphate (APS) and catalysed by N, N, N', N' − tetramethylethylendiamine (TEMED) [125]. Polyacrylamide is mainly used for separating proteins or smaller fragments of nucleic acids. It has advantages over agarose gels on higher chemical stability, providing higher resolution, sharper peaks, greater capacity to load large number of DNA fragments and efficient separation of molecules with smaller sizes [152]. The pore size of the polyacrylamide gels can be controlled by varying the concentrations of monomer and cross-linker. Higher concentrations of monomer and cross-linker yield smaller pores and hence the gel can be used for separation of smaller size molecules. The concentration of polyacrylamide gel is characterized by the relationship given below [153]

$$\%T = \frac{acrylamide\ (g) + cross{-}linker\ (g)}{Total\ Volume\ (ml)} \times 100 \qquad (7)$$

Where $\%T$ is equal to the total concentration of monomer and cross-linker. The higher values of %T results in gels with smaller pores and lower values of %T produce gels with larger pore sizes. The normal values of %T used for protein separations are 1-10%. The proteins have zwitter ion properties due to the presence of amino acid groups, therefore a surfactant such as SDS is used to denature proteins from tertiary structures to simple structures. SDS breaks the sulphide bonds between the proteins, denaturing them into their sub units and provides overall negative charge to the proteins [129].

Polyacrylamide gels are also cured inside the separation channels by UV based photoinitiation mechanism. Herr *et al.* [154] miniaturised SDS-PAGE for the first time for protein-SDS separations. Firstly, the separation channels were washed with DI water and then NaOH to deprotonate the silanol groups on the glass surface (Fig. 3.3A). Secondly, acrylamide/bisacrylamide and 0.2 % (w/v) photoinitiator solutions in tris/glycine/SDS buffer were filled in the separation channel and exposed to UV light to initiate the polymerization as shown in Fig. 3.3B-C. A mask was also used to cross-link monomer in only unmasked regions for the purpose of fabricating gradient gels (Fig. 3.3D). Finally, the SDS-PAGE separation of R-lactalbumin, trypsin inhibitor, carbonic anhydrase, and alcohol dehydrogenase was performed in a microchannel polymerised with 6% polyacrylamide gel as shown in Fig. 3.3E. In another study, Kirby *et al.* [155] developed a two-step method to coat microchip glass surface. Firstly, the microchannels were functionalised using 3-(trimethoxysilyl) propyl, methacrylate, and glacial acetic acid. Secondly, acrylamide with 5% photoinitiator was flushed through the channel and then exposed to UV light. This method prepares a thin layer of polyacrylamide coating on the surface of the glass to control the polymerization of the separation gels.

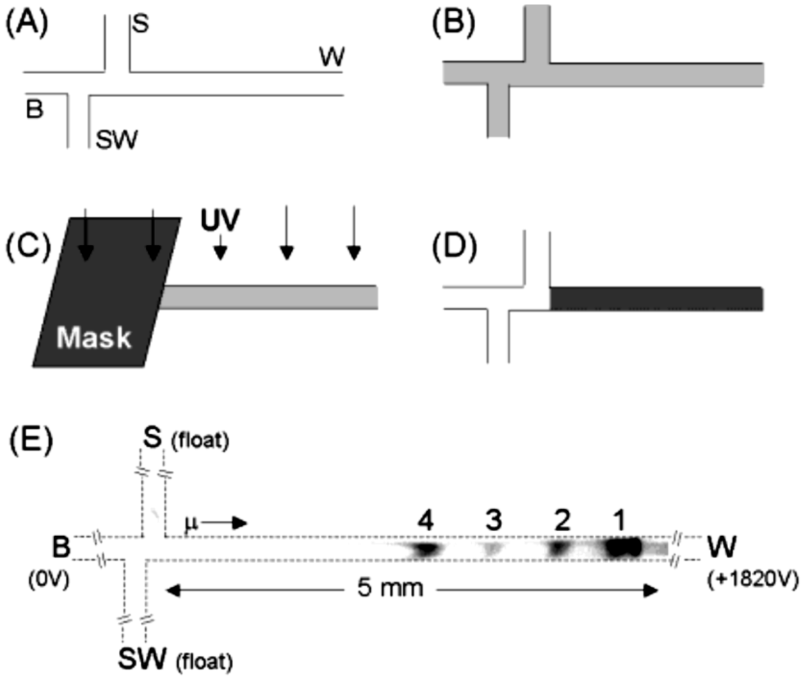

Figure 3.3 Photopolymerization of polyacrylamide gel inside microchannel A) NaOH treated channels, B) Monomers solutions filled in a microchannel, C-D) Exposure of UV source and cross-linked region in the microchannel, E) SDS-PAGE separation of proteins on 6% photopatterning gel [154].

Photopolymerized gels have been vastly used for SDS protein separations in microchannels. Hughes *et al.* [156] photopolymerized gels inside the microchannels and developed a protocol for high specificity protein isoforms. In another development, Amy Herr’s group [157] designed and fabricated free-standing photopolymerized polyacrylamide gels for protein electrophoresis. Without fabricating separation channels, the authors only used polymerised gel on glass cover sheet and separated proteins in free-standing gels. Han *et al.* [158] also used polymerised gel to separate proteins on a microchip. The authors photopatterned SDS-PAGE in microchannels and separated fluorescently labelled proteins. Gradient gels were also fabricated by controlling the UV exposure on the microchips [159]. The polyacrylamide gels with 3.5-10% concentration were polymerised on the chip used for protein separations. It was shown that the gradient gels provide protein separation in 4 s at an ultra-short distance of 3 mm. Mei *et al.* [160] photopatterned gels inside a microfluidic chip and studied protein immunoblotting. Proteins were separated in two dimensions by applying electric fields and integrated several immunoblotting steps onto the chip to improve the efficiency of the separation and provide faster analyses.

Over the last decade, microfluidic chips have been fabricated with arrays of channels for high throughput on-chip detections. In a study done by He *et al.* [161], the authors fabricated three channels on the microchip and achieved parallel separations of 100 bp DNA weight marker, feline panleukopenia virus (FPV) DNA and a negative control. The method proved to be 100 times faster than the gel electrophoresis for DNA separations. Aborn *et al.* [20] presented a high-throughput system for DNA sequencing with 786 channels. The study used two plates with each 384 channels and the automatic system for sample handling, separation, detection and plate movement. One plate was investigated first and after completion of the analysis, the detector was automatically moved to the second plate.

Bousse *et al.* [23] developed microchip-based gel electrophoresis of proteins with sequential separation of proteins or DNA fragments for up to 12 samples. Dye staining and destaining steps were also integrated onto the microchip for high-throughput results. Herr et al. [12] fabricated the microchip for the analysis of MMP-8, which is a disease biomarker for periodontitis in saliva. The microchip integrated the sample loading channels with larger pore size photopolymerized gel, separation channels with smaller pore size gel and a membrane for on-chip sample concentration. Kelly *et al.* [13] reported the first rapid and sensitive chip based immunoassay device to measure tear related disease biomarker from human tear fluids. The authors detected the Lactoferrin (Lf) which is a tear-specific biomarker for Sjogren's Syndrome, and the results were comparable to ELISA measurements of Lactoferrin.

3.3.3 Microchip Western Blotting (μWB)

Western blotting (WB) is a powerful technique to detect specific and rare proteins from cell extracts [162]. The proteins are separated by SDS-PAGE and transferred to a membrane for immunodetection [163]. The working principle of western blotting involves three steps. Firstly, proteins extracted from cells are loaded onto the polyacrylamide gel for separation by SDS-PAGE. Secondly, the gel containing protein bands is placed on a membrane to adsorb the molecules on the surface, and protein bands are transferred to a nitrocellulose or polyvinylidene fluoride (PVDF) membrane upon application of an electric field in a vertical direction. Thirdly, membranes are incubated with antibodies (fluorescently labelled) to visualise the distinct protein bands from the cell. Western blotting can qualitatively analyse the proteins, but it cannot provide quantitative analysis and also takes 8 hours to 1 day to complete the analysis [163]. Microchip western blotting (µWB), on the other hand, provides fast and sensitive assays. For example, R. T. Kennedy’s group [164] attempted to miniaturise the western blotting by precisely interfacing microchip electrophoresis with protein capture membrane as shown in Fig. 3.4A. The authors separated SDS-complex proteins in a cross-chip and captured protein bands on a moving PVDF membrane. The membrane was further used for incubation with antibodies and detection purposes.

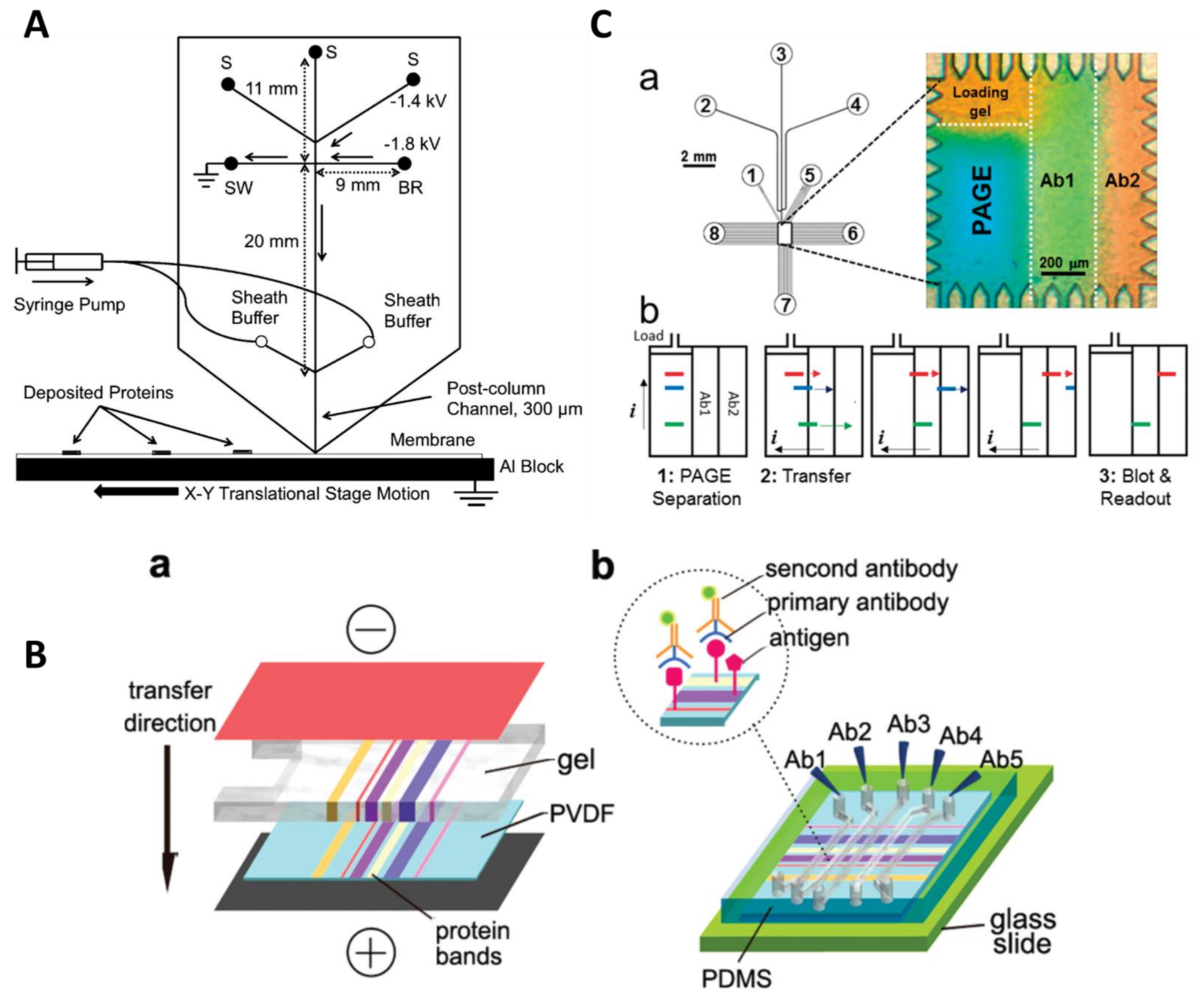

Figure 3.4 Overview of the µWB techniques A) Schematic of the microchip interfaced with PVDF membrane. Proteins separated are captured on the membrane in narrow bands moving under the separation channels [164]. B) Schematic of the microchip electroblotting a) Protein transfer to membrane, b) PDMS microchip is interfaced with the membrane and different antibody solutions are filled in the channels [163], C) Schematic of the immunoblotting device, a) Design of the microfluidic chip and microfluidic chamber showing native gel electrophoresis and antibody labelling regions, b) Schematic of the protocols for western blotting regions [165].

Pan *et al.* [163] developed a method for microfluidic western blot and integrated sample loading, separation and antibody labelling on a single microchip as shown in Fig. 3.4B. Briefly, proteins were separated by SDS-PAGE on a microchip, transferred to a PVDF membrane incorporated into the microchip device, and immune-reacted with antibodies introduced into the parallel microfluidic channels. The authors were able to separate 10 different proteins in parallel on a single microchip. Amy E. Herr's group [165] established another method to incorporate fully automated western blot analysis on a microchip device as shown in Fig. 3.4C. Using native polyacrylamide gel electrophoresis, the authors fabricated multiple immunoblotting regions on a single microchip for multi-analyte detections. Without any pre-relabelling steps, the robust and automated analyses required only 5 minutes to complete and provided the highest sensitivity as compared to the previous western blot analyses [163], [164].

3.3.4 Microchip Isoelectric Focusing (Microchip IEF)

The amphoteric molecules like proteins can be separated by adjusting different pH conditions in the buffer system. Briefly, the proteins in various regions of pH gradients have different net charge and migrate in opposite direction under the presence of an electric field. Each protein reaches in a particular region of pH where its net charge becomes zero and the migration of protein stops. This point is known as isoelectric point (pI). It results in focusing of different proteins along the gradient known as isoelectric focusing (IEF). The focused bands are passed through the detector by hydrodynamic or electrophoretic movement [166]. However, this movement adds band-broadening effect and hence, other techniques such as whole column imaging can reduce this effect [167].

From its earlier development [168], Microchip IEF has been developed with the advancement of fabrication methods [77], [169]–[171]. Shameli *et al.* [169] developed PDMS hybrid chip for separation of proteins by Microchip-IEF and detection by imaging the whole microchannel as shown in Fig. 3.5A. The device was designed with full integration of modified PDMS membrane to separate electrolytes, an SU-8 slit for enhanced detection sensitivity and injection capillaries for high-throughput analysis. Recently, Zhao *et al.* [77] developed a Slipchip-based method to perform Microchip-IEF in discrete droplets. The device was composed of two micromilled plastic layers with wells fabricated on both. The layers were aligned in such a way that the continuous zig-zag channel was formed as shown in Fig. 3.5B. After the generation of the pH gradient along the channel, a relative movement of layers was performed to generate droplets in the wells. Furthermore, these droplets containing IEF components were collected for further analysis. Fig 3.5C shows six focused pI markers (pI 4.0, 5.5, 7.2, 7.6, 8.1 and 9.0) in IEF channel. The fluorescent images illustrate the focussed band (pI 5.5) before and after compartmentalization in a zig-zag channel.

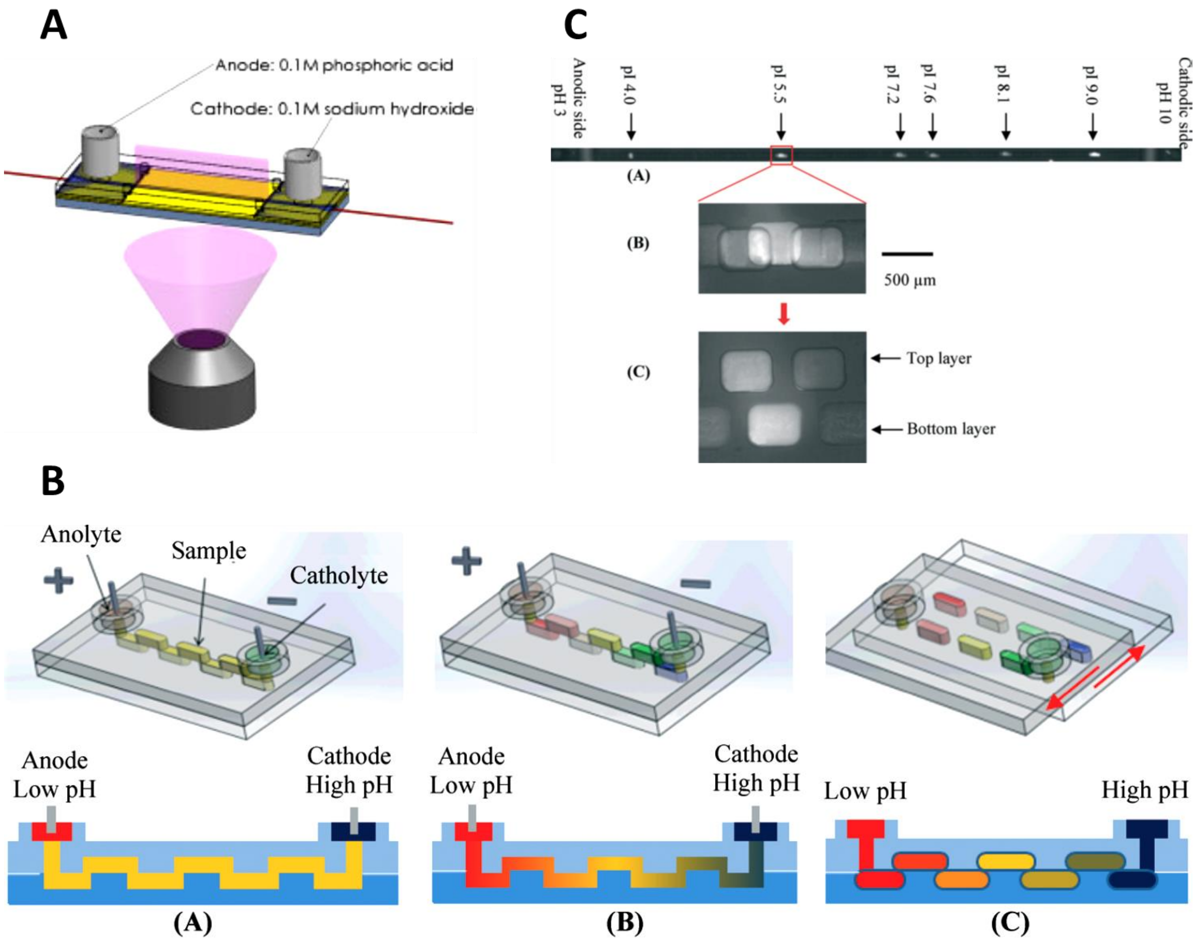

Figure 3.5 Overview of IEF-MCE A) Schematic of the quarts substrate with whole chip imaging via SU-8 slit [169]. B) Schematic of IEF Slipchip illustrating sample loading and pH gradient establishment in zig-zag channel (A-B) and droplet generation (C) of IEF fragments [77]. C) Separation of pI markers (pI 4.0, 5.5, 7.2,7.6, 8.1 and 9.0) in IEF channel (A) and fluorescent images of focused band (pI 5.5) before (B) and after (C) compartmentalization [77].

IEF is usually coupled with electrophoresis to increase the resolving power known as 2D-Gel electrophoresis and was first used by Farrel [172] in 1975 to separate proteins by isoelectric focusing in one direction and further separation by SDS-PAGE in other direction. The separation in 2D-electrophoresis is achieved in three steps. Firstly, proteins are separated on the basis of the differences in their pI value at different pH regions. Secondly, proteins focussed by IEF are equilibrated with SDS to break disulphide bonds and provide them with net negative charges. Thirdly, the proteins are separated in the second direction with SDS-PAGE. The ampholytes are removed by mixing trichloroacetic acid (TCA) with staining dye, and the gel is discoloured with acetic acid [173], [174].

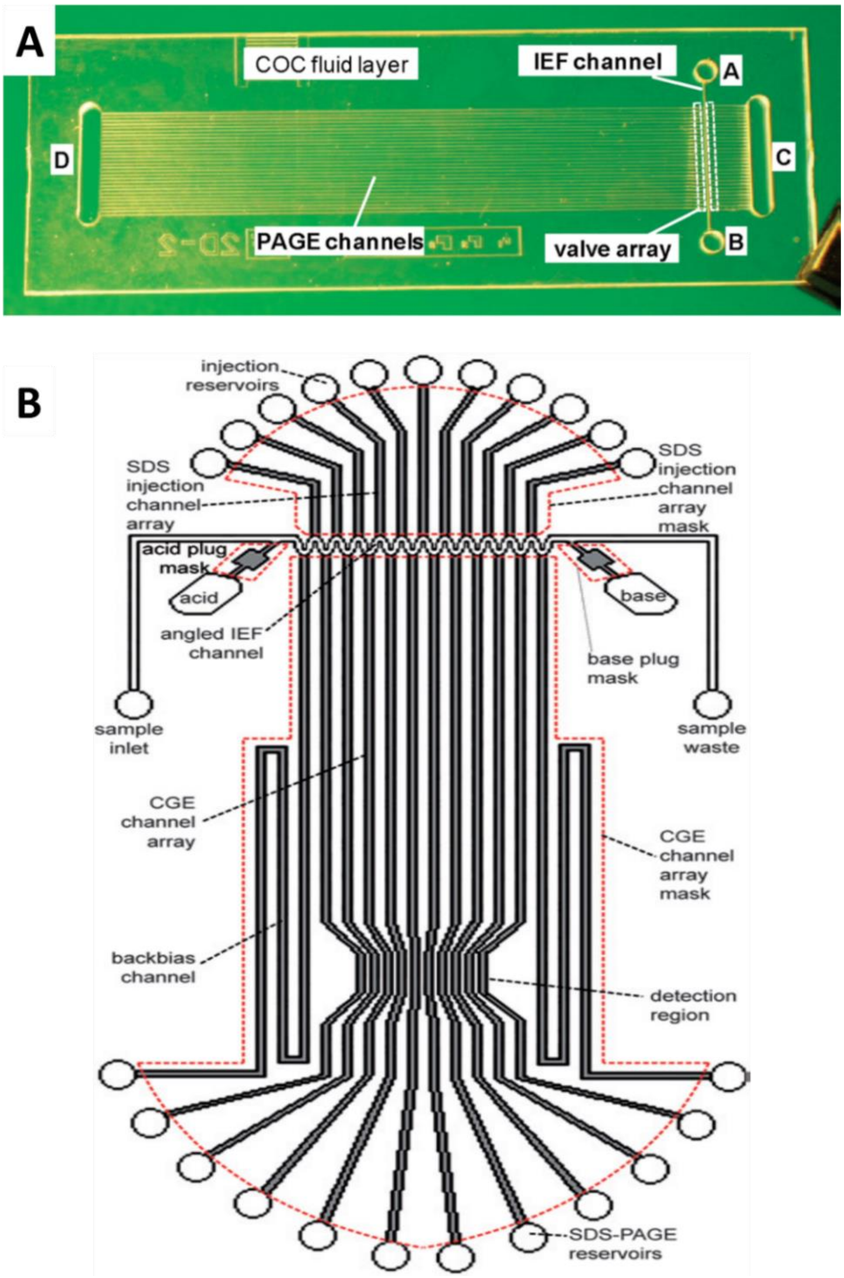

Figure 3.6 Overview of 2D-electrophoresis A) Snapshot of a COC substrate that functioned as a fluid layer. The device was designed for protein separation. Channel A-B is for the first dimension (IEF) while channels C-D are for the second dimension (SDS-PAGE). Valve arrays are indicated by the dashed lines on the both sides of the IEF channel [175], B) Schematic of the IEF-MCE with SDS-PAGE channels in the second direction. Photopolymerized gels were used in the CGE channels to separate anolyte, catholyte and IEF buffer solutions [21].

2D-electrophoresis in microfluidics can be very advantageous as IEF can focus proteins in very narrow and concentrated bands. For instance, plastic microchip was fabricated with IEF channel in one direction and CE channels perpendicular as shown in Fig. 3.6A. Actuated valves embedded in PDMS layer were used to inject IEF focussed proteins into separation channels [175]. In another development, Shuang *et al*. [21] fabricated a 2D separation device with 10 channels for isoelectric focussing in one direction and the cross channel for electrophoretic separation in second direction as shown in Fig. 3.6B. The microchip ran IEF separation in one direction and after focussing protein bands in the channel, the second dimensional SDS-PAGE was achieved in 10 long channels.

3.4 Recent Developments of Sample Injection in MCE

A particular interest of research in this area is the sample injections in MCE systems. Reliable and reproducible sample injection into separation channel is significantly important for resolving a mixture of biomolecules such as nucleic acids, proteins, and amino acids, etc. Sample injection in MCE involves containment of the sample on the same microchip as opposite to CE where the sample is injected separately. The majority of the MCE systems have used one of the two common sample injection methods, i.e. electrokinetic or hydrostatic injection. Hydrostatic sample injection technique controls the fluid flow in the small microchannels via pressure control and requires sophisticated microvalve systems due to which it has limited throughput [18] and is not discussed in this report.

In electrokinetic injection method, the sample is mobilized electrophoretically, and a fraction of the sample is dispensed into the separation channel [16], [17] as shown in Fig. 3.7A. Electrokinetic mode of sample injection may introduce bias as different analytes have different electrophoretic mobilities and the sample is dispensed from the cross-junction. More than 90% of the sample goes to the sample waste reservoir. Therefore, the injected sample may not reflect the concentration and composition of the original sample [9]. Jacobson *et al.* [176] described the pinched and floating sample injection methods into the separation channel as shown in Fig. 3.7B-D. Cross-chip design injects the sample into the separation channel via the intersection, and the volume of the sample injection can be controlled by the width of the channel intersection. The working principle of cross-chip is previously described in section 3.2 and Fig. 3.1. To reduce the sample bias, a greater volume of sample can be injected into the loading channels. However, this increases the band-broadening effect in the separation channel due to the diffusion. This method only uses electrokinetic movement of the sample in the loading channel known as floating sample injection (Fig. 3.7B) [176].

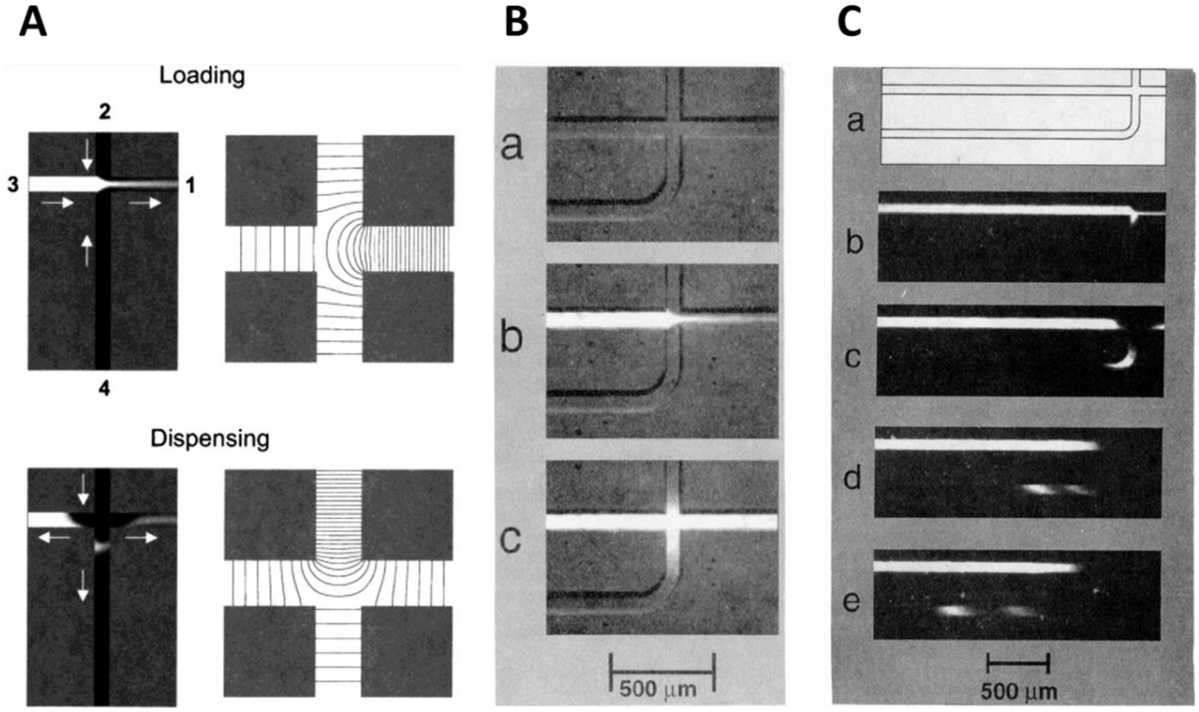

Figure 3.7 Electrokinetic sample injection into the separation channel A) Pinched sample injection into the separation channel. The lines on the right show electric field direction [17], B) Cross-chip sample injection device without any fluorescent molecule (a), a pinched sample loading mechanism (b) and a floating sample loading mechanism (c) [176], C) A schematic of the pinched sample loading cross-chip (a), A CCD image of the pinched sample injection (b) and a CCD images of separation of rhodamine and sulphorhodamine (c-e) [176].

Droplet-based microfluidics encapsulates samples into discrete droplets allows the manipulation of droplets in a high-throughput format (See Chapter 1), therefore, it has been applied to inject droplets into the separation channels such as Edgar *et al.* [31] developed a microfluidics device to inject droplets into the separation channel. The authors fabricated the chip with integrated droplet generation part and separation region and introduced the membrane between these two parts. The droplets were generated in the channels and then transported towards the separation channel where aqueous droplets were diffused into the separation channel by the aqueous membrane as shown in Fig. 3.8A. In contrast, Niu *et al.* [28] fabricated a droplet connector for two-dimensional separations of peptides. The droplets were generated after the first dimension separation (via capillary HPLC) and the merged with the separation channel buffer. Pillar array was used which automatically extracted the oil at the injection part, and the droplets were merged to the separation channel by the electric field (Fig. 3.8B). The connector injected entire droplets into the separation channel reproducibly. In another development, a K-shaped device was fabricated by Rowan *et al.* [177] to inject the sample into the separation channels. The authors used the V-shaped flow channel in which the sample was moved towards the separation channel, and a plug of the sample was injected into the separation channel (Fig. 3.8C). The serial injection of the amino acids was performed by using this device, and a controlled separation was achieved.

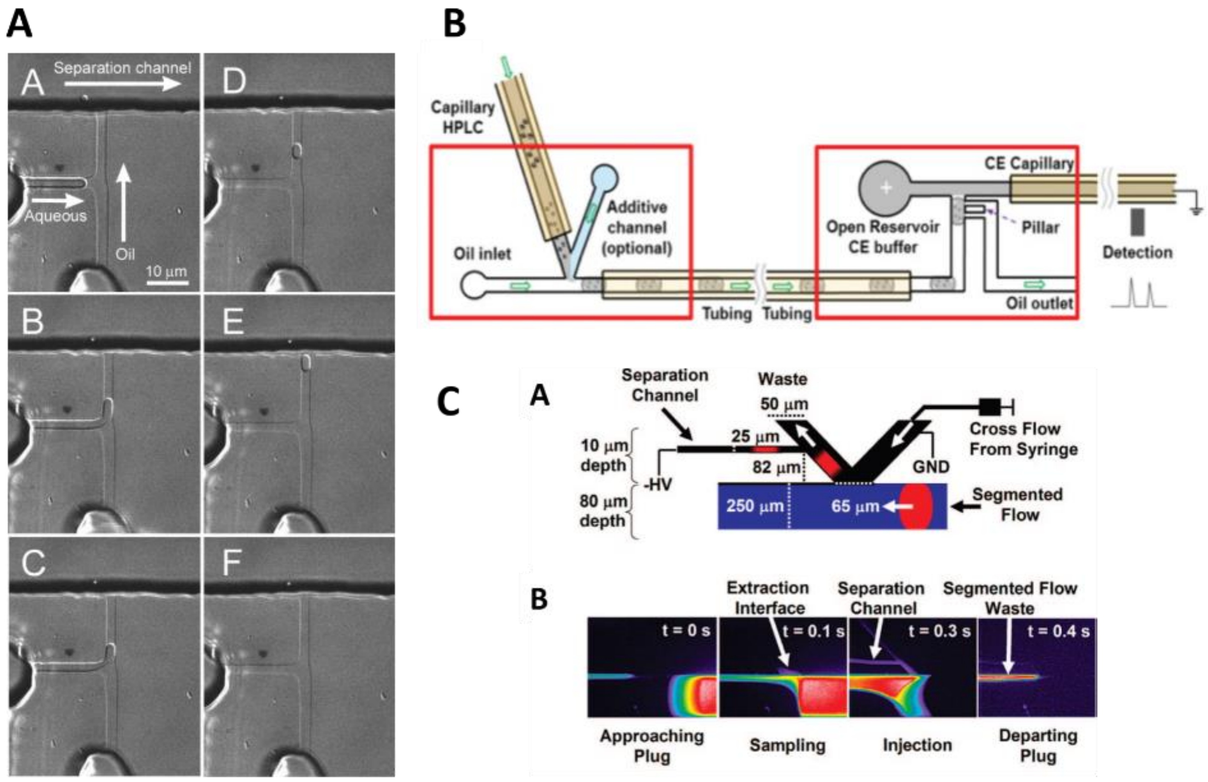

Figure 3.8 Droplet-interfaced sample injection into separation channels A) Generation and movement of sample droplet by applying pressure to aqueous sample (A-B) and carrier oil (C), movement of droplet in the microchannel (D-E) and injection into the separation channel (F) [31], B) Compartmentalisation of separated molecules from capillary HPLC column into droplets and interface with capillary electrophoresis. Pillar array was used to extract oil at the injection part, and electric field was applied to merge droplets into separation channel [28], C) Schematic of the K-shaped device illustrating droplet merging in the V-shaped channel and sample injection into the separation channel [177].

Recently, our group developed a droplet-based platform for separation of analytes encapsulated in droplets [32]. The platform allowed serial injection of pL to nL droplets into the separation channel. The sample droplets were generated in Teflon tubing and injected into the separation channel. Droplet generation was achieved by using FC-40 oil and the oil was removed with the help of an oleophilic membrane (Fig. 3.9A). The electric field was then applied to the separation channel, and the droplets were merged in the separation channel as shown in Fig. 3.9B. The droplets of 50bp DNA step ladder were injected into the device and separated into its fragments. The results were comparable with the standard electropherograms from capillary electrophoresis and agarose gel separations provided by the company. This method allows sequential injection of droplets into the separation channel, and each droplet is separated into its components within a time frame of 1-2 min i.e. the device is capable of analysing hundreds of droplets sequentially.

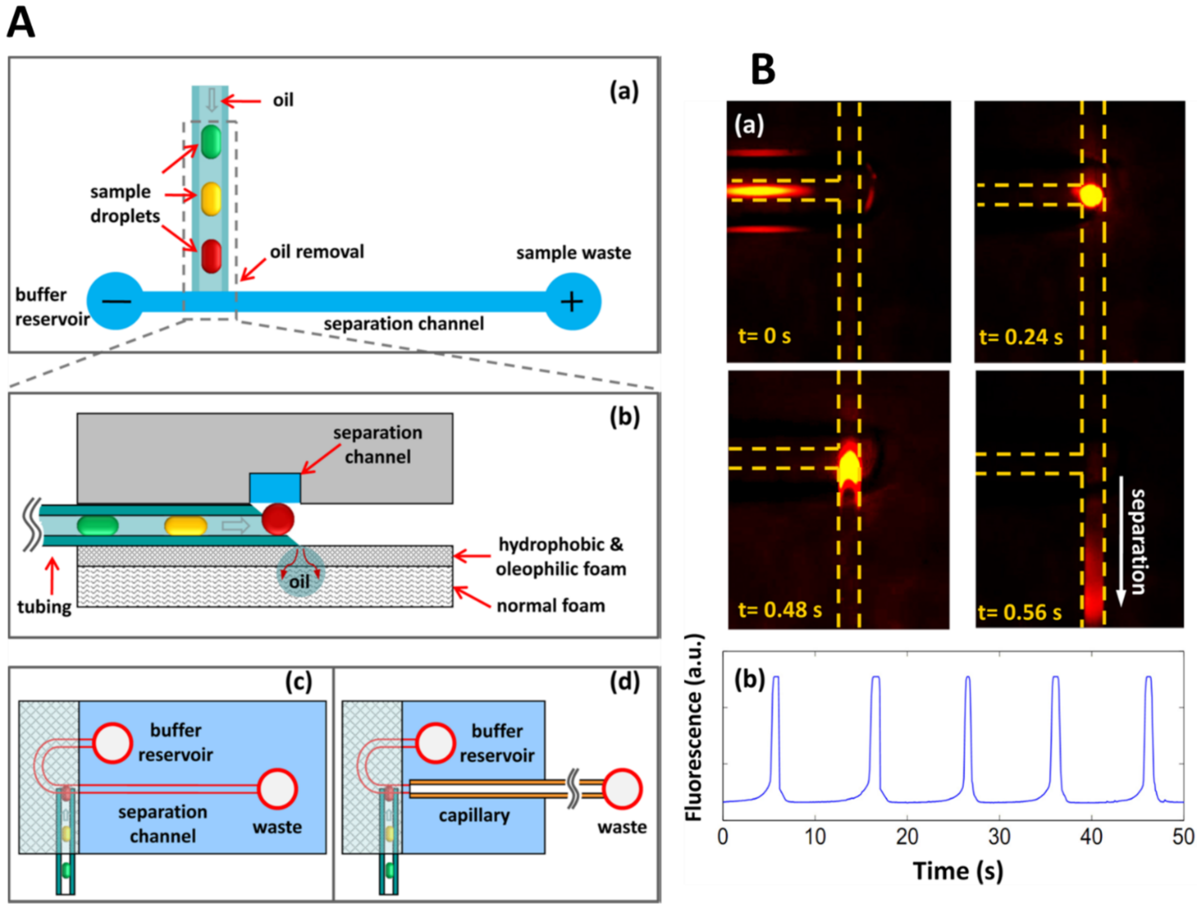

Figure 3.9 Droplet-interfaced sample injection into the separation channel (Sequential) A) Schematic of the device illustrating generation of droplets perpendicular to the separation channel (a), droplet injection into separation channel and oil removal via PTFE foam (b), (c) and (d) show the interface of the droplet injection channel with the PDMS separation channel and capillary connected to the separation channel respectively [32], B) CCD images of the droplet injection into the separation channel, electrokinetic movement of the FITC sample (a) and fluorescent signal of the sequentially injected sample droplets (b) [32].

3.5 Conclusions

This chapter reviewed basic principles of electrophoresis and microchip electrophoresis and several modes of MCE. Electrophoresis is a standard technique to separate macromolecules such as nucleic acids (DNA, RNA) and proteins, etc. The technique has become a routine method for DNA size fragmenting and separating protein mixtures in most laboratories around the world. SGE is commonly used for protein sizing, DNA sequencing, western blotting, etc. SGE uses porous gel medium to separate biomolecules based on the charge to size ratio of the molecules. Microchip electrophoresis (MCE) is a miniaturized form of capillary electrophoresis. MCE offers application of higher voltages to achieve fast and efficient electrophoretic separations. Droplet-based microfluids offers a promising platform for high-throughput sample injections into separation channels. This review demonstrates that the high-throughput MCE device with simple and user-friendly operational procedures has not been shown in previous studies.

Chapter 4 Droplet-Interfaced Microchip Electrophoresis Platform

The first part of the Chapter describes the design, working principle and fabrication of the newly developed droplet-interfaced MCE. The second part describes the characterisation of the droplet-interfaced platform using fluorescent dyes and biomolecules (DNA).

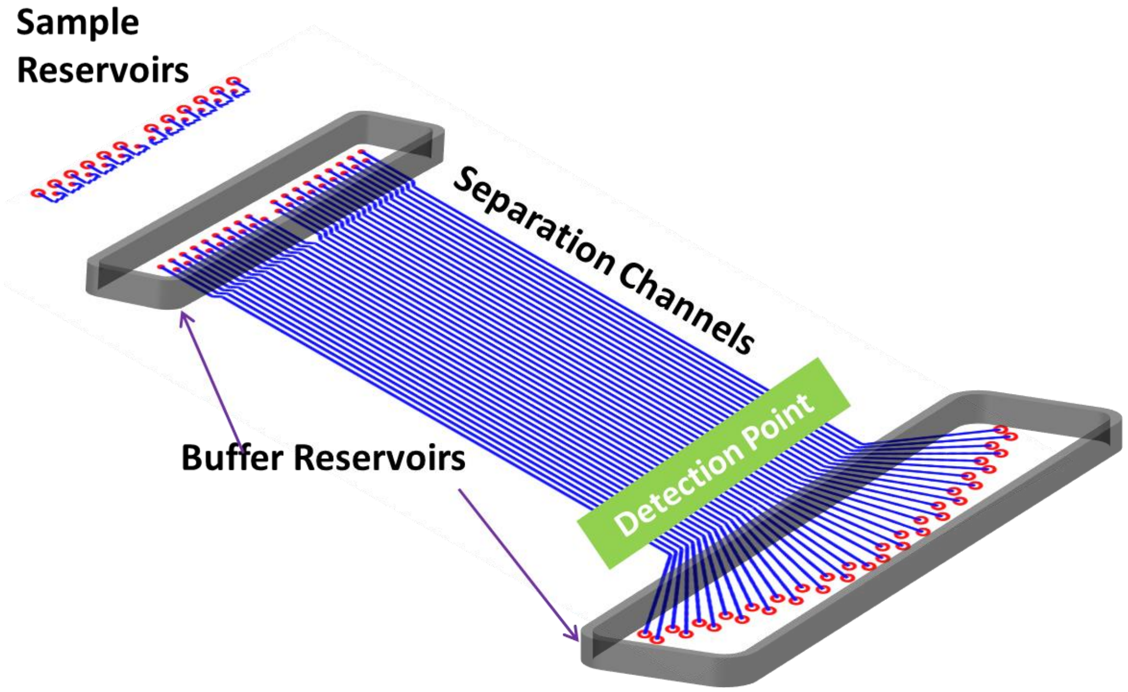

4.1 Introduction

A novel droplet-based high throughput MCE device for quantitative and high-throughput electrophoretic separations of nucleic acid fragments, protein mixtures, and biomarkers from biofluids such as saliva, blood, dialysate, etc. has been developed in the current study. Disposable MCE chips were fabricated by micromilling of plastic sheets, and a 3D printed Slipchip holding platform was used to control the movement of the microchips. The separation was run in parallel in 30 channels to achieve separation of 5 fluorescent molecules within 2 minutes, with detection by a CCD camera attached to a fluorescent microscope. Furthermore, 100 bp DNA step ladder was separated in 30 channels with high reproducbility.

4.2 Design and Fabrication of Droplet-Interfaced Separation Platform

Our approach was to combine the concepts of the Slipchip and MCE, develop a novel Gelchip device that can achieve parallel droplet-interfaced separations, by loading droplets into separation gel/medium with the ‘slipping’ function. With this sample loading method, the entire volume of the sample droplets could be separated, and therefore, it will be able to quantify biomolecules in sample droplets. Fig. 4.1 shows the schematic design of the Gelchip. The Gelchip consists of two separate plates; separation channels, sample loading channels, buffer reservoirs and via holes are on the top plate, and droplet wells are on the bottom plate. Hereafter, the top plate is referred to as the separation plate and the bottom plate as the droplet plate (Fig. 4.1). Droplet plate links the wells with the sample reservoir channels on separation plate forming a continuous channel for sample loading as shown in zoomed part in Fig. 4.1. Buffer reservoirs were glued on top of the separation chip, and holes were drilled to load the samples into the sample loading channels. The holes in the buffer reservoirs provide an electric field connection between reservoirs and separation channels.

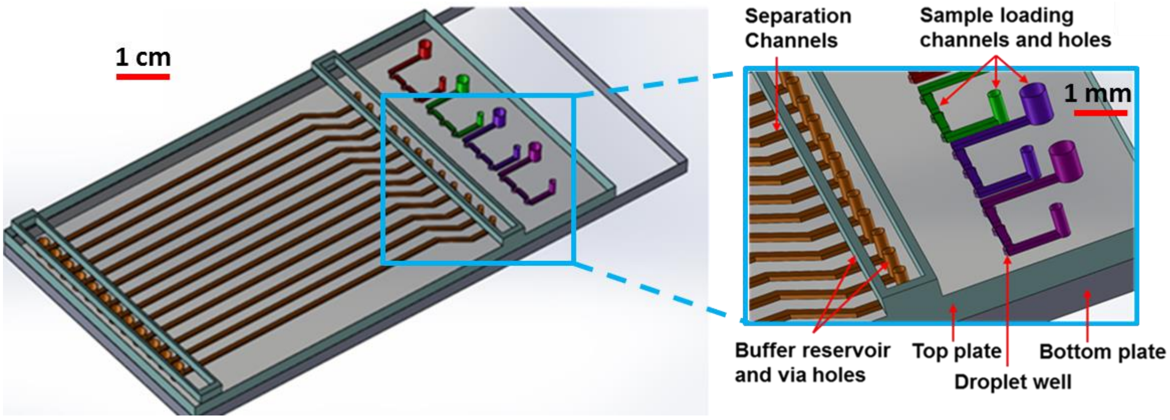

Figure 4.1 3D schematic of the Gelchip showing the assembly of separation chip (top) and droplet chip (bottom). The zoomed part shows the sample loading channels and holes, buffer reservoirs and separation channels. The schematic is not drawn up to the scale for illustration purposes.

Duxback was coated on the surface of the plates to increase hydrophobicity and reduce aqueous sample sticking on the plates. Briefly, both the MCE chips were treated with Duxback (Duxback Ltd) and heated at 65 ^{o}C for 10 min in an oven to evaporate the remaining solvent. To seal the microchannels and minimise sample sticking on the surface, 30-50 µL of FC-40 fluorinated oil (3M, UK) was added to the interface, mainly covering the areas between the droplet generation and the sample loading channels. The oil lubricates the two plates and minimises surface friction during movement of the plates. The separation plate was then joined with the droplet plate in such a way that the sample loading channels were connected with droplet wells forming continuous channels. The schematic of the working principle of the MCE device is shown in Fig. 4.2. The device works in three different stages. Firstly, samples are loaded to the sample reservoir channels. Secondly, the sample is injected into the separation channels and thirdly, the sample is separated in the presence of an electric field.

The two halves were clamped together using magnets and/or clips on opposite sides to assure a tight contact of the two plates [77]. Separation gel was cured in the separation channels by a simple protocol provided in the results section. Briefly, gel reagents were mixed in a container, degassed and poured into the separation channels. Invisible adhesive tape (Office Depot, Inc.) was pressed over the channels, and the extra gel was removed. Once the gel was cured, the tape was gently removed to leave the gel in the channel. Fig. 4.3a shows the 3D schematic of the separation and droplet plate in place before assembly.

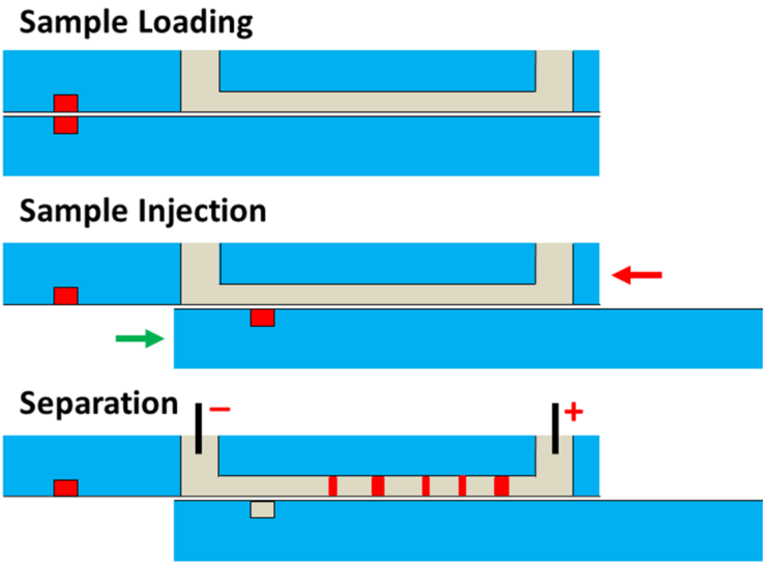

Figure 4.2 Schematic side view of the working principle of MCE device. The Gelchip works in three steps; sample loading via drilled holes, sample injection into separation channels with relative movement of droplet plates, and separation upon application of electric field.

After assembly, the sample mixture was loaded into the sample loading channels via inlet holes (0.8 mm diameter) that fitted with the end of a pipette tip. The separation buffer (TBE/Tris-Ches) was then loaded to the two buffer reservoirs connecting to the both end of the separation channels. A 0.5 mm diameter platinum wire electrodes were placed in each reservoir to provide a uniform electric field to all of the parallel channels. Noted in certain separation modes when liquid sieving matrices were required, such as PEO solution for microchip capillary gel electrophoresis (microchip CGE) or microchip capillary zone electrophoresis (microchip CZE) buffers, the separation channels were left empty during chip assembly. Separation matrices were then added to the channels before sample loading, by gentle liquid pumping to the inlet holes (0.8 mm diameter) with a peristaltic pump at a flow rate of 3 µL/min. The 3D Schematic of the MCE device after assembly is shown in Fig. 4.3b.

The droplet plate was then moved by a screw micrometre stage from its initial position; thereby generating droplets in each of the wells as shown in 3D Schematic of the Fig. 4.3c. During this process, sample droplets were first generated from the sample loading channels and further moved to overlap with the separation channels as shown in Fig. 4.3c. (The FC-40 oil membrane trapped in between the two plates keeps the aqueous sample droplets inside the droplet wells whilst they were moved towards the separation channels). Finally, a DC electric field was applied across the reservoirs, migrating the sample molecule towards the opposite charge end performing electrophoresis separations. The separated components were detected by a fluorescent CCD camera attached to a microscope.

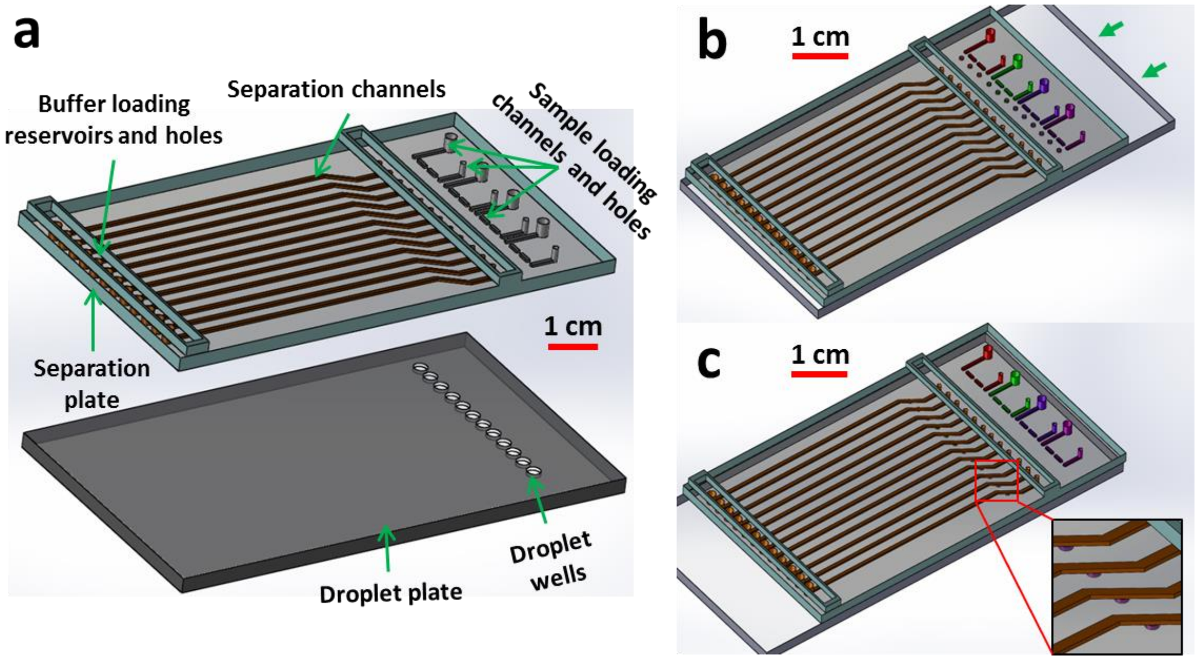

Figure 4.3 3D schematic of the working principle of the Gelchip a) Separation and droplet plate in place before assembly, b) Slipping bottom layer to generate droplets (arrow shows movement direction), c) Injection of droplets into the separation channels. The zoomed part shows the injected droplets into the separation channels.

The most common detection methods for electrophoresis are electrochemical and optical detections. Electrochemical detection is very sensitive and compact method to detect minute amounts of analytes with the use of the electrode. The distinct bands pass through the detector, where the change in current occurs and band peaks are recorded. The electrochemical detector can be very compact and embedded in the MCE device. However, specific electrodes are required for different analytes, and electrochemical detectors are expensive due to the disposable electrodes or requiring replacement after few analyses [178]. Optical detections are most commonly used for MCE separations. It uses a light source to illuminate the molecules at various wavelengths, and the emitted or absorbed lights are detected by a photodiode, charge-coupled device (CCD) or photomultiplier tube (PMT) as discussed previously in chapter 2. Unlike electrochemical detectors, optical detectors can move from one position to another and therefore, offer the possibility of scanning multiple separation channels for high throughput detections.

An electrical field of 50-260 V/cm was applied to the separation channels for electrophoresis. The fluorescence intensity of the separated analytes was measured by collecting images using a microscope (Olympus BXFM, Japan) with an attached CCD camera. A mercury lamp was used to excite the sample through a FITC filter and focussed through a 10x objective. ImageJ software was used to analyse the recorded images and the electropherograms, and pseudo-gel plots were drawn by Matlab programming (Mathworks) (Appendix 1.3.1). Briefly, the electropherograms collected by ImageJ were transported to Matlab, and a pseudo-gel plot was drawn as a colour map. The data was further normalised by an in-house developed Matlab code according to retention times of the first and last peaks (Appendix 1.3.2) as discussed in results section.

4.2.1 Fabrication

Ultra high-throughput can be achieved by fabricating hundreds of parallel arrays of channels. The most common fabrication techniques used for MCE are soft lithography and glass etching which are tedious and time-consuming. Plastic microchips such as PMMA chips have the advantages over glass and PDMS microchips such as mechanical strength, inexpensive, simple fabrication steps and disposability. Numerous such devices have been fabricated by laser ablation [179], micromilling [180], and hot embossing or plastic moulding [181] briefly outlined below.

Laser ablation involves the application of a laser beam on the polymer material. Laser beam breaks the covalent bonds on the polymer chain molecules, and the shock wave is produced which ejects the decomposed fragments. Most of the polymers can be laser ablated especially PMMA is widely used for fabricating microchannels [179]. The micromilling is quite a cheap method to fabricate separation channels on plastic microchips and it provides very reliable dimensions with small variations. The micromilling apparatus consists of a milling bit attached to a moveable platform and works by x-, y- and z-axis actuators installed on the machine [182]. A camera can also be connected with a platform to monitor the progress of the micromilling. The micromilling tools are available in different sizes from 25 µm to 3 mm. Hot embossing and plastic moulding are very common methods for mass production of microchips. Plastic moulding involves fabrication of the master and microstructure transfer from the mould to the polymer substrate. Moulds can be fabricated by micromilling and lithography [183] and microchips can be replicated from the mould by hot embossing [184]. The mould and polymer material are heated just above the glass transition temperature of the plastic material. This method takes few minutes to produce the microchip. Therefore, it can be used for mass fabrication of microchips.

In the current work, both plates were fabricated by a precision micromilling of PMMA sheets using LPKF Protomat S100 micromilling machine (LPKF Laser & Electronics Ltd, Berkshire, UK) as shown in Fig. 4.4a. The designs were drawn by AutoCAD software, and the dxf file was imported to CircuitCAM software (LPKF laser and electronics, Garbsen, Germany). The wells were milled with a 150-300 µm diameter end milling bits (LPKF Laser & Electronics Ltd, Berkshire, UK), and holes were drilled with a 250, and 800 µm diameter drilling bit. The milling of the droplet plate took 30 min, and the milling of the separation plate took about 3 hours. On the top plate the separation channels (150 x 200 μm width x depth, 7 cm long), via holes (300 μm diameter), cathode and anode reservoirs were milled as shown in Fig. 4.4a. The separation channels were filled with red food dye for better vision of the separation chip as shown in Fig. 4.4b. Microwells for sample droplets (150 x 200 x 200 μm width x length x depth) were milled on the droplet plate.

Several other chip designs were also considered during the experimental work (Appendices 1.2.1-1.2.5). However, the current design was used in later experiments because of the following reasons 1) The sample loading channels allowed small volume of sample (300-1750 picolitre) to be loaded onto the chip, 2) Multiple samples are allowed by be loaded to a single chip with 3 repeat droplets for each sample, and 3) The straight separation channels with smooth turns allowed easier filling of the separation medium and less dispersion of bands. The distance between each channel was designed to allow the droplets moving towards the separation channels experience no contamination or sample tailing at the start of the separation channels. This distance depends on the droplet size and can be increased to accommodate bigger droplets (as in the case of DNA sample used later in this section). Furthermore, a discontinuous separation channel shown in appendix 1.2.1 was also used to provide a more uniform electric field distribution. However, the breakage of the channels added extra challenges to both chip fabrication and chip alignment and hence was replaced with continuous channels (Fig. 4.4). The distance droplet travel from the initial position to injection into the separation channels was also calibrated, because small leakage of the liquid sample was always present and could tailgate into the separation channels. The distance of 1.6 cm was found to be optimum to stop the leakage reaching the channels and was used throughout all experiments.

The fabricated plates were rinsed with DI water and sonicated in isopropyl alcohol (IPA) for 7-8 min. The chips were then rinsed with DI water and dried with compressed air. The surface of the separation channels, sample loading channels and droplet wells was found rough after micromilling analogous to the study done by Ogilvie *et al.* [185]. The authors treated the microchips with chloroform and generated optically clear surfaces. Therefore, the fabricated plates were reflowed with chloroform to smooth the surfaces of the channel and droplet wells (Fig. 4.4c). The method produced optically transparent surfaces as shown in Fig. 4.4c (A1, B1, and C1). Briefly, the chip was placed on the top of a container filled with chloroform. The chips were faced downwards that all of the channels were exposed to chloroform vapour. The distance between the chip and the chloroform layer was kept at 5 mm and an exposure time of 3-4 min was found to be suitable for reflow of the PMMA surface. A longer exposure time of more than 4 min was found to be damaging the channels with cracks appearing on the surface. Fig. 4.4c illustrates the optical quality of the MCE chip before and after chloroform reflow after 3 min's vapour exposure. Chloroform is a hazardous material and the vapours can cause acute toxicity, irritation or carcinogenicity. Therefore, the reflow process was performed in a fumehood and using personal protective equipment. Fig. 4.4d illustrates the schematic of the sample loading into the assembled Gelchip. The droplet wells act as the bridge between the discontinuous channels and allow the fluid to flow via droplets wells as indicated by arrows in Fig. 4.4d.

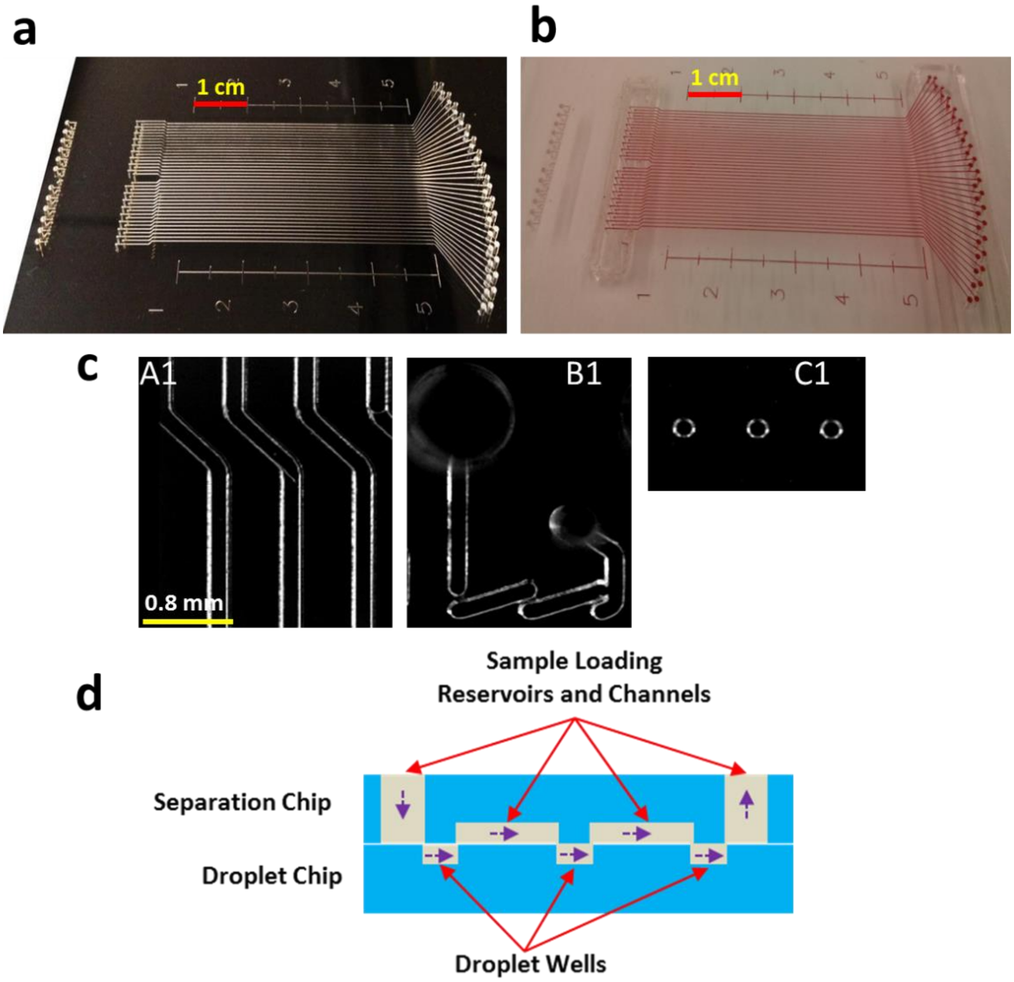

Figure 4.4 Micromilling of droplet and separation plates a) Snapshot of micromilled separation plate, b) Snapshot of the separation chip filled with red food dye, c) Snapshots of Separation channels (A1), Sample loading channels (B1), and droplet wells (C1) after chloroform reflow, d) Schematic of the assembled Gelchip illustrating sample loading into the droplet wells. Arrows show the direction of fluid during sample loading.

Slipchips are usually joined together by binder clips [70] or paper clips [72], and the slipping is achieved manually. Therefore, a slight misalignment of the droplet wells could cause a leakage and contamination of the parallel samples. To solve this problem, a Slipchip holding platform has been developed by our group [77] to mount and align microchips in a controlled manner. The platform consisted of three layers as shown in Fig. 4.5a. The bottom layer of the platform is to support and provide a solid base to the whole device. Middle layer offers the mechanism to hold and slide the droplet plate. The middle layer is also attached with a micrometre to control the movement of the droplet plate precisely. The top layer is the fixed layer and holds the separation chip. Fig. 4.5b shows the platform after assembly. Two pairs of magnets were used to provide a uniform pressure on the two chips for a tight sealing.

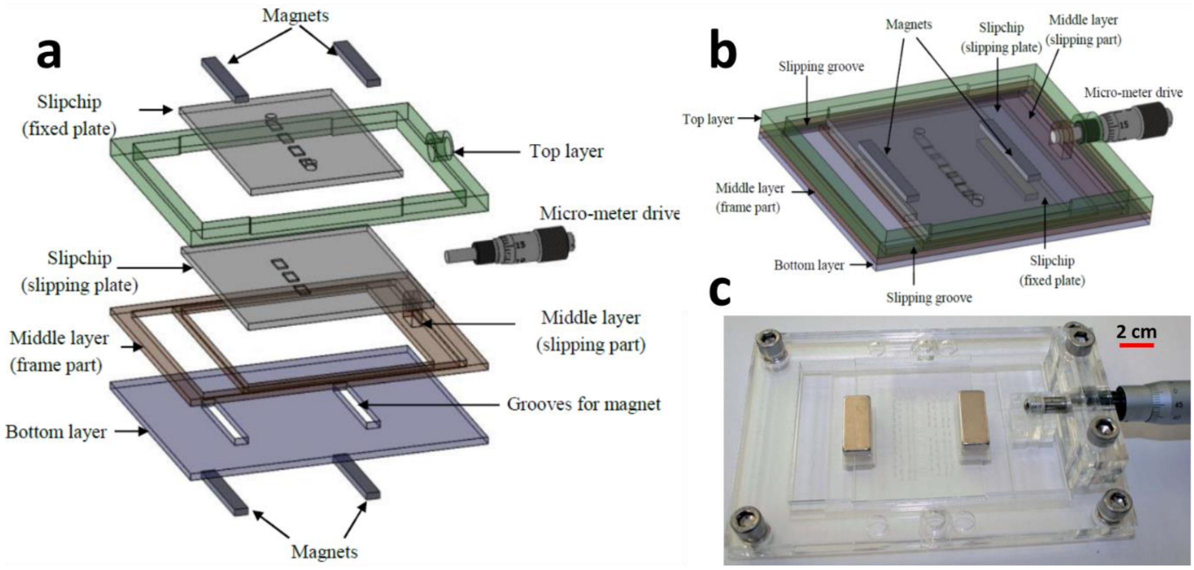

Figure 4.5 3D Schematic of the Slipchip holding platform a) Illustration of different layers of platform before assembly showing top, middle and bottom layers, and Slipchips used for IEF separations, b) 3D schematic of the fully assembled platform including micrometre, magnets, and Slipchips used for IEF separations, c) Snapshot of the fully assembled IEF separation platform. [77].

Slipchip holding platform was fabricated by Epilog 18 CO_2 laser system (Epilog Laser, CO, US). It uses the power of 30 watts, and the diameter of the laser beam is 75 µm. Laser power and movement speed of the head determines the cutting depth of the material. The designs of the platform layers were drawn on the AutoCAD software, and the dxf files were imported to the CorelDraw software which provides an interface between the laser machine and design. The sheets of PMMA (2mm and 5 mm) were cut with different powers of the laser. Briefly, the 100% power and 100% speed of laser ablate 60 µm of the material. The snapshot of the fabricated platform is shown in Fig. 4.5c. The dimensions of the platform were 20 x 10 x 1.5 cm (length, width, and height respectively).

The platform was also fabricated by 3D printing as shown in Fig. 4.6. The design of the platform was drawn in SolidWorks (Dassault Systemes) and printed in black poly(lactic acid) (PLA) material using an Ultimaker-2 3D printer. The platform is composed of a single printed holder with spaces fabricated for droplet generation and separation plates as shown in Fig. 4.6a. 3D printing was chosen because of the ease of fabrication. Fig. 4.6b shows the schematic of the droplet and separation plate in place in the platform for separation. Once fully assembled, the platform only measures 15 x 5 x 1.5 cm (length, width and height respectively) as shown in Fig. 4.6c. The buffer reservoirs were glued on the separation chip and platinum electrodes were fixed on the platform to apply voltage to the separation channels.

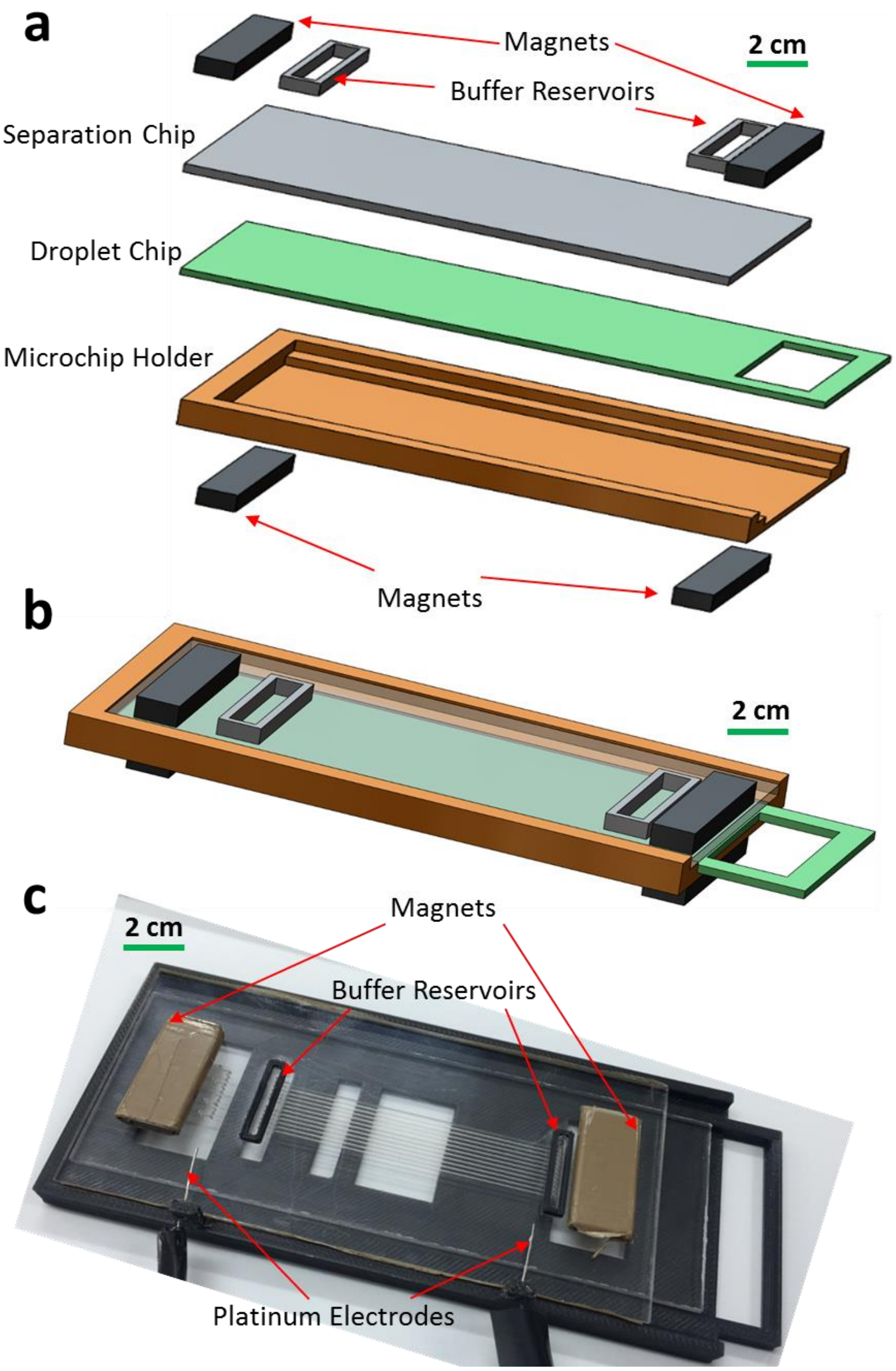

Figure 4.6 3D Schematic of the 3D printed Slipchip holding platform a) Illustration of different layers of platform before assembly showing microchip holder, and separation and droplet plates in place for MCE separations, b) 3D schematic of the fully assembled platform including separation and droplet plates, magnets, and buffer reservoirs, c) Snapshot of the fully assembled platform.

4.3 Experimental Results and Discussion

This section of the chapter describes all the experimental results including separation medium and sample loading into the Gelchip, characterisation of droplet generation and injection, the effect of droplet sizes on separation efficiency, separation of fluorescent and DNA molecules.

4.3.1 Separation Medium

The buffers and/gels were filled or cured inside the separation channels to carry out the separation on MCE channels. Different formats of MCE require different separation mediums and the ones used in this project are discussed below.

Tris-borate buffer usually referred as TBE buffer is mostly used for nucleic acid fragment separations previously discussed in chapter 3. It is used with agarose gel electrophoresis and also with polyacrylamide gel for separation of single stranded DNA molecules [186]. Tris-ches and Tris-glycine buffers are used for SDS-PAGE separation of proteins [187], [188]. All the buffers were bought from Sigma (Dorset, UK) and diluted to the required concentrations as per company instructions. Buffers were loaded to the separation chip by a pipette and/or syringe pump.

Polyethylene oxide is commonly used for microchip CGE. The PEO gel is used for separation of DNA fragments and proteins [149], [189], [190]. PEO is a well-known sieving matrix used for separating DNA molecules and provides homogeneous solutions [190]. PEO (500 kDa) was bought from Alpha Aesar (Lancashire, UK) and poured slowly in TBE or Tris-ches while the solution was stirring. It was filtered by using 0.2 µm pore size syringe filter and degassed after being stirred for 24 h. In this way, 1-3% PEO (w/v) in TBE/Tris-ches was prepared. SDS was also added to the gel for protein separations at a concentration of 0.2-1 %. PEO gel was loaded to the separation channels after assembly of the device by a pipette or syringe pump.

A simple protocol was developed to prepare the ‘Gelchip’ for curing agarose gel inside separation channels. Agarose powder was mixed in the buffer, heated in a microwave oven to above 90°C to melt the powder. As shown in Fig. 4.7a-e, the agarose liquid was degassed and cooled down to 50°C and poured on the microchannels. A lab tape was then applied on the plate surface with the aid of a roller, to remove extra liquid gel from the surface of the plate and to prevent drying of the gel during curing. Fig. 4.7f shows the cured gel inside channels under microscope (with mixed fluorescein for indication). The lab tape was peeled off from the plate before its usage for electrophoresis separation, and no damage of the gel surface in the channels was found (and no gel sticking on the tape as verified under a fluorescent microscope). The gel filled chips were stored at

4 °C prior to use. In initial test, the Gelchips could be stored in the fridge for 5 days and used off-the-shelf. A container with statured water vapour might can help to extend the shelf life.

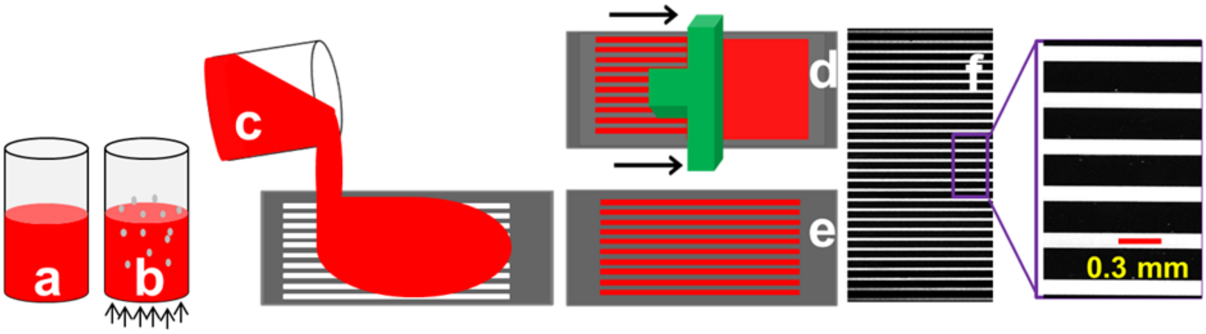

Figure 4.7 Gel curing procedure a) Reagents mixed in buffer, b) Degassing in a sonicator, c) Pouring liquid/gel on microchannels, d) Removing extra fluid/gel from the microchip, e) Casting the gel in the channels, f) Snapshot of the microchannels with gel cured inside (fluorescein was mixed with gel for visual purposes).

Polyacrylamide gel was also cured inside separation channels by mixing the gel reagents (acrylamide/bisacrylamide, ammonium persulphate, Tris-ches and SDS), degassing in a sonicator and then gently mixing TEMED in the solution. The mixture was poured on the channels; the tape was pressed to bond on the chip surface to seal the channels. After 30 mins, the gel was completely cured, and the tape was removed. The gel filled chips were also stored at 4 °C prior to use. The cured polyacrylamide gel in the channels is shown in Fig. 4.8b. Polyacrylamide gels were cured with different %T values required for separation of fluorescent dyes or biomolecules and the %T values were calculated using Eq. 7 (Chapter 3). Acrylamide monomer is a hazardous material and the vapours can cause acute toxicity, irritation or carcinogenicity. Therefore, the curing process was performed in a fumehood and using personal protective equipment.

Fig. 4.8 shows fluorescent images of the gels cured inside the separation channels. Fluorescein was mixed with the gel reagents before curing for indication. Part of the cured gel was removed out of the channels with a pair of tweezers to demonstrate the cross-section of the gels (Fig. 4.8a for agarose and 4.8b for polyacrylamide gels). The purpose of the development of the simple gel curing method was to provide an easy way to cure gels inside channels which can be stored in the fridge and used for experiments. This approach eliminates the need for filling separation channels and hence can be used off-the-shelf for POC applications.

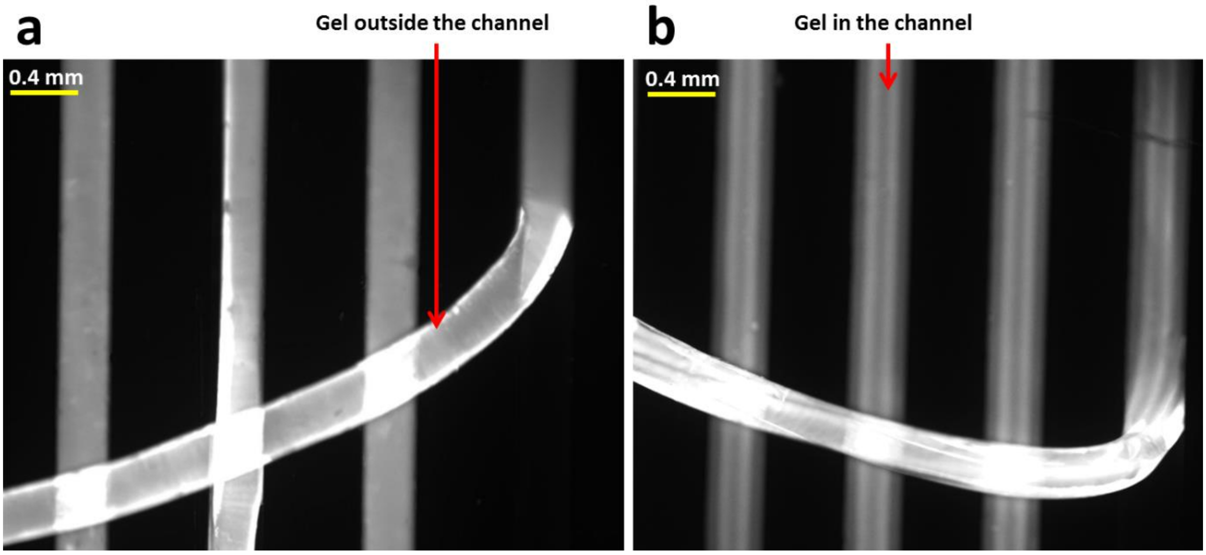

Figure 4.8 Preview of the gel cured inside separation channels a) Agarose gel cured in the channels by heating reagents in a microwave oven, pouring liquid onto the channels and removing the extra gel, b) Polyacrylamide gel cured in the channels by mixing reagents and filling them into the assembled Gelchip via holes. Fluorescein was added to the gel reagents for visual purposes.

4.3.2 Droplet Generations in MCE Device

Droplet generation was initially calibrated by loading fluorescein dye solution into the sample loading channels connected to the droplet wells (Fig. 4.4) as shown in Fig. 4.9a. After slipping the chip, droplets were generated in parallel. Each sample produced 3 repeat droplets. As shown in Fig. 4.9b, there is no fluorescent signal out of the droplets and sample loading channels (i.e. no leakage). Fluorescence intensity profiles of the generated droplets were analysed by ImageJ; this gives information on the reproducibility of the area of droplets (an estimation of droplet volumes) (Fig. 4.9c). The percent relative standard deviation (%RSD) of peak area for all of the 30 droplets in more than 3 runs was <3%.

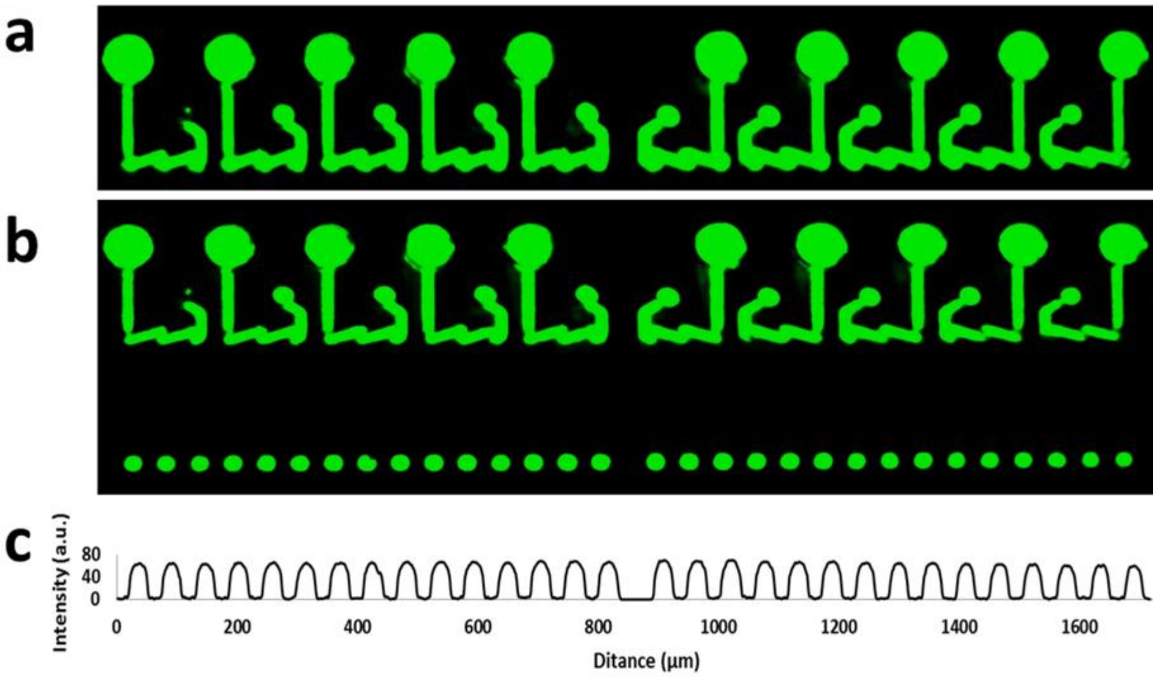

Figure 4.9 Droplet generation in Gelchip (Fig. 4.4) a) Fluorescein filled in the sample loading channels, b) Droplets generated after slipping the chip, c) Fluorescence intensity profile of the droplets (the corners show low intensity which is due to the uneven brightness of the light source).

In initial experiments, leakage was observed (Fig. 4.10) during the slipping operation on untreated plate surfaces. This leakage was attributed to the PMMA surface which is not hydrophobic enough, and the aqueous sample sticks to the surface. This leakage can have the detrimental effect on the separation because the aqueous sample leaked from the sample reservoir channels introduces the tailing effect i.e. sample continues to move towards the separation channels and some extra small sample peaks are observed. However, this was controlled by a coating of a hydrophobic material (Duxback) to the separation and droplet plates. This minimised the leakage, and the aqueous droplets stayed inside the droplet wells (Fig. 4.9b).

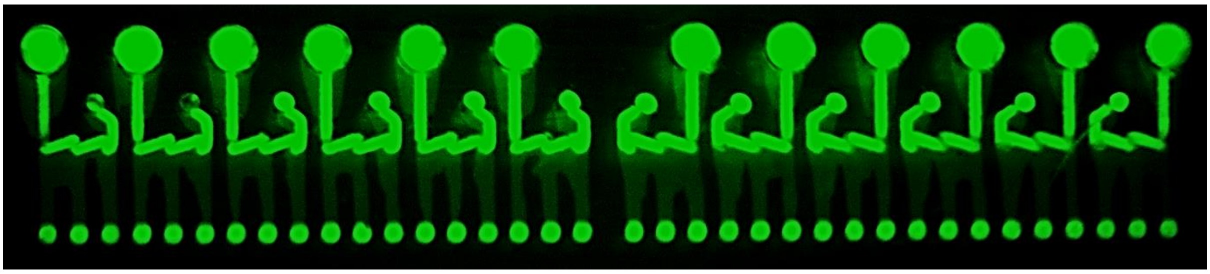

Figure 4.10 Microscopic view of the Gelchip with droplets generation and showing leakage of the sample from the sample loading channels. This leakage is due to the PMMA surface being slightly hydrophilic and affects the droplet volume reaching the separation channels.

4.3.3 Sample Injections in Separation Channels

The droplets were further moved to be in contact with the separation channels (Fig. 4.11). There was no surfactant added into the oil and the aqueous droplet merged with the gel immediately. The sample molecules started to diffuse into the separation channels. In Fig. 4.11, the droplets in the right half of the channels are less bright in colour; this is due to the limit of current experimental setup. To illuminate the large area of the chip for imaging, the light source was placed at the top left side of the chip. The different orientations of separation channels in the left group and the right group gave rise to the different visual effect in Fig. 4.11. However, this does not affect the detection of distinct bands where all of the separation channels are in parallel and are detected by moving the platform under the microscope (15 channels at once).

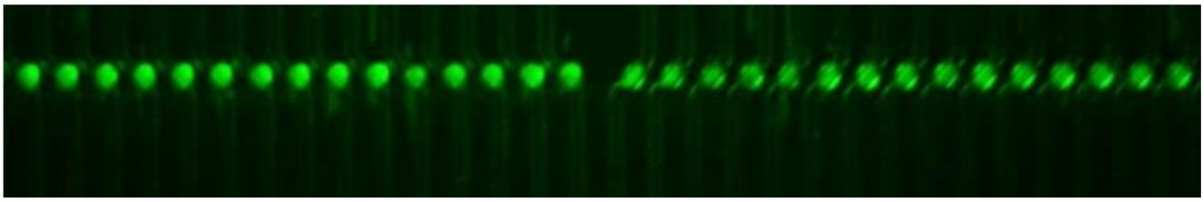

Figure 4.11 Droplet injection of fluorescein sample in the separation channels with the movement of the droplet chip. The snapshot was taken at 0 s from the injection. The opposite orientation of the channels gives a different visual effect which is due to the light source placed at the top left side of the platform.

To characterise sample injection into the separation channels, droplets containing fluorescein were generated in the Gelchip and injected into the separation channels filled with PEO gel (1.5%). The aqueous sample spreads quickly on the separation medium as shown in Fig. 4.12a. Fluorescein molecules diffused into the highly hydrophilic PEO gel even without the application of electric field. However, the electric field should be applied as soon as the droplet reaches in contact with the separation medium (less than 10 s) to avoid elongation of the injected volume and hence band-broadening. It was observed that 30 seconds was enough for the diffusion of almost all of the sample into the separation channels (based on a volume of 1 nanolitre droplet and 0.4 mm channel width).

Confocal imaging of the droplets diffused into the separation channel was obtained by a Zeiss confocal microscope (Inverted Zeiss LSM 510)) using the Gelchip (Fig. 4.4) as shown in Fig. 4.12b. The purpose of the experiment was to observe how does the aqueous droplet diffuse into the separation channel and whether the thin oil layer in between the separation medium and droplets hinders the diffusion of the molecules in the separation medium. The fluorescein droplets of 1 nanolitre volume were generated in Gelchip and injected into the separation channel (0.4 mm ID) filled with PEO gel (1.5%). Soon after injection, the 3D imaging of the merging was achieved by recording the z-stack images (100 slices were recorded based on the channel depth of 0.4 mm).

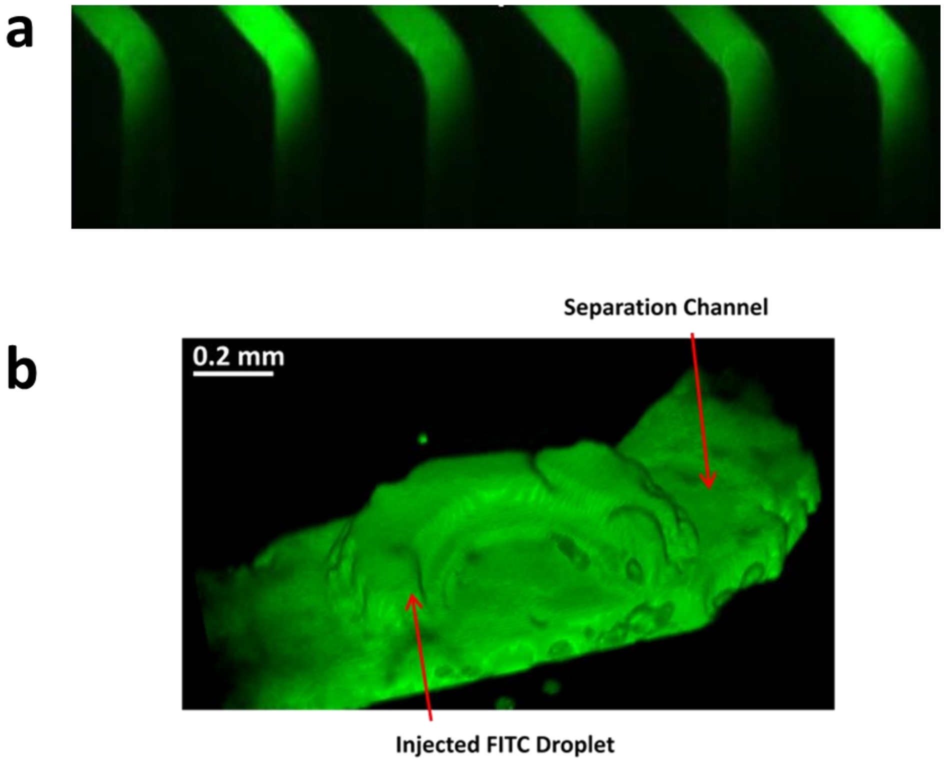

Figure 4.12 Diffusion of sample droplets in separation channels (Fig. 4.4) a) Fluorescein droplets after merged in the separation channels, b) Z-stack 3D confocal imaging and fluorescein diffusion in agarose gel after merging. The green area represents diffused fluorescein molecules in agarose gel and remaining droplet.

Briefly, the top and bottom surface of the channels were manually focussed before the droplet injection to fix the positions for the first and the last slice. The platform was fixed on the microscope movement stage in order to avoid changing in focussing due to the movement of the plate, and the z-stack images were taken at an exposure time of 100 ms (the whole channel was scanned within 10 s after sample injection). The 3D image showed that the fluorescent molecules already diffused into the separation gel within 10 seconds after the droplet merging to the separation channel without the application of electric field (Fig. 4.12b). It can be inferred from the 3D image that the sample droplet volume was reduced by more than 50% within 10 seconds of initial merging.

4.3.4 Separation Calibrations

Separation reproducibility was calibrated by separating fluorescent dyes into the microchannels. PEO, agarose, and polyacrylamide gels were used to calibrate the sample injection and separation efficiency in the separation channels as discussed below.

4.3.4.1 Fluorescein-5(6)-Isothiocyanate (FITC), Fluorescein (FL), 5-Carboxyfluorescein (CFL), and Eosin Y (EY) Separation in PEO Gel

FITC, FL, EY and CFL at concentrations of 25, 10, 144 and 13.5 µM respectively were prepared in 0.1x TBE buffer and separated using 1.5% PEO gel (500 kDa). In this calibration, all of the sample droplets contained the same sample mixture. The dyes were negatively charged at a pH of 8.4 and migrated towards the anode when an electric field (90 V/cm) was applied. The bands of separated dyes were detected at 3.5 cm from the sample injection point (within 60 s), and the images were recorded and analysed by ImageJ. FITC had two isomers FITC 1 and FITC 2. The two isomers travelled at different velocities due to the presence of thiocyanate group at various positions on the benzene ring.

The experimental velocities of CFL, FL, FITC 1, FITC 2 and EY were calculated to be 0.0173, 0.0122, 0.0095, 0.0085, and 0.0073 cm/s respectively (overall %RSD >5%) using Eq. 3 (Chapter 3). In the case of FITC 1 and 2, it was found that a 2 cm was the shortest distance to separate both molecules (FITC 1 and 2), and the separate bands were not visible in shorter distances. Furthermore, the FL (332.31 g/mol) band moved slower than CFL (376.32 g/mol) even though the CFL molecule is bigger than FL. This is due to the presence of 3 hydroxyl groups on CFL (as compared to 2 on FL) which increases the charge on the CFL molecule, and hence its velocity (Eq. 1).

The unprocessed data was drawn as electropherograms by a homemade Matlab (Mathworks) code (see appendix 1.3.1) as shown in Fig. 4.13a. The first peak at about 30 s shows the eluted band of CFL, followed by FL, FITC 1, FITC 2 and EY. The electropherograms were realigned according to the peaks from CFL by using a Matlab code (appendix 1.3.2). The representative electropherograms (Fig. 4.13b) and pseudo-gel plot (Fig. 4.13c) were drawn. Briefly, the data from electropherograms was transported to Matlab, and a pseudo-gel plot was drawn as a colour map for 30 channels. Differences in electrophoretic velocities of fluorescent molecules were observed from different lanes of the separation chip. The possible reasons can be attributed to the current and/or voltage variation due to the gel properties such as air bubbles, gel pore size homogeneity or different electrode contact between the reservoirs and the gel. This difference in velocity resulted in variable retention times which was normalised by considering the retention times of first (CFL) and last (EY) peaks (appendix 1.3.2). Moreover, slight differences in light intensity were also observed due to the uneven light source on the corners. These differences were normalised by the intensity of the first peak (CFL) (appendix 1.3.2).

To obtain larger imaging area, a 2.5X objective was used which was only able to detect 15 channels (attached to BXFM, Olympus microscope). Therefore, the separation chip was moved on the microscopic stage to obtain 2 images for each run, and these images were combined to show the separation in 30 channels (the shaded blocks on the pseudo-gel plot and electropherograms were added just to distinguish them from the left 15 lanes because the chip was designed to be symmetric).

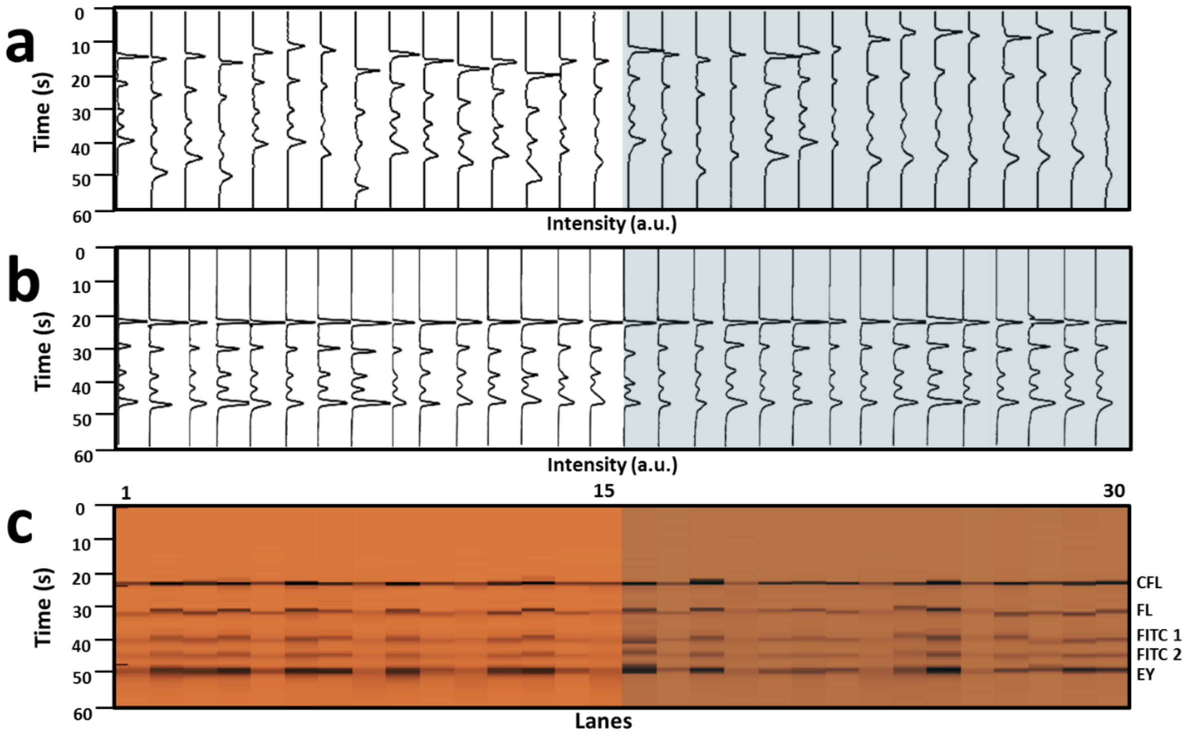

Figure 4.13 Separation of fluorescent dyes in PEO gel a) Unprocessed electropherograms of sample mixture (Eosin Y, FITC 1, FITC 2, Fluorescein, 5-Carboxyfluorescein), b) Normalised electropherograms, b) Pseudo gel, Field strength: 90 V/cm, detection point: 3.5 cm, Separation medium: 1.5% peo gel. The shaded blocks on the pseudo-gel plot and electropherograms distinguish right 15 channels from the left 15.

The theoretical plates were calculated to be 7560/s at a distance of 3.5 cm by Eq. 6 (Chapter 3), which is in good comparison with previously reported values in droplet-interfaced microfluidic separations [32]. However, this value is one magnitude less than in the glass chip-based separations previously achieved [190]. This lower number of theoretical plates can be attributed to three main factors. First, there was molecular diffusion at the injection point and in the separation channels. The diffusion was more evident for small fluorescent molecules than larger biomolecules (as shown in the later DNA separation with higher plate numbers); second, separation conditions such as buffer/gel concentrations, surface coating, and electric field strength have not been optimised in this study and third, droplet volume (800 pL) used here was larger as compared to 10 ms injection time in the cross-piece injections [177].

4.3.4.2 FITC, FL and CFL Separation in Agarose Gel

FITC, FL and CFL at concentrations of 100, 50, and 9 µM respectively were also used to calibrate the separation in precast agarose gel (2% agarose). The distinct bands were detected from the injection point to the distance of 6 mm. The representative pseudo-gel plot and electropherograms were drawn in Fig. 4.14a-b. The fluorescent images of the separated bands in the gel medium are also shown in Fig. 4.14c. Fig. 4.14b-c shows the electropherograms and pseudo-gel plot. The experimental velocities of CFL, FL, and FITC were calculated to be 0.0052, 0.0035, and 0.0022 cm/s respectively (overall %RSD > 5%) using Eq. 3 (Chapter 3). These velocities were found to be lower than in PEO gel which can be attributed to the slightly low voltage applied to the agarose gel, and the movement of molecules is hindered by pores in the gel. The theoretical plates were calculated to be 1890/s at a distance of 6 mm (Eq. 6, Chapter 3). The peaks were normalized using CFL and FITC peaks as discussed above.

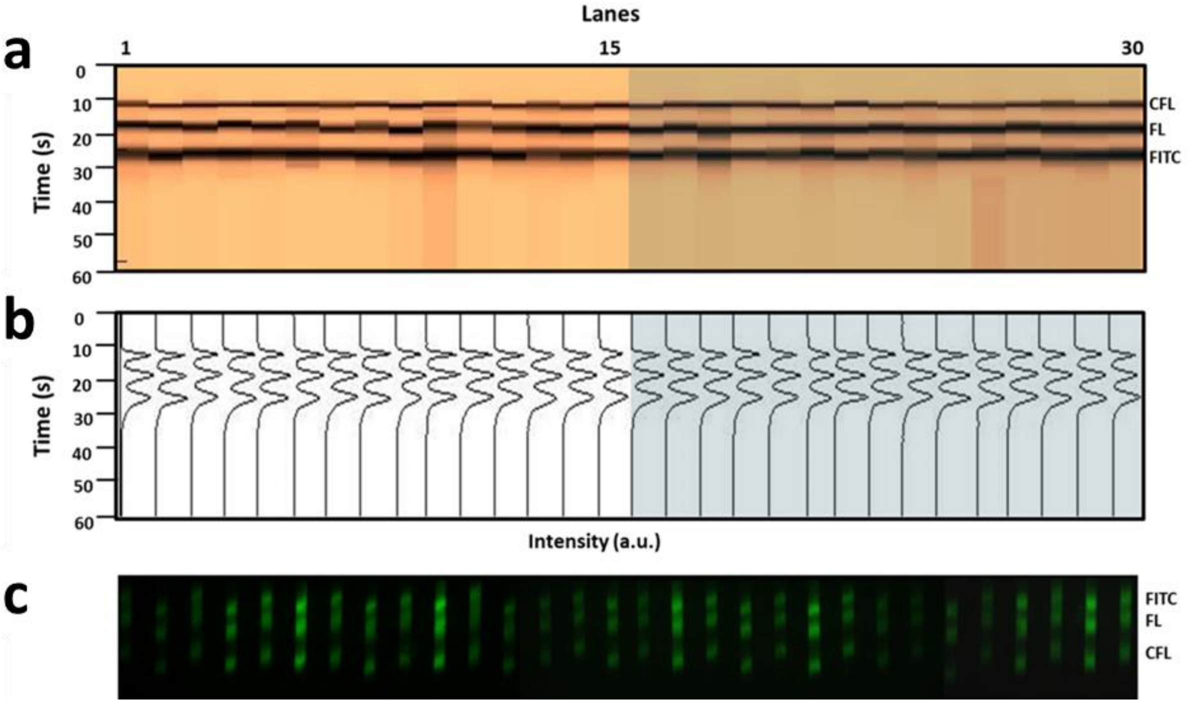

Figure 4.14 Separation of fluorescent dyes (FITC, FL, AND CFL) in agarose a) Pseudo gel plot of the sample mixture, b) Corresponding electropherograms, e) Corresponding separated bands under a microscope. Field strength: 80 V/cm, detection point: 6 mm, Separation medium: 2% agarose gel. The shaded blocks on the pseudo-gel plot and electropherograms distinguish right 15 channels from the left 15.

4.3.5 Droplet Size Calibrations

In this droplet-interfaced MCE device, sample molecules in the whole droplets are electrokinetically injected into the separation channels. Therefore, the droplet volume and positioning of droplets on the channels could affect the separation efficiency. To study these effects, droplet wells were fabricated with different volumes (320, 800, 1280, 1750 picolitres) by changing the depth of the wells on the same droplet plate, and tested the separation efficiency of droplets produced from these wells (Fig. 4.15a). These droplets contained the same sample mixture (fluorescein and FITC). Fig. 4.15b shows the moment when the droplets were in contact with the separation channels (and merged), with Fig. 4.15c showing a snapshot of separated peaks in the channels at about 8 mm from the injection. The corresponding electropherogram was obtained at 8 mm, shown in Fig. 4.5d. Separation resolution was calculated by Eq. 5 (Chapter 3) and plotted in Fig. 4.15e for different droplet volumes. It was found that the sample resolution increases linearly with decreasing sample volume. From Fig. 4.15d, it can be seen that baseline separation was not achieved. These results all infer that bigger droplets will introduce initial elongated injections. The bands were highly resolved for the smallest droplet volume as shown in Fig. 4.15e. However, there are slight deviations from a linear fit which can be due to the differences in droplet size, variations in electric field strength in different channels and wettability of the channels which affects aqueous droplet merging. The theoretical plates achieved by this separation are 2220/s (corresponding to the smallest droplet) to 1480/s (the largest droplet) at a distance of 8 mm.

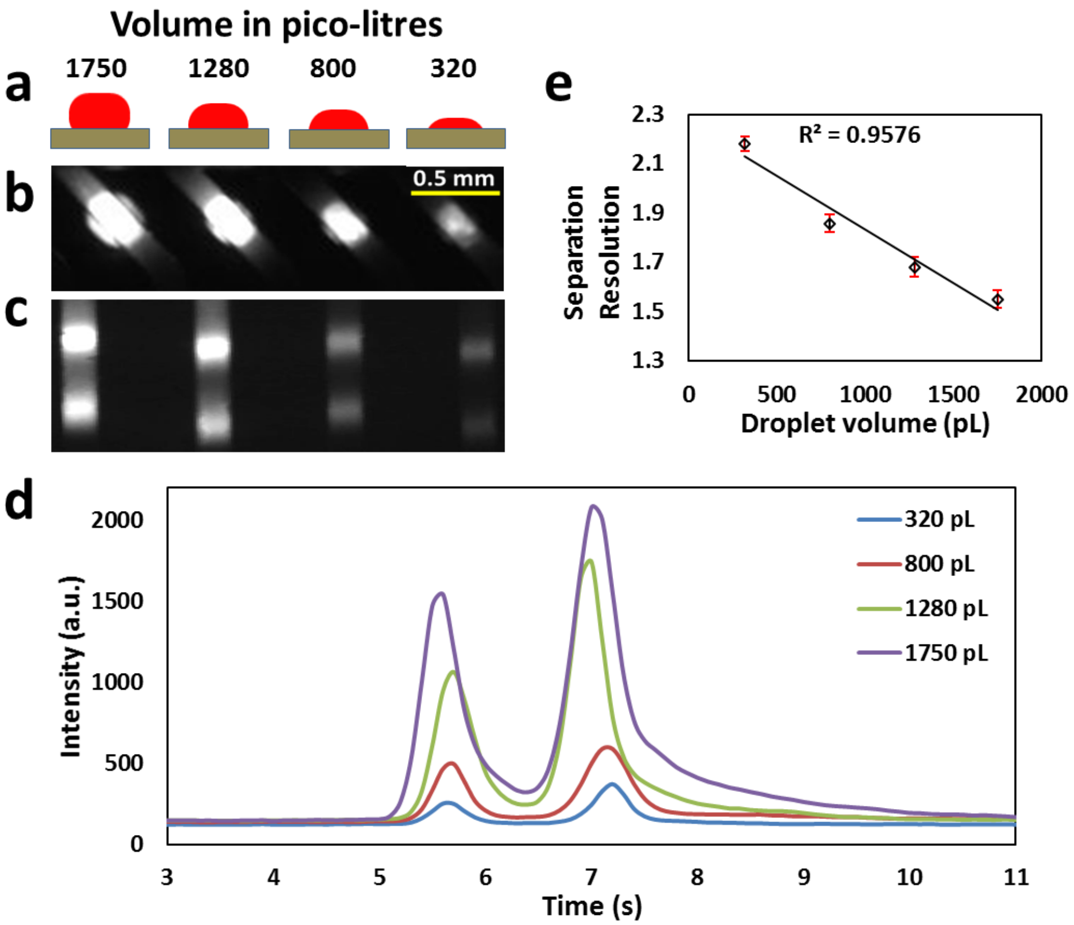

Figure 4.15 Droplet size calibration a) Schematic of droplet wells with different depths, b) Droplets after merging with the separation gel, c) Separation of FITC and Fluorescein in given droplet volumes, d) Representative peaks, e) Separation resolution vs. droplet volume. Field strength: 80 V/cm, detection point: 8 mm, Separation medium: 2% agarose.

This longer injection length can be explained by the non-uniform electric field distribution at the start of the electrophoresis. Fig. 4.16a illustrates a COMSOL simulations of the electric field distribution for different droplet height (and volume). The simulation is based on a simple model that assumes the electrical conductivity is same for the sample droplet and separation medium. The separation channel height is 200 µm and droplet well depths are variable (100, 200, 300 µm). It can be clearly seen that the electric field close to the top of the droplet (merged) is the weakest. Therefore, the higher the droplet, it takes longer time for the electric field to move out all of the sample molecules from the droplet, thereby the initial band of injection is longer for a higher droplet.

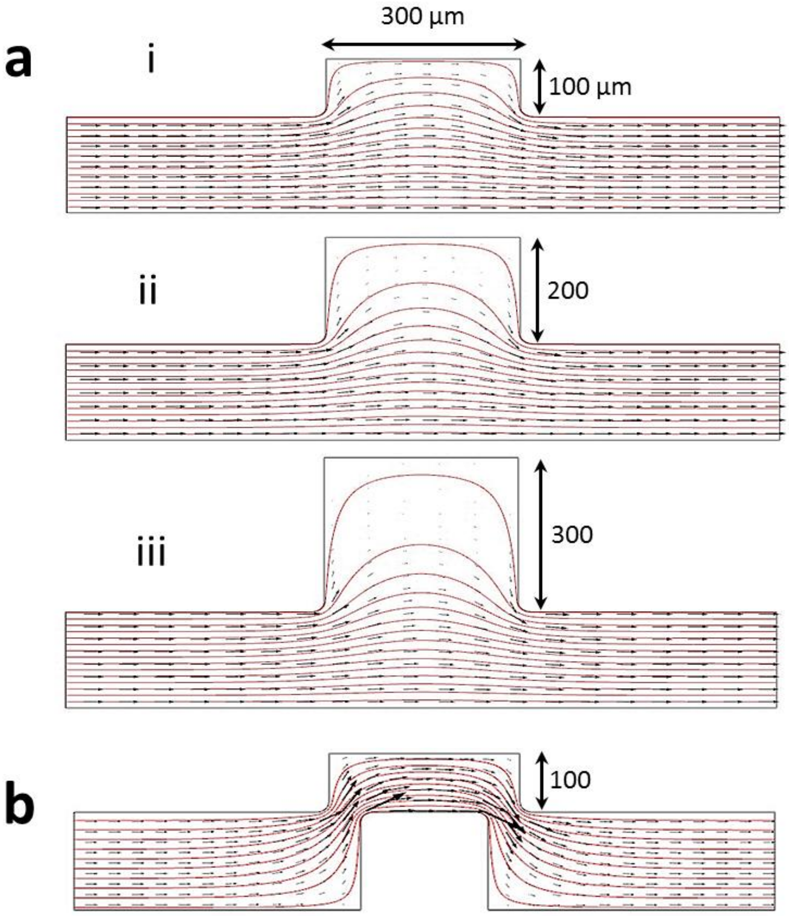

Figure 4.16 Vector plot of the current density a) Droplet wells with different heights, b) Separation channel with breakage. The black arrows and red lines show the directions and streamlines, respectively. The channel dimensions have units in µm.

Such a band broadening suggests if the non-uniformly electric field distribution is removed, the separation efficiency could be improved, for example, a discontinuous separation channel shown in Fig. 4.16b could be adapted to provide a more uniform electric field distribution. However, this breakage adds extra challenges to both chip fabrication and chip alignment, not practical for the current device that is targeting for a portable device. Additionally, the confocal 3D imaging of the droplet merged with the separation channel (Fig. 4.12b, obtained by a Zeiss confocal microscope (Inverted Zeiss LSM 510)) shows that the sample droplet volume was reduced by more than 50% within 10 seconds of initial merging, due to the spreading of the aqueous buffer on the separation medium in the separation channel. This lowered down the average height of the droplet and reduced non-uniformity of the electric field. This droplet size calibration studies stress the importance of droplet size uniformity in the system which can affect the separation efficiency of the system. The variability in droplet sizes has been minimised effectively by precise and accurately sized micromilling of droplet wells and the treatment of plates with a hydrophobic material to stop leakage from the well.

4.3.6 Quantitative Sample Analyses

This method of droplet interfaced separation allows a whole sample injection from the droplets to the separation channels without any sample waste. Therefore, quantitative analysis of analytes within the sample mixture can be achieved. For each sample mixture, the chip produces multiple sample droplets (3 in this setup). The separation results can be compared to provide a standard calibration curve that is generally required in a biochemical analysis. Since these sample repeats are analysed in parallel, no extra separation time is needed in our system.

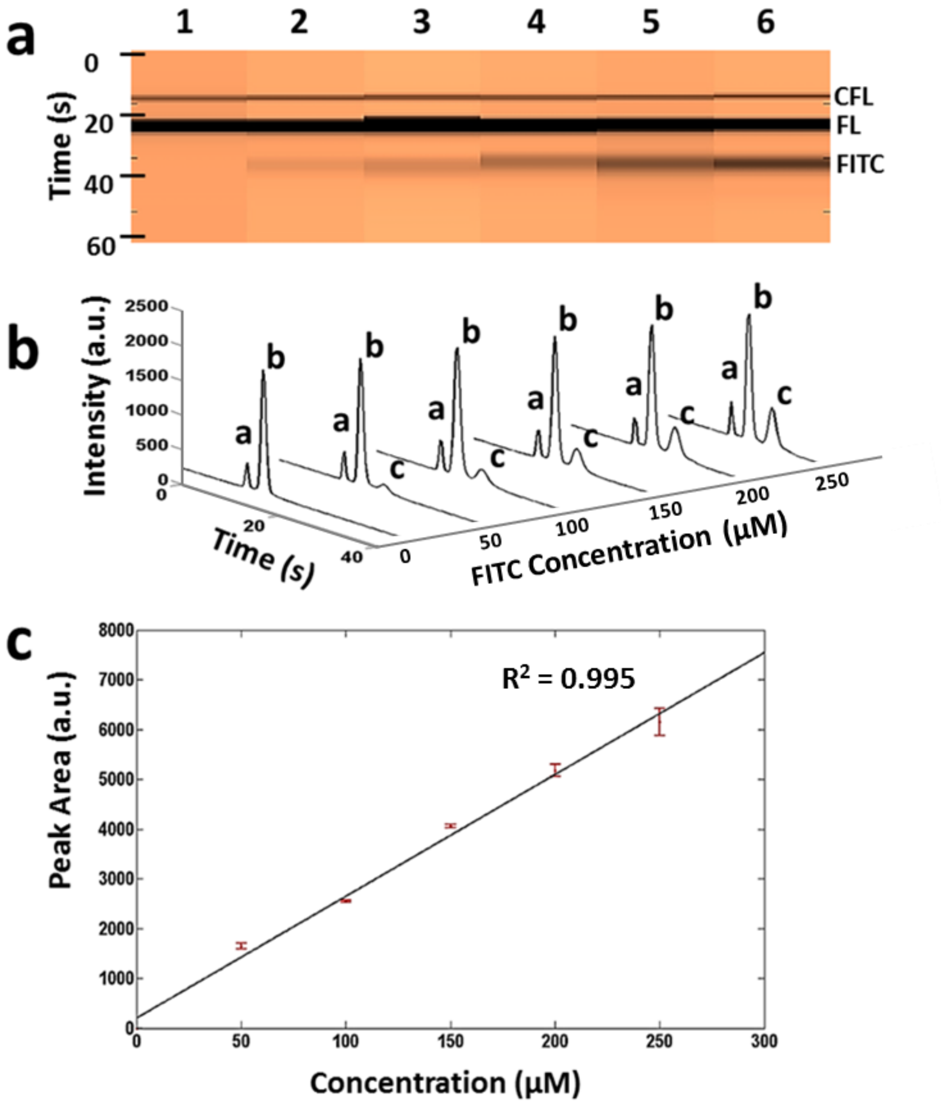

Figure 4.17 Quantitative analysis. a) Pseudo gel plot, b) Electropherograms, c) Standard curve for peak area vs. concentrations of fitc. FITC concentrations from left to right are 0, 50, 100, 150, 200, 250 µM. Field strength: 80 V/cm, detection point: 8 mm, Separation medium: 2% agarose gel.

To validate, mixtures of samples were prepared by fixing the concentrations of 5-carboxyluorescein (9 µM), fluorescein (50 µM) and varying FITC concentration from 0 to 50, 100, 150, 200 and 250 µM. Each sample was injected into one sample channel to produce 3 droplet copies and being separated in corresponding channels. The pseudogel plot and electropherograms were plotted in Fig. 4.17a. In Fig. 4.17b, peaks ‘a’ and ‘b’ represent 5-carboxyfluorescein and fluorescein respectively in fixed concentrations while peak ‘c’ is FITC with varying concentrations. A homemade Matlab code (Appendix 1.3.3) was used to extract the peak areas, and these areas were further normalised using the peak area of 5-carboxyfluorescein as an internal standard. The change of peak areas was found in linear correspondence (3.6% RSD) with the original sample concentrations illustrated in Fig. 4.17c.

4.3.7 High Throughput Separations of DNA Fragments

DNA sizing and protein separations are important applications of gel electrophoresis in biochemistry, forensics, and immunoassays. As a proof of principle, separations of DNA step ladder were performed in this novel platform. DNA step ladder was separated in 2.5% PEO gel (500 kDa) to assess the performance of the Gelchip. Different concentrations of PEO gel or other hydrophilic polymers can be used to separate DNA fragments with different molecular weights. According to Fiona *et al*. [8], the separation in PEO gel depends on pore size and electrophoretic mobility of the molecules. The authors separated nucleic acid fragments of 25 bp dsDNA ladders with UV detection and compared separation using low molecular weight polyethylene oxide (PEO), methyl cellulose, linear polyacrylamide and hydroxyl (poly) methylcellulose. Separation achieved in PEO gel was well resolved as compared to the other matrices.

BioVentures Mapmaker FAM labelled DNA ladder (50, 100, 150, 200, 300, 400, 500, and 600 bp) was prepared as per company instructions. Briefly, DNA samples were prepared by mixing standard Mapmarker ladder with formamide at equal volumes and diluted with 1x TBE to achieve 10x diluted standard sample. The sample mixture was pre-denatured at 95^{o} C for 2 min and snap-cooled on ice prior to loading to the sample channels. Eight DNA fragments were separated and detected at a 13 mm distance from the point of injection within 120 seconds, as shown in Fig. 4.18.

The number of theoretical plates at a distance of 13 mm was calculated to be 79800/s, which is one magnitude higher than previously achieved theoretical plates [32]. This is attributed to the presence of greater sample diffusion in the peo gel because the sample droplet is injected vertically to the channel while the electric field was switched on before injection. These theoretical plates can be further increased by decreasing the sample volume from 5 nanolitres to sub-nanolitre. Noted to obtain high-resolution images, the 10X objective was used which can only detect 3-4 channels each time, therefore, the separation chip was moved on a microscopic stage to obtain 8 images for each run, and these images were combined to show the separation in 30 channels. A high sensitivity scanning detector is currently under development in our lab targeting on a self-sustained portable device for the point-of-care application.

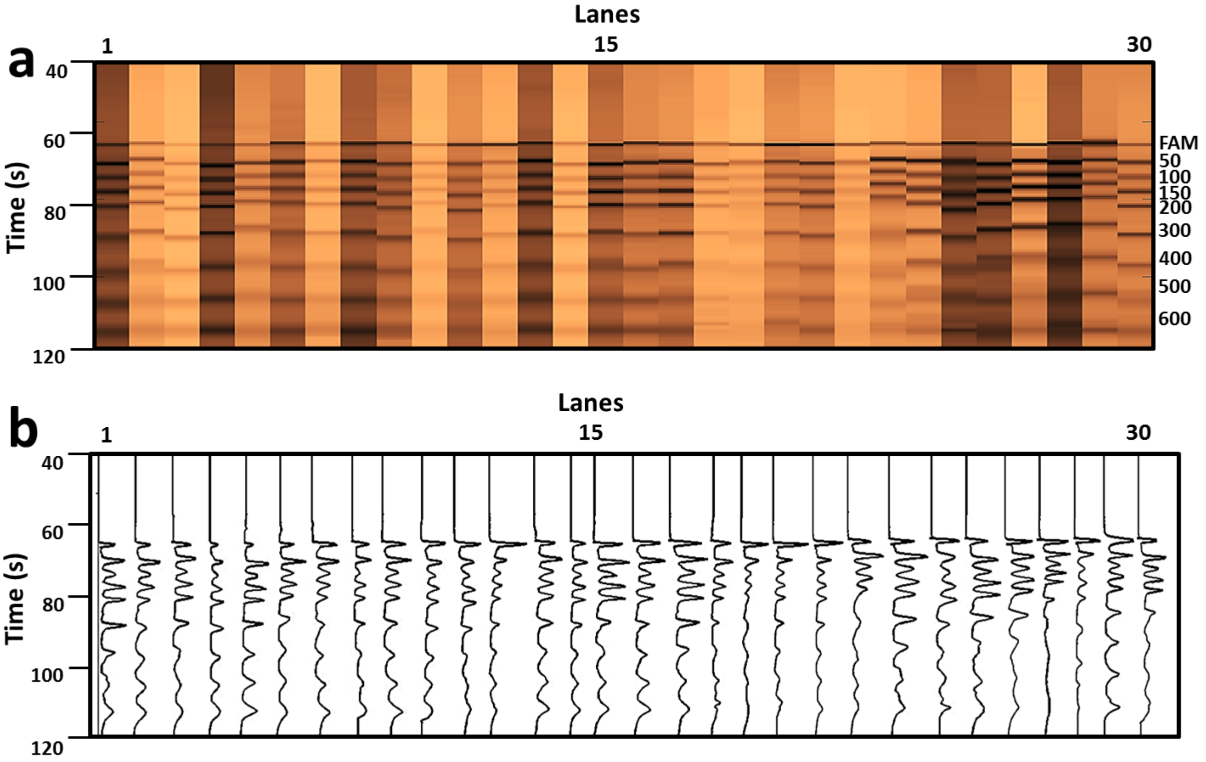

Figure 4.18 DNA ladder Separation a) Pseudo gel plot of DNA fragments. b) Electropherograms. Field strength: 100 V/cm, detection point: 1.3 cm, Separation medium: 2.5% PEO. Separation of 50, 100, 150, 200, 300, 400, 500, and 600 bp DNA ladder (BioVentures Mapmarker FAM labelled), a) Pseudo gel plot of DNA fragments. b) Electropherograms. Field strength: 100 V/cm, detection point: 1.3 cm, Separation medium: 2.5% PEO.

The first peak in the electropherogram belongs to FAM when separated in PEO gel. The short gap between the FAM and DNA fragments could be a result that the dye is weakly charged as compared to DNA fragments at a pH of 8.4. As evidenced by experiments, the dye moves much faster at lower concentrations of PEO gel. However, the movement is slower at 2.5% PEO gel. The platform can also be applied to other DNA or RNA studies including PCR, forensics, RNA electrophoretic mobility shift assays, etc.

The parameters optimised for DNA separation include PEO concentration, detection distance, applied voltage and droplet volume. Detection distance of 1.3 cm was found to be optimum for detecting all fragments. PEO concentration was optimised to be 2.5 % as the lower concentrations provided fewer and unresolved bands. The separation started at 6 mm, however, the DNA fragments were not resolved completely until 1.3 cm. Applied voltage of 100V/cm was found to be optimum. Higher voltages provided faster separations, but the bands were more diffused, and smearing of DNA fragments along separation channels occurred. The volume of the sample injection into separation channel was optimised to be 5 nanolitres. This high droplet volume was used due to the limit of detection of the microscope (BXFM, Olympus) as each band was almost 0.6 nanolitre the droplet volume can be reduced by using sensitive fluorescent systems in the future.

Table 4.1 Electrophoretic velocities and electrophoretic mobilities of DNA ladder calculated on the basis of experimental conditions.

DNA Fragment (bp)	Velocity (cm/s) %RSD<10%	Electrophoretic Mobility ($cm^2/V.s$) %RSD<10%
50	0.0194	0.000194
100	0.0183	0.000183
150	0.0173	0.000173
200	0.0160	0.000160
300	0.0147	0.000148
400	0.0132	0.000133
500	0.012	0.000121
600	0.0111	0.000111

As previously discussed (Chapter 3), the surface of the PMMA chips requires a coating to stabilize the EOF and sample loss on the channels walls. In our design, the chips were coated with Duxback, which helped reduce the sample sticking on the channels and PEO was filled in the channels which stabilised the EOF. In these experiments, no backflow was observed, however, smearing of DNA bands was observed which can be attributed to the PEO gel concentration (higher concentration of PEO gel can further narrow bands but in the current setup, only 2.5% was able to fill in the channels).

Fig. 4.18 shows differences in intensity from similar bands but in different lane. This is due to the limitation of the detection setup; only 3 channels were detected each time and this, in turn, added some differences in light intensity values. Moreover, slight leakage before droplets injection into separation channels can also add some variability. The bands were normalised according to the method discussed previously. Degassing of PEO gel was found to be crucial as the bubbles in the gel slowed down the movement of the bands in the channels. This is likely due to the decrease in electric field strength in separation channels and hence introduces variability in retention times of the bands.

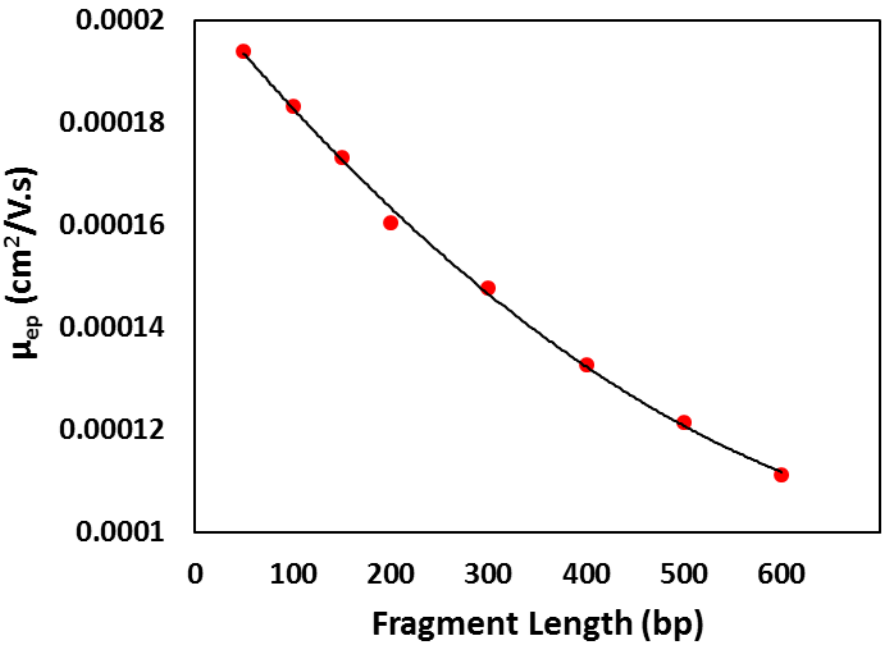

Figure 4.19 Plot of the electrophoretic mobility versus size of the DNA fragment. Field strength: 100 V/cm, detection point: 1.3 cm, Separation medium: 2.5% PEO. Separation of 50, 100, 150, 200, 300, 400, 500, and 600 bp DNA ladder (BioVentures Mapmarker FAM labelled).

The electrophoretic velocities and electrophoretic mobilities of 50, 100, 150, 200, 300, 400, 500, and 600 bp are shown in Table 4.1 calculated by Eq. 3-4 (Chapter 3). The electrophoretic mobilities were plotted against the size of the DNA fragments as shown in Fig 4.19. These electrophoretic mobilities are in good comparison with the previously reported values [8], [191].

4.4 Conclusions

A novel droplet-based high throughput MCE device has been developed in the current study for quantitative and high-throughput electrophoretic separations. The prototype device has been calibrated for the electrophoretic separations of fluorescent molecules, DNA fragments and protein mixtures. The key advantages of the invention lie in its ability to handle and analyse truly small sample volume down to nanolitre, to provide quantitative analysis and in high-throughput. The device has the potential to analyse hundreds of samples in a single run and provide results within minutes. The simplicity, robustness and user-friendly operational procedures of the MCE device can further lead this to be used for POC and clinical diagnostics.

Chapter 5 Optical Flow Cell for Continuous Measurement of Enzyme Kinetics in Droplet Flow

The first part of the Chapter describes absorbance based colorimetric assays and enlists enzymatic reactions. The second part describes the design, fabrication and working principle of the multi-detector flow cell. The third part of the Chapter describes the characterisation of the multi-detector flow cell using food dyes and glucose enzymatic reaction. It also monitors the continuous change in glucose concentration in vitro.

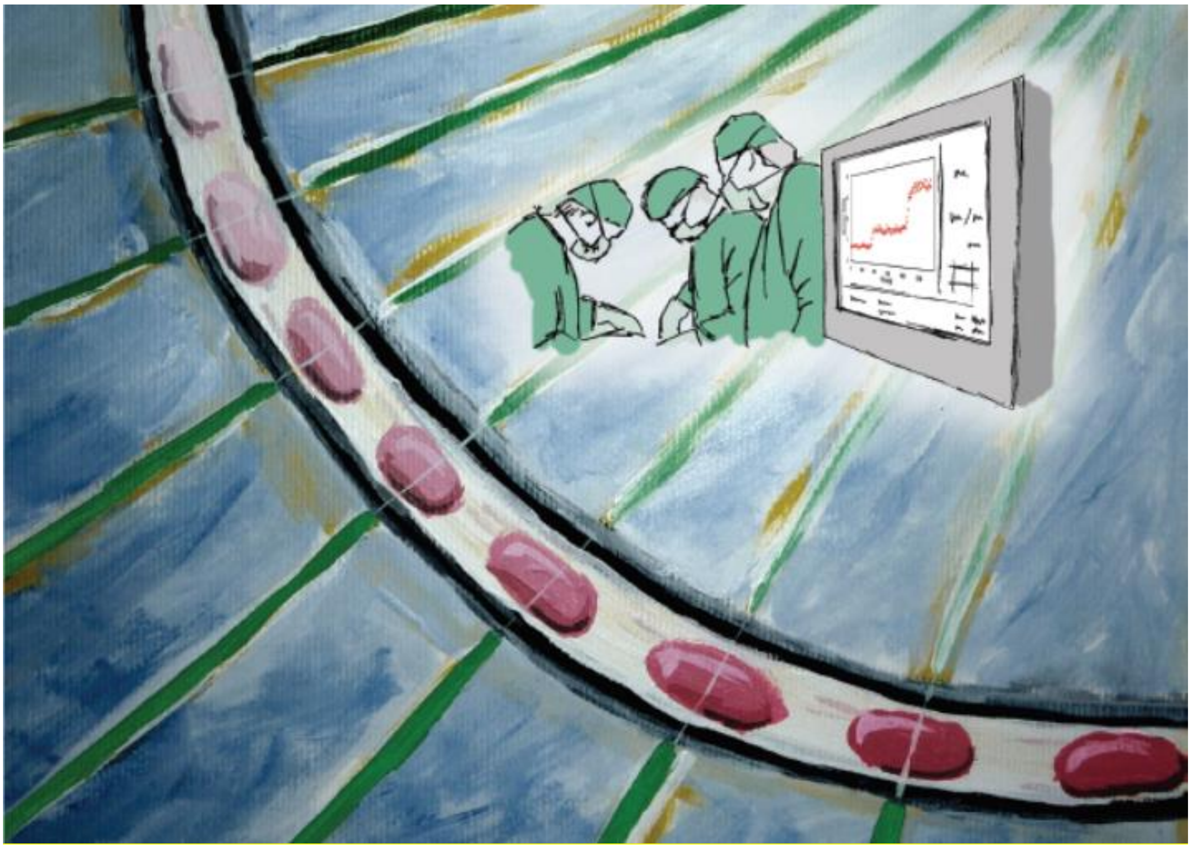

5.1 Introduction

With the development in recent years, microfluidics has shown the potentials of providing practical miniaturization by miniaturizing chemical and biological assays into mini reactors with channels of tens to hundreds of microns and with the advantage of reduced amounts of samples and reagents, cost effectiveness, improved robustness and sensitivity [35]. Colorimetric and fluorescent assays are essential techniques for wet chemical based assays in laboratories; thus the miniaturisation of these assays and detections holds particular importance for developing POC devices to take advantages of the vast amount of well-calibrated assay kits already available. Absorption spectroscopy relies on the well-known Beer-Lambert law to quantify analytes of interest by measuring absorption as shown in Eq. 8.

$$A = -log_{10}\left(\frac{I}{I_o}\right) = \varepsilon cl \qquad (8)$$

where A is the absorbance, I is the transmitted light intensity, I_o is the blank light intensity, ε is the molar absorption coefficient, c is the concentration, and l is the optical path length. Spectrophotometers typically use 1 cm path length cuvettes and offer higher sensitivity but require large amount of samples (0.5-1mL) while microfluidic devices require less sample quantities (nanolitres-microliters). However, microfluidic devices use channels with smaller path length which can hamper the sensitivity of detections. Unsurprisingly, analytes with high physiological concentrations are among the first to be measured with absorbance spectrophotometry in miniaturised systems. Srinivasan *et al*. [192] used microfluidic system to measure absorbance of glucose molecules in nanolitre samples, with 475 µm optical path length and achieved sensitive detection of glucose in range of 0.5-25 mM. Similarly, Wu *et al*. [193] used 250 µm optical path length to measure lactate levels in microfluidic channels and achieved 0.5 mM LOD. Nevertheless, the sensitivities of these microfluidic systems have been lower as compared to standard spectrophotometric measurements which are normally in the range of micromolars.

Research efforts have been devoted to increasing the optical path length of the microfluidic channels. For instance, Sieben *et al*. [5] developed a device to increase the optical path length of the microfluidic channel by collecting light from the fluid flow direction and achieved 25 mm of path length in microfluidic channels. Recently, Rushworth *et al*. [6] developed a new device with cavity mirrors to enhance the optical path length by 28 times and increased the sensitivity up to 5 times which enabled micromolar measurements of nitrate solutions in 50 µm channels. These continuous microfluidics devices are sensitive but rely on intensive microvalve control to switch between samples and cleaning reagents, require strategies to enhance mixing out of laminar diffusion. Critically, fluidic sample experience dispersion in the channel and signal smearing exists. Taylor dispersion and band-broadening are caused by the parabolic flow profile that limits the throughput of the microfluidic device and hence decreases the temporal resolution of the system. In this chapter, I developed detectors suitable for droplet-based microfluidics to overcome some of the problems related to fluidics as aforementioned.

5.1.1 Colorimetric Assays

Colorimetry, in which an analyte-specific reagent reacts with the target analyte to give a coloured product, offers a promising platform to quantify analytes via absorption spectroscopy. Colorimetry is shown to be highly suitable for accurate quantitative analysis in microfluidics and for many biochemical assays and with multiple assays already developed for many metabolites and other important biomarkers [49]–[52].

Colorimetric assays for quantifying biomolecules are particularly challenging for POC monitoring as the reactions are typically slow, taking up to an hour to go to completion and develop the full colour [194], [195]. This means the typical method of end-point quantification is unsuitable for POC monitoring. One way to circumvent this is to measure the kinetics of the reaction – using the initial rate of colour development as the measure of analyte concentration. Several groups have recently demonstrated enzyme-based colorimetric assays in droplet-based microfluidics. Srinivasan *et al*. [192] developed a droplet-based system to measure the kinetics of glucose in droplets. The optical detection was performed on a plane perpendicular to microfluidic chip consisting of LED and photodiode with a path length of 475 µm. Droplets of glucose and reagents were pipetted onto the electrowetting plate, merged to produce a final volume of 2 µL, mixed for 15s, and the absorbance measurements were taken for the 30s to generate Michaelis-Menten parameters. Similarly, Fradet *et al*. [196] fused droplets of sample and reagent (β-d-glucosidase and 4-nitrophenyl β-d-glucopyranoside), immobilised the resulting droplet and followed the colour development over time using an optical microscope. The authors studied different enzyme concentrations, generated Michaelis-Menten kinetics, and quantified the effect of the inhibitor on enzyme activity. In a recent study, Gielen *et al.* [197] developed a sampler that was able to generate high-resolution concentration gradients of haloalkane dehalogenase DbjA and analysed 150 combinations of enzyme and substrate in less than 5 min.

In contrast Gielen *et al*. [198] chose to monitor the similar enzymatic reaction by oscillating reaction-containing droplets back-and-forth through an absorption flow cell. The authors generated droplets of 4-nitrophenyl glucopyranoside hydrolysis by sweet almond β-glucosidase and passed through the detector consisting of LED and photodiode with a path length of 200 µm. Different concentrations of the substrate were loaded in droplets, merged to initiate the reaction, and the absorbance was measured for each set of concentration by flowing the droplets back and forth in the detector to generate Michaelis-Menten parameters. The above-mentioned methods were able to follow the colour development in detail and obtained accurate reaction rates, however, the throughput is still low. The chief reason for such a low throughput analysis is due to a single detection point to measure the colour development in the droplets, therefore, either stop flow or oscillation flow is needed. This low throughput analysis has yet to match the potentials of high throughput analysis that droplet-based microfluidics can offer, for example, thousands of droplets can be produced per second in a single T-junction [199].

Tissue metabolites such as glucose, lactate, pyruvate, glycerol and glutamate are also quantified via Colorimetric assays [35]. These assays are usually quantified reacting with dyes to produce a coloured product such as conversion of 4-aminoantipyrine and phenol into quinoneimine. Glucose is enzymatically oxidised to gluconolactone by glucose oxidase and produces hydrogen peroxide [200]. Similarly, lactate [201] is also converted into pyruvate by lactate oxidase, and hydrogen peroxide is produced. Other tissue metabolites such as pyruvate, glycerol and glutamate have also been converted into hydrogen peroxide via the reactions shown in Table 5.1. The hydrogen peroxide reacts with phenol (or 4-chlorophenol or N-ethyl-N-(2-hydroxy-3-sulfopropyl)-m-toluidine or 3, 5-Dichloro-2-hydroxybenzenesulphonic acid) and 4-aminoantipyrine in the presence of horsedish peroxidase and forms a coloured product (quinoneimine) as shown in Table 5.1. These reactions are widely used for detection of tissue metabolites from microdialysis (Technical Manual for ISCUSflex Microdialysis Analyzer, Feb 2013). The analyte concentration is directly measured by measuring the absorbance of red-violet colour at a maximum of 545 nm [192].

Table 5.1 Equations showing the conversion of metabolites into a coloured product.

Metabolite	Equation
Glucose	$D - Glucose + O_2 \xrightarrow{Glucose\ Oxidase} D - Gluconolactone + H_2O_2$ $2H_2O_2 + Phenol + 4 - Aminoantipyrine$ $\xrightarrow{Peroxidase} Quinoneimine + 4H_2O$
Lactate	$L - Lactate + O_2 \xrightarrow{Lactate\ Oxidase} Pyruvate + H_2O_2$ $H_2O_2 + 4 - Chlorophenol + 4 - Aminoantipyrine$ $\xrightarrow{Peroxidase} Qunoneimine + 2H_2O + HCl$
Pyruvate	$Pyruvate + O_2 + Inorganic\ Phosphate$ $\xrightarrow{Pyruvate\ Oxidase} Acetylphosphate + CO_2 + H_2O_2$ $H_2O_2 + N - ethyl - N - (2 - hydroxy - 3 - sulfopropyl) - m$ $- toluidine + 4 - Aminoantipyrine$ $\xrightarrow{Peroxidase} Qunoneimine + 4H_2O$
Glycerol	$Glycerol + ATP \xrightarrow{Glycerol\ kinase} Glycerol - 3 - phosphate + ADP$ $Glycerol - 3 - phosphate + O_2$ $\xrightarrow{Glycerol-3-phosphate\ Oxidase} Dihydroxyacetone\ phosphate + H_2O_2$ $H_2O_2 + 3{,}5 - Dichloro - 2 - hydroxybenzenesulphonic\ acid + 4 -$ $Aminoantipyrine \xrightarrow{Peroxidase} Qunoneimine + 2H_2O + HCl$
Glutamate	$Glutamate + O_2 \xrightarrow{Glutamate\ Oxidase} 2 - Oxoglutarate + NH_3 + H_2O_2$ $H_2O_2 + N - ethyl - N - (2 - hydroxy - 3 - sulfopropyl) - m$ $- toluidine + 4 - Aminoantipyrine$ $\xrightarrow{Peroxidase} Qunoneimine + 4H_2O$

5.2 Multidetector Flow Cell

Here is presented a device that allows high-throughput analysis of metabolites and other biomarkers, comprising multiple concatenated measurement points. As a droplet flows through these measurement points, the rate of enzymatic reaction can be fully characterised without stopping the flow. Since there is no cross-talk between the droplets, the device is capable of continuously measuring metabolites in a droplet flow and thus suitable for continuous POC monitoring. This report describes the design and operation of the device and its validation by application to the accurate and continuous quantification of unknown glucose concentrations using an enzymatic assay.

5.2.1 Design and Fabrication of Multi-detector Flow Cell

The miniaturised multidetector flow cell was designed using SolidWorks as shown in Fig. 5.1 and printed in black PLA material using an Ultimaker-2 3D printer. The flow cell is composed of two interlocking 3D-printed structures, a cartridge, and a detection cell. Fig. 5.1b shows the cartridge and detection cell in position for droplet detection. The cartridge holds the tubing in place and is inserted into the detector cell, which houses the main optical components. Once fully assembled, the flow cell measures only 45 x 10 x 15 mm, therefore, it can be easily accommodated within a field-deployable POC device.

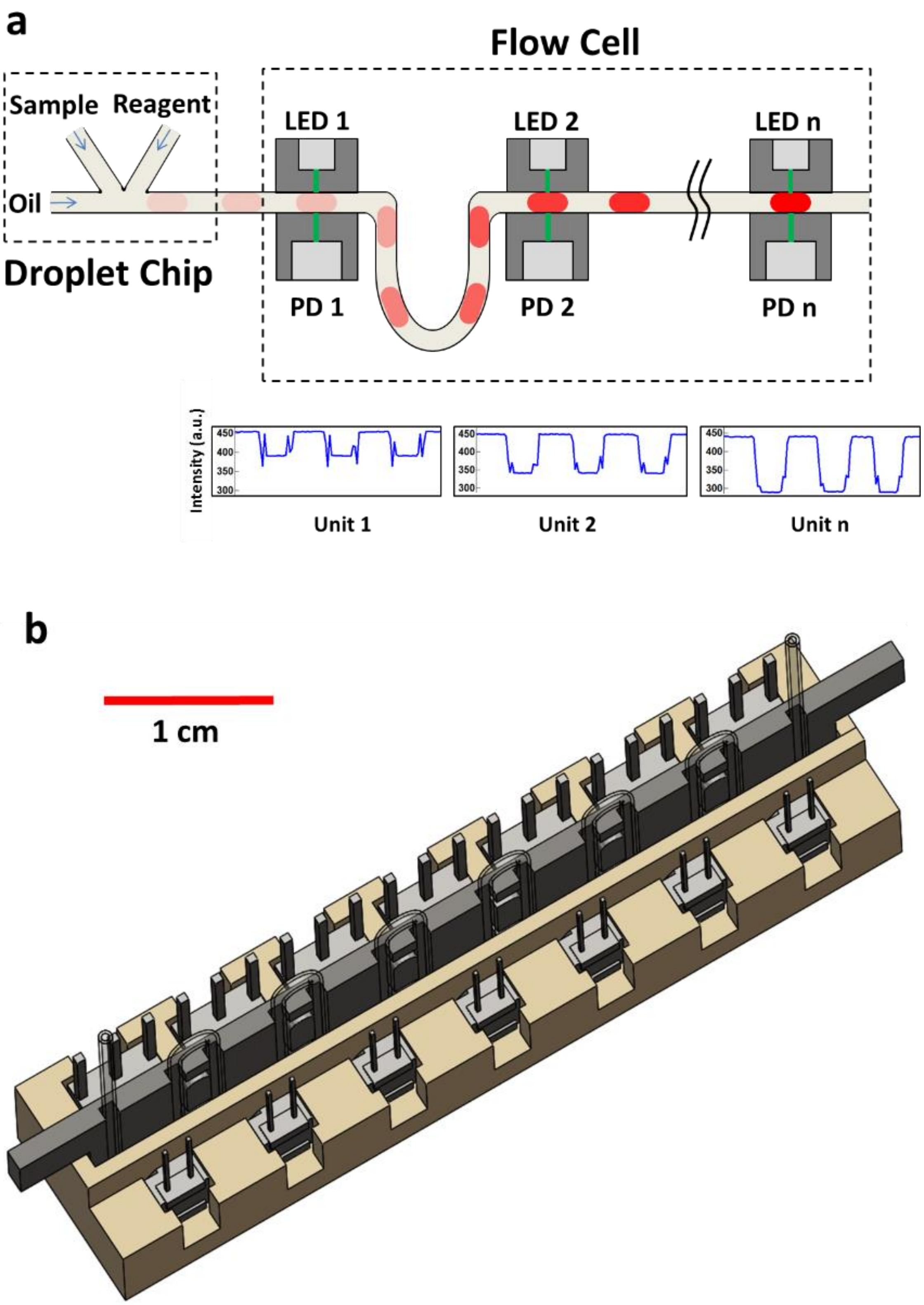

Figure 5.1 Schematic of the multi-detector flow cell a) working principle of the device, illustrating droplet generation and travelling through the flow cell. The bottom part shows an example intensity change during a glucose reaction droplet passes through consecutive detectors in the flow cell, b) Fully assembled flow cell showing cartridge, optical detection cell, LEDs, photodiodes and tubing inserted into the cartridge.

The cartridge is 1 mm thick and has grooves cut into one side such that 0.7 mm OD PTFE tubing can snugly fit into it (Fig. 5.2a). The tubing can be inserted into the groove in numerous different geometries to give different distances (and hence travel time of the droplets) between detectors, as appropriate to the assay time being implemented. The cartridge has 7 horizontal slits (400 µm width) that allow light to pass through the tubing and the cartridge itself, and these horizontal slits are co-located with vertical slits (400 µm width) in the detection cell. The detection cell houses 7 pairs of light emitting diodes (LED, ASMT-QGBE-NFH0E, Avago Technologies) and photodetectors (PD, TSL257, Texas Advance Optical Solutions), each of which corresponds to an individual absorption detection point (Fig. 5.2b). Here, green LEDs (peak wavelength = 516.5 nm) were used to coincide with the main absorption band of the colorimetric product of the glucose assay (peak value 545 nm). It should be noted, however, that the LEDs can be changed, depending on the specific colorimetric assay being implemented. Fig 5.2c-d shows the components after fabrication and wiring.

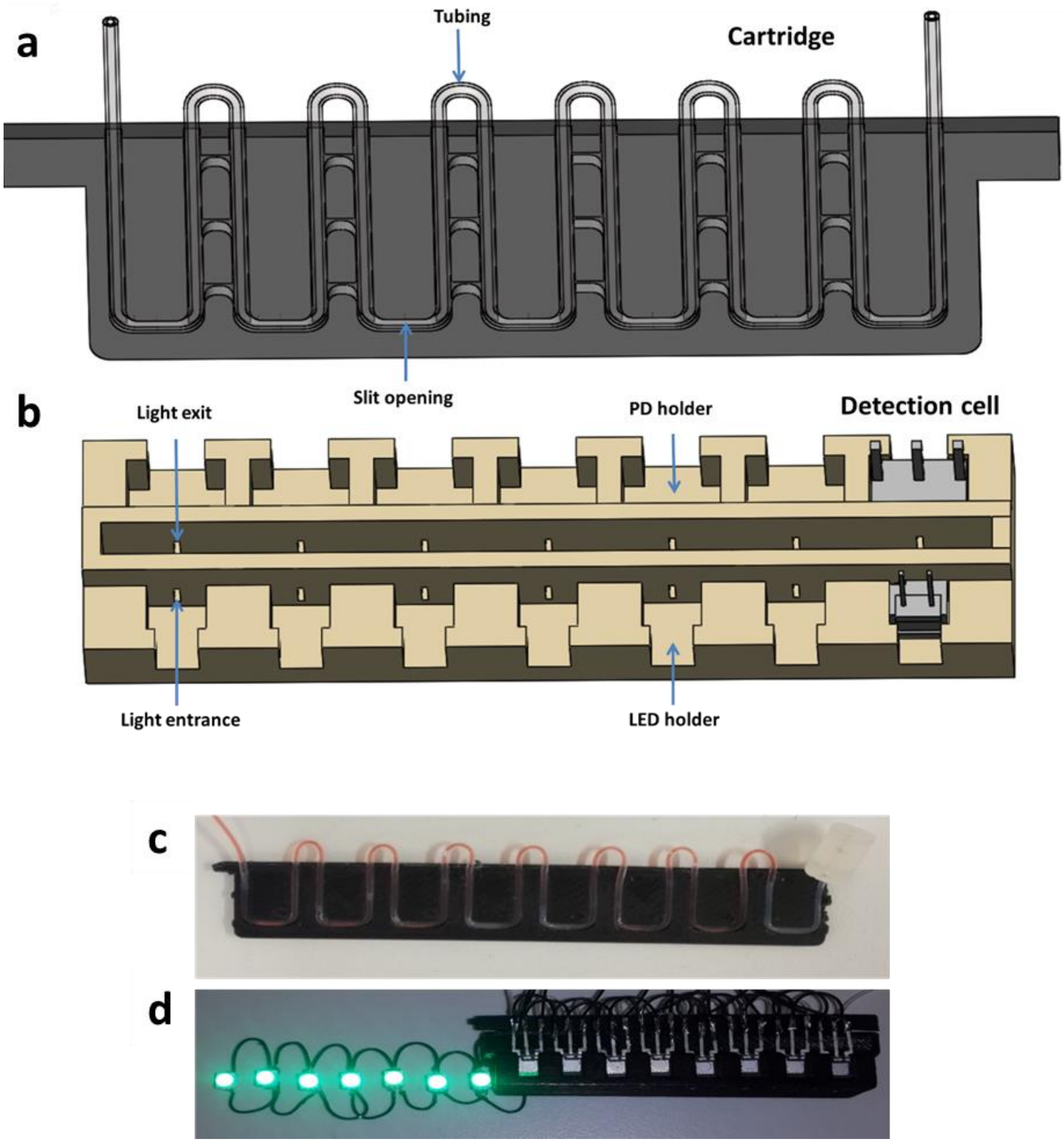

Figure 5.2 Cartridge and optical detection cell a) 3D schematic of the flow cell showing the cartridge which holds the tubing, b) the detection cell which holds the LEDs and photodiodes. Both cartridge and detection cell have slits incorporated such that once the cartridge is inserted into the detection cell, there is a clear light path from LED to photodiode through the tubing, c) 3D printed cartridge with poly(lactic acid) (PLA) and tubing inserted into the grooves, d) 3D printed optical detection cell with LEDs and photodiodes. LEDs are not fixed in the detection cell for illustration purposes.

5.2.1.1 Microchip fabrication and Droplet Generation

The T-junction chip used to generate droplets was fabricated as follows: Firstly, a mould was designed in 3D CAD software (SolidWorks) as shown in Fig. 5.3a. and printed in VeroClear material using an Objet500 Connex3 3D printer (Stanford Marsh Ltd). The microchannels were designed to have dimensions of 200 µm in width and 400 µm in height. These printed channels were used as a mould for Polydimethylsiloxane (PDMS) microchips. The surface of the 3D printed mould was found greasy after printing and did not allow complete baking of the PDMS on the surface which damaged the channels. Therefore, after printing the surface of the mould was cleaned with isopropyl alcohol (IPA), dried and left in an oven overnight at 60 °C. The mould was further washed with IPA, dried, and treated with a non-stick coating Duxback to aid removal of the PDMS chip after casting. The PDMS channel layer was cast using the mould and bonded to another flat piece of PDMS using the standard 'half-cure' technique [202].

Silicone elastomer Base (Sylgard 184, Dow corning) was mixed with the curing agent (Dow corning in a clean petri dish and the ratio was kept at 10:1 (w/w), respectively. The base and curing agent were mixed quickly using a polypropylene pipette tip. The mixture was then added onto the PDMS mould to achieve a required thickness, and the remaining mixture was left in the petri dish for curing the base layer to bond with the PDMS layer with channels. In our experiments, 10 g of the base was mixed with 1g of curing agent of which about 6 g was added to the mould and 4 g was left for a base layer. Degassing was achieved by putting the mould and base layer in the vacuum desiccator for 10 min. It is important to remove air bubbles completely from the PDMS mixture because the bubbles on the surface could make holes and hence can produce leakage.

The mould was then left in the oven for 2 hours at 60 °C, and the base was left in the oven for 40 min. The PDMS layer was removed from the mould with all the channels transferred to the PDMS surface and the holes were punched for liquid inlets and outlet. The punching was achieved with blunt syringe needles sharpened with sandpaper. It is pertinent to note here that the un-sanded needles did not punch the PDMS completely and introduced invisible cracks which started leakage when tubing was installed with microchips. Therefore, care is taken to punch the holes vertically and remove the punched PDMS piece which can cause a blockage if not removed entirely.

The PDMS layer with channels was then bonded to the base layer and left in the oven for 4 hours at 60 °C. Moreover, a clean surface during fabrication was used because the dust can sit on the channels and affect the bonding between the two layers. Finally, the microchip was removed from the oven, flushed with duxback to render the channels hydrophobic and used for droplet generation as shown in Fig. 5.3b. Two inlets were used to inject red and green dyes, and the third inlet was used to pump carrier fluid for droplet generation. The dyes mixed in a ratio of 1:1 and dispersed into regular sized droplets. Polythene tubing was glued on the outlet, and the droplets were transported to the cartridge for detection as shown in Fig. 5.3b. The carrier fluid used was FC-40 fluorinated oil containing a 0.35 % w/w concentration of non-ionic tri-block copolymer surfactant synthesized in-house [26]. Syringe pumps (PHD 2000/Harvard Apparatus) were used to pump all fluids. Following generation, the droplets flowed into a polytetrafluoroethylene (PTFE) tubing (0.4 mm ID, 0.7 mm OD, Adtech Polymer Engineering Ltd.) connected to the flow cell for optical detections.

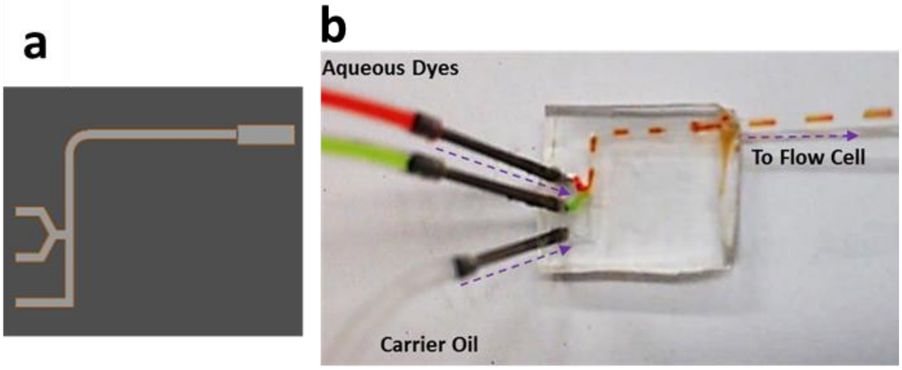

Figure 5.3 Microchip fabrication and droplet generation a) SolidWorks design of T-junction microchip mould, b) Droplet generation using red and green food dyes as aqueous phases and FC-40 oil with 0.35% Raindance surfactant (w/w).

5.2.1.2 Operation of the Flow Cell and Data Processing

The operation of the flow cell is illustrated in Fig 5.1a. Initially, droplets composed of a 1:1 ratio of sample and reagent are generated with the T-junction microfluidic chip. Droplets exit the chip into PTFE tubing which is woven into the flow cell such that the droplets will sequentially pass through each detector in turn. As the colorimetric reaction progresses, the colour of the droplet will deepen, and the absorbance as measured by each detector will increase. The absorbance gives a measure of the concentration of the end-product (Eq. 8). The time for a droplet to travel from the T-junction to the detection point was calculated by dividing the total length of channel and connection tubing with the flow velocity. By measuring the absorbance of a droplet at all of the 7 detectors, the initial rate of reaction can be obtained.

The voltage readout from each photodiode was collected using a microcontroller (Arduino Nano) which relayed the information in real-time to a computer, where the data was recorded using LabVIEW (National Instruments) (Appendix 2.1). Absorption values for the droplets were calculated using a modified version of the Beer-Lambert law (Eq. 9). To allow for small changes in the light intensity of the LED, the equation includes terms for the light transmitted through the carrier fluid. As the composition of the carrier fluid doesn't change, it will give a constant absorption and can thus be used to adjust for any variations in the intensity of incident light between the measurement of the blank and all subsequent measurements.

$$A = -log_{10}\left(\frac{I_{sample\ droplet}}{I_{blank\ droplet}} \times \frac{I_{blank\ oil}}{I_{droplet\ oil}}\right) = \varepsilon cl \qquad (9)$$

Where $I_{sample\ droplet}$ and $I_{blank\ droplet}$ are the photodiode responses corresponding to light transmitted through the sample droplets and blank droplets (introduced at the start of an experiment) respectively; $I_{blank\ oil}$ and $I_{droplet\ oil}$ are the photodiode responses for light transmitted through the carrier fluid adjacent to the blank and sample droplets. Absorbance is equal to εcl where ε is the molar absorption coefficient, c the concentration and l the optical path length.

5.2.2 Experimental Results and Discussion

The single detectors were initially characterised within the flow cell by flowing droplets of red food dye at different concentrations through the flow cell and measuring the response (Powdered red food dye, East End Foods plc. was used in solution for all calibrations). Fig. 5.4a shows droplets in tubing passing through the detector with an LED light on the top and photodiode on the bottom. Flow cell was used to detect droplets inside the tubing as shown in Fig. 5.4b. In this experiment, the droplets of two different concentrations of red food dye (50 and 250 µg/mL) were generated and passed through the flow cell. As each droplet enters the light path, the transmitted light intensity drops from a higher value (corresponding to light passing through the carrier oil) to a lower value. As the droplet exits the light path, the measured intensity returns to its high initial value.

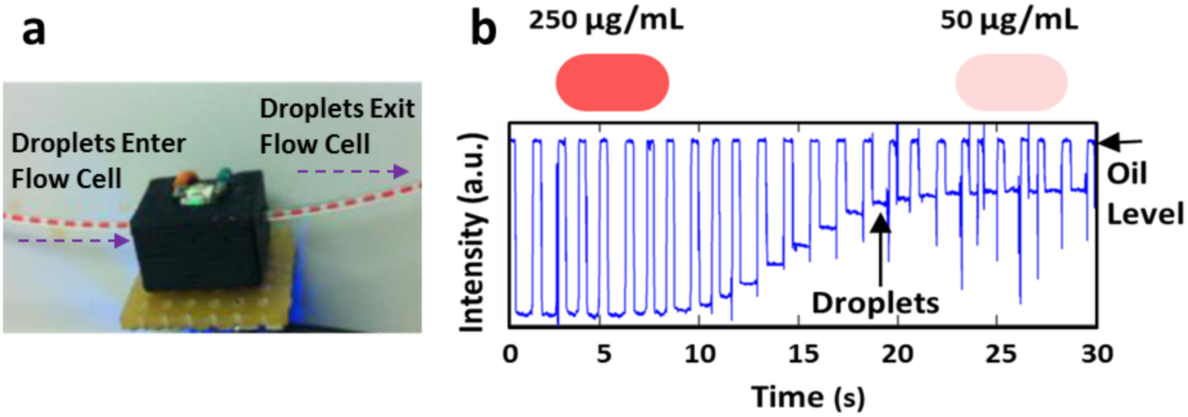

Figure 5.4 Droplet detection in single detector flow cell a) Droplet transportation through the flow cell in a tubing b) Signal collected from the droplet detection in a flow cell for switching concentration from 250 µg/mL to 50 µg/mL. The change in intensity shows the change in absorbance due to the weak colour of the red dye. The fixed signal at the top indicates oil intensity levels and the changing signal at the bottom indicate droplet levels in the flow cell.

Fig. 5.5a shows the light intensity (as a voltage output from the photodiode) obtained for five series of droplets containing different dye concentrations (0.10, 0.25, 0.50, 1.00 and 2.00 mg/mL). The detector shows a high reproducibility for each group of droplets, with %RSD of the light transmitted through the droplets below 0.5%. As the dye concentration in the droplets drops from high to low, the magnitude of the intensity drop also decreases – consistent with the absorbance of less light, as expected. The absorbance of each concentration of droplets was calculated against a set of blank droplets composed of pure water using the modified Beer-Lambert law (Eq. 9). Each concentration was repeated 3 times and the overall %RSD was found to be ~ 2%.

Fig. 5.5b shows the measured absorbance values versus dye concentration. As expected a linear relationship is seen at lower concentrations with deviation from linearity at absorbances > 0.25 [203]. The limit of detection, defined as three times the standard deviation of a series of blank measurements, was found to correspond to an absorbance of 0.01. This value could be further improved by increasing the optical path length by, for example, controlling the channel geometry [50] or implementing cavity mirror enhancement [51]. These measurements confirmed that the absorption flow cell can be used to perform quantitative absorption measurement and has an operational range of absorbance values of 0.01 and 0.25.

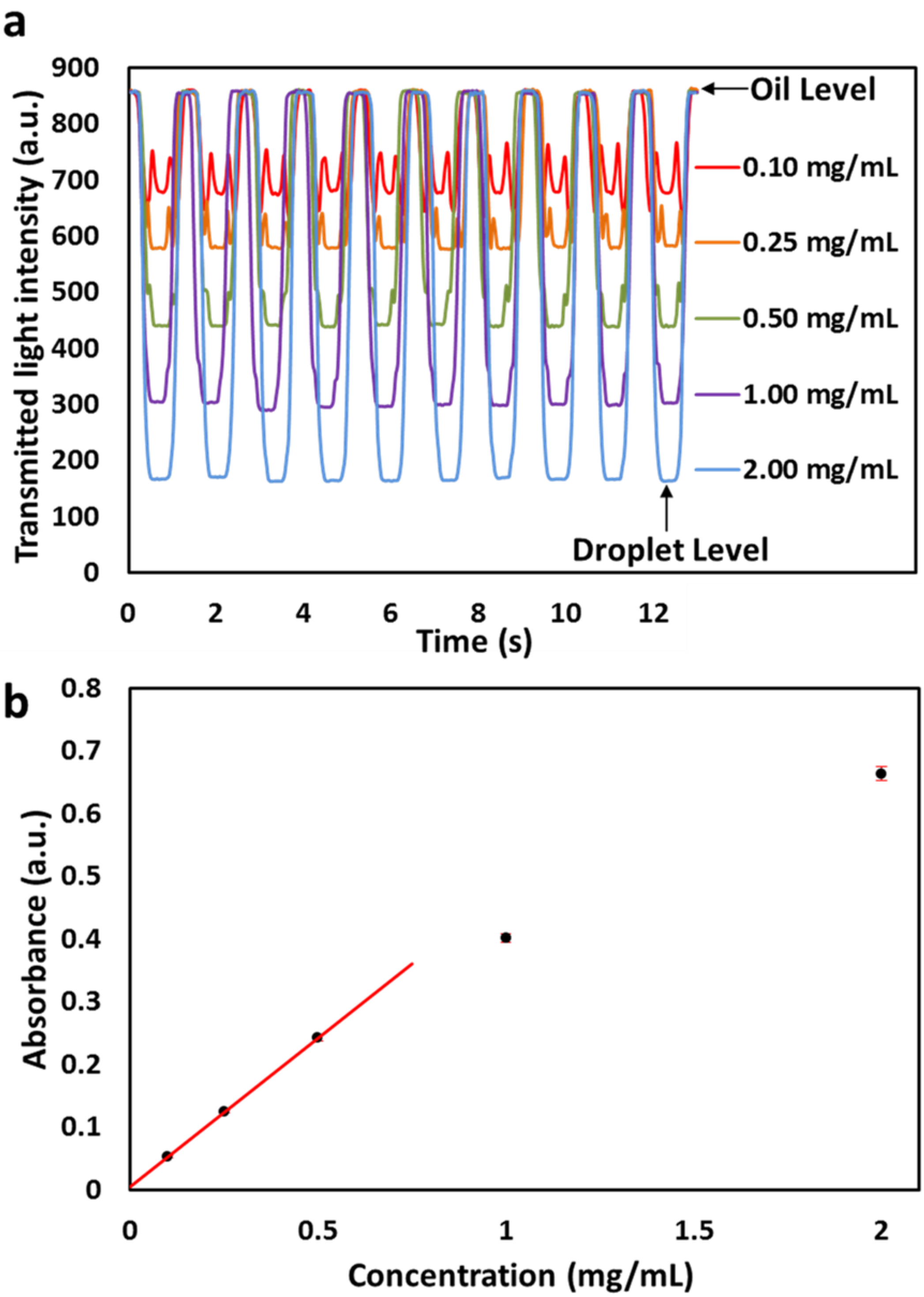

Figure 5.5 Characterisation of a single detector in the flow cell using droplets containing red food dye (a) Transmitted light intensity over time as droplets travel through the light path. Five distinct populations of droplets with different dye concentrations are observed: 0.10, 0.25, 0.50, 1.00, 2.00 mg/mL, (b) Droplet absorbance against dye concentration. A line of best fit ($R^2 = 0.998$) shows the linear response for absorbance values < 0.3.

Following calibration of a single detector, multiple detectors were tested. A first experiment was done by turning on and off a single LED and measuring the readout from the adjacent photodiodes.

The readout showed no noticeable change meaning there is no cross talk between the detectors. Therefore, the black PLA material and the bending of the grooves in the cartridge is effective in preventing light from straying between detection channels. Next, the dye solution entering the droplet generation chip was alternatively swapped between a high concentration (250 µg/mL) and a low concentration (50 µg/mL).

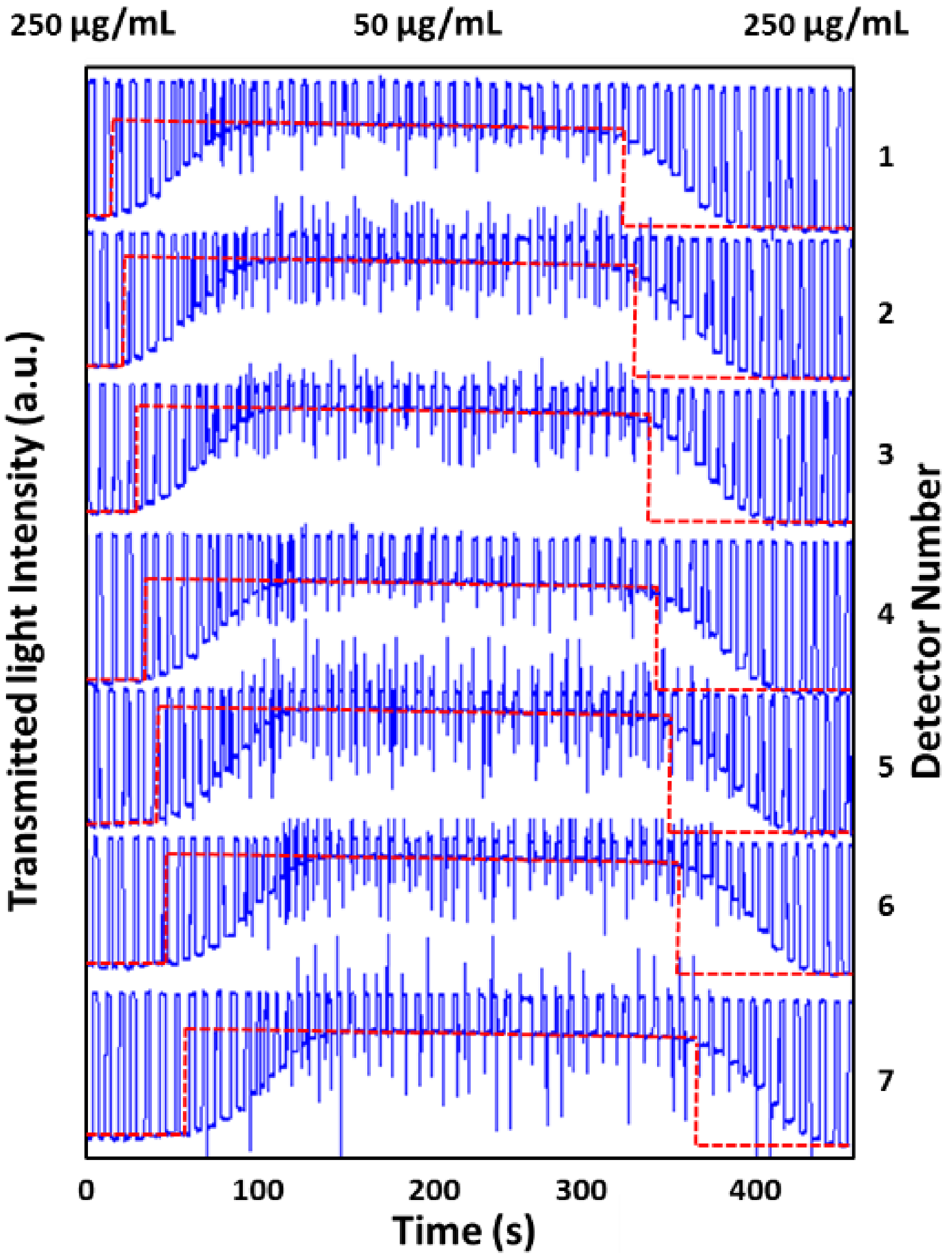

Figure 5.6 Characterisation of the multi-detector flow cell using red food dye. Absorbance from 7 detectors (top to bottom) with changing dye concentration from high (250 µg/mL) to low (50 µg/mL) and to high again. The red dotted lines indicate where the concentration was switched and along the detectors.

Fig. 5.6 shows the measured signals from all 7 detectors. For each detector, the carrier oil gave constant high signals, while the response of the droplets changed with the concentration change. In the experiment, about 14 droplets and a time of 25 s (Temporal resolution) were required to switch from one concentration to the other completely. The red dotted lines in Fig. 5.6 highlight the onset of the transitions. Comparing the signals from these 7 detectors, it can be seen that the start of transition times shift sequentially to the right (later time) following the sequential order of the detectors. This trend is more apparent in Fig. 5.7, which shows the same data normalised such that each point represents the measured average light intensity of a single droplet. This plot also emphasises that the shape of the transitions is identical for each detector and the train of droplets travels between detectors without the cross contamination or Taylor dispersion commonly found in continuous microfluidic sensors [204]. Additionally, it also shows the high-throughput nature of the flow cell, as individual droplets can be identified in each subsequent flow cell detector. Thus each droplet constitutes a single discrete set of measurements.

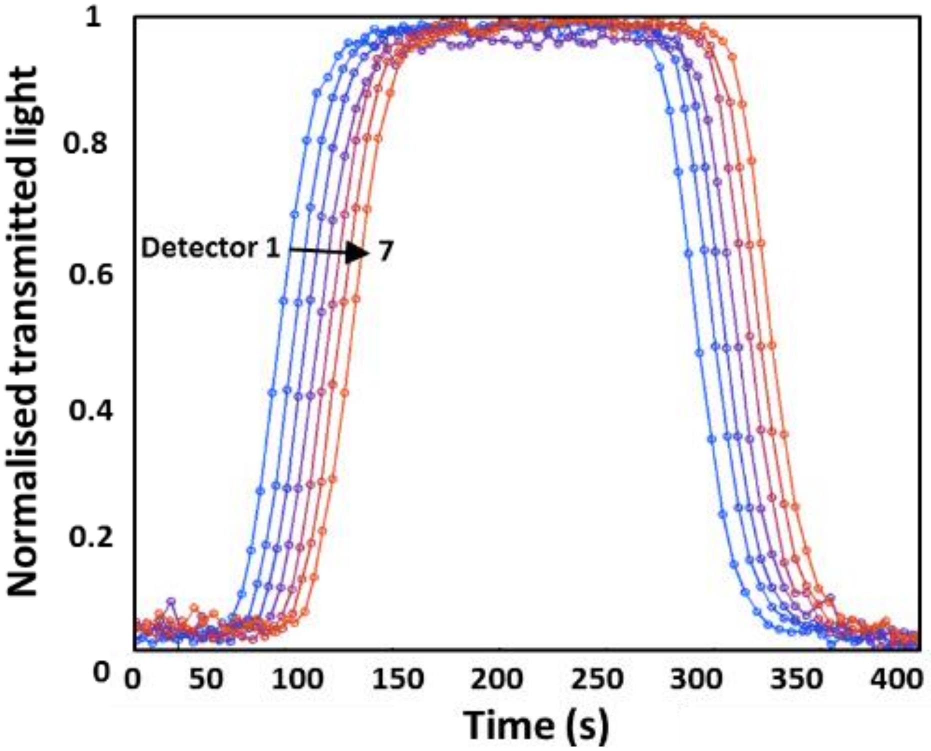

Figure 5.7 Normalised transmitted light plot against time illustrates that the profile of concentration switch is identical at each detector. Each point in the figure represents a single droplet.

5.2.2.1 Glucose enzymatic assay

Having calibrated the flow cell using food dye, a colorimetric assay was implemented to quantify glucose concentrations in sample solutions. Glucose measurement was chosen because it is a widely measured biomarker for a range of medical conditions and procedures including metabolic diseases [35], diabetes [36], TBI [38] and free flap surgery [39]. Glucose can be determined *via* an enzyme-based colorimetric assay based on Trinder's reaction [200] as shown previously in Table 5.1.

Lee *et al*. [205] previously used this method to measure glucose after the reaction has gone to completion. However, the reaction can take up to 30 min [Cayman glucose colorimetric assay kit, Item no 10009582] - too long for real-time or near real-time monitoring applications. Another method is to measure the initial reaction rate, and accurate measurements of analyte concentrations can be obtained within 1 minute [206].

In order to convert the measured reaction rates to a known concentration, the method must first be calibrated using the Michaelis-Menten model [207], [208] which relates the initial rate of reaction (V_0) to the concentration of the substrate (glucose in this case) as shown in Eq. 10.

$$V_0 = \frac{V_{max} \cdot [S]}{[S] + K_m} \qquad (10)$$

Where [S], V_{max} and K_m are the substrate concentration, maximum rate at saturating substrate concentration, and substrate concentration at half the maximum rate ([S] at ½V_{max}). V_{max} and K_m are constants at constant temperature and constant enzyme concentrations, therefore, V_0 increases with substrate concentration [194].

Commercially available reagents were bought and used without further purification. Glucose oxidase, horseradish peroxidase (HRP), 4-aminoantipyrine, phenol and phosphate buffered saline (PBS) were purchased from Sigma-Aldrich (Dorset, U.K). The reagents were prepared in 0.1 M PBS at pH of 7.4. The reagents were mixed such that the final reagent mixture consisted of glucose oxidase (30 U/mL), HRP (30 U/mL), 4-aminoantipyrine (1.54 mM) and phenol (22 mM). This solution of reagents will be referred as reagent mix in later sections. Glucose solutions were prepared by dissolving glucose (Sigma-Aldrich, U.K) in 0.1 M PBS at pH of 7.4. Ultrapure water was used throughout (18.2 MΩ, MilliQ).

For the calibration, droplets composed of a glucose solution and reagents (containing glucose oxidase, HRP, phenol, and 4-aminoantipyrine) mixed at a 1:1 ratio were generated and then flowed through the flow cell. The reagent mix and glucose solutions were injected at the same flow rate, and the flow rate of oil (1.31 µL/min) was tuned to achieve droplets measuring approximately 10 nL. This was repeated using six different known glucose concentrations (0.5, 1.0, 2.5, 5.0, 15 and 25 mM). Blank measurements were taken by using 0 concentration glucose solution and used to calculate the absorbance of the glucose-containing droplets. In the experiment, the droplet flow rate was kept constant, and droplets were measured to pass through the detectors (1-7) at times of 4.94, 8.58, 13.52, 18.46, 23.4, 28.34 and 33.28 s respectively (the time was defined to be 0 at the moment when the droplet was generated at the T-junction.)**.**

Fig. 5.8a shows the absorbance against time for each set of glucose concentrations. For each glucose concentration, the absorbance increased linearly as expected and was fitted with a straight line to obtain the initial reaction rate. It is notable that none of the lines of best fit pass through the origin, indicating that the reaction had started before $t = 0$. This is likely to be due to the reaction having started in the T-junction at the interface where the two aqueous streams met before they had been partitioned into droplets. Nonetheless, the shift of origin time does not affect the measurement of reaction rate which is the slope of the line. The obtained reaction rates were then plotted against the glucose concentration and fitted with a Michaelis-Menten curve using nonlinear regression, (see Fig. 5.8b and Appendix 2.2.2). The curve fits the data exceptionally well ($R^2 \approx 0.999$) with V_{max}= 0.0062 a.u./s and K_m= 11.52 mM.

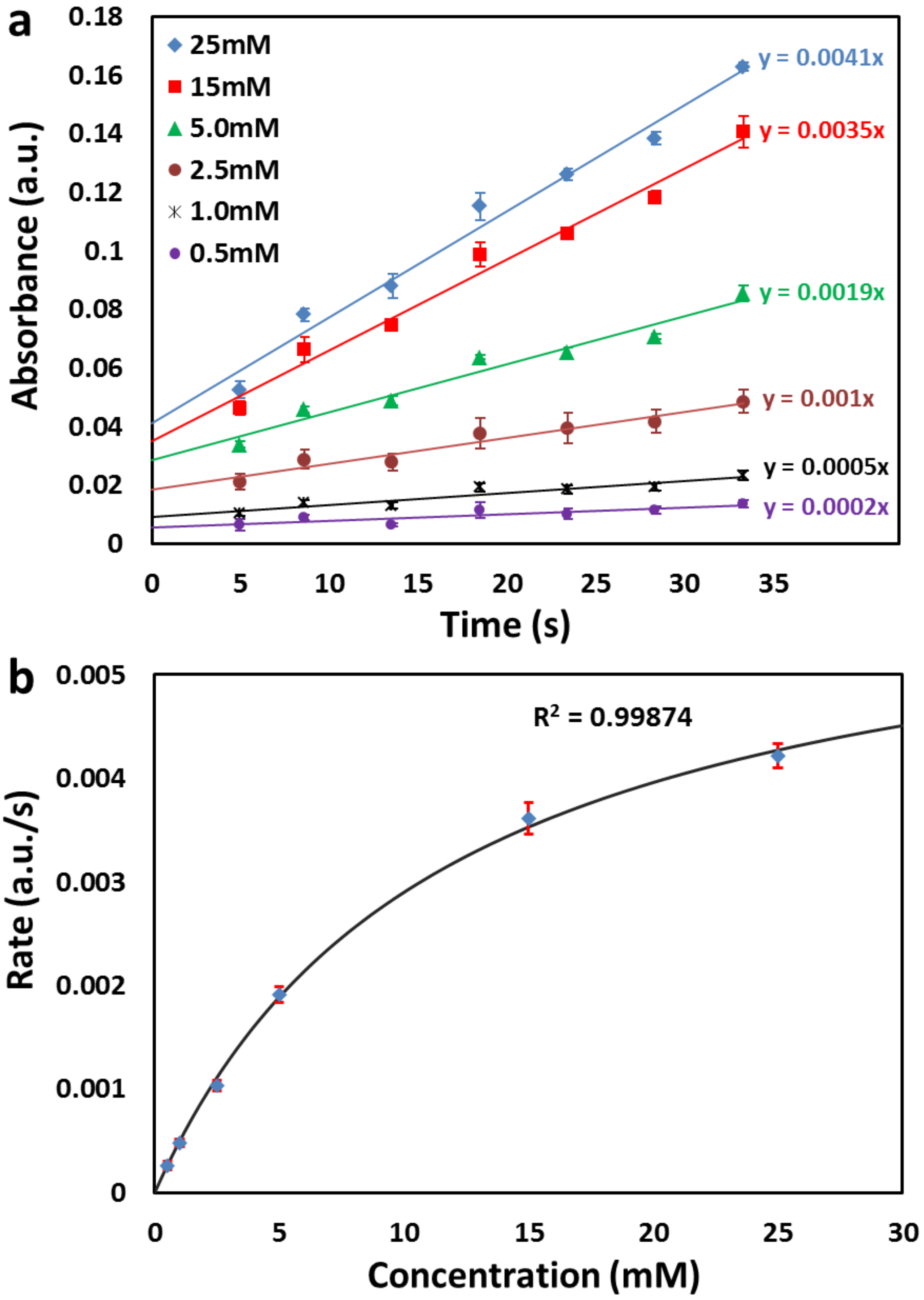

Figure 5.8 Use of the flow cell in determining glucose concentrations with a Trinder's assay (a) Absorbance of droplets flowing through the flow cell expressed in relation to the time since generation. Each result is a repeat of three separate experiments with the standard deviation expressed as the error bars (mean 6.4% RSD). The lines of best fit constitute the initial reaction rate and are shown plotted against the glucose concentration in (b). The data is fitted by nonlinear regression with a Michaelis–Menten curve.

Having obtained the Michaelis-Menten curve and along with it, the values for V_{max} and K_m, it was then possible to use the flow cell to determine the glucose content of unknown solutions. To confirm this and to test the accuracy of the flow cell, four new glucose solutions (1.5, 4, 7 and 16 mM) were formulated as ‘unknown’ samples and determined their concentrations from their initial reaction rates. Droplets of these ‘unknown’ samples were generated and taken through the flow cell as discussed before. The linear increases in absorbance of the droplets with time were recorded and the initial reaction rates obtained from the gradient of the lines of best fit. The concentrations of glucose were calculated by using a rearranged form of the Michaelis-Menten equation:

$$[S] = \frac{V_0 \cdot K_m}{V_{max} - V_0} \tag{11}$$

The experiments were carried out in triplicate, and the recovered concentrations were 1.59, 3.80, 6.90 and 15.3 mM, with small average errors of < 5% RSD. These measured concentrations are plotted against the actual concentrations in Fig. 5.9.

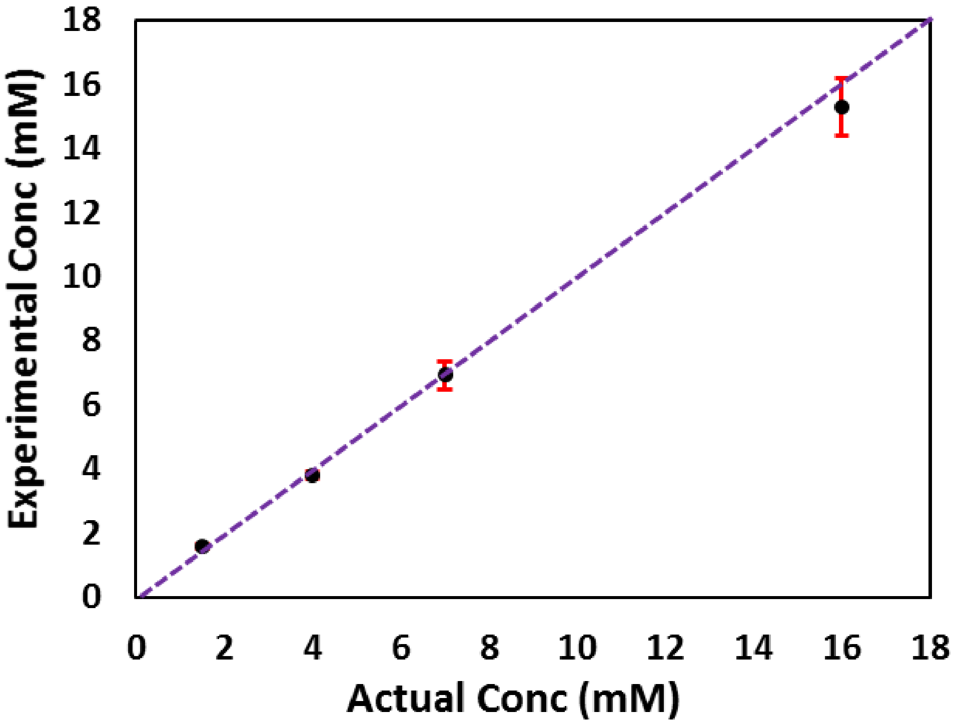

Figure 5.9 Comparison of the experimentally determined concentrations of a series of glucose solutions versus their actual concentrations. The experiments were carried out in triplicate, and the standard deviations are expressed as the error bars. The dotted line shows the 1:1 equivalence.

It is interesting to note that the error (as shown by the error bars) increases with concentration, which is likely due to the increased influence of experimental error in Eq. 11. V_0 increases with concentration and as it becomes more significant with respect to V_{max}, so too does the error contained within the denominator of Eq. 11. Nonetheless, the relative error is still small and the measured concentrations are in excellent agreement with the actual values. This shows that, despite being small in size and being fabricated from low-cost components, the flow cell can be used for accurate quantitative analysis of metabolite concentration *via* measurement of enzymatic kinetics.

5.2.2.2 High Throughput in Vitro Measurement of Glucose

In addition to the high accuracy just demonstrated, the flow cell is intrinsically high-throughput (unlike other previous droplet-based devices) making it suitable for POC monitoring by continuous measurement of a time sequence of sample droplets. To demonstrate this, the glucose concentration in the droplets was changed sequentially using a similar method to Fig. 5.6, with stabilised concentrations at 4, 6.5 and 16 mM. Droplets were automatically identified from the detected signals using computer code written in Matlab (Mathworks). The absorbance of each droplet at different detectors was correlated with reaction time, and the initial reaction rates were obtained from lines of best fit. This gave the reaction rate for each droplet, as shown in Fig. 5.10a. These reaction rates were then converted to give the glucose concentration for each sample droplet using Eq. 11 as shown in Fig. 5.10b. Each point constitutes a distinct measurement with a time interval of 4.2 s between neighbouring droplets in this experiment. While this frequency should be more than sufficient for most of the POC applications (e.g. glucose monitoring), even higher measurement frequencies could be obtained by simply increasing the linear velocity of the droplets while also extending the length of tubing in between detectors to provide enough reaction time.

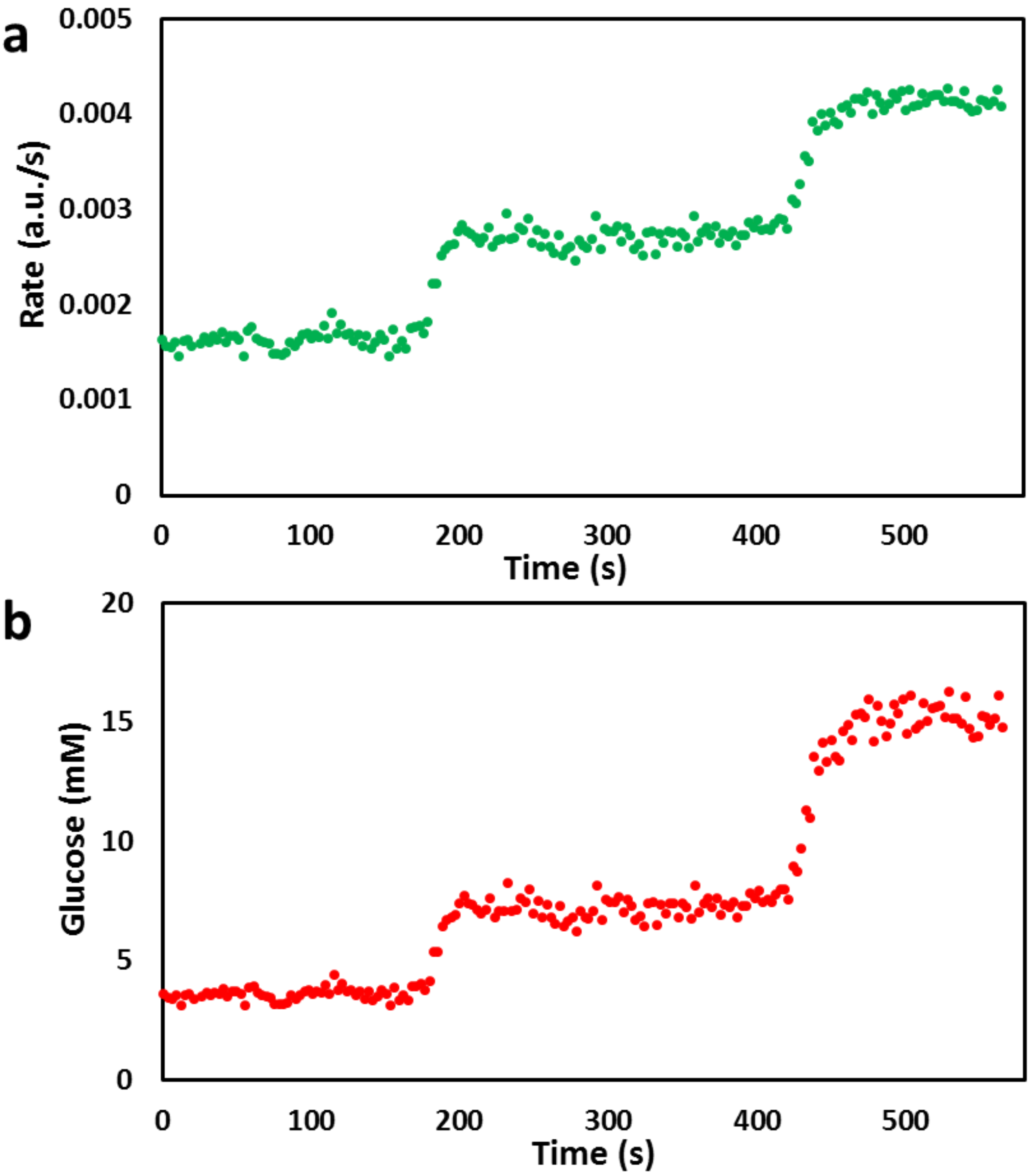

Figure 5.10 High throughput determination of glucose concentration in the flow cell. (a) Initial rate of reaction of droplets flowing through the flow cell, expressed in relation to the time since generation, (b) actual concentration of each droplet calculated via rearranged Michaelis–Menten equation (Eq. 11).

The initial rate of glucose reaction was also studied with a change in temperature. Glucose (15mM) was reacted with reagent mix at different temperatures (10.5, 16, 21, 27, 33, 38 and 43 °C) as shown in Fig. 5.11. Each result is a repeat of 3 experiments, and the %RSD was found to be 3%. The rate of reaction increases with increase in temperature up to 28-30 °C and decreases afterwards due to the enzyme degradation as analogous to the previous enzyme based studies [209]–[211]. This result shows that care must be taken to keep the temperature of the droplet reactor constant for any field applications. Otherwise, the reading of glucose level (or another analyte) will be less accurate, or even bring in false reading or wrong clinical decisions. For a human wearable device, this risk can be addressed by either providing a reaction chamber with constant temperature or by mounting the reactor close to human body so that the ambient temperature is largely stable.

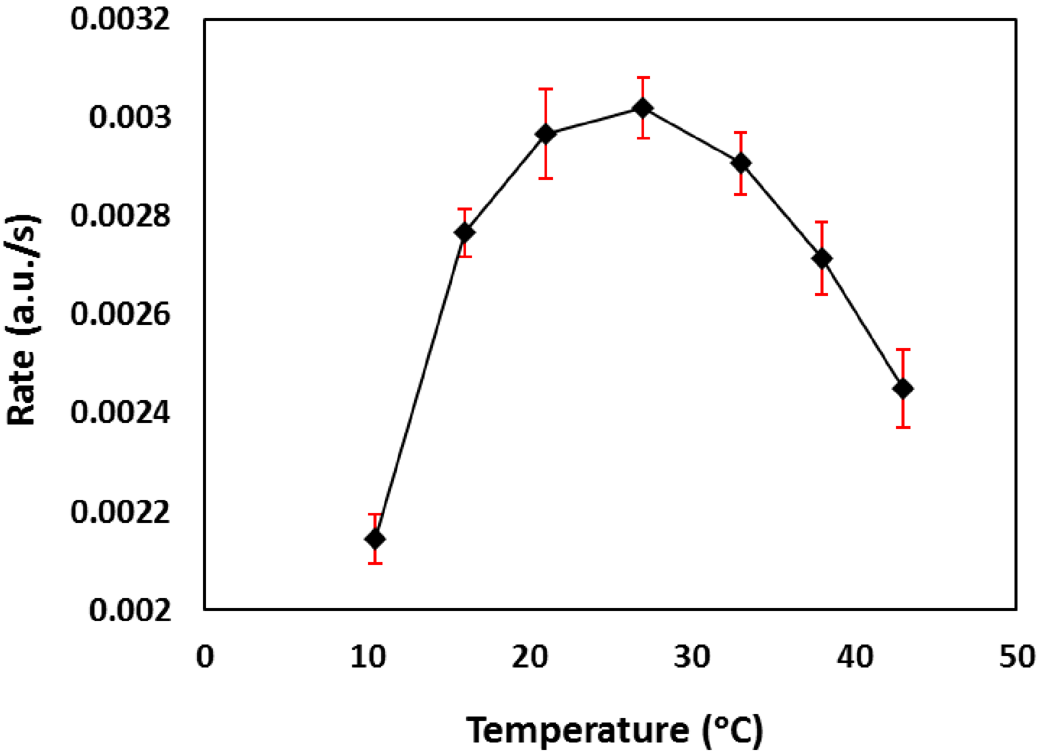

Figure 5.11 Effect of temperature on initial rate of glucose reaction. The rate increases with increase in temperature up to 30 ºC and then decreases onwards. This is due to the degradation of the glucose oxidase example which takes place at higher temperatures.

5.3 Conclusions

In this chapter, a multidetector flow cell is developed for the study of enzymatic reactions within droplets. The flow cell has been successfully applied to glucose analysis and determination of unknown samples using Michaelis-Menten kinetics. This ‘mix-and-read’ glucose assay represents a significant class of homogeneous and heterogeneous enzymatic assays routinely performed in biolabs. Therefore, the device may find broad applications in the measurement of other biomolecules, for example, lactate, pyruvate, glutamate, glycerol, etc. The flow cell has a small footprint made of low-cost components, makes it a suitable choice to be integrated into portable or even wearable point-of-care applications. There are recent exciting developments on ‘digitalising’ various continuous chemical signals into sequential droplets [14], [28]. This flow cell can measure these sequential droplets colorimetrically and without stopping the flow, enabling continuous and near real-time monitoring with droplet microfluidics. Combined with its small footprint, low-powered, and low-cost components, this device is highly suitable for application in portable field-deployable devices. It is envisaged that flow cell could find applications in continuous measurement of enzyme kinetics, droplet-based PCR, and droplet sorting, etc.

Chapter 6 Droplet-Based Continuous Chemical Sensing

The first part of this Chapter highlights the importance of continuous point-of-care monitoring and describes key studies on microdialysis and droplet-based microdialysis. The second part describes the fabrication and experimental characterization of the screw-driven pump and upgraded flow cell for continuous sensing of glucose and lactate enzymatic assays.

6.1 Introduction

Over the last two decades, biosensing research community has focused on lateral flow tests that are uniquely simple and cheap to manufacture, and to meet the ASSURED criteria for diagnostic tests developed by the World Health Organization. However, most lateral flow tests lack the sensitivity and quantitation capabilities required for biomarker-based treatment, where sensitivities in the range of physiological levels are paramount to support patient triage and treatment. Rapid and automated POC tests are beneficial especially in an emergency setting where the time window is linked to survival rate and discharging of patients. Currently, high sensitivity biomarkers measurement requires sophisticated assay and detection equipment renders those tests being restricted to bulky, high-performance equipment only available in clinical pathology laboratories, and the ASSURED criteria of short time (2-5 min) sample-to-result remains seen as incompatible with automation.

Another less asked question is whether a *single point* POC test is adequate for guiding clinical decisions, especially when fast changing biomarkers are involved, such as metabolites like glucose, lactate or others that could change in minutes or seconds. Ideally, these biomarkers shall be measured continuously over a period of time or in the entire course integration. Indeed, studies on real-time and online monitoring of such species for traumatic brain injury [35] or diabetes [36] patients have shown that continuous and rapid testing could be lifesaving. Real-time monitoring of abrupt changes in metabolism inside intensive care unit (ICU) for traumatic brain injured (TBI) patients or during liver transplant could be lifesaving and are direct applications for portable droplet sensor.

A droplet-based portable chemical sensing device for continuous sampling of body fluids developed in Dr. Niu’s group has been used to generate and analyse sample droplets. The fundamental idea of the device is to pump sample and reagent fluids continuously with a screw-driven pump, perform biochemical assays inside droplets using the upgraded version of the flow cell described in chapter 5. The aim of the continuous droplet generation and online detection is to collect dialysate from microdialysis probe attached to the sensor and to quantify metabolic changes inside body tissue such as changes in concentrations from glucose, lactate, and pyruvate.

6.2 Microdialysis for Probing Tissue Biochemistry

Microdialysis is a technique used to collect molecules from interstitial fluid of tissues. The semi-invasive nature of microdialysis has led it to be utilised for the study of metabolites in tissues even from the brain. Biological events occurring in vivo are difficult to be quantified in real time. However, microdialysis has made possible to sample biomolecules from the tissue continuously and capture the events happening during illness or critical conditions. The critical application of microdialysis has been found in neurological research and used as a primary technique to quantify neurotransmitters for almost three decades [212]. It has also been widely used in drug development and metabolism studies [213], and drug delivery into the interstitial fluid [214]. Although microdialysis has been extensively used for human and animal brains, it has also been used for the study of other tissues and organs including liver, skin, blood and heart [215].

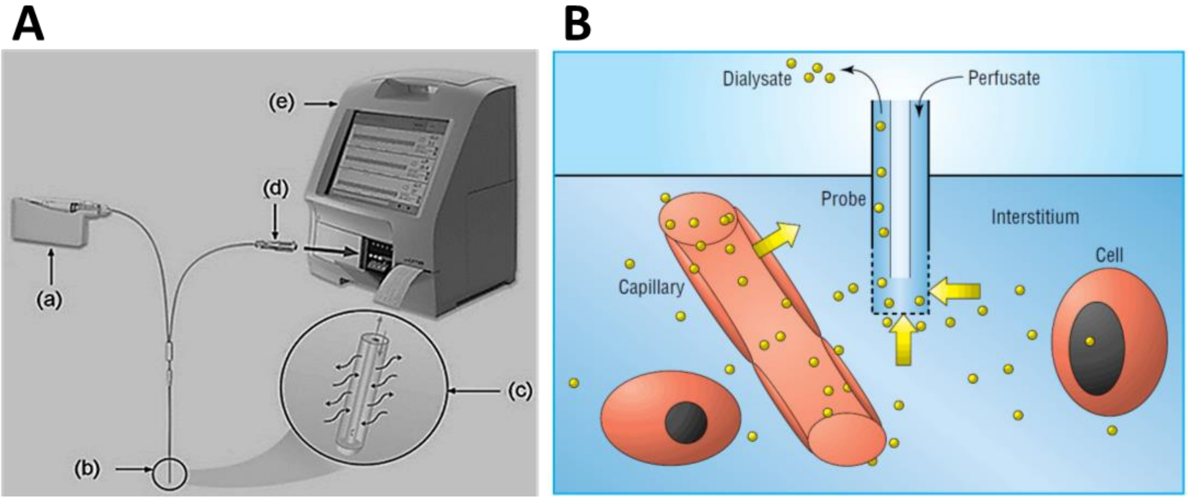

Figure 6.1 Overview of the microdialysis A) CMA Microdialysis bedside analyzer illustrating different components including CMA pump to perfuse tissue (a), a microdialysis probe (b-c), the sample injecting connector to CMA analyzer (d), and output signal display (e), B) Standard microdialysis probe illustrating the working principle of the probe. The semipermeable probe allows the exchange of small molecules to and from the tissue [216].

The working principle of the microdialysis lies in inserting a microdialysis probe into the tissue of interest, perfusing with artificial interstitial fluid with a syringe pump and collecting the dialysate in vials which represent the concentration of the biomolecule inside the interstitial fluid. The collected sample is then analysed via bench top analytical instruments. Fig. 6.1A shows a typical microdialysis setup used in clinical research (CMA Microdialysis) for the analysis of tissue metabolites such as glucose, lactate, pyruvate, etc. Artificial cellular fluid is used to perfuse the tissue which has similar ionic composition and strength to the extracellular fluid. Biomolecules not present in the perfusate diffuse into the membrane and are transported via an outlet, and the sample is collected every 10-30 mins in vials for analysis [216], [217]. This longer sample collection time is due to the bigger sample requirement for detection in spectrophotometers. The length of collection tubing placed at a certain distance (typically 5 cm) from the patient also requires a longer time to bring the new concentration from the membrane to the collection vial. Biomolecules can also be diffused in the cellular fluid via microdialysis probe for drug metabolism or pharmacokinetics studies.

The core of the microdialysis system is a semi-permeable membrane which allows molecules to diffuse from the interstitial fluid with zero net fluid loss. The probe consists of a semi-permeable membrane with a limit of permeability less than 20 KDa (for tissue metabolites). Usually, the probe is designed as a concentric tube where perfusate enters from one inlet, passes through the membrane and exits through the outlet as shown in Fig. 6.1B. The diffusion occurs between two fluids as concentration gradient and the concentration recovered by microdialysis probe reflects the actual concentration inside the tissue. The diffusion of biomolecules is also characterized by relative recovery of the molecule. Relative recovery depends on the length of the membrane, weight cut-off, concentration gradient, perfusate flow rate and viscosity of the fluid [217], [218].

The relative recovery of molecules can also be affected by the change in temperature [218], therefore, in vitro experiments must be performed at constant temperature and the body temperature is preferable for mimicking in vivo experiments. The viscosity of the fluids and particle radius also play a vital role in determining relative recovery and hence, smaller particles with low fluid viscosity diffuse much faster than larger particles with viscous fluids and vice versa. Numerous such studies have been devoted to measuring the recovery of the microdialysis probe such as Moon *et al.* [219] evaluated in vitro recovery rate of glucose solutions at different flow rates and different probe lengths as shown in Fig. 6.2. The authors found that the membrane with 3 cm length had higher recovery rate as compared to 1 cm membrane (the longer probe length would allow more diffusion). In addition, more than 95% recovery rate was achieved with flow rates of 500 nL/min with probe lengths of 1 and 3 cm and the recovery rate decreased with increase in flow rate.

Glucose and lactate are smaller molecules and diffuse much faster as compared to larger molecules such as proteins (35-500KDa). Proteins are present in low concentration in interstitial fluid, and their movement is also restricted by hydrophobic interactions with tubings. Wide pore membranes are usually used to diffuse proteins, but perfusate solution can also leak into the tissue. 1-5% recovery rate for proteins is generally achieved with a flow rate of 1 μL/min and 100, 000 Da microdialysis membrane which is much smaller than usual recovery rate of 20-30% for smaller molecules [35]. In summary, microdialysis is widely used for the study of tissue metabolites and brain neurotransmitters.

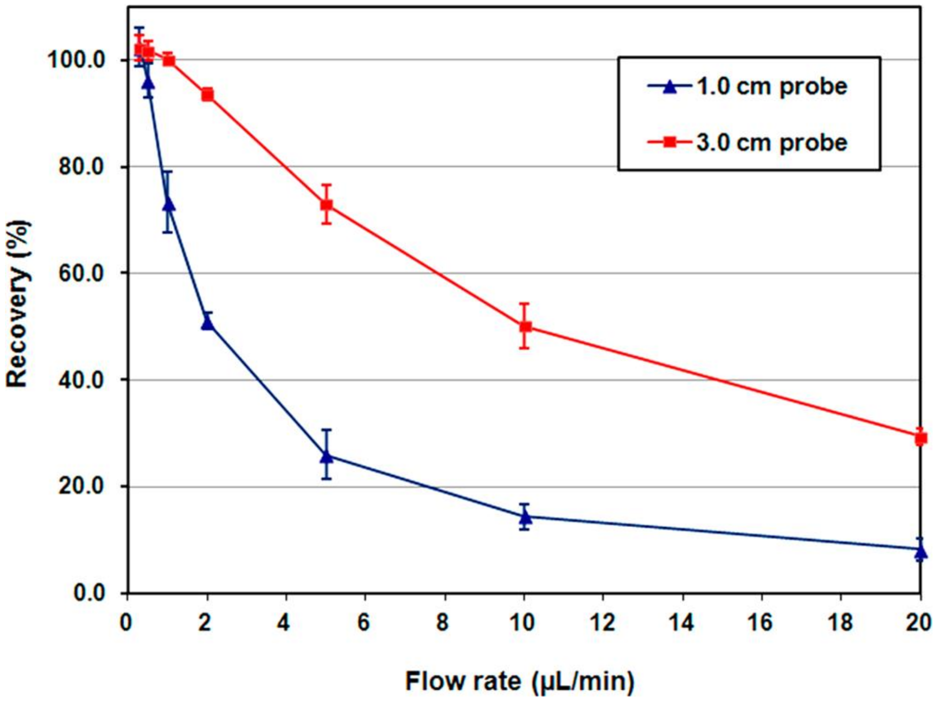

Figure 6.2 Calibration of membrane length vs. recovery rate. The recovery rate of glucose is higher at 500 nL/min and lower above 10 µL/min. The recovery is also higher for 3.0 cm probe length [219].

6.2.1 Tissue Metabolism

Critical chemical changes such as tissue metabolism can lead to an early surgical intervention and prevent further tissue damage following injuries or transplantations. This can be achieved much faster with microdialysis sampling as compared to blood sampling where the changes take a significant amount of time to be detected in blood [216] (diffusion into blood capillaries). Microdialysis has been used in clinical practice and has been shown to reduces mortalities up to 70% [220]. Brain pressure is a common parameter to indicate further damage towards brain tissues. However, metabolic changes occur well before the pressure changes take place in the brain, and the risk can be reduced by continuously measuring glucose, lactate, and pyruvate levels.

Microdialysis is widely used in ICU for detection of glucose, lactate, and pyruvate in TBI patients. Pyruvate is metabolised into carbon dioxide and water in the citric acid cycle when the oxygen and glucose levels are normal [221]. However, after tissue damage the consumption of glucose increases and produces more pyruvate. Because of the increased NAD^+ consumption and oxygen deprivation in tissues, pyruvate metabolises to lactate rather than metabolized in the citric acid cycle; the condition is known as hypoxia (Fig. 6.3) (also referred as ischemia). Oxygen is essential to oxidise glucose in mitochondria and reduced oxygen supply to injured brain produces less ATP and more lactate which leads towards mitochondrial dysfunction. For this reason, lactate to pyruvate ratio is an important parameter for overlooking respiratory conditions of tissue and early detection of brain ischemia [222]. In 1999, intracerebral microdialysis was used to monitor delayed ischemia, and the results showed glucose and lactate levels changed with patient's condition. The results encouraged the use of microdialysis for critically injured patients [223]. Microdialysis has been widely used for detection of glucose, lactate and pyruvate levels and this report will only look at applications involving real-time monitoring of metabolism.

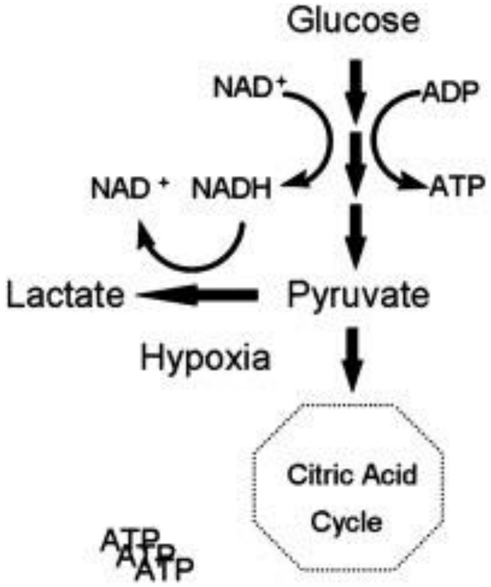

Figure 6.3 Glucose conversion into pyruvate and pyruvate consumption inside citric acid cycle to produce ATPs. Pyruvate to lactate shows a hypoxia; a condition which leads to ischemia [222].

6.2.2 Real-Time Clinical Monitoring

Standard microdialysis procedure in ICU involves the collection of samples 10-30 minutes in vials, sample analysis and reporting results back to the clinicians for diagnosis. This process takes place outside ICU in analytical labs or inside with bedside analysers. However, the cellular metabolism changes can happen in seconds to minutes and are not present in the interval based measurements. Continuous monitoring can provide near real-time information about patient's metabolism status.

Microdialysis is a powerful method to monitor glucose levels from subcutaneous tissue and the membrane is safe and compatible with tissues. Microdialysis system could rather be bulky because of the need for a pump to perfuse tissue, tubings to collect dialysate, liquid reservoirs and bedside detector. Also, the time lag for each measurement is long (30 mins) and miniaturization is required to lessen the analysis time, consumption of fewer reagents and cheaper analyses. In one of the glucose measuring study [219], microfluidic chip was connected to the microdialysis probe, and the recovery rate for glucose was optimised by implanting probe in animals. The experiments were based on glucose and insulin injection to the subcutaneous tissue of rat and continuous detection of glucose levels as shown in Fig. 6.4. Nanolitre sized sample was reacted with enzymes in the microreactor and detected with the platinum electrodes amperometrically. The time lag between microdialysis probe and the signal was found to be 18 mins which is mainly due to the longer tubing and can be minimised by miniaturising all components and putting closer to the probe.

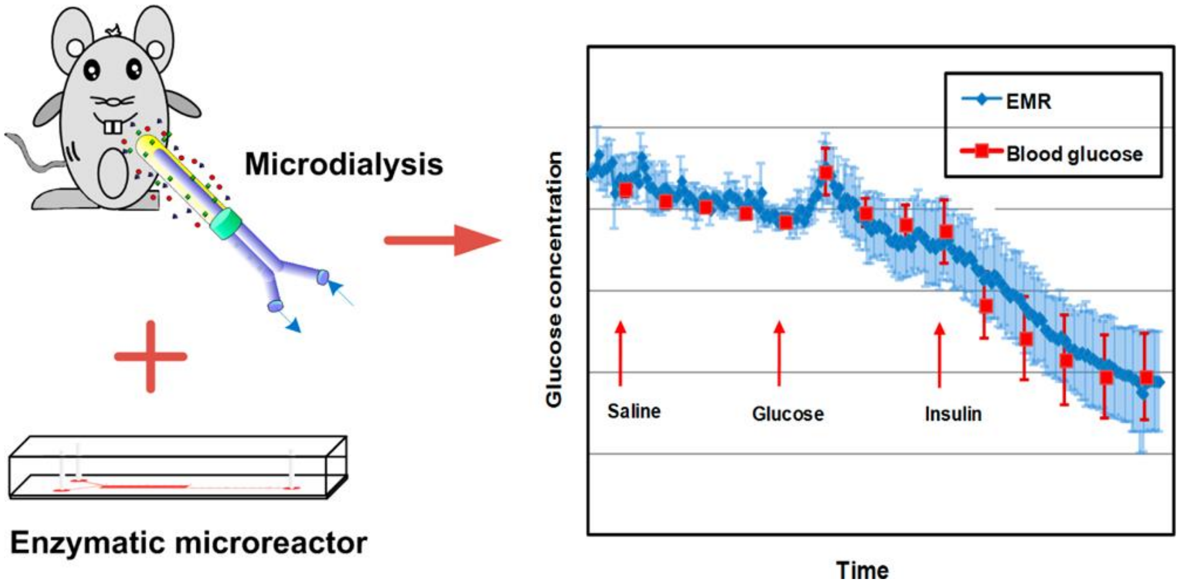

Figure 6.4 Enzymatic detection of glucose on microreactor and real-time monitoring of glucose and insulin injection in adipose tissue of rat. The continuous measurement of glucose via microdialysis is achieved with a time lag of 18 min, and the results are compared with blood glucose levels [219].

With low flow rates, microdialysis achieves a high recovery of biomolecules, but the sample volumes accumulate slowly which poses a challenge to be detected by standard analysers. Therefore, in clinical setup microdialysis samples are collected on an hourly basis. Boutelle’s group [224], [225] developed continuous based microdialysis system known as rapid sampling microdialysis system (rsMD). In this system, 200 nanolitre sample is injected into the microreactor for enzymatic reaction of both glucose and lactate and each sample is analysed in every 15 seconds as shown in Fig. 6.5. The dialysate tubing of 1 m length was connected with enzyme microreactors. Glucose enzyme reagents and lactate enzyme reagents are separately added into the microreactors and a custom built valve is used to introduce the dialysate into each microreactor which is controlled by a computer. However, the sample from tissue to microreactor takes 15 min due to the longer tubing and can be reduced by miniaturizing components.

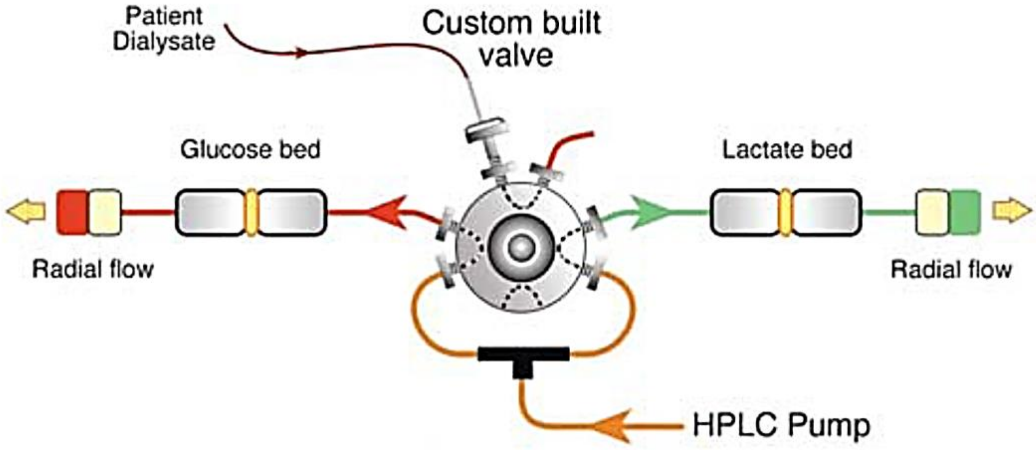

Figure 6.5 Enzymatic detection of glucose and lactate by the rsMD system. 200 nanolitre sample is injected into each microreactor via a valve switching. The sample reacts with enzyme-based reagents and provides electrochemical detection after 15 s [224].

Furthermore, Jone *et al*. [225] used the rsMD system with traumatic brain injury patients in ICU and measured glucose and lactate levels with 30 s time intervals (the time lag was 15 min). The authors detected low glucose and lactate levels which were difficult to be detected by standard methods. In another study done by the same group [39], rsMD was used to monitor muscle ischemia during free flap surgery. Lactate and glucose were measured throughout the entire surgery, and it was found that the ischemia started with free flap failure. Free flap surgery is an important and expensive surgery, and early detection of ischemia could prevent it a failure. Glucose and lactate measurements by the rsMD system were also used to detect metabolic changes with spreading depolarization (SD) waves which occur with specific interval inside traumatically injured brain. The glucose levels decrease with SD wave and the lactate levels increased, and the value adds up with each SD wave and substantially depletes brain glucose. These results are used for better understanding of the mechanisms of secondary brain injury in patients [226].

However, the temporal resolution of these systems is still low and requires new strategies to implement. Droplet-based microfluidics has emerged as a promising tool to increase the temporal resolution of microdialysis-based systems and is discussed in the following section.

6.2.3 Droplet-Based Microdialysis

Temporal resolution is defined as the time over which the abrupt change in concentration is observed. Temporal resolution is an important parameter in microdialysis monitoring of neurotransmitters because concentration changes occur at a time scale of seconds to minutes [227]. This requires a fast detection of analytes after collection from microdialysis probe because of the fact that these changes could be diluted along the tubing, and the signal will represent the average of the concentrations inside that time interval. If the sampling rate is increased, this on the other end requires highly sensitive instruments to detect these changes in a small amount of volume.

Sampling volume is the key to determining temporal resolution. Consequently, slow flow rates can also achieve higher recovery rate, but the volumes generated are tiny and sensitive systems are required to detect these changes in real time [228]. Small volumes can also be injected into the capillary electrophoresis system to be quantified with LIF such as amino acids because of their higher concentrations in dialysate can be detected easily with LIF detections [14]. If the slow sampling rate is used to collect dialysate with enough concentration to be analysed in the analytical device, then Taylor dispersion will reduce temporal resolution because of the zone broadening effect (Chapter 2). Taylor dispersion can be reduced by using shorter or thinner tubing, but this can be difficult for moving animals or TBI patients where the pump and reactors cannot be placed very close to the patient's head.

Segmented flow can localise concentrations inside droplets and avoid any dispersion along the tubing. This approach has been successfully applied to measure temporal resolution for different fluorescein concentrations in droplets as shown in Fig. 6.6 [229]. In this study, a microfluidic device was used to generate droplets of dialysate and transported to the detection system. Temporal resolution was measured by changing fluorescein concentrations at the probe surface and measuring intensity at the other end. Flow rate and the distance between the probe and detection point did not affect temporal resolution because of the segmented flow generated near microdialysis outlet. The authors changed the flow rates from 200 nL/min (Fig. 6.6A) to 1 uL/min (Fig. 6.6B) with 2 mm probe length and found that the temporal resolution was 30 s. Temporal resolution was improved with the probe length of 1 mm and was found to be 15 s as shown in Fig. 6.6C-D. In this setup, temporal resolution was calculated by the step increase in intensity from 10% to 90%.

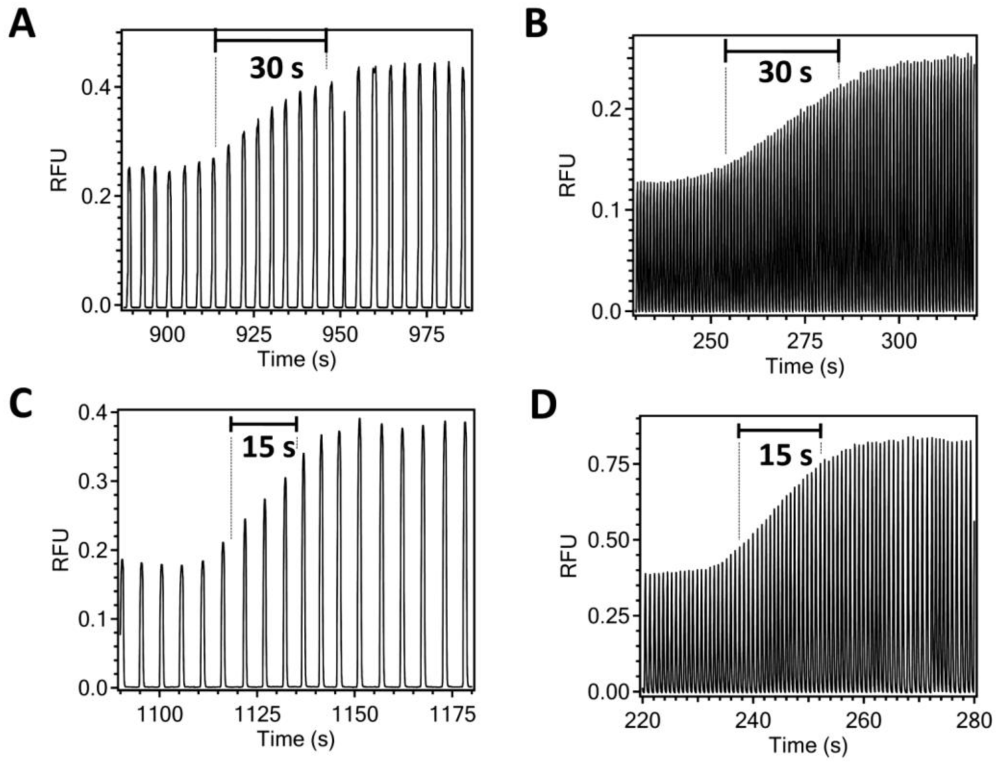

Figure 6.6 Effect of flow rate and probe length on temporal resolution using fluorescein droplets A) 200 nL/min flow rate and 2 mm probe length, B) 1 uL/min flow rate and 2 mm probe length, C) 200 nL/min flow rate and 1 mm probe length, D) 1 uL/min flow rate and 1 mm probe length. Change in flow rate do not change temporal resolution while smaller probe gives higher temporal resolution [229].

In another study, push and pull perfusion method [230] was used to collect samples of L-glutamate from an anesthetized rat at a temporal resolution of 7 s using droplet-based microfluidics. The tissue was perfused with artificial CSF and brain cellular liquid was pulled to generate droplets in a tee microchip as shown in Fig. 6.7a. These droplets were then stored in a capillary tube and analysed offline by injecting into another Teflon tee as shown in Fig. 6.7b. In the microchip, droplets were merged with the fluorescent enzymatic assay and the LIF detection was used to analyse the fluorescent signal inside droplets. This method of sample generation preserved the concentration changes inside droplets and provided the highest temporal resolution.

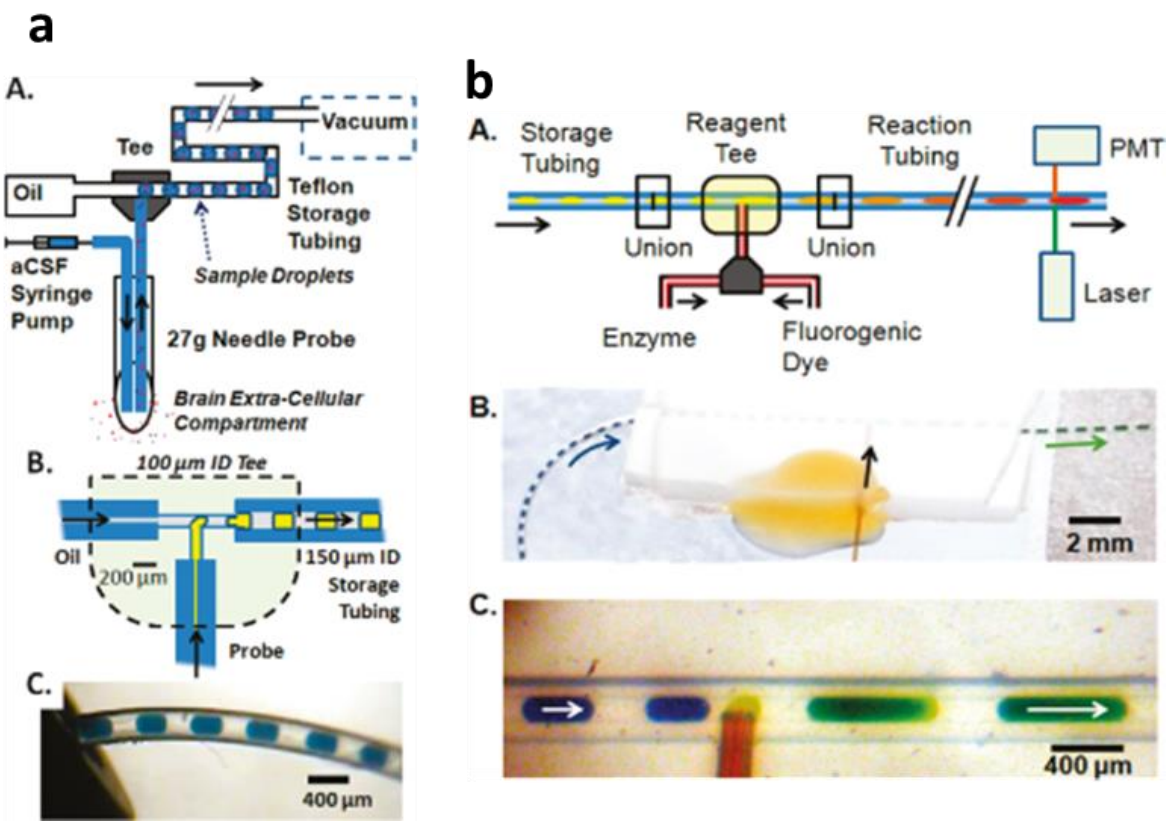

Figure 6.7 Push and pull method of probe sampling to generate droplets of brain cellular liquid a) Generation of aCSF droplets from brain and storage in tubing for later use illustrating schematic of the push and pull method (A), Droplet generation (B), and droplets stored in the tubing, b) Droplet merging and detection showing schematic of the droplet merging with fluorogenic dye to generate a fluorescent signal by LIF detection (A), photograph of the droplet merging using blue and red dyes for illustration purposes (B,C) [230].

6.3 Continuous Chemical Sensing Device

Although there are continuous and droplet-based microdialysis devices as discussed above, the sampling and handling of microdialysis samples are still driven by bulky pumps. Moreover, the droplet generation can be affected by disturbance from flow rate, sample change, etc. Niu’s group started to develop a new method of sampling and droplet generation in the last few years. The key design involves the screw-driven pump (a mini peristaltic pump) with a target to generate droplets robustly and sample near patients. The screw-driven pump works on the principle of squeezing the flexible tubing and pushing the liquid. This is contrary to the syringe pumping, a widely used method to pump fluids for microfluidic devices. However, the syringe pump is bulky, and the sample volume is limited [231], [232] whereas, the peristaltic pump can continuously supply fluids for microfluidic systems and can be miniaturized with simple fabrication techniques.

The schematic of the screw-driven pump is shown in Fig. 6.8. The droplets generated in the microchip (Chapter 5) were transported to the flow cell for detection. The design, fabrication and working principle of the continuous chemical sensing device including screw-driven pump was reported elsewhere (Yu Zhang, PhD Thesis, Submitted to University of Southampton, 2016). This chapter will only describe the fabrication and characterization of the screw-driven pump and flow cell mainly used for continuous chemical sensing device.

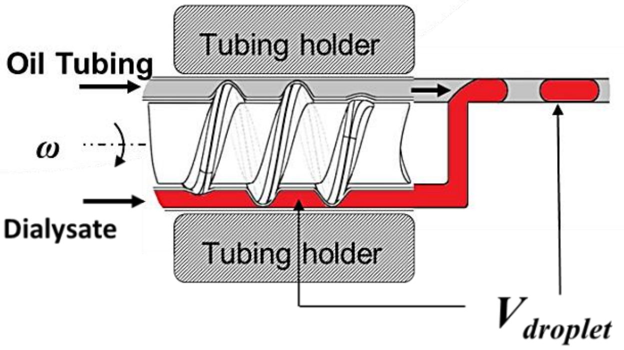

Figure 6.8 Schematic of the principle of the screw-driven pump and droplet generation. The shaft squezes the tubing and the flow is generated in oppositely placed aqueous and oil tubings to generate droplets. The pitch of the screw shaft determines the volume of the droplet ($V_{droplet}$) and is known as shaft pitch.

The screw-driven pump is easy to fabricate (3D printing of pump and shaft), easy to operate and the pump relies on the rotation of the shaft from DC motor. As the shaft rotates, it squeezes the tubings and generates a flow with constant pulsation (Fig. 6.8). The aqueous and oil tubings were fixed at the opposite end of the pump which drives aqueous and oil fluids one after other. This out of phase fluid movement is very helpful for droplet generation because the carrier phase breaks the aqueous phase much easily. At the T-junction, the aqueous phase elongates in the hydrophobic tubing and the elongated part breaks when the carrier phase moves. This pulsation pattern generates very stable droplets, which is hard to produce by other types of pumps. Additionally, the pump has the ability to drive multiple channels which allows analysing of multiple assays at the same time. For microdialysis experiments, the pump drives the perfusate to the probe and withdraws the dialysate from probe outlet. This dialysate is then pumped to the microchip along with oil and reagents to generate droplets.

6.4 Experimental Results and Discussions

Experiments were performed by using microchips and the droplets were generated by screw-driven pump. The detection of the droplets firstly was achieved by a CCD camera and then optical flow cell was integrated into the device. The performance of the screw-driven pump and flow cell was tested by generating droplets at different conditions such as different screw shaft pitch diameters, tubing sizes, glucose and lactate assays.

6.4.1 Droplet Generation and Size Calibration

Initially, droplet size was calibrated by changing the screw shaft pitch (the distance between the two hinges on the shaft which determines the volume of the droplet as shown in Fig. 6.8) and tubing diameters. Firstly, droplets were produced in microchips by changing pitch sizes of the shaft (4, 5.5 and 7 mm) as shown in Fig. 6.9a and it was found that the droplet size increased with increase in pitch diameter. Secondly, the aqueous inlet tubing diameters were changed (0.13 and 0.19 mm ID) and it was also observed that the inlet tubing with 0.13 mm ID generated smaller droplets than 0.19 mm ID (0.25 mm ID of oil tubing was fixed in all experiments). The experiments were designed in two different arrangements; 0.13 and 0.19 mm tubing were used to generate red food dye droplets with three different shaft pitch sizes, and the droplet length was calculated using imageJ. Snapshots from top to bottom show an increase in droplet size with shaft pitches of 4 mm, 5.5 mm and 7 mm. The increase in droplet size (with an increase in shaft pitch size) was found to be linear for both tubing diameters as shown in Fig. 6.9b.

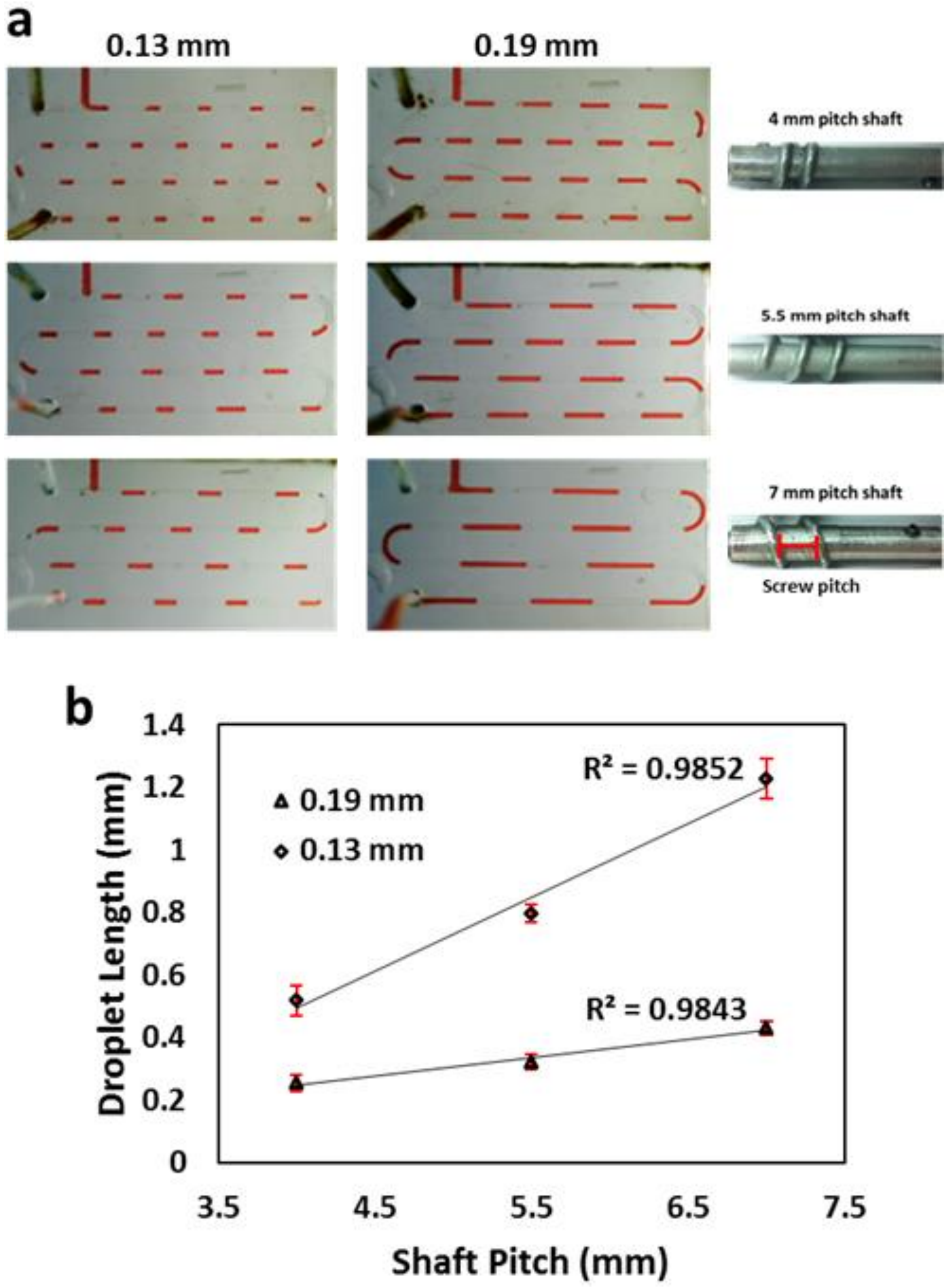

Figure 6.9 Droplet size calibrations a) Screw shafts with different pitch sizes, Droplet generation with different shaft sizes (4, 5.5, and 7 mm) and tubing ID (0.13 and 0.19 mm, b) Plot between droplet and shaft pitch sizes with 0.13 mm and 0.19 mm tubing showing the increase in droplet sizes with increase shaft pitches.

The temporal resolution of the screw-driven pump was also tested by changing the green food dye with the red food dye. The dye was changed manually by switching inlet tubing from green dye reservoir to red dye reservoir, and it was found that about 8-10 droplets were required to modify the signal completely as shown in Fig. 6.10. The colour changes in droplets were recorded with a handheld camera (Dino-Lite, Germany), and analysed by imageJ to plot an intensity profile of the droplet generation. The onset shows the snapshot of the droplet generation during switching of the food dyes (Fig. 6.10). The temporal resolution was found to be 15 s which is comparable to the previously reported values [229]. The number of droplets and switching time depends on the length of the dye inlet tubing and size of the droplet which will be further discussed in later sections.

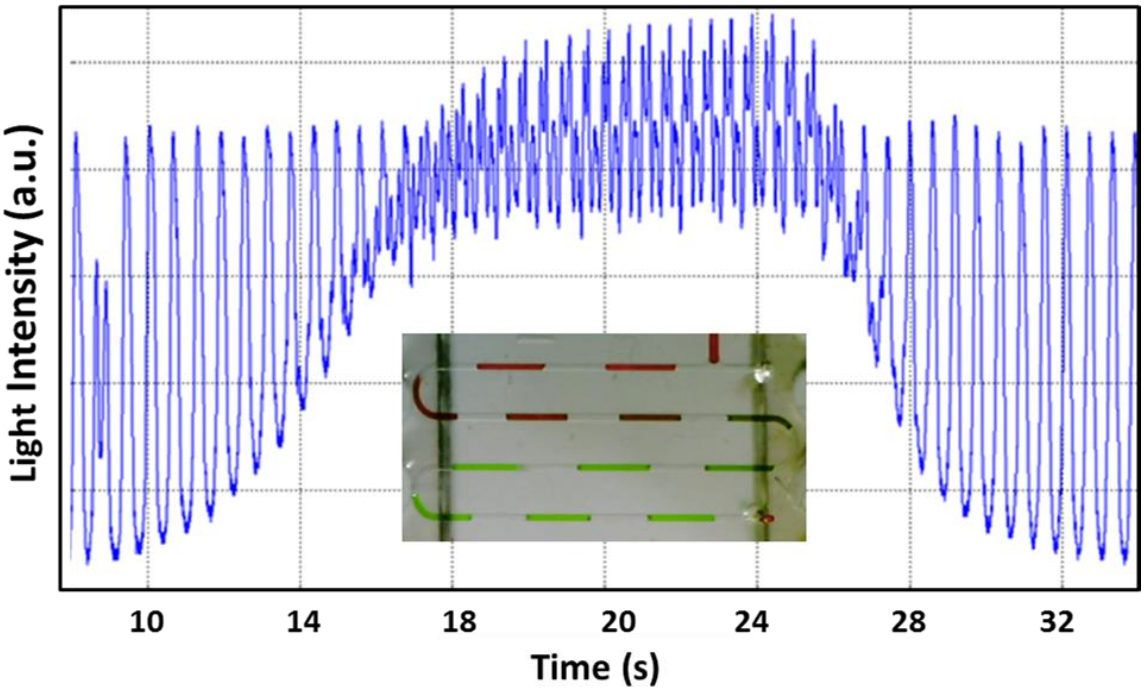

Figure 6.10 Droplet generation with the screw-driven pump. Switching of green dye with red dye shows 8-10 droplets and approx. 15 s were required to change one sample completely to another. The onset indicates the snapshot of the dye switching in droplets.

6.4.2 Droplet Detection in Flow Cell

Flow cell for optical detection of droplets was designed with SolidWorks and printed with 3D-printer as previously discussed in chapter 5. The flow cell is composed of 2 interlocking parts, the cartridge and detection cell, which allows accurate alignment of the optical components. Fig. 6.11a shows the schematic of the fully assembled 4-detector flow cell (the size of the device is 28 x 8 x 6 mm). Droplets were generated in a T-junction chip and flowed through the 4-detector flow cell as shown in a Fig. 6.11b. Previously, the 3D printed cartridge (Chapter 5) had variability in slit-sizes due to the limitation of the 3D printer (Ulitimaker 2). As a result of this, the absorbances measured at each detector for a droplet of fixed concentration of red food dye were found to have 6.5% RSD. It was also observed that slight misalignment of cartridge slit with tubing and/or detection cell could lead to significant change in intensity value. The tubing ID was 0.4 mm, and the wall thickness of tubing was 0.15 mm, thus the slight movement of the tubing in the 3D printed grooves of the cartridge affected the light intensity reaching the droplet and hence, the transmitted light to the detector.

For the above-mentioned reasons, the cartridge was fabricated by a precision micromilling of PMMA sheet (black) using LPKF Protomat S100 micromilling machine as previously described in chapter 4. The channels for holding tubing were micromilled with a 700 µm diameter end milling bits (LPKF Laser & Electronics Ltd, Berkshire, UK), and the holes were drilled with a 400 µm diameter drilling bit as shown in Fig. 6.11c. The second part was also fabricated with similar dimensions and holes, and both the parts were glued (Super Glue, Loctite) together with the tubing inserted into the channels using alignment pins to align the holes precisely.

The cartridge is 6 mm thick and has channels micromilled into one part such that 0.7 mm OD PTFE tubing can snugly fit into it. The tubing can also be inserted into the channels in numerous different geometries to give different distances and hence travel time of the droplets between detectors. As indicated in the Fig. 6.11c, there are 4 opening holes in the channels that provide the passage for light. The cartridge can slot into the detection cell (Fig. 6.11a-b). 4 pairs of LEDs (ASMT-QGBE-NFH0E, Avago Technologies) and photodetectors (TSL257, Texas Advance Optical Solutions) were fixed in the detection cell. Fig. 6.11d shows a transmitted light intensity signal from 4 detectors while droplets of red food dye flowed through the flow cell. The absorbances were calculated for each detector, and the %RSD was found to be lower (3.3%) as compared to 3D printed cartridge (6.5%).

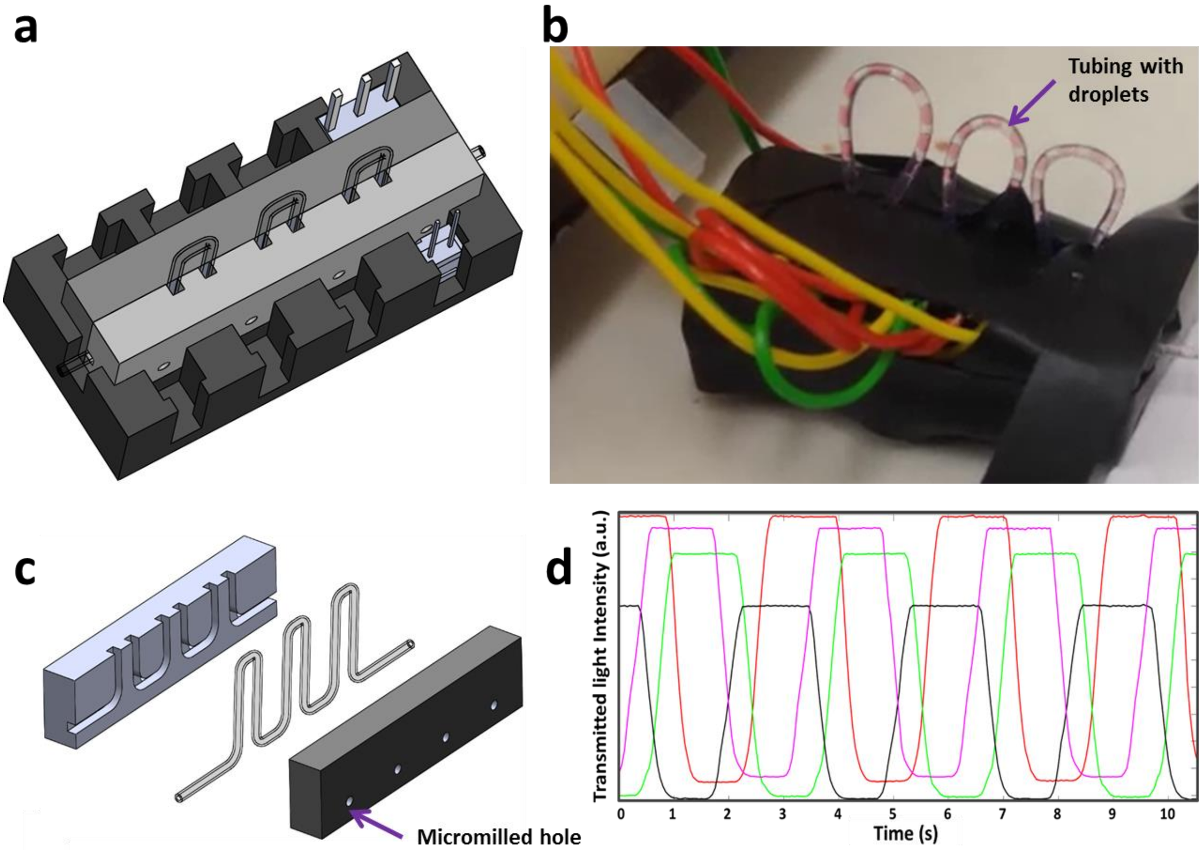

Figure 6.11 Multi-detector flow cell a) 3D schematic of the fully assembled 4-detector flow cell illustrating cartridge, tubing, LED and photodiode, b) Snapshot of the detector showing cartridge in place and tubing with droplets flowing through the flow cell, c) 3D schematic of the micromilled cartridge showing two PMMA parts with holes channels, and tubing, d) Transmitted light intensity graph signal of the droplet of red food dye for 4 detector. Notably, the intensity levels for each detector are slightly different due to the differences in LED brightness and/or tolerances in tubing diameter but the differences in absorbances are very low (3.3% RSD).

The reproducibility of the 4-detector flow cell was calibrated by generating droplets containing food dye and flowing them through the flow cell. Fig. 6.12 shows the droplets of three different food dye concentrations (50, 150 and 250 μg/mL) passed through the flow cell, and the level of intensity at the top of the graph shows oil which was constant during the experiment. As the light passed through the droplet, the transmitted light intensity decreased as per Beer-Lambert law. The signal was then collected from the photodiode and plotted (as shown previously in Chapter 5). The variation in intensity for each droplet at single concentration was found to be very low (%RSD < 0.5%).

Fig. 6.12 indicates (from top to bottom) that the change in colour intensity of the droplets generated at T-junction is preserved without contamination or smearing along the tubing and hence, without depending on the length of the tubing or time the droplets take to reach the detector. In this experiment about 20 s were required to switch from one concentration to the other completely which can be further reduced by shortening the tubing lengths from the inlet reservoirs and droplet generation.

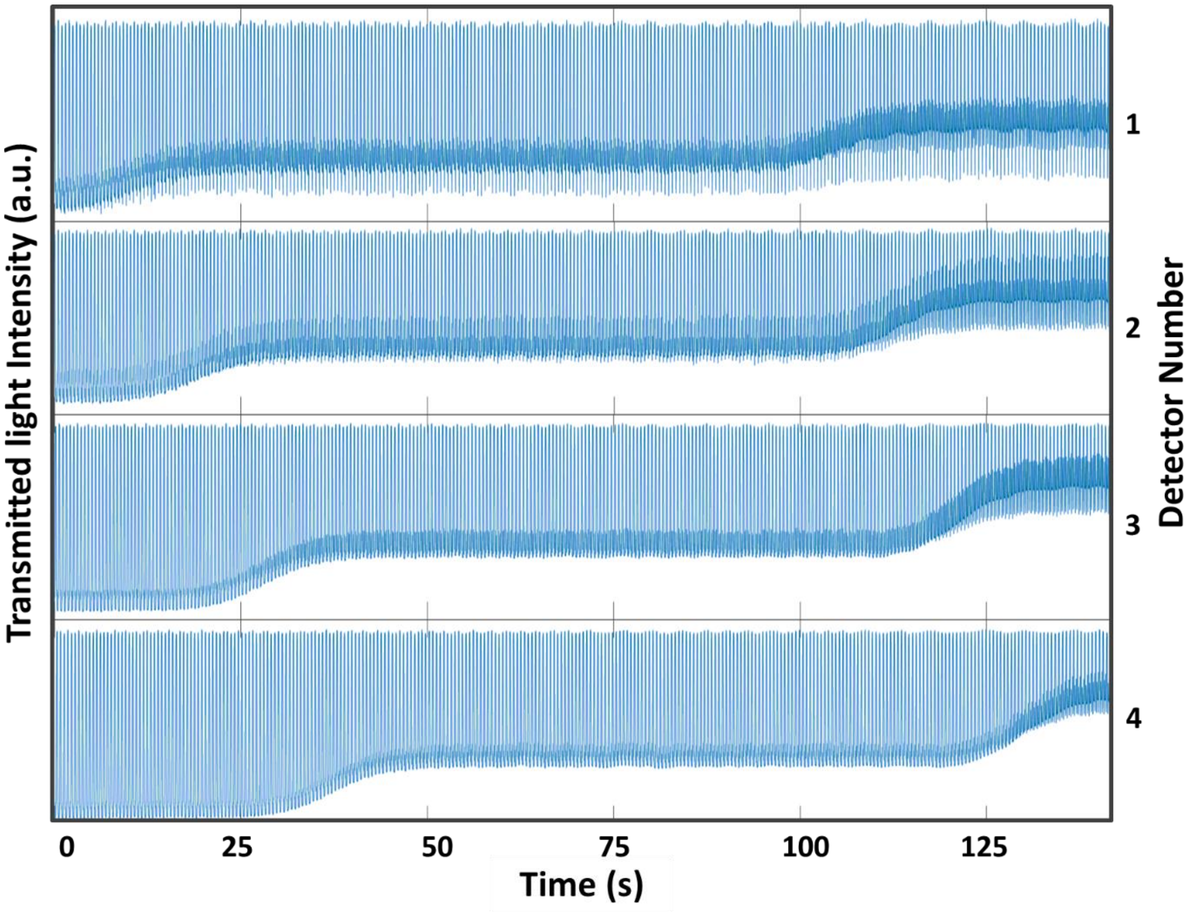

Figure 6.12 Calibration of the 4-detector flow cell via recording intensity change in 4 detectors (top to bottom) with changing dye concentrations from 250 µg/mL to 150 µg/mL and 50 µg/mL. It shows that the change in colour intensity is preserved from top to bottom (detectors 1-4) and travels to next detectors without contamination or smearing.

6.4.3 Glucose Enzymatic Assay in Continuous Chemical Sensing Device

Colorimetric assay of glucose is usually done in a spectrophotometer by using enzymatic reaction, as detailed in chapter 5. Initially, glucose reaction droplets generated by a screw-driven pump were detected in a microchip by handheld microscope (Dino-Lite) or a CCD camera attached to a microscope (Olympus BXFM). Furthermore, a miniaturised 4-detector flow cell aforementioned in this chapter was used to characterise glucose assay mainly for continuous chemical sensing device.

Glucose oxidase, HRP, 4-aminoantipyrine and phenol (PBS) were prepared in 0.1 M phosphate buffered saline (PBS) at pH of 7.4. The reagents were mixed such that the final reagent mixture consisted of glucose oxidase (30 U/mL), peroxidase (30 U/mL), 4-aminoantipyrine (1.54 mM) and phenol (22 mM) as reported previously in chapter 5.

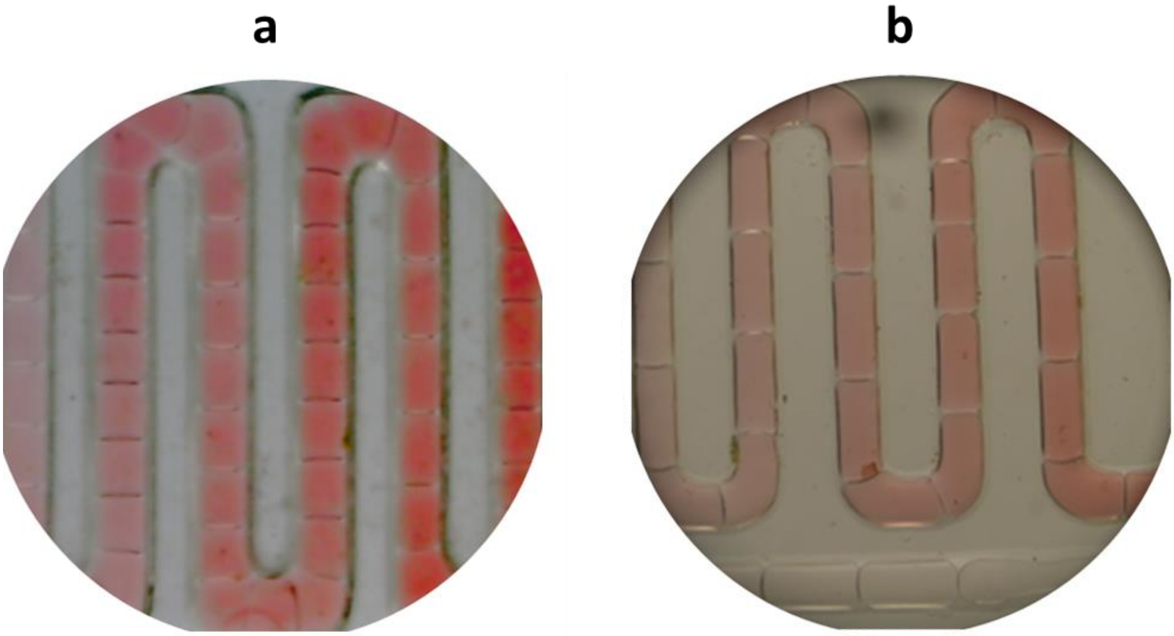

Figure 6.13 Glucose reaction droplets (22 mM) after generation in the T-junction chip. a) A snapshot taken by Dino-Lite Hand-held microscope, b) A snapshot taken by a CCD camera attached to a microscope (BXFM Olympus) and using a 2.5x objective lens.

Droplets composed of a glucose solution and reagents (containing glucose oxidase, peroxidase, phenol, and 4-aminoantipyrine) were generated in a T-junction chip using FC-40 with 0.35% surfactant. The reagents and glucose sample were mixed in 1:1 ratio in a microchip (the aqueous and carrier phase tubing internal diameters were 0.19 mm). Fig. 6.13a shows the 15 mM glucose droplets in the microchip (the snapshot was taken by Dino-Lite handheld microscope). Glucose droplets were also observed under a CCD camera attached to a microscope (Fig. 6.13b). The different colour intensity of the droplets at different points in the microchip shows the progression of the reaction with time.

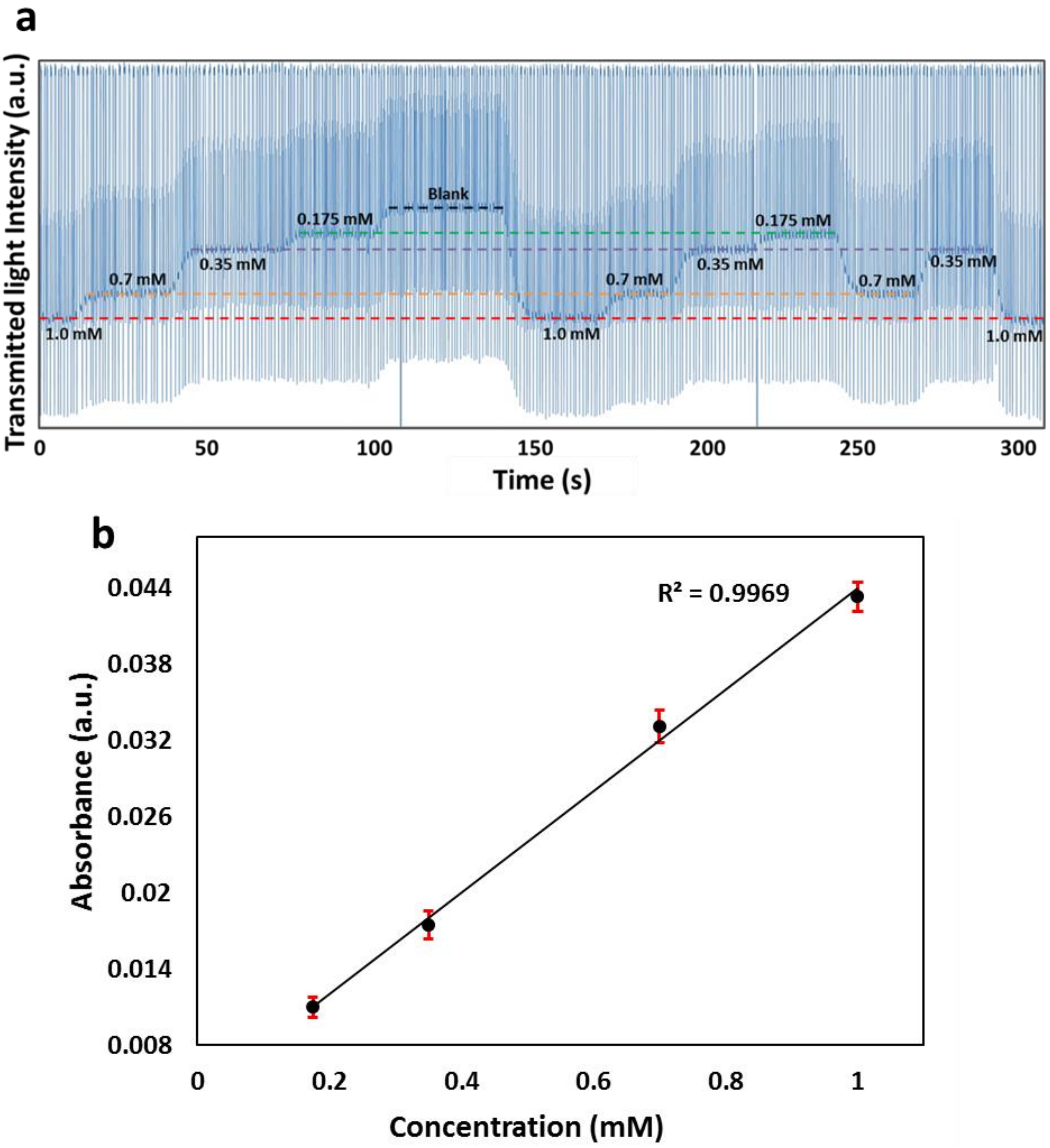

Figure 6.14 Rapid glucose change detection in the flow cell a) Glucose concentrations of 0.175, 0.35, 0.7 and 1.00 mM were injected into the microchip randomly, and the transmitted light intensity signal was recorded. The concentrations were changed by switching the glucose solution inlet tubing without stopping the screw-driven pump. The dotted lines indicate the intensity levels of each specific concentration after switching, b) The linear best fit of absorbance values versus concentration shows that the change in absorbance is linear for all concentrations at a detection time of 21.6 s.

Having calibrated the droplet generation and glucose reaction in droplets, the optical flow cell discussed earlier in this chapter was used for detection of glucose assay droplets. Firstly, the sensitivity of the flow cell was tested by generating droplets of glucose reaction mixture with screw-driven pump and injecting them into the single detector flow cell. One inlet was pumped with reagent mix and the other inlet was pumped with glucose concentrations (0.175, 0.35, 0.7, and 1.0 mM) at room temperature. Blank measurements were also taken by injecting blank in one inlet and reagent mix in another inlet. The concentrations were switched randomly by switching the inlet tubing of the glucose solutions to observe the sensitivity of the detector towards lower glucose values. Droplets travelled through the tubing and entered the flow cell at a time of 21.6 s. The transmitted light intensity was recorded as shown in Fig. 6.14a which clearly shows that a small change in glucose concentration can be quantified with a micromilled version of the cartridge as compared to the 3D printed cartridge shown previously in chapter 5 (the lowest quantifiable concentration was 0.35 mM in 3D printed cartridge). Fig. 6.14b shows calibration curve for absorbance versus concentrations and the absorbance values fit very well with linear best fit (R^2 = 0.9969).

Furthermore, the single detector performance was tested by injecting 4 different glucose concentrations (0.5, 2.5, 5.0, and 15 mM) and the absorbance was measured as shown in a plot in Fig. 6.15a. The absorbance values fitted very well with the polynomial fit (R^2 = 0.9995) at a detection time of 21.6 s. The polynomial curve was then used to determine three “unknown” glucose concentrations (1.5, 4, and 10 mM) from their absorbance values. Droplets of unknown samples were generated at similar conditions and their absorbance values were measured. The experiments were carried out in triplicate, and the recovered concentrations were 1.36, 4.14, and 9.54 mM with a small average error of < 3% (%RSD). These experimental concentrations were plotted against actual concentrations as shown in Fig. 6.15b which illustrates an accurate estimation of the unknown samples.

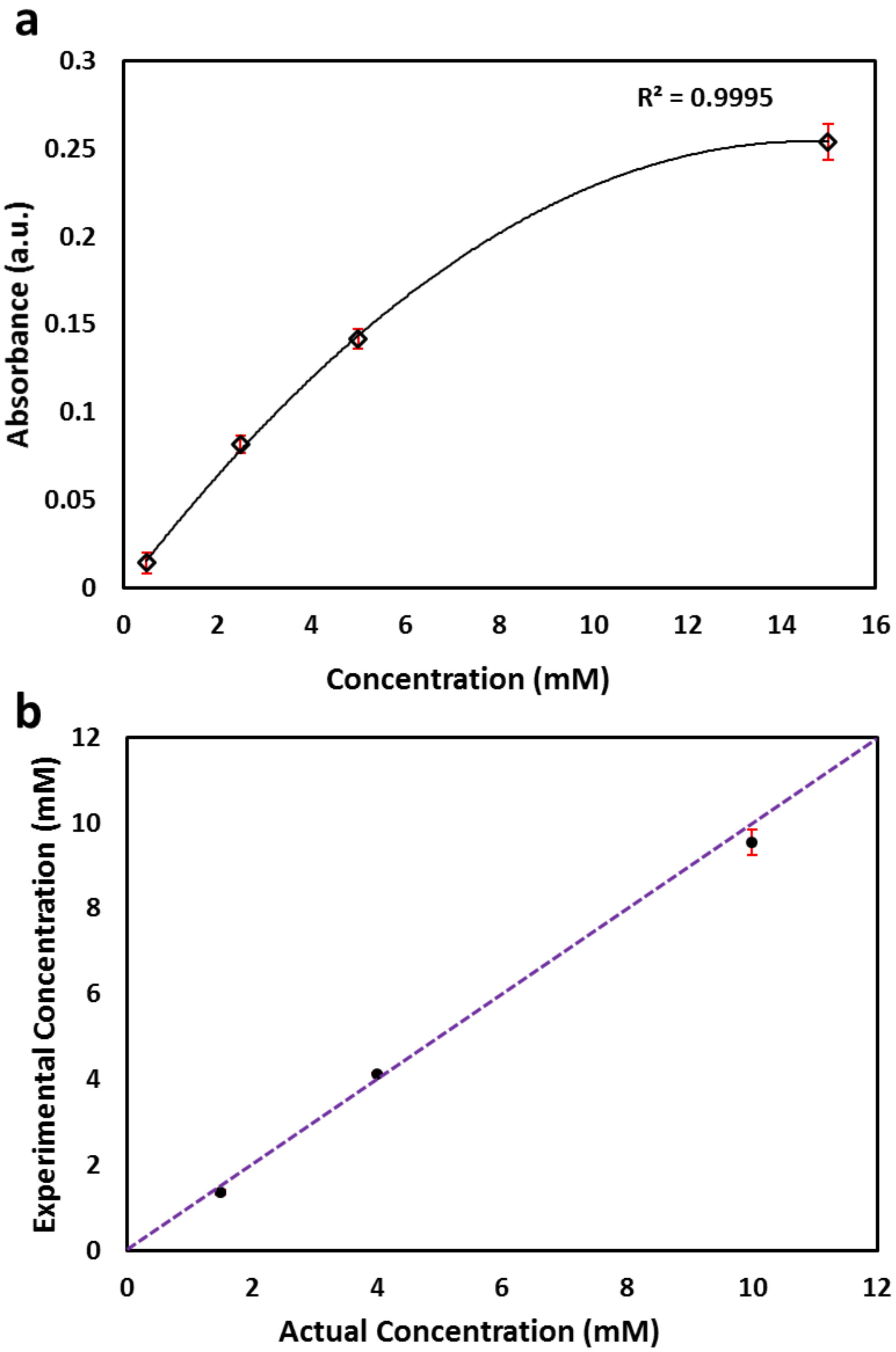

Figure 6.15 Glucose assay in droplets in single detector flow cell a) Polynomial fitted curved showing experimental absorbances versus concentration, b) actual concentrations (1.5, 4, and 10 mM) plot against experimentally recovered concentrations (1.36, 4.14, and 9.54 mM) by polynomial curve fitting method.

Additionally, analogous to the study done by Gielen *et* al. [198] for measuring enzyme kinetics, droplets of different concentrations of glucose (0.9, 1.4, 2.8, 8.0, 14, 25, and 33 mM) were generated in the microchip and passed through the flow cell placed nearer to the chip outlet. The first droplet reached the flow cell at a time lag of 10 s. The pump was stopped, and the droplet flow was switched back and forth continuously for fixed volume (3µL) using a peristaltic pump ((ISM 597, REGLO, ISMATEC). The colour intensity of the droplet changed due to the production of quinoneimine along with time, and the signal was recorded as shown in Fig. 6.16.

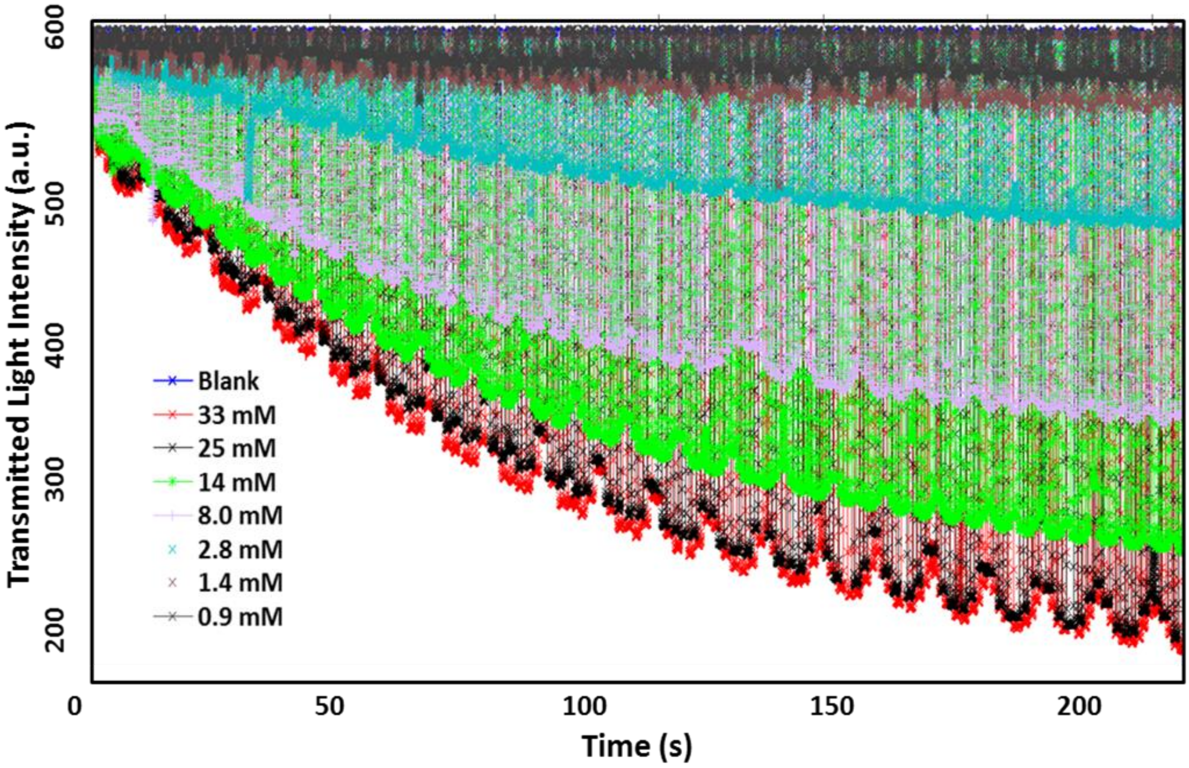

Figure 6.16 Transmitted light intensity plot versus time of different concentrations of glucose (0.9, 1.4, 2.8, 8, 14, 25, 33 mM). The droplets flowed back and forth in a single detector flow cell and the progress of the reaction was monitored.

From the transmission intensity plot (Fig. 6.16), absorbance values were calculated for up to 80 s as shown in Fig. 6.17a. Droplets passed through the tubing and entered the detector at a time lag of 10 s after the initiation of the reaction. The data was fitted with the linear best fit, and the initial rates of reaction were calculated as the slope of the best fit. The initial rates of reaction were then plotted against standard Michaelis-Menten fit (Chapter 5) and achieved a good fit (R^2 = 0.9902) as shown in Fig. 6.17b. From the Michaelis-Menten, V_{max}= 0.00329 a.u./s and K_m= 13.72 mM were calculated.

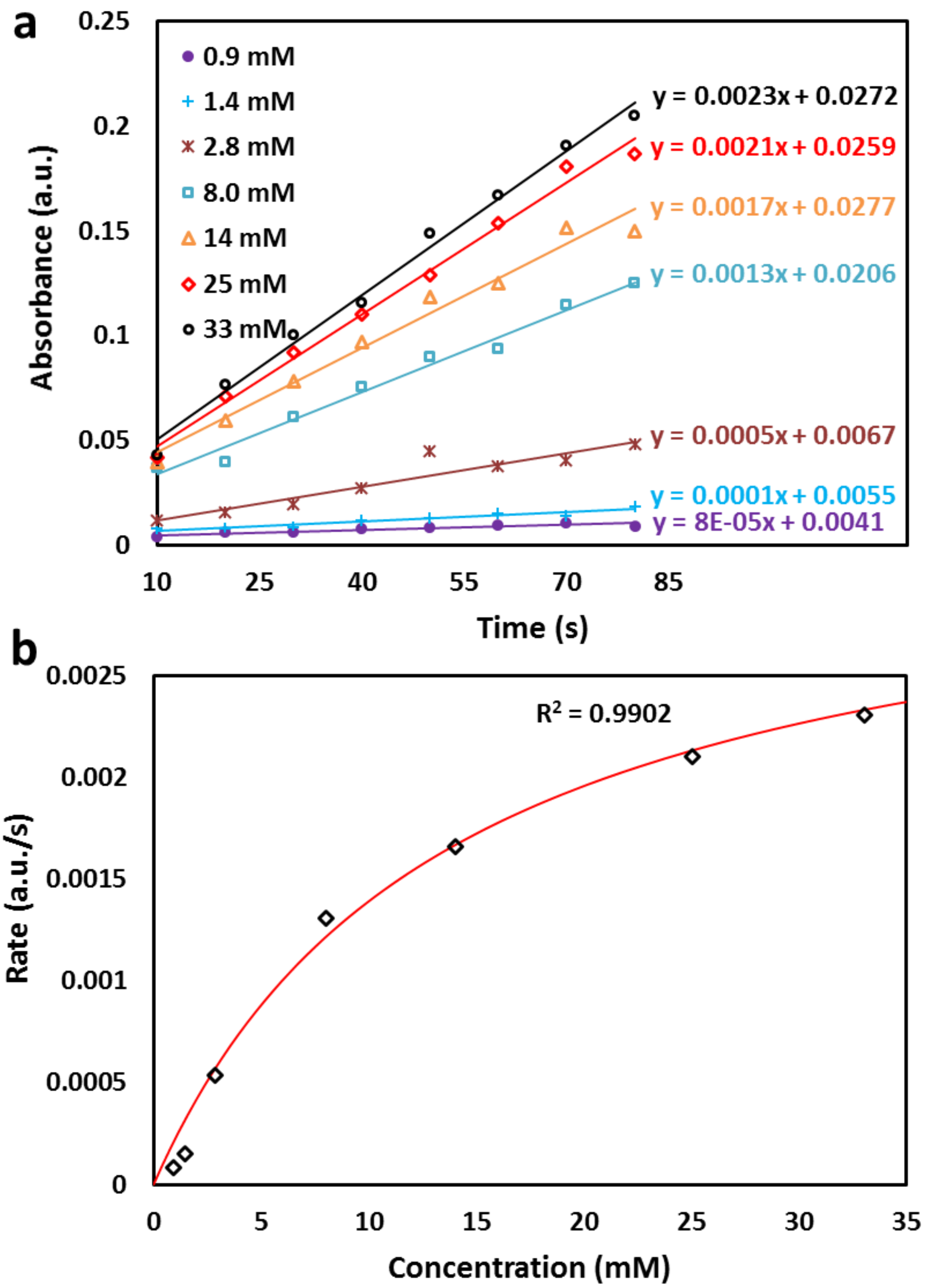

Figure 6.17 Use of the single detector flow cell in measuring absorbances via back and forth oscillation of droplets a) The absorbance of droplets flowing through the flow cell, expressed in relation to the time with a time lag of 10 s, b) The lines of best fit constitute the initial reaction rate and are shown plotted against the glucose concentration. The data is fitted by nonlinear regression with a Michaelis-Menten curve generating V_{max}= 0.00329 a.u./s and K_m= 13.72 mM.

Having calibrated the single detector with glucose reaction droplets, a multi-detector (4 detectors) flow cell was used to determine glucose concentrations via Trinder's assay (see chapter 5 for more details). Droplets of different concentrations of glucose (0.5, 2.5, 5, 15 mM) were generated and flowed through the multi-detector flow cell. The droplets passed through the consecutive detectors at times of 6.9, 11.8, 16.7 and 21.6 s and the absorbance was measured as shown in Fig. 6.18a.

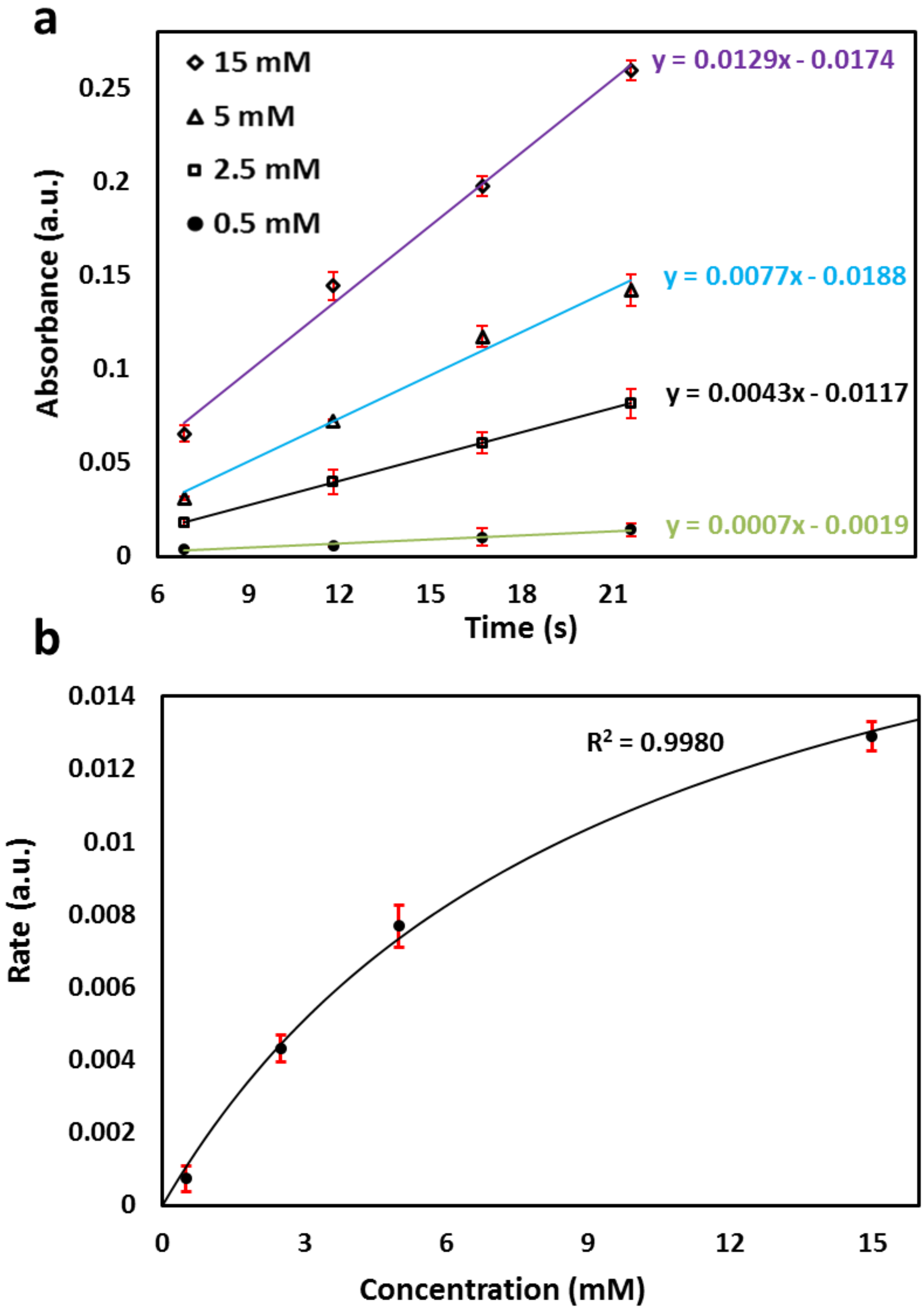

Figure 6.18 Glucose assay in the multi-detector flow cell a) Droplets of different concentrations of glucose (0.5, 2.5, 5.0, and 15mM) were produced, and absorbance was measured for 4 detectors at times of 6.9, 11.8, 16.7 and 21.6s, b) Michaelis-Menten curve showing experimental data against Michaelis-Menten fit. The Michaelis-Menten parameters V_{max} and K_m were calculated to be 0.019 a.u./s and 10.92 mM respectively.

Absorption increased linearly over the first 25 s, with the gradient of the line-of-best-fit giving the initial reaction rate (coloured quinoneimine). The initial rates of reaction were then plotted against standard Michaelis-Menten fit and achieved a good fit (R^2 > 99%) as shown in Fig. 6.18b. From the Michaelis-Menten, V_{max}= 0.019 a.u./s and K_m= 10.92 mM were calculated.

Furthermore, the Michaelis-Menten equation (Eq. 11) was used to calculate the concentrations of unknown glucose solutions (1.5, 4, and 10 mM). The droplets of unknown glucose concentrations were flowed through the flow cell and using V_{max} and K_m values obtained from the Michaelis fit, the unknown concentrations were calculated. The experimental values calculated were in good agreement with actual values as shown in Fig. 6.19.

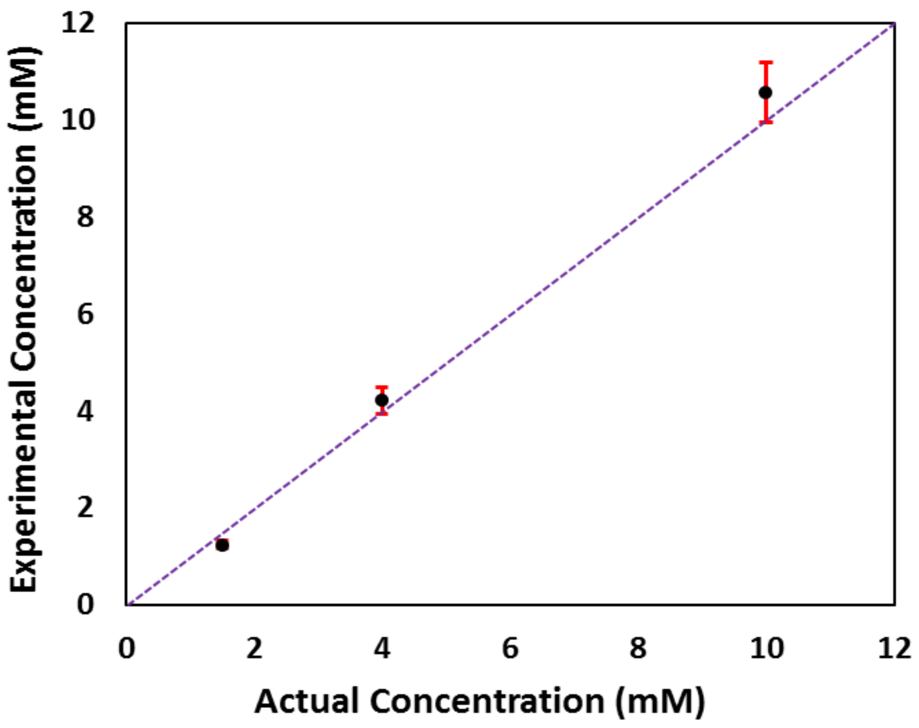

Figure 6.19 Actual concentrations (1.5, 4, and 10 mM) plot against experimentally recovered concentrations (1.19, 4.42, and 11.3 mM) by Michaelis-Menten method.

After the characterisation of the 4-detector flow cell, the device was used for in-vitro measurement of glucose samples via microdialysis probe. Firstly, the device was calibrated using different concentrations of glucose (1.0, 5.0, and 15 mM) by injecting glucose solutions into the dialysate pumping line and the absorbances were measured using aforementioned 4-detector flow cell (Fig. 6.20a). Michaelis-Menten curve fitting described previously was used to obtain V_{max} and K_m (Fig. 6.20b) which were found to be 0.0105 and = 15.91. It is important to run the calibration before microdialysis experiments because V_{max} and K_m values can be slightly different depending on the actual flow rate, temperature and enzyme activity change over the storage time.

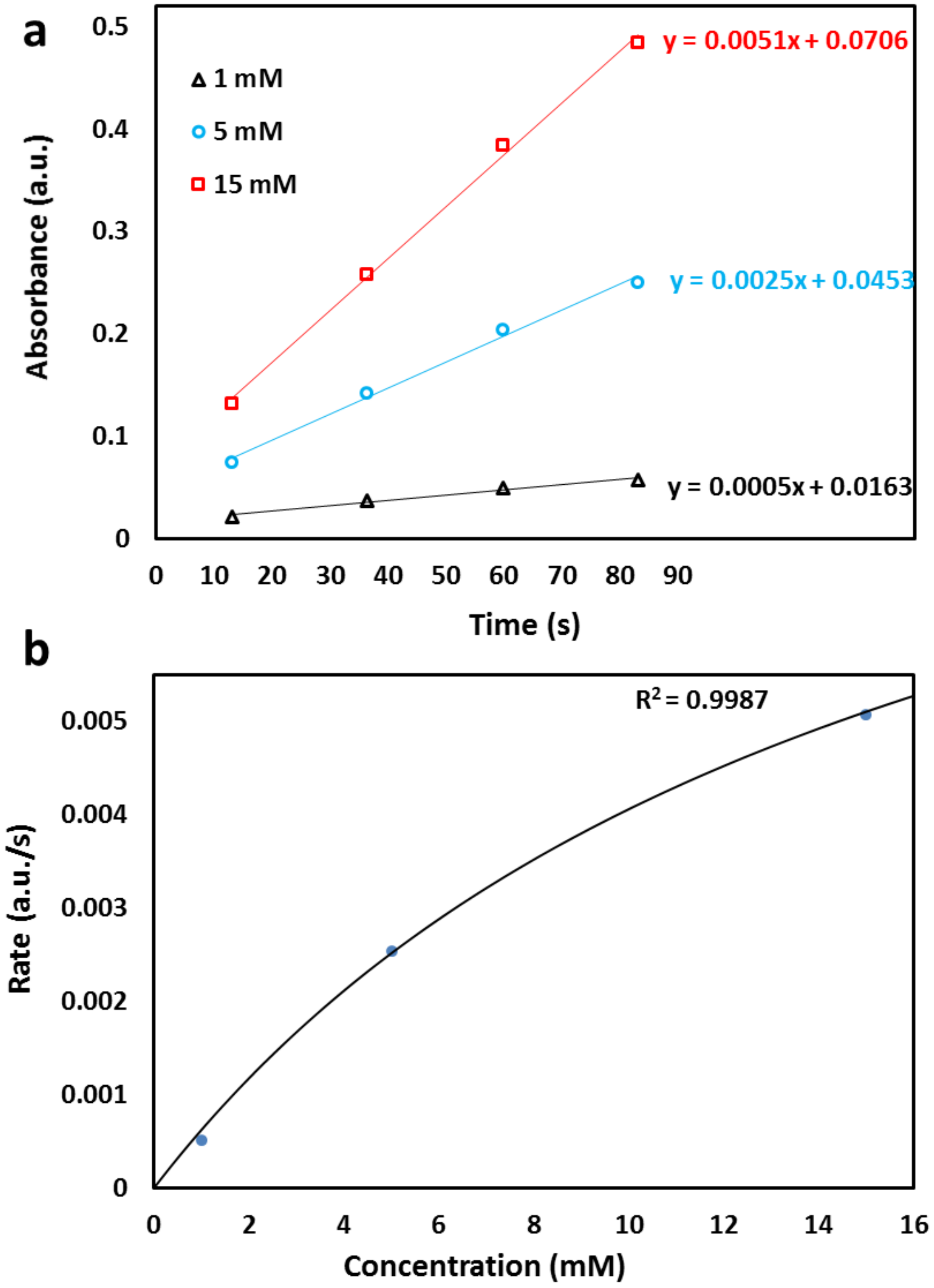

Figure 6.20 Calibration of the glucose concentrations 4-detector flow cell a) Absorbances measured for three concentrations of glucose to calculate initial rates of reaction, b) Michaelis-Menten fit to obtain V_{max} (0.0105 a.u./s) and K_m (15.91 mM) before running microdialysis experiments.

The microdialysis probe (20 KDa cut off, CMA 12) attached to the device was placed in a solution of 10 mM glucose, and the perfusate was pumped through the microdialysis probe. The dialysate was collected from the outlet in the T-junction chip and was separated into droplets. These droplets then flowed through the flow cell and absorbances were measured as shown in Fig. 6.21a.

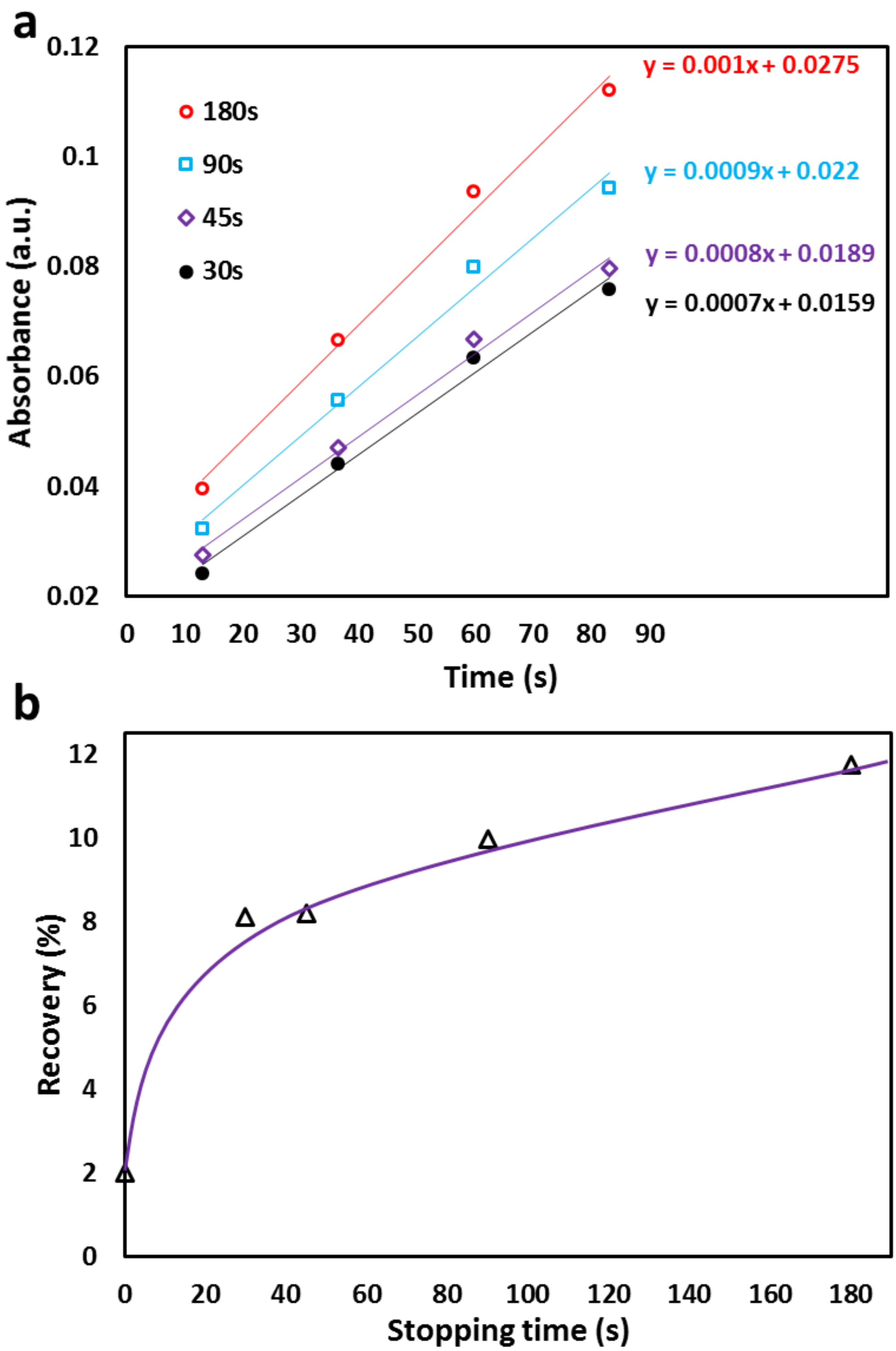

Figure 6.21 Glucose recovery rate experiments via microdialysis probe in vitro a) Absorbances of the glucose recovered from the probe at varying pump stopping time. The pump was stopped for different times (30, 45, 90, and 180s) to increase the diffusion of glucose molecules in the probe, b) Recovery rate versus pump stopping time indicates the recovery increases with increase in stopping time of the pump.

The flow rate was kept constant throughout all experiments (2.8 µl/min) so that droplets of all concentrations and dialysate reached at similar times to the detector. Michaelis-Menten equation (Eq. 11) was used to calculate the recovered glucose concentrations from the dialysate. The recovery rate was calculated to be 2% at a flow rate of 2.8 µL/min. This recovery rate was lower as compared to previously reported values [219]. The low recovery rate of glucose can possibly be attributed to the longer dialysate tubing length (20 cm for initial experiments) and can be increased by reducing it. Also, the flow rate of the oil can be increased to pass the droplets from the detector at shorter times (i.e. less than 60 s). Fig. 6.21a shows the absorbances measured for 10 mM glucose solution. The pump was stopped to increase the diffusion rate of glucose molecules into the probe for times of 30, 45, 90, and 180s, and the recovered glucose concentrations were 1.215, 1.230, 1.450, and 1.761 mM respectively. The recovery rates were calculated to be 8.10, 8.20, 9.96 and 11.74% as shown in Fig. 6.21b.

6.4.4 Lactate Enzymatic Assay in Continuous Chemical Sensing Device

Colorimetric assay of lactate like glucose is also mostly done in a spectrophotometer by using enzymatic reaction as shown in Table 5.1. Lactate oxidase, HRP, 4-aminoantipyrine, 4-chlorophenol and phosphate buffered saline (PBS) were prepared in 0.1 M PIPES buffer at pH of 6.8. The reagents were mixed such that the final reagent mixture consisted of lactate oxidase (2.5 U/mL), HRP (2.5 U/mL), 4-aminoantipyrine (0.4 mM) and 4-chlorophenol (5.4 mM).

Bulk experiments of lactate assay were performed in a petri dish. Briefly, 25 uL of sample reagents (lactate oxidase, HRP, 4-aminoantipyrine, and 4-chlorophenol) and 25 uL of lactate sample (2 mM) were mixed in a petri dish, and the reaction was recorded with the coloured camera at different times as shown in Fig. 6.22a. The recorded images were analysed by imageJ software to measure the intensity of the coloured product formed, and the intensity was then plotted against time as shown in Fig. 6.22b. The graph indicates that the intensity of lactate enzymatic reaction linearly increases for up to 100 seconds.

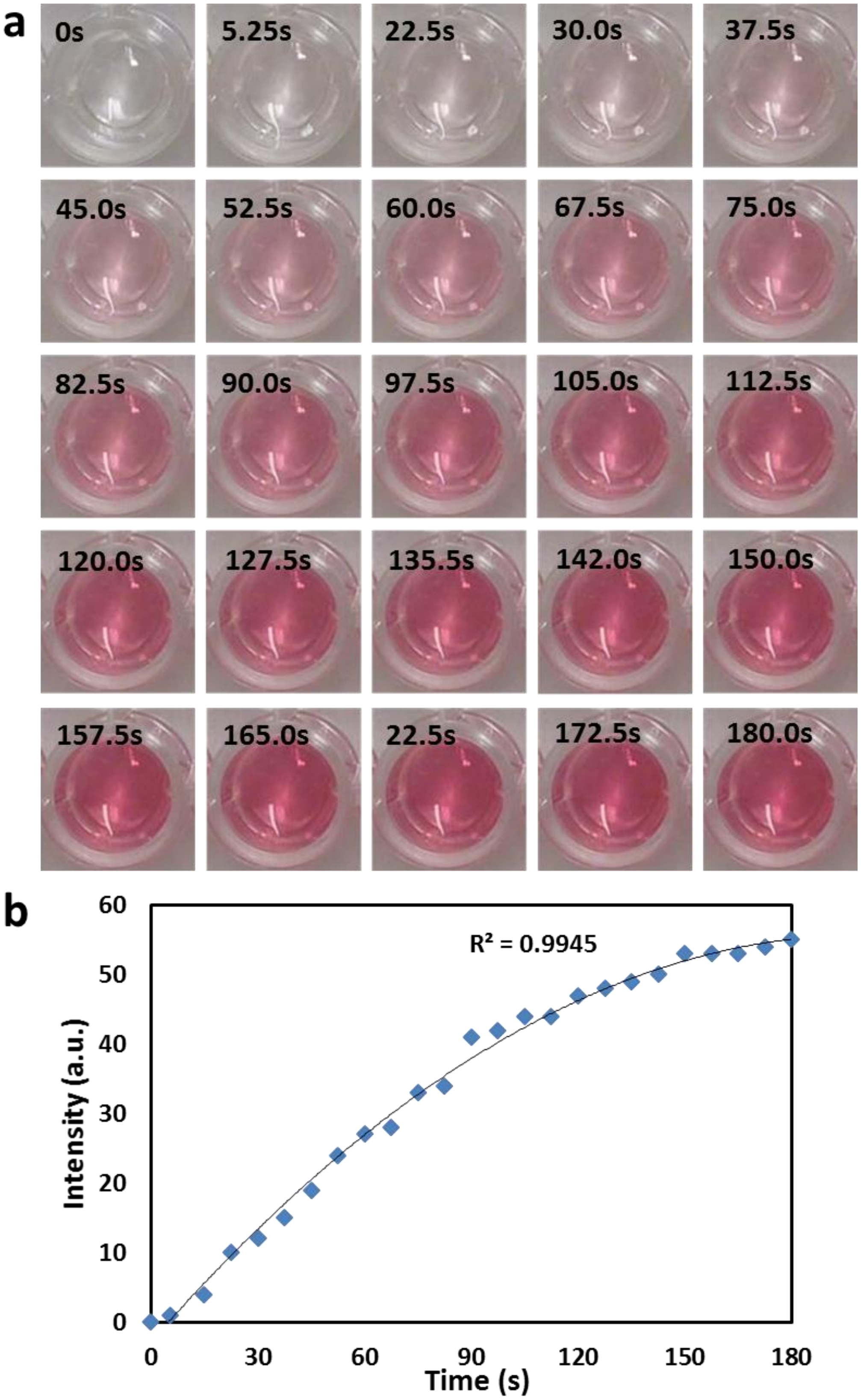

Figure 6.22 Lactate enzymatic reaction in a petri dish a) Lactate assay reagents and lactate sample (2 mM) were mixed in a petri dish, and the reaction was monitored by taking snapshots at different time intervals for 0s to 180s, b) Time versus intensity of reaction measured by imageJ at each time point. The polynomial best-fit line shows the increase in colour intensity is no linear after 100s.

Following the calibration of the lactate reaction in a petri dish, droplets composed of a Lactate sample and reagents were generated in a T-junction chip using FC-40 with 0.35% surfactant. The reagents and sample were mixed in a 1:1 ratio in microchip and the droplets of lactate reaction mixture flowed through the single detector flow cell (micromilled version). Four different lactate concentrations (0.1, 1.0, 2.5, and 5 mM) were injected into the microchip, and the droplets were generated (Chapter 5). These droplets flowed through the flow cell and the absorbances were measured as shown in a plot in Fig. 6.23.

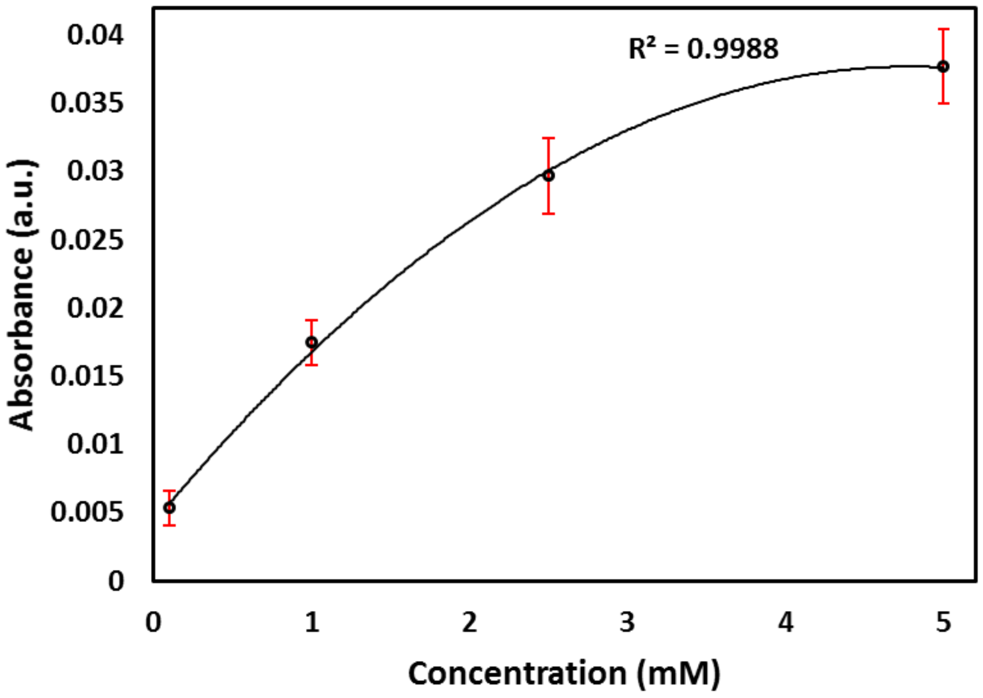

Figure 6.23 Lactate assay in droplets in s single detector flow cell showing polynomial fitted curve of experimental absorbances versus concentration.

The absorbance values fitted very well with the polynomial fit ($R^2 = 0.9988$) at a detection time of 2.2 min. The experiments were carried out in triplicate, and the %RSD was found to be < 10%. These absorbance values were found approx. 15 times lower than glucose values measured (Fig. 6.15a). Also, the reaction was found slower as compared to petri dish calibrations (10 times) because the colour intensity change was very small. Therefore, a time of 2.2 min was found to be the shortest time to detect intensity change in droplets for lowest concentration (0.1 mM). It was also observed that the intensity of droplets started to increase at a much faster rate upon exiting the tubing and therefore, suggests that there might be the supply of oxygen is limited inside the tubing (these observations are not quantified in the current work).

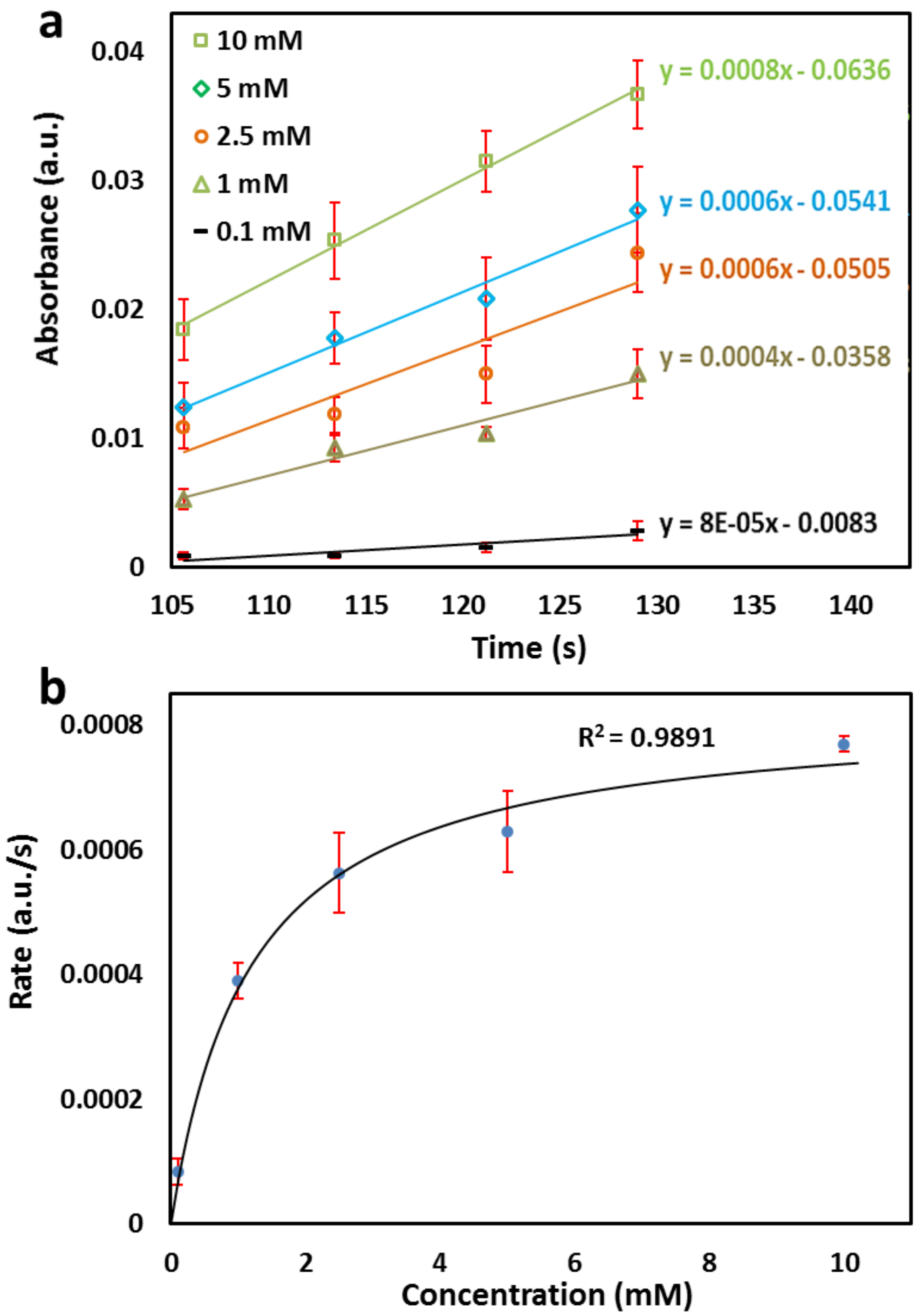

Figure 6.24 Lactate assay in 4-detector flow cell a) Droplets of different concentrations of glucose (0.1, 1.0, 2.5, 5.0, and 10 mM) were produced, and absorbance was measured for 4 detectors at times of 105.6, 113.4, 121.2, and 129.0s, b) Michaelis-Menten curve showing experimental data against Michaelis-Menten fit. The Michaelis-Menten parameters V_{max} and K_m were calculated to be 0.00549 a.u./s and 11.07 mM respectively.

Following the calibration of the single detector with lactate reaction droplets, a 4-detector flow cell was used to investigate enzyme kinetics of lactate assay. Droplets of different concentrations of lactate (0.1, 1.0, 2.5, 5, and 10 mM) were generated and flowed through the flow cell. The droplets passed through the detectors (1-4) at times of 105.6, 113.4, 121.2, and 129.0 s respectively and the absorbances were measured as shown in Fig. 6.24a. Absorption increased linearly, with the gradient of the line-of-best-fit giving the initial reaction rate. The absorbance values were measured 3 times with the relative standard deviation of 9.6% (%RSD). The initial rates of reaction were then plotted against standard Michaelis-Menten fit and achieved a good fit ($R^2 > 0.989$) as shown in Fig. 6.24b. From the Michaelis-Menten curve, were V_{max} = 0.00549 a.u./s and K_m = 11.07 mM were calculated. Each experiment was repeated 3 times with an overall %RSD of 10.8%.

6.5 Conclusions

In this chapter, the development of a droplet-based continuous chemical sensing device has been described for quantification of metabolic changes in body tissues such as changes in concentrations of glucose and lactate. The newly developed screw-driven pump has been utilised to generate droplets of reagents and sample (glucose and lactate) and flow them through the multi-detector flow cell. The flow cell has been upgraded via fabrication of precise micromilling of the cartridge and successfully applied to glucose and lactate analysis and determination of unknown samples using Michaelis-Menten kinetics. The screw-driven pump and flow cell were made of low-cost components and can be integrated into portable or even wearable point-of-care applications. Continuous chemical sensing device allows the continuous generation and detection of sample droplets making it suitable for portable and real-time detection of biomolecules for clinical applications.

Chapter 7 Optical Flow Cell for Measuring Size, Velocity and Composition of Flowing Droplet

The first part of the Chapter highlights key methods for measuring size and velocity of droplets. The second part introduces the newly developed flow cell for measuring size, velocity and composition of droplets in a continuous flow and describes fabrication, working principle of the device and experimental results.

7.1 Introduction

The accurate and precise measurement of flow rates is crucial for high throughput applications such as flow cytometry, particle counting, enzyme kinetics and cell sorting. [233]. In droplet-based microfluidics, droplets travelling in the microchannels require detection of droplet position, size, and velocity for real-time manipulation. For example, several studies have explored enzyme kinetics in continuous droplet stream using multi-point detection [234], [235] and rely on accurate measurement of velocity and droplet size. Any fluctuation of flow rate could affect the characterization of the rates of reaction which is detrimental to the accurate measurement of Michaelis-Menten kinetics.

Electrical and optical detection are most common methods for detection of droplets. Electrical method of droplet detection involves the detection of contrast present between oil and aqueous droplet due to the differences in their electrical properties. Electrochemical and capacitive based detection methods have been used widely. Electrochemical detections work on the principle of interaction between analytes and electrodes while capacitive sensing works via detecting the change in capacitance between two electrodes produced by the changing dielectric constant from oil and water.

Electrochemical detections only distinguish analytes which are electroactive [45], and the electrodes require frequent calibrations after short intervals because of the electrodes prone to changes in pH, ionic concentration and temperature [44]–[47]. Moreover, electrochemical detection requires droplets to be in contact with the electrodes, but a thin oil layer can separate the droplet from the electrode and limits the signal. Droplets can be wetted on the surface of the electrode but the wetting can lead to contamination of the sample between the droplets [48]. On the other hand, capacitive detections offer the detection of droplets without the requirement of contacting the electrodes.

Several capacitance-based detectors have been developed for detection of droplet position, size and velocity [48], [236]–[240]. For example, Chen *et al*. [238] developed the miniaturized capacitance-based sensor for detection of droplet position, size, composition and percentage water uptake for hygroscopic liquids. Elbuken *et al*. [48] presented capacitance based system for detecting the presence, size and speed of droplets using commercially available inexpensive capacitive sensors. Niu *et al*. [237] reported the design and implementation of capacitive detection and control of droplets using integrated microfluidic and control circuits to monitor *in situ* the volume, velocity and even composition of the droplet.

Optical detection methods have been developed to analyse size and velocity of droplets mostly based on the analysis of videos recorded by high-speed camera. This approach demands higher specification hardware when analysing the frames from the high-speed videos, and limits the recording time of videos due to data storage capacities. As a result, it is not applicable for portable and real-time detection of droplets due to the requirement of the stationary microchip, camera and further processing of the data [241]. Several other optical methods have been reported to overcome these challenges such as Jakiela *et al*. [242] reduced data storage requirement and performed real-time detection of droplet velocity and size by imaging the centre line of the microchannel. Revellin *et al*. [243] used two fibres at a fixed distance and photodiodes on the opposite sides to measure the mean velocity and length of the slugs (gas bubbles). Similarly, Vincent *et al*. [241] developed an optical detector using two photodiodes to measure the velocity, length, and frequency of droplets. The real-time measurement of droplet characteristics was performed by collecting a differential signal from illumination observed during the passage of droplet. Apart from the illumination, Doppler-based optical method [233] has also been developed to detect the flow velocities of the droplet flow. The authors detected the Doppler shift from the scattered light while the droplet passed through illumination source.

However, the above-mentioned systems were bulkier and had not been miniaturized for portable systems. Here an optical flow cell with two light paths is reported that can accurately quantify the size and velocity of droplets flowing through microchannels. The flow cell operates by measuring the time taken for droplets to pass between and through two conjoined probe light paths and is analogous to a previously reported capacitive-based device [237]. By implementing in an optical system, however, the composition of the droplet can also be accurately quantified via absorption spectroscopy. The device has a small footprint and uses low-powered, low-cost components, which make it ideally suited for use in field-deployable and portable analytical devices.

7.2 Design and Working Principle of Dual Light Path Flow Cell

The miniaturised flow cell with dual light paths was designed using SolidWorks and printed in black PLA material using an Ultimaker-2 3D printer. A 3D schematic of the flow cell is shown in Fig. 7.1. The flow cell consists of two interlocking structures, a cartridge, and a detection cell. The cartridge is composed of two interlocking micromilled PMMA pieces with a channel cut into one piece to hold 0.5 mm OD tubing. The detection cell houses the cartridge, LED, and photodiodes. Once fully assembled, the flow cell measures only 10 x 10 x 15 mm, therefore, it can be easily accommodated within a field-deployable POC device.

Light emitted from an LED shines on the droplets in a tubing, and transmitted light reaches photodiode as previously discussed in chapter 5. As shown in Fig. 7.1, two holes with 0.2 mm ID were micromilled in the cartridge via precise micromilling and aligned (see chapter 5 for more details) and a distance between two holes was fixed to 0.5 mm (centre-to-centre distance = L). The voltage readout from each photodiode was collected using a microcontroller (Arduino Nano) which relayed the information in real-time to a computer, where the data was recorded using LabVIEW (Appendix 2.1).

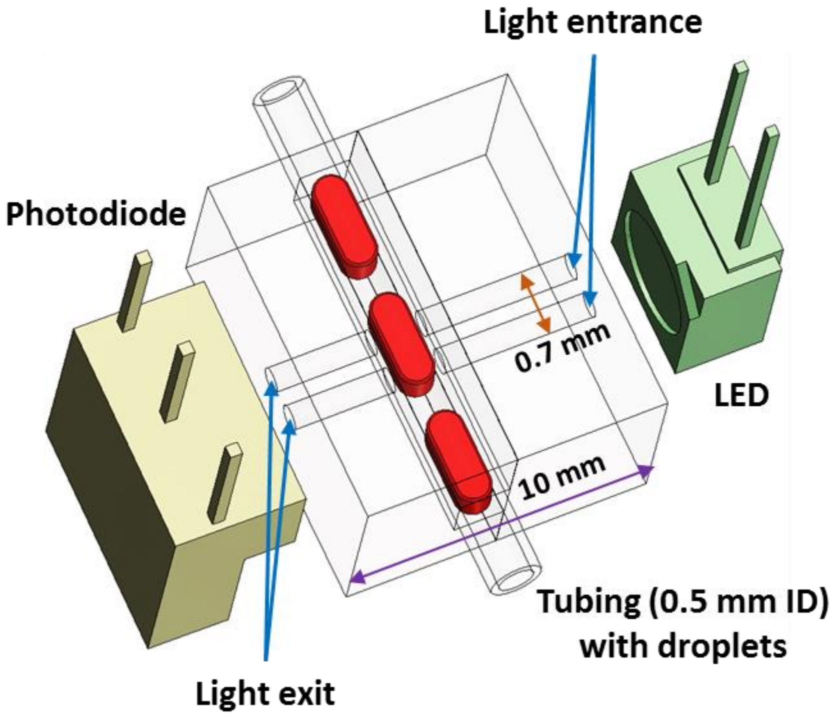

Figure 7.1 3D schematic of the flow cell with dual light paths showing the cartridge which holds the tubing, LED, and photodiode. The holes (0.2 mm) were precisely micromilled and aligned visa alignments pins.

The working principle of the flow cell is shown in Fig. 7.2. The transmitted light measured by the photodiode clearly shows when a droplet enters ($t_1 \rightarrow t_2$, $t_3 \rightarrow t_4$) and exits ($t_5 \rightarrow t_6$, $t_7 \rightarrow t_8$) each separate light path. As each droplet enters the light path, the transmitted light intensity drops from a higher value (corresponding to light passing through the carrier oil) to a lower value ($t_1 \rightarrow t_2$) as shown in Fig. 7.2a. The intensity value of the droplet stays constant ($t_2 \rightarrow t_3$) and further drops when the droplet passes through the second light path ($t_3 \rightarrow t_4$). The droplet intensity level stays the same while droplet remains under both light paths ($t_4 \rightarrow t_5$). Similarly, the intensity level increases when droplet exits the first light path ($t_5 \rightarrow t_6$), stays constant ($t_6 \rightarrow t_7$) and returns to its initial high level when droplet exits both light paths ($t_7 \rightarrow t_8$). Defining Δt as the time taken by a droplet to travel between two light paths, L as a distance between two light paths and Δt_L as the time requiredfor a droplet to pass through a light path (see Fig. 7.2b), thus the velocity, v of the droplet is given by $L/\Delta t$ and the droplet length by $v\Delta t_L$. Similarly, $L/\Delta t'$ and $v\Delta t_L'$ are also used to measure the velocity and size of the droplet respectively.

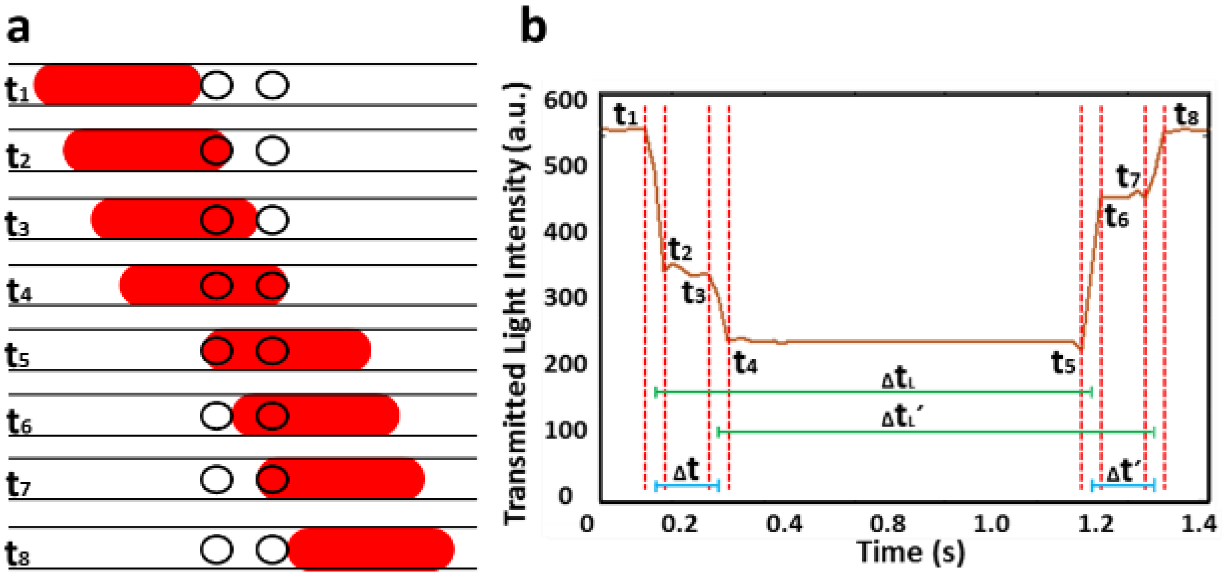

Figure 7.2 Working principle of flow cell with dual light paths a) Schematic of the device, b) plot of transmitted light intensity over time as droplet travels through the holes. The times $t_1 \rightarrow t_8$ relate to the moment when droplet enters and exits the holes.

7.3 Experimental Results and Discussions

I initially characterised the distance between the holes (L=0.3, 0.4, 0.5, and 0.6 mm) in the cartridge by flowing droplets of red food dye at fixed flow rate and droplet length as shown in Fig. 7.3. It can be seen from the intensity signal that Δt decreases with a decrease in L values at a fixed flow rate. Noted the droplet intensity for entering and exiting the light path was not equal which can be attributed to the slight misalignment of the 0.2 mm holes or the position of the holes in reference to the photodiode. Nonetheless, this difference in intensity level is less important in accurately measuring the size and velocity of the droplets.

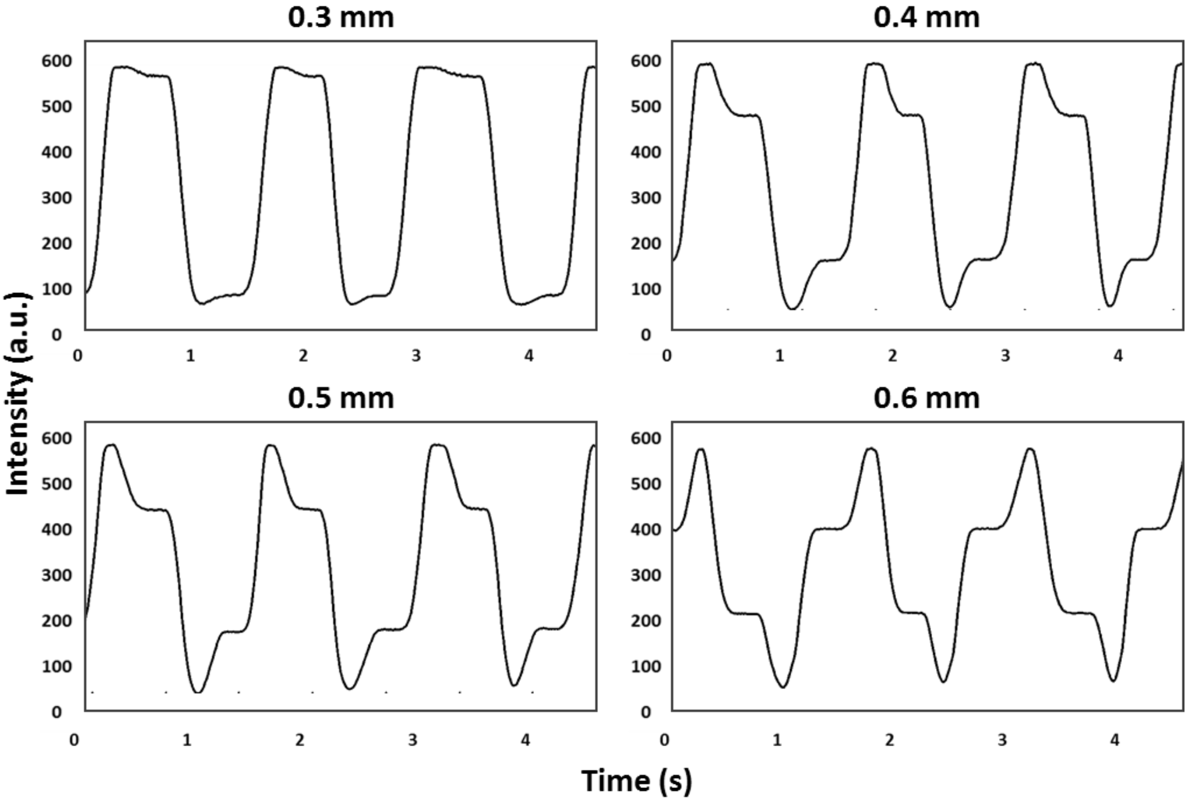

Figure 7.3 The graphs showing a drop in intensity levels during the passage of droplets (Droplet velocity and length were 1.65 mm/s and 0.94 mm respectively) from light paths of different distances (L=0.3, 0.4, 0.5, and 0.6 mm).

Droplet velocity (1.65 mm/s) and length (0.94 mm) were measured from the intensity plots shown in Fig. 7.3. The %RSD of droplet velocity and length for each L value was found to be 3 and 4% respectively. This low error proves that the velocity and length of droplets do not change with change in L values, but the L value of 0.3 mm was found to be too small to observe clearly the sharp drop in intensity. Hence, in later experiments, the L value of 0.5 mm was used.

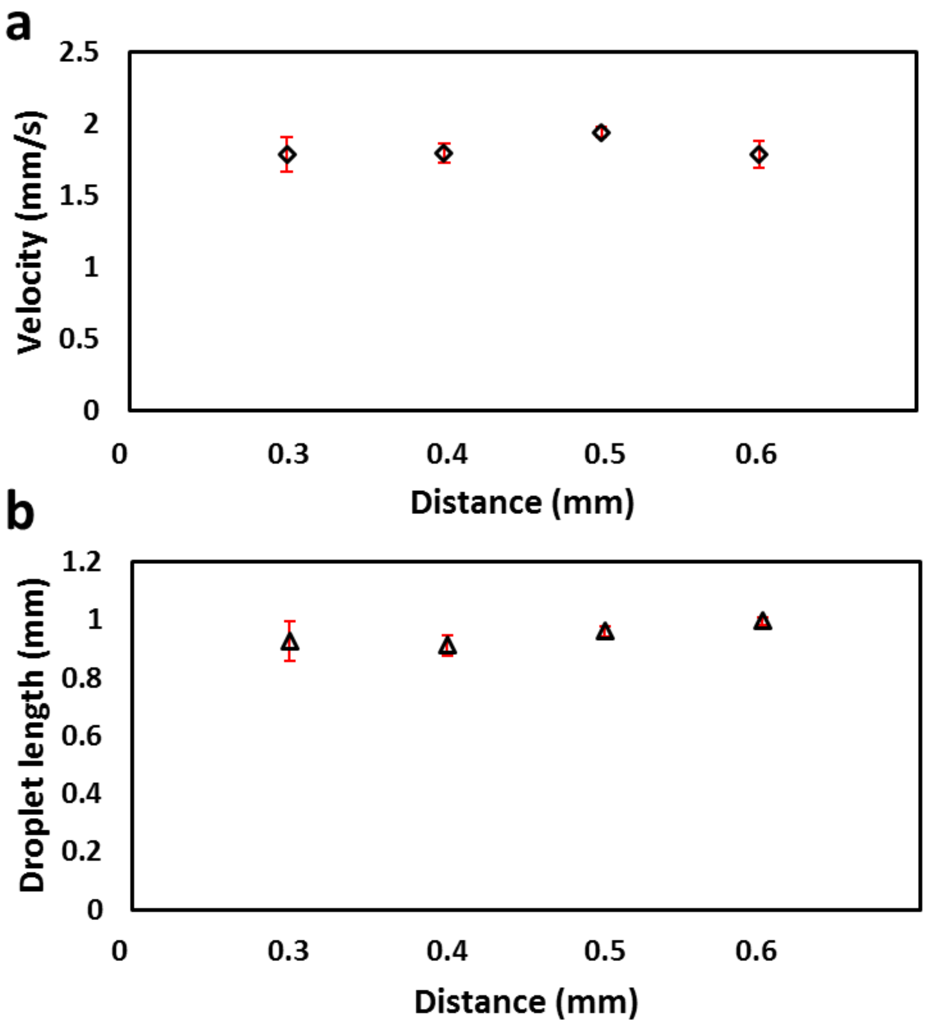

Figure 7.4 Droplet velocity and length measurements in dual light paths with different distances (L=0.3, 0.4, 0.5, and 0.6 mm) a) Velocity measured by flow cell with a dual light path using different L values, b) Droplet length measured by the sensor using different L values. Both droplet velocity (1.65 mm/s) and length (0.94 mm) were measured to be similar with %RSD values of 3 and 4% respectively.

To observe the shape of the peak intensity change, droplets of different velocities (0.6, 1.2, 1.8, 3.0, 3.9, and 5.1 mm/s) were flowed through the flow cell and the intensity plots were drawn as shown in Fig. 7.5. It clearly shows that as the velocity increases, the number of droplets passing through the flow cell also increases but the droplet retains its shape. Hence, the flow cell can be used for variety of velocities between 0.6-5.1 mm/s. These values can be improved by decreasing the sampling time of the processor (Arduino Nano was used in this experiment with sampling time of 100 ms).

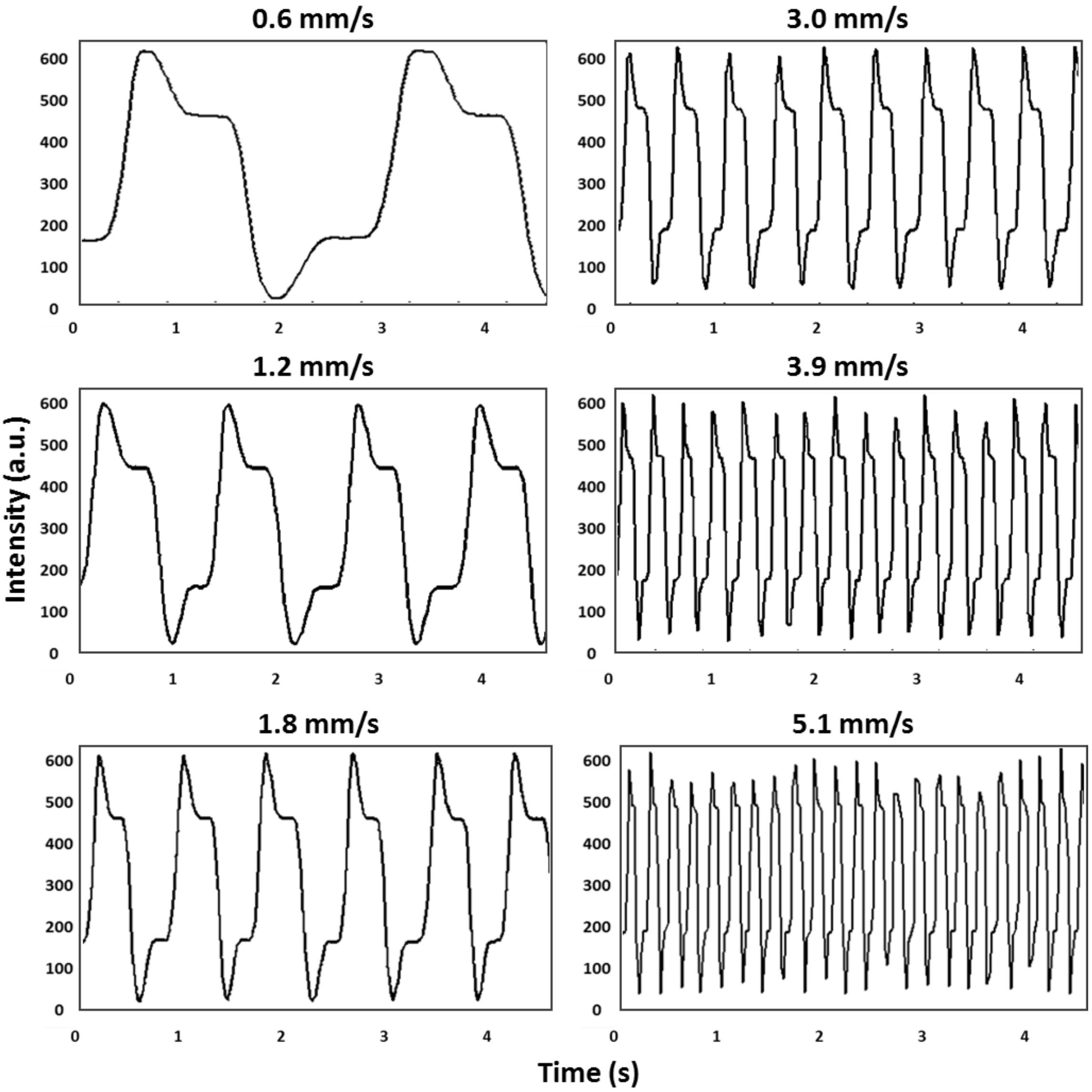

Figure 7.5 Droplet velocity measurement in dual light paths flow cell with different velocities (0.6, 1.2, 1.8, 3.0, 3.9, and 5.1 mm/s). The distance between light paths was 0.5 mm.

To test the performance of the flow cell, droplets of different velocities (0.77, 0.99, 1.12, 1.32, 1.62, 1.74, 2.95, 3.68, 4.13, and 5.44 mm/s) and lengths (1.10, 1.53, 1.94, 2.82, 3.85, 5.51, and 7.90 mm) were generated, measured using the flow cell and then compared with actual values obtained from recorded videos. As shown in Fig. 7.6, there was excellent agreement between the two methods, with errors for the optical flow cell relative to the video results of < 6 % for droplet velocity and < 5% for droplet size.

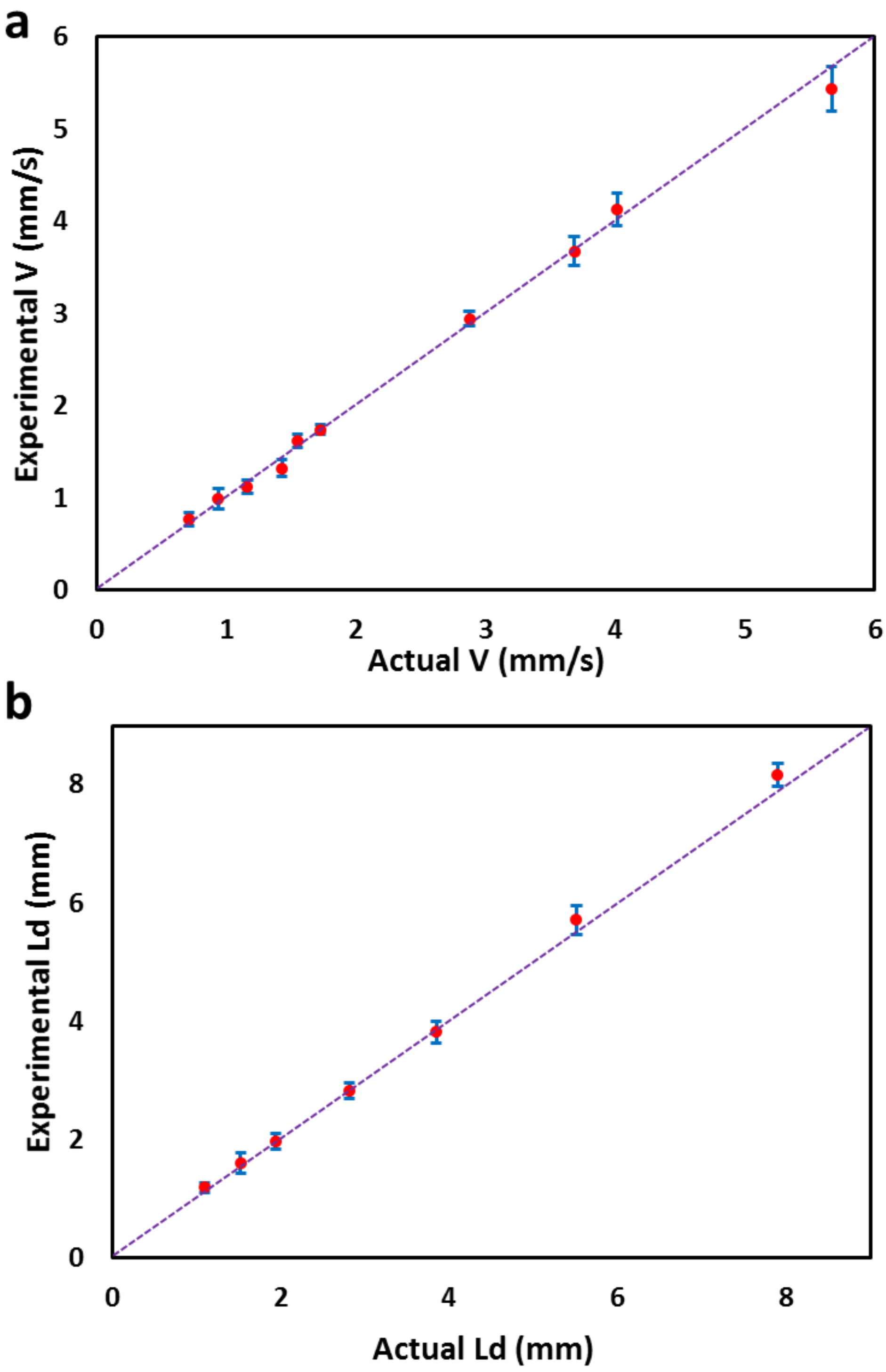

Figure 7.6 Droplet velocity and length measurements a) Experimental velocity vs. actual velocity, b) Experimental droplet length vs. actual droplet length. The dotted line shows the 1:1 equivalence.

A key advantage of this optical flow cell over other previously reported devices [48], [233], [237], [241] is that it can additionally be used for accurate measurement of droplet composition via absorption spectroscopy. The flow cell was characterised by flowing droplets of red food dye at different concentrations (0.10, 0.25, 0.50, 1.00 and 2.00 mg/mL) through the flow cell and measuring the response as a voltage output from the photodiode. As the dye concentration in the droplets dropped from high to low, the magnitude of the intensity drop also decreased. The absorbance of each concentration of droplets was calculated against a set of blank droplets composed of pure water using the modified Beer-Lambert law (Eq. 9). Each concentration was repeated 3 times and the overall %RSD was found to be ~ 2 %. Fig. 7.7 shows the measured absorbance values versus dye concentration.

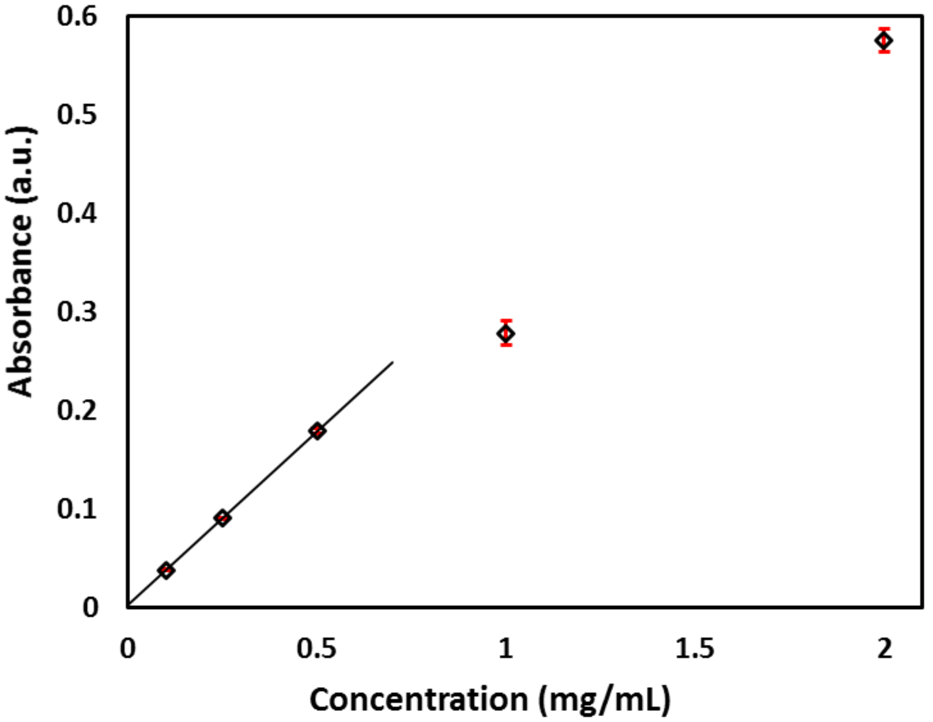

Figure 7.7 Plot of absorbance against droplets containing red food dye concentration (0.10, 0.25, 0.50, 1.00 and 2.00 mg/dL) measured in flow cell with dual light paths. Droplet absorbance against dye concentration. A line of best fit ($R^2 = 0.999$) shows the linear response for absorbance values <0.2.

Having calibrated the flow rate sensor using food dye, a colorimetric assay was implemented to quantify glucose concentrations in sample solutions. Fig. 7.8a shows the schematic of the quantification of the progress of a colorimetric glucose assay over time by placing the flow cell at a set distance (3.8 cm) downstream of a T-junction generating droplets. The droplets composed of 1, 5, and 15 mM glucose and a glucose-specific colorimetric reagents (containing glucose oxidase, HRP, phenol, and 4-aminoantipyrine) were generated in a stream of fluorous oil (Chapter 5). Blank measurements were taken by using 0 concentration glucose solution and used to calculate the absorbance of the glucose-containing droplets. The total flow rate was varied, the linear flow rate was quantified inline using the sensor (found to be 0.77, 1.28, 1.75, 2.17 and 2.85 mm/s) and then used to calculate the reaction times (14, 18, 23, 29, and 36 s). The absorbance was seen to increase linearly with reaction time (Fig. 7.8b) as expected and shows that the flow cell with dual light paths can be utilised for quantitative chemical assaying.

The obtained reaction rates were then plotted against the glucose concentration and fitted with a Michaelis-Menten curve using nonlinear regression, (Fig. 7.8c). The curve fits the data exceptionally well ($R^2 \approx 0.998$) with V_{max} = 0.0068 a.u./s and K_m = 10.77 mM.

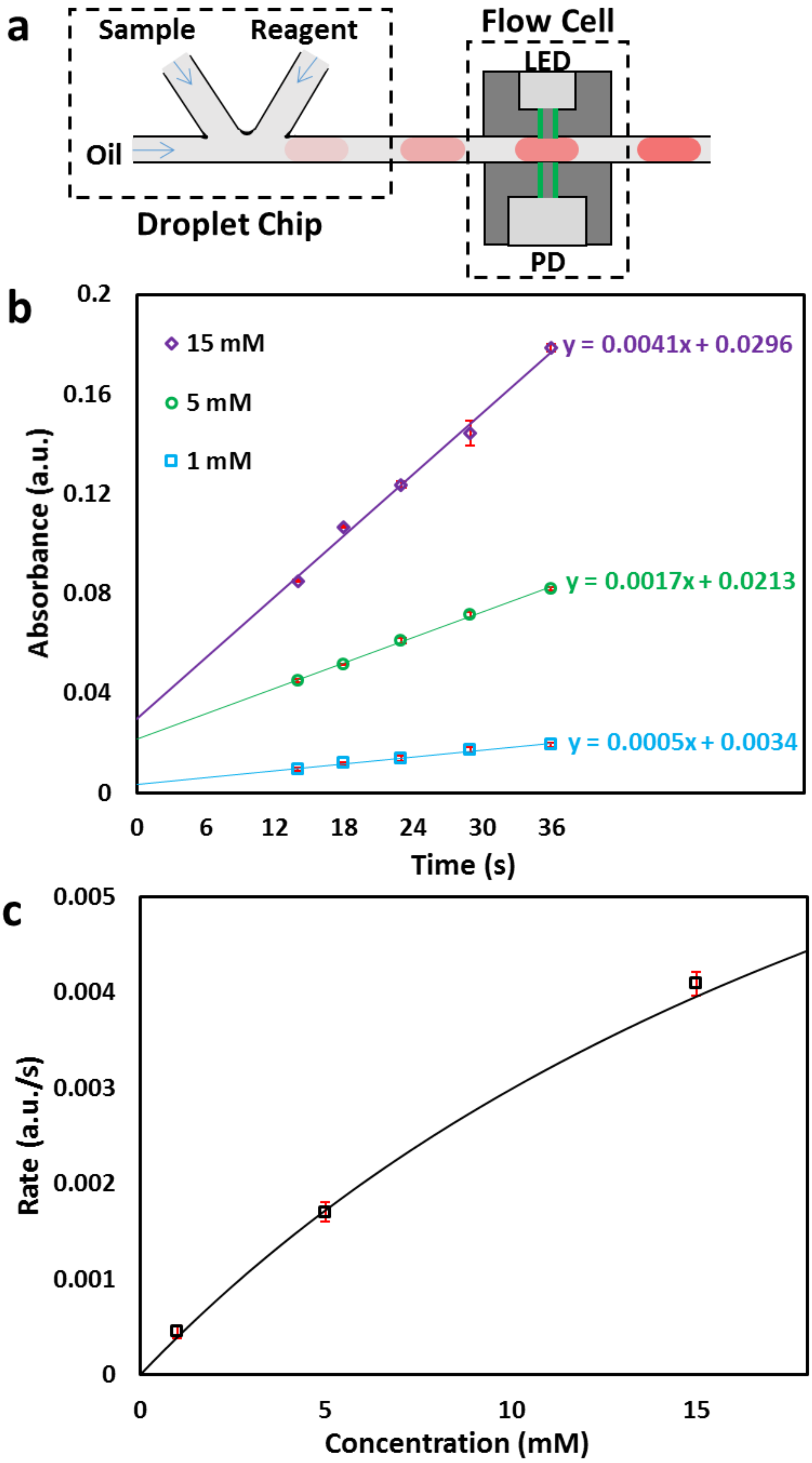

Figure 7.8 Enzymatic glucose reaction in droplets at different velocities a) Schematic of the droplet generation and injection into the flow cell, b) The absorbances of glucose droplets (1, 5, 15 mM) plotted as lines of best fit against time. Each time point corresponds to velocities of 0.77, 1.28, 1.75, 2.17 and 2.85 mm/s at a distance of 3.8 cm, c) The data is fitted by nonlinear regression with a Michaelis–Menten curve. V_{max} = 0.0068 a.u./s and K_m = 10.77 mM.

Furthermore, the rate of reaction of glucose via colorimetric assay was studied in flow cell attached to an absorbance detector (Fig. 7.9a-b). In this experiment, droplets flowed through the device at four different velocities (0.202, 0.375, 0.845 and 1.271 mm/s). Absorbances were measured at each velocity and a line of best fit was plotted as shown in Fig. 7.9c. The dotted line shows the expected absorbance values against time.

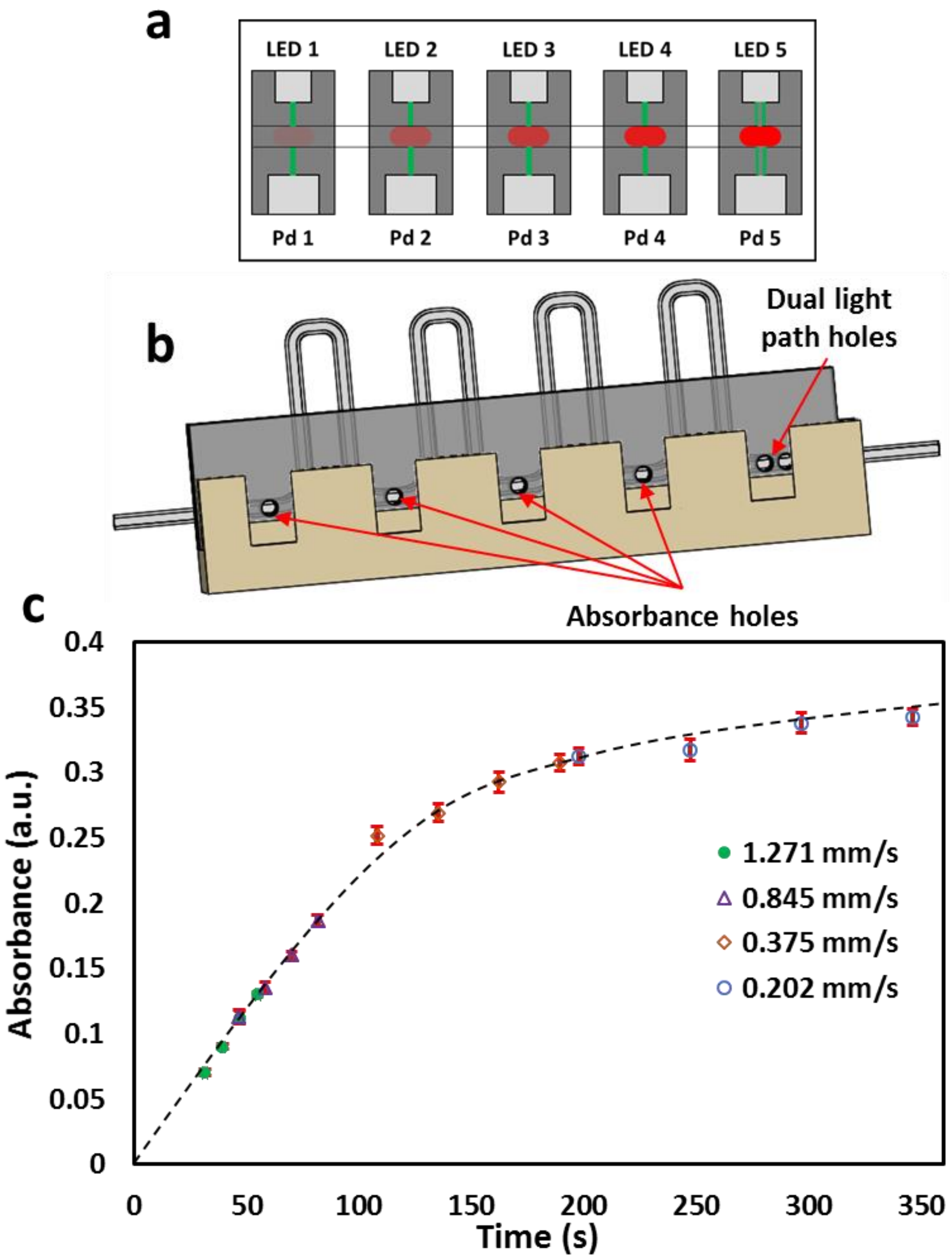

Figure 7.9 Glucose enzymatic reaction in droplets a) Schematic of the device with 4 absorbance detectors and dual light path flow cell, b) 3D schematic of the 4 absorbance detectors with dual light path flow cell, c) The absorption of glucose droplets (5mM) plotted as lines of best fit against time. Each line corresponds to velocities of 0.202, 0.375, 0.845 and 1.271 mm/s. The dotted line shows the expected absorbance values against time.

To apply the flow cell for accurate glucose measurements, the droplets generated by a screw-driven pump (Chapter 6) flowed through the absorbance detectors attached to dual light path flow cell. Similar to the method discussed in chapter 6, Michaelis-Menten parameters (V_{max} and K_m) were measured, and the unknown concentrations of glucose (1.5, 4, 10 mM) were quantified using Eq. 11. The recorded data was used to measure the velocity for the whole of the experiments, and it was found that the velocity changed over the course of the time while running different concentrations of glucose even though the flow rate was fixed. This suggests that the single point velocity measurement cannot be used to calculate the time each droplet takes to reach the four detectors in the flow cell and hence can affect the rates of reaction. This, in turn, increases the errors in the glucose concentrations quantified based on single velocity measurement. Fig. 7.10 showed the decrease in error when the continuously measured velocity values were used to calculate the time for reaction rates.

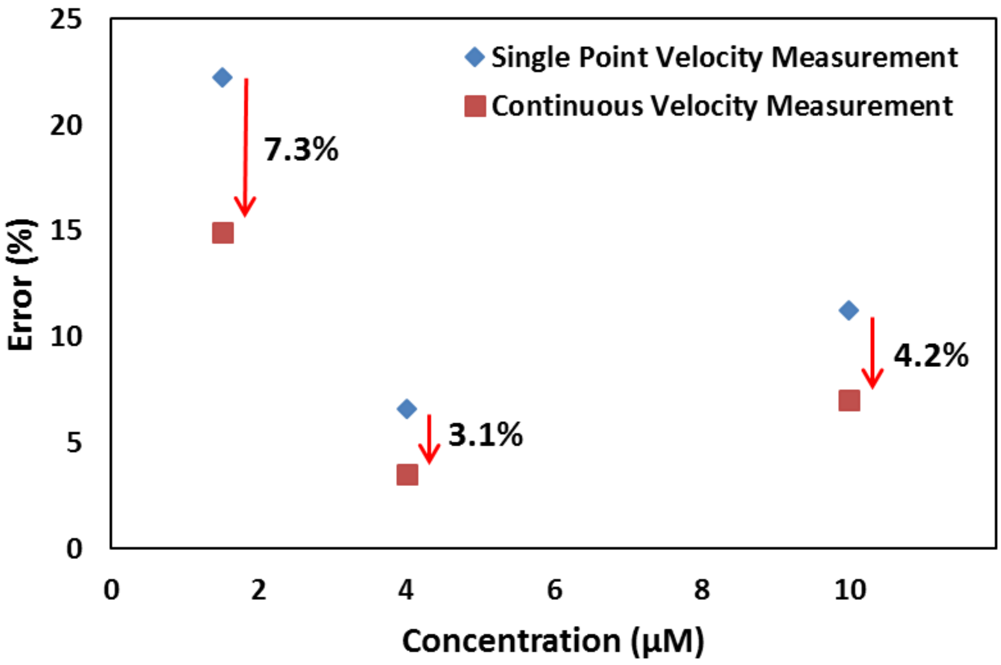

Figure 7.10 The plot of the %error against the concentration of glucose showing the decrease in error values with multiple point measurement of velocities in flow rate sensor. The glucose concentrations were by Michaelis-Menten kinetics.

7.4 Conclusions

This Chapter presents the development of a flow cell for accurate measurement of the length, velocity and composition of droplets. The optical flow cell was fabricated with dual light paths, analogous to a previously reported capacitive-based device [237]. The sensor was capable of measuring droplet velocities and lengths with errors of < 6% and < 5%, respectively. The flow cell has a small footprint and uses low-powered, low-cost components, which makes it ideally suited for use in field-deployable and portable systems.

Chapter 8 Conclusions and Future Directions

This Chapter concludes the Thesis and describes possible future directions beyond the current work.

8.1 Conclusions

This Thesis describes the development of droplet-interfaced microchip electrophoresis (MCE) and continuous chemical sensing device for conducting on-chip electrophoretic separations and real-time continuous measurement of tissue metabolites respectively.

The droplet-interfaced separation device is built as a step change of method presented by Niu *et al.* [32] in which droplets were generated in a tubing and injected into the separation channel. In the original design, droplets were *sequentially* injected into the separation channel with a throughput limited by a number of resolving bands and required time for completely separating the sample. In this current work, the device provides *parallel* and quantitative separations of analytes from sub-nano litre droplets having higher throughput. The chip contains pre-cured agarose or polyacrylamide gel, making it a ‘Gelchip’ that can be used off-the-shelf; liquid separation medium (e.g. PEO) can also be loaded into the channels *in situ*. Therefore, the device supports a broad range of separation methods.

Fluorescent dyes were separated in 30 droplets by injecting parallel into the separation channels, and the theoretical plates were calculated to be 7560/s at a distance of 3.5 cm. Gelchip was further characterised by studying the effect of different droplet sizes on separation efficiency (theoretical plates and resolution separation increase with a decrease in droplet size). Quantification of fluorescent dyes was accurately performed by separating different concentrations of FITC with a small error of 3.6% relative standard deviation (%RSD). As proof-of-concept applications, separation of DNA step ladder was performed on Gelchip and theoretical plates were achieved to be 79800/s at a distance of 1.3 cm. Although in the initial study, each channel was loaded with uniform gel, advanced separation abilities could be added by curing of gradient gels or forming of preconcentration zones in the channels, or online labelling by curing derivatization dyes into the gel.

The microfluidic devices (miniaturized colorimetric assays) built upon previous studies [49]–[51], [204] has been developed using continuous microfluidics but are bulky, and the throughput is low. This is due to the multiple microvalve switching of samples, slow mixing, sample dispersion and band-broadening in microfluidic channels. As a result, the system can only achieve low temporal resolution and with high reagent and energy cost. Droplet-based microfluidics requires low sample volumes (nanolitre to picolitre volumes) and offers high temporal resolution due to the compartmentalization of sample molecules in discrete droplets which eliminates dispersion and band-broadening along the channels. It has the potential of miniaturising a wide variety of wet chemical assays into POC devices.

A droplet-based portable continuous chemical sensor capable of generating droplets-on-demand and analysing glucose or lactate from dialysate was developed. The sensor worked via pumping fluid samples, generating droplets and analysing them in a flow cell. The newly developed screw-driven pump was used to generate droplets of reagents and sample (glucose and lactate), and flow them through the multi-detector flow cell.

To measure the reactions in droplets calorimetrically, a miniaturised 7-detector flow cell to analyse enzyme kinetics, with an example application of continuous glucose assay in droplets has been developed. The multi-point detection technique is perfect for the continuous measurement required for POC monitoring. Crucially, however, all of the previous reports employed sophisticated and bulky microscope-based setups unsuitable for application in clinical settings [234], [244]–[246]. The small size (45 by 10 by 15 mm) and use of affordable components combined with its ability to perform continuous, accurate biochemical quantification make it highly suitable for use in field-deployable POC monitoring devices. This section describes the design, and operation of the device and its validation by application to the accurate continuous quantification of unknown glucose concentrations using an enzymatic assay. The results show that reaction rates and Michaelis-Menten kinetics can be studied quantitatively for each droplet, and the device can measure sample droplets continuously with short sample-to-result time ((~30 s) and glucose concentrations were accurately determined (error < 5%) with the LOD of 0.35 mM.

The flow cell was further upgraded via fabrication of precise micromilling of the cartridge and successfully applied for detection of glucose and lactate droplets for clinical applications. Another significant development of the optical flow cell is dual light paths for accurately quantifying the size and velocity of the continuously flowing droplets, as well as quantifying the composition of the droplet. The sensor was capable of measuring droplet lengths with errors of < 5%. With all these features, a fully functional optical flow cell is built that can be readily used in wearable/portable microfluidic devices. Such a flow cell is expected to find applications in the fields of neurology, drug development, drug metabolism and drug distribution in the body, glucose monitoring for diabetes or environmental monitoring for pollutants.

8.2 Future Directions

8.2.1 Further Applications of Gelchip

In the prototype, the sample droplets were generated by one slip of the chip and sample breaks up in the continuous zig-zag continuous channels to form droplets. Droplets could also be pre-generated by the other droplet generation or collection devices and trapped in these channels/wells for CE analysis. With on-chip PCR or immunoassay functions also shown in the other Slipchips, multiple step assays could be further integrated to facilitate a self-contained diagnostic device. Droplet interfacing is a new approach of sample loading relying on the segmentation and loading of the sample droplets. Therefore, appropriate oil shall be chosen to prevent unwanted droplet breakup, sample leakage or surface contamination. SDS was found to destabilise the oil-water interface (FC-40 oil and TBE buffer combination) and causing severe sample loss to the interface of the two plates. Therefore, SDS-PAGE requires optimisation on Gelchip. After separation process, the Slipchip plates can be detached, and the gel can be exposed to other chemicals. This could facilitate post-separation staining and de-staining or MALDI-MS that are currently under study. With the future improvement in the detection capacity and sensitivity of the system, the device has the potential to be applied for resolution of complex mixtures in hundreds of droplets or be used for the 2D separations of serum protein, quantitative immunoassays, and western blot analyses.

8.2.1.1 Carcinoembryonic Antigen (CEA) Separation

Carcinoembryonic antigen (CEA) is an important tumour marker used in the clinical diagnosis of colorectal, pancreatic, gastric, and cervical carcinomas. Fanggui *et al*. [147] fabricated a microchip to quantify the carcinoembryonic antibody-antigen reaction for the detection of cancer disease in blood serum samples. Carcinoembryonic antigen (CEA) standards and serum samples from patients were incubated first with primary antibody (Ab1) and secondly with the fluorescently labelled secondary antibody (Ab2*). CEA can react with the fluorescently labelled anti-CEA primary and secondary antibodies. Gelchip can be used to quantify the separation of antibody-antigen complex (Ab*-CEA) and free antibody (Ab*). Similarly, other important biomarker have also been studied on a microchip and can be optimised for separation on Gelchip such as MMP-8 disease biomarker for periodontitis in saliva and Lactoferrin (Lf) tear-specific biomarker for Sjogren's Syndrome [12], [13].

8.2.1.2 Quantification of SNAP-25 Cleavage

Botulinum Neurotoxin Type-A (BoNT-A) is used in the clinical industry to treat conditions such as cervical dystonia. The paralytic effects of BoNT-A lead it to be used advantageously to treat neurological conditions relating to muscle hyperactivity. The toxin activity can be measured by detecting relative amounts of cleaved SNAP-25 and full-length SNAP-25. The Gelchip can be used in quantifying the SNAP-25 cleavage. The main steps involved in the study will be 1) antibody-antigen reaction and incubation off the chip, 2) Gel preparation inside separation channels, and 3) separation and data analysis (See Appendix 1.6).

8.2.1.3 Droplet Gel Chip

Direct injection of droplets into separation channel can be achieved by generating droplets offline or even online and injecting into the straight channel for parallel separation shown below. Further details are provided in Appendix (1.7).

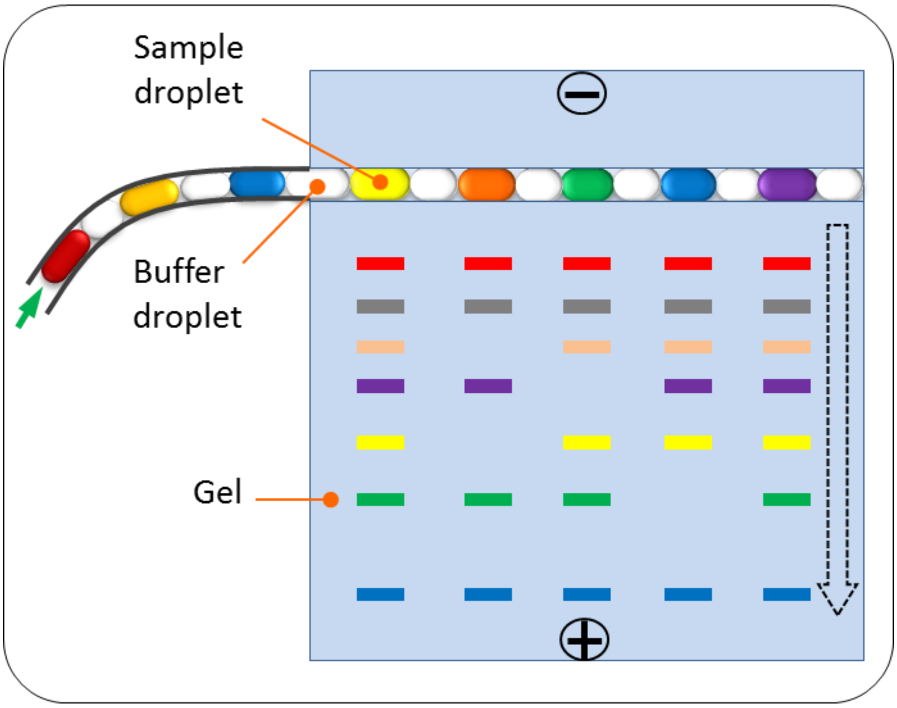

8.2.2 Further Applications of Continuous Chemical Sensing Device

The portable screw-driven pump is tested for continuous sampling of droplets from tissue fluids or the other environmental fluids. The sensor can also find applications in the fields of neurology, drug development, drug metabolism and drug distribution in the body, glucose monitoring for diabetes or environmental monitoring for pollutants.

Self-calibration and parallel droplet generation for multiple assays on chip can be performed by simply increasing the pumplines on the screw-driven pump. The data collected by flow cell can provide information about the patient's health in real time and allow the doctors to act accordingly in a short period rather than waiting for results from labs. For example, insulin injection to the diabetic patient can be controlled more efficiently by continuously monitoring glucose change inside tissues. The secondary brain injury could be avoided by early detection of ischemia for TBI patients. The continuous sensor needs to be optimised for biochemical assays of lactate, pyruvate, glutamate and glycerol for real-time detection in droplets and microdialysis calibrations including recovery rates and clinical testing.

The continuous chemical sensing device could also be combined with the droplet gel chip, making a POC sampling and analysis system, for monitoring complex mixtures of biological samples from dialysate such as amino acids previously achieved in lab-based systems [227], [229], [230], [247].

Appendix

1. Droplet-Interfaced Separation Platform

1.1 3D Schematic of Gelchip and Separation

The 3d schematics a-f show the principle of droplet generation in Gelchip, injection into the separation channels and separation upon application of electric field.

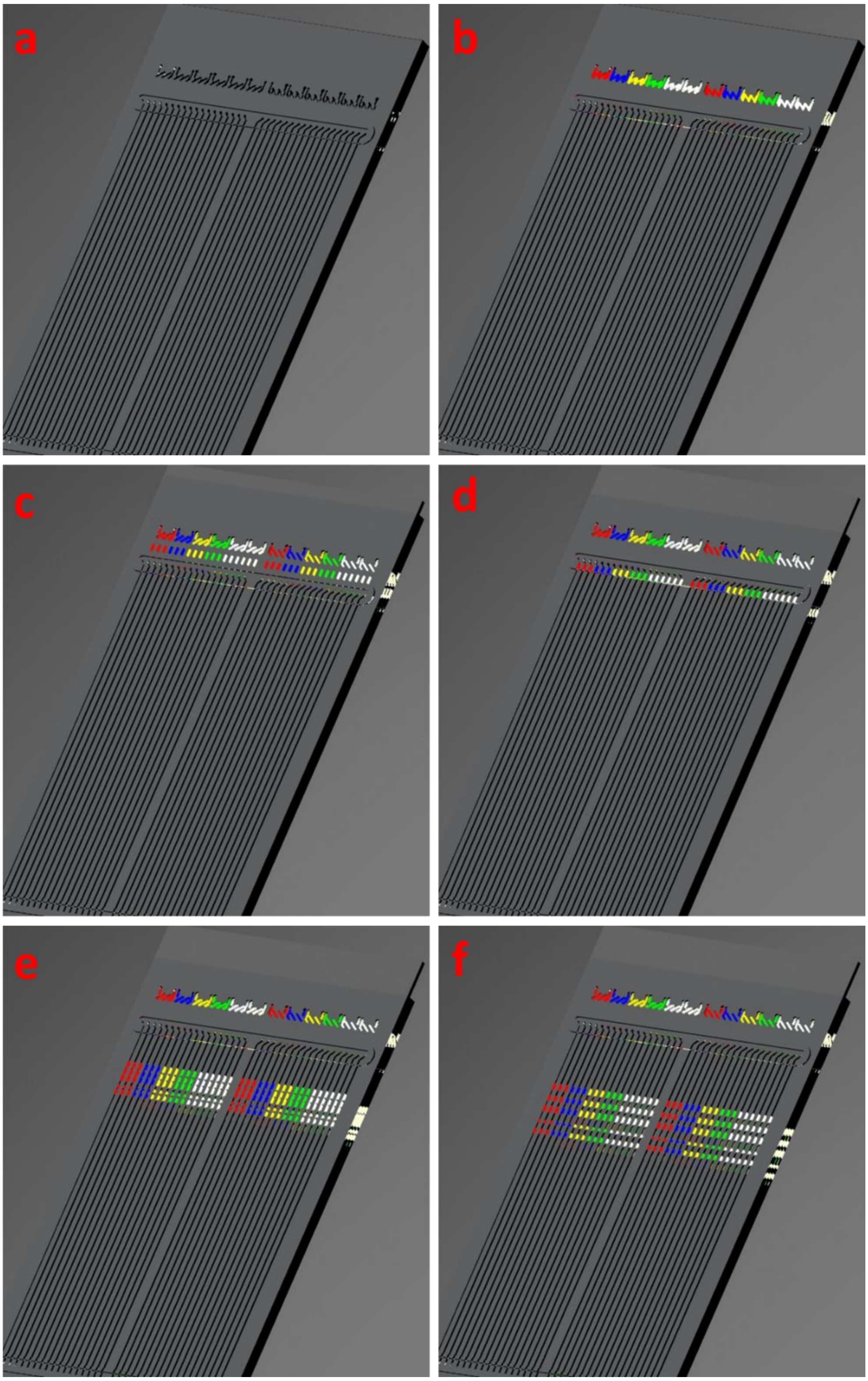

Fluorescein droplets in Separation channels filled with 1.5% PEO gel. The diffusion occurred as the droplets injected into separation channels.

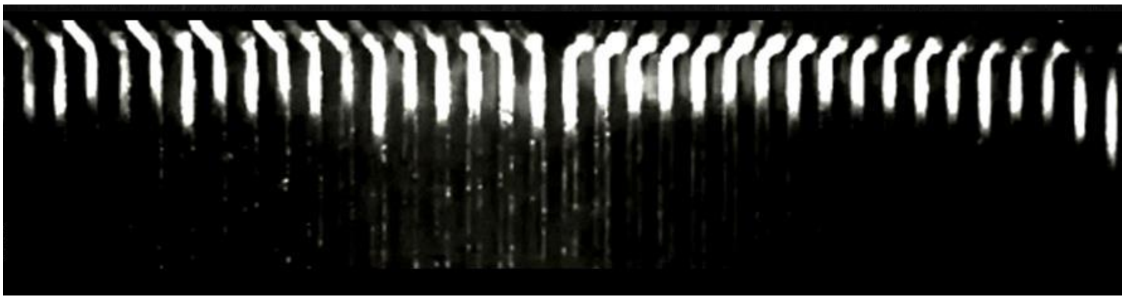

Separation of FITC and Fluorescein. Separation conditions: 1.5% PEO gel (500 KDa) FITC 250 μM, Fluorescein 150 μM, detection distance 1.5 cm.

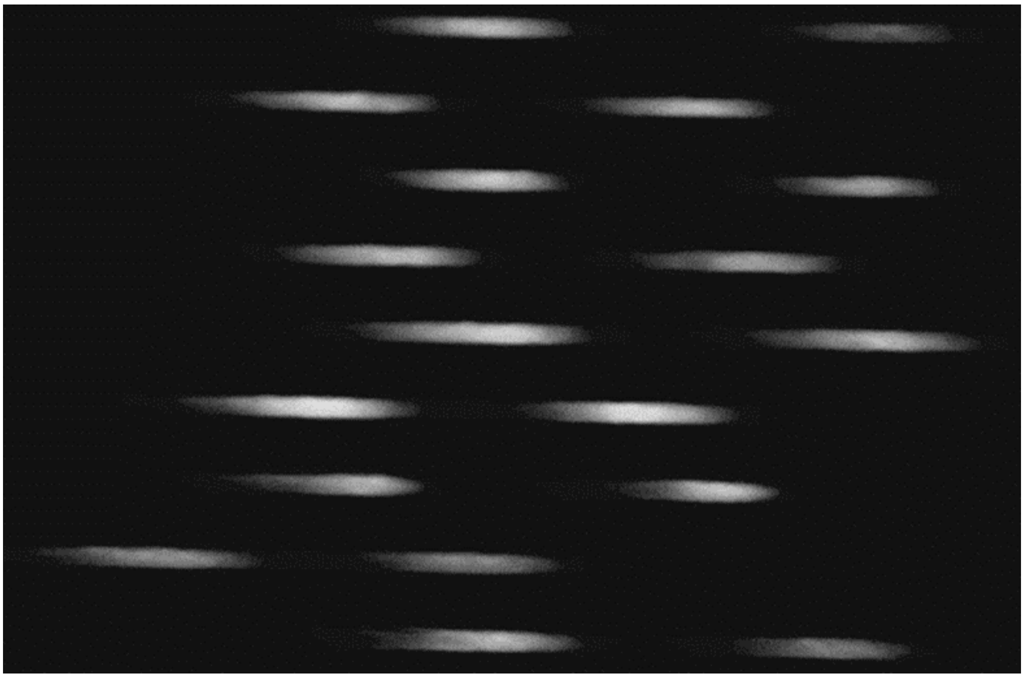

1.2 Separation Chip Designs

Below are some of the separation chip designs fabricated and considered during experimental work.

1.2.1 Design 1

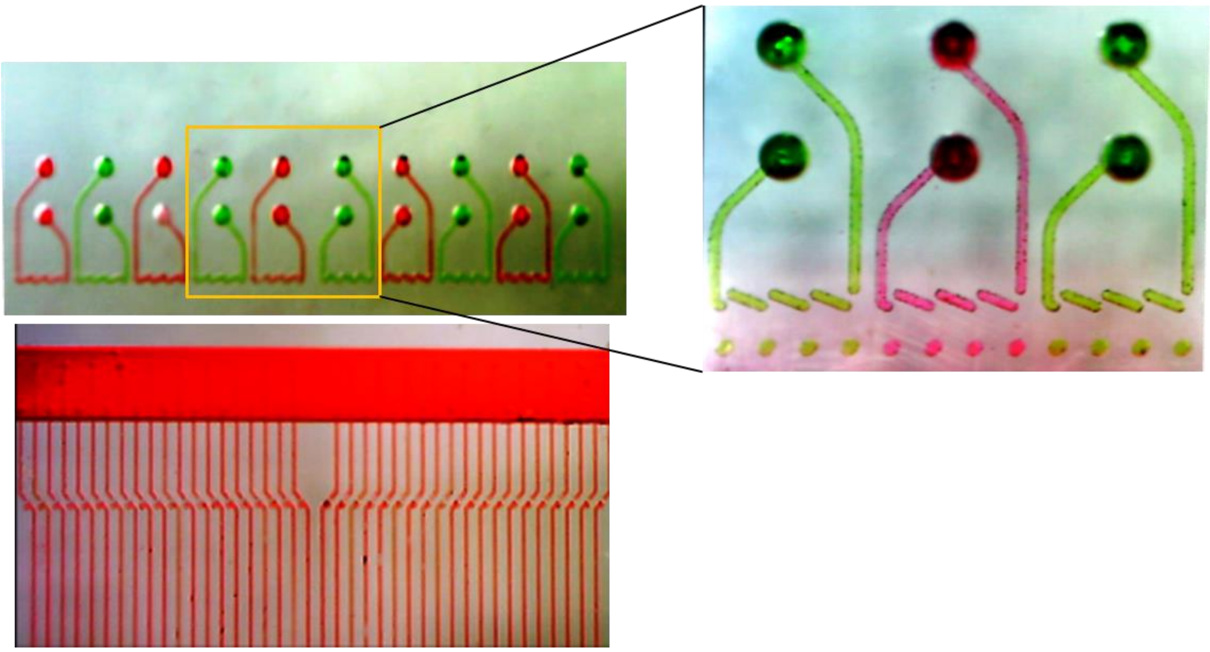

1.2.2 Design 2

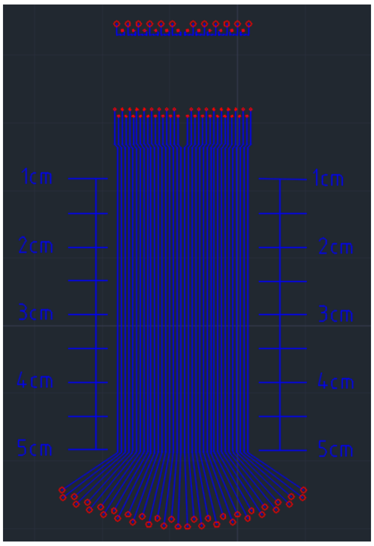

1.2.3 Design 3

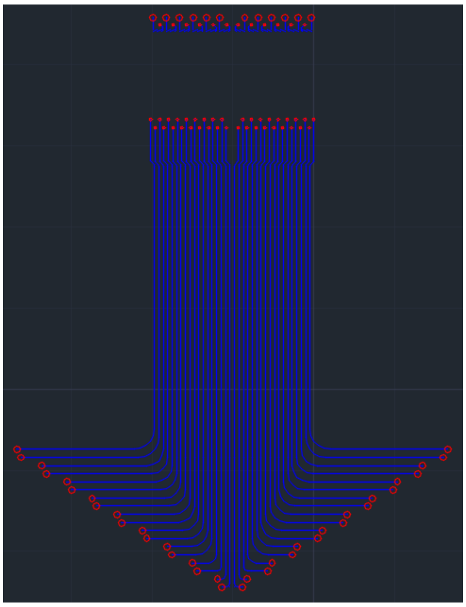

1.2.4 Design 4

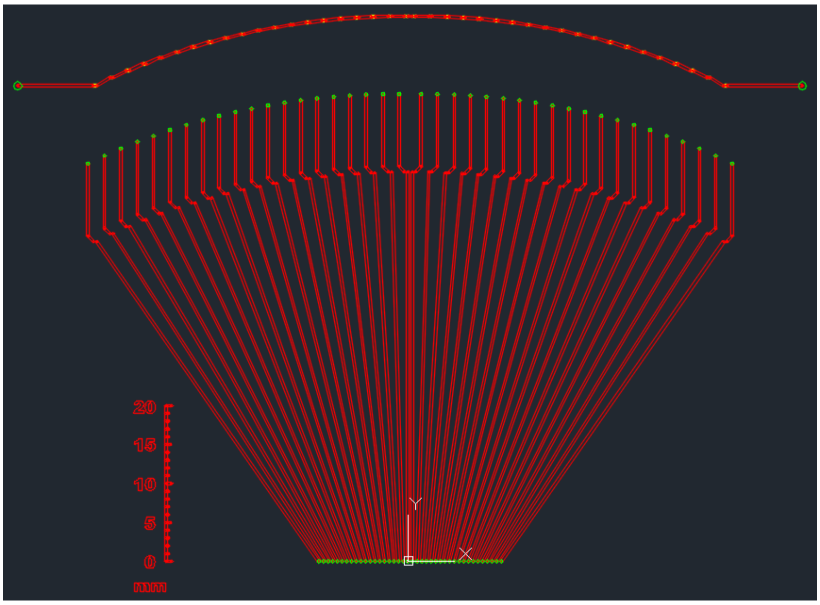

1.2.5 Design 5

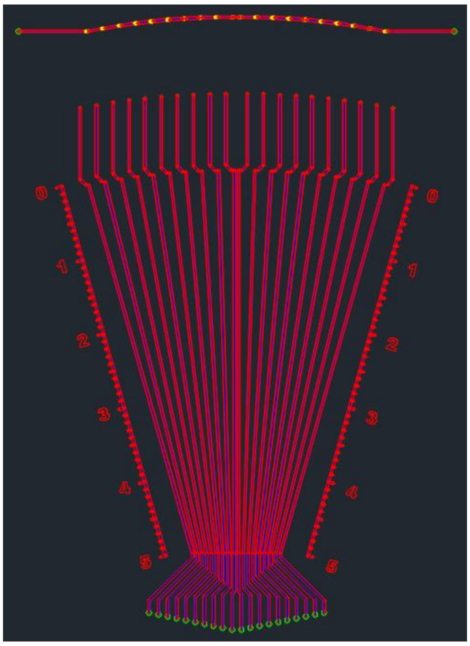

1.3 Matlab

1.3.1 Plotting Data

```
% this program reads the data from Excel file and plot all in a
figure
% Figure 1: plot raw data
% Figure 2: self aligned according to the first peak.
% Fig 3 self aligned and pseudo gel plot

a=xlsread('File Name', 3);  % read from the Excel file.

timestep=1;          % please input exposure time.

[m,n]=size(a);
peakmax=max(max(a));

% Fig 1
time=(1:m)*timestep;

figure(1)
hold
for i=1:n
    newdata=a(:,i)+(i-1)*peakmax*1/1.25;
    plot(time, newdata);
end

figure(2)
hold
before length=0;     % this is a trial value, select these number
of data points before the peak
after length= 0;    % this is a trial value, select these number
of data points after the peak depends on the time of the last
peak
time=(0:(before_length+after_length))*timestep;
for i=1:n
     [c,d]=max(a(:,i)); % c is the peak value and d is the peak
time
     newdata= a((d-before_length):(d+after_length),i)/c*peakmax
+(i-1)*peakmax*2/3;
    plot(time, newdata);
end
xlim([0 (before_length+after_length)*timestep])

figure(3)      % gle plot of the original data
X_color=256-round((New_data)/peakmax*400);   % flipud(a)
image(X_color);
colormap(copper(256));  % can use 'gray', 'copper' or 'jet' or
the others
```

1.3.2 Normalisation of Peaks

```
clear;

a=xlsread('File Name', 1);  % read from the Excel file.
timestep=0.2;          % please input exposure time.
[m,n]=size(a);
peakmax=max(max(a));

peaknumber=5;  % this number need to be defined by the
experiment, how many real peaks

ref_peak=5;    % the number of the reference peak used to adjust
the whole electropharagram.

% datapoint_before_firstband=15;   % need to manually set. means
after alignment how many data points left before the first band.

%%%%%%%%%%%%%%%%%%%%%%%%%%%%%%%%%%%%%%%%%%%%%
% Fig 1
time=((1:m)*timestep)';

msheatmap(time, a)
 xlabel('Time (s)')
 ylabel('Lanes')
 title ('Before alignment')



% Ys = mssgolay(time, a, 'SPAN', 3, 'SHOWPLOT', 3);
band_peak=[];
band_loc=[];
for i=1:n;
    [pks,locs]=findpeaks(a(:,i),'minpeakdistance',2);  % find out
all of the peaks
    % pick out the first peaknumber of peaks
    [pp_sort, IX] = sort(pks);
    np=length(pks);
    peaks_loc=IX((np-peaknumber+1):np);
    peak_loc_final = sort(peaks_loc);
    peak_info = [];

    for j=1:peaknumber;
        peak_info=[peak_info; pks(peak_loc_final(j))
locs(peak_loc_final(j)) ];
    end
    band_peak=[band_peak peak_info(:,1)];
    band_loc=[band_loc peak_info(:,2)];
end

% find out the mean loc of all of the bands
band_mean=mean(band_loc,2);
```

```
Dm=band_mean(ref_peak)-band_mean(1);    % distance between the
ref_peak to the first peak


New_T=[];

for i=1:n;
    da=band_mean(1)-band_loc(1,i);  % distance nee to move
    T=1:m;
    DD=band_loc(ref_peak,i)-band_loc(1,i);
    T_adj=[ T(1:band_loc(1,i))+da  T(band_loc(1,i))+da+(1:(m-
band_loc(1,i)))*Dm/DD]';
    New_T= [New_T T_adj];
end

New_T=New_T*timestep;

New_data=[];
for i=1:n;
    TT=New_T(:,i);
    vq2 = interp1(TT,a(:,i),time,'spline');   %  1-D data
interpolation
    New_data=[New_data vq2];
end

msheatmap(time, New_data)
 xlabel('Time (s)')
 ylabel('Lanes')
 title ('After alignment')

figure(3)     % gle plot of the original data
X_color=256-round((New_data)/peakmax*400);   % flipud(a)
image(X_color);
colormap(copper(256));  % can use 'gray', 'copper' or 'jet' or
the others

 ylabel('')
 xlabel('Lanes')
 title ('Gel format')

%  find the peaks again after realignment and calculat the
variation
%
band_peak=[];
band_loc=[];
for i=1:n;
    [pks,locs]=findpeaks(New_data(:,i),'minpeakdistance',2);  %
find out all of the peaks
    % pick out the first peaknumber of peaks
    [pp_sort, IX] = sort(pks);
    np=length(pks);
    peaks_loc=IX((np-peaknumber+1):np);
    peak_loc_final = sort(peaks_loc);
```

```
    peak_info = [];

    for j=1:peaknumber;
        peak_info=[peak_info; pks(peak_loc_final(j))
locs(peak_loc_final(j)) ];
    end
    band_peak=[band_peak peak_info(:,1)];
    band_loc=[band_loc peak_info(:,2)];
end

New_data=New_data(10:202,:);  %%%%%  !!!!!! this sentence is only
for this group of data.
New_data1=[];
 for i=1:n;
     New_data1(:,i)=(New_data(:,i)-
min(New_data(:,i)))/(max(New_data(:,i))-min(New_data(:,i)));
 end

figure(5)      % gle plot of the original data
X_color=256-round((New_data1)*256);   % flipud(a)
image(X_color);
colormap(copper(256));  % can use 'gray', 'copper' or 'jet' or
the others

 ylabel('')
 xlabel('Lanes')
 title ('Gel format')

% this program is not ideal (move according to peak 1 then
stretch according peak 5). Experimentally the variations might
come from the following two effects:
%
% (a) the field strength in each channels is different, due to
the uneven gel loading.
% (b) The droplet merge with the channel later than other
%
% (a) will cause elongation of the electropherogram, while (b)
may cause
% the shift of the whole electropherogram. We hope can avoid (b)
as much as possible in experiments. To compensate (a) and to get
a meaningful alignment of the electropherograms,
% it's better to know the starting time, then align each
electropherogram according to the first peak,
% by multiplying a factor from mobility (E-filed).

% SO, for different experiments, it's very important to start
recording at the same time after switching on the E-field.
```

1.3.3 Peak Area

```
a=xlsread('File Name, 1);  % read a group of CE data from the
Excel file.

timestep=0.33;          % please input exposure time.

[m,n]=size(a);    % the size of the matrix

peak_number=input('enter how many peaks  ');
peak_bottoms=peak_number+1;

base=[];

lane_peaks=[];
for i=1:n;
    plot(a(:,i));
    pb = ginput(peak_bottoms);  % click on the graph where you
think the bottom of the peak should be
    xx = round(pb(:,1))         % find the corresponding x values
    area=[]
    for j=1:peak_number;              % calculate area for each
peak
    area_peak= sum(a(xx(j):xx(j+1),i)-min(a(:,i)));
    area=[area; area_peak];
    end
    lane_peaks=[lane_peaks area];     %un-normalised results
end

first_lane_peaks=max(max(lane_peaks));

 normalize_peak_area=[];
 for i=1:n;
     normalize_peak_area=[normalize_peak_area
lane_peaks(:,i)*first_lane_peaks/ max(lane_peaks(:,i))];
 end

 normalize_peak_area      % shows the peak areas in each channel
                          % the areas can be used for statistics

a=xlsread('File Name', 1);  % read from the Excel file.

timestep=0.33;          % please input exposure time.

[m,n]=size(a);
peakmax=max(max(a));
base_line=min(min(a));

% Fig 1
time=(1:m)*timestep;

x=a;
% set the base line
```

```
base=[140
      140];  % set base for electrophogram 1, 2,3,..

peakarea=[];
flag=0;
current_area=0;
peak_area_in_all_channels=[];
for j=1:n;
for i=1:m;
    if x(i,j)>base;
        current_area=current_area+x(i,j)-base(j);
        flag=1;
    elseif flag>0.1
        peakarea=[peakarea; current_area];
        current_area=0;
        flag=0;
    end
    peakarea
    peak_area_in_all_channels=[peak_area_in_all_channels
peakarea];
end
```

1.4 Separation of Protein Mixture

Protein ladder consisted of six fluorescently labelled proteins i.e. Trypsin Inhibitor (20,000 Da), Carbonic Anhydrase (29,000 Da), Alcohol Dehydrogenase (39,800 Da), Albumin, bovine serum (66,000 Da), b-Galactosidase (116,000 Da), Myosin (200,000 Da). These proteins were separated in the channels in 1.5% PEO and 100mM Tris-ches with pH 8.4. SDS was added with 0.1% concentration to denature the proteins. The protein mixture was heated at 60° C in a hot water tank before loading to the sample reservoir channels as directed by the product manual (Sigma-Aldrich). Electropherogram of the protein ladder: Peak a (Trypsin Inhibitor), Peak b (Carbonic Anhydrase), Peak c (Alcohol Dehydrogenase), Peak d (Albumin, bovine serum), Peak e (b-Galactosidase), Peak f (Myosin). Separation conditions: 1.5% PEO gel (500 KDa), Separation distance 3cm, Electric Field 130 V/cm.

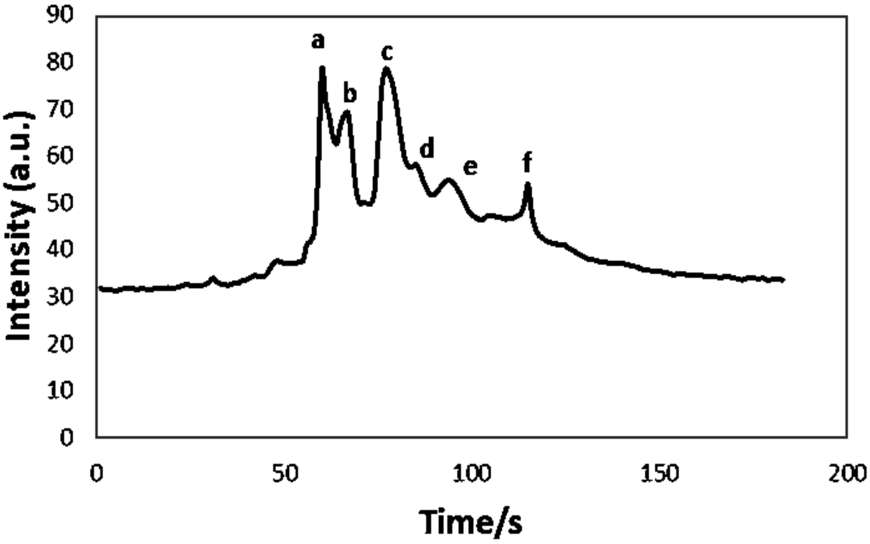

1.5 Carcinoembryonic Antibody-Antigen Reaction

Carcinoembryonic antigen (CEA) as one of the most widely used tumour markers is used in the clinical diagnosis of colorectal, pancreatic, gastric, and cervical carcinomas. Carcinoembryonic antigen was reacted with the fluorescently labelled anti-carcinoembryonic antibody under dark and incubated at 38° C for 1 hour. The separation of antibody-antigen complex (Ab*-CEA) and free antibody (Ab*) was achieved by using 1.5% PEO (500 KDa) as shown below. Electropherogram of the antibody-antigen complex (Ab*-CEA) and free antibody (Ab). Separation conditions: Separation distance 5 cm, Electric Field 130 V/cm.

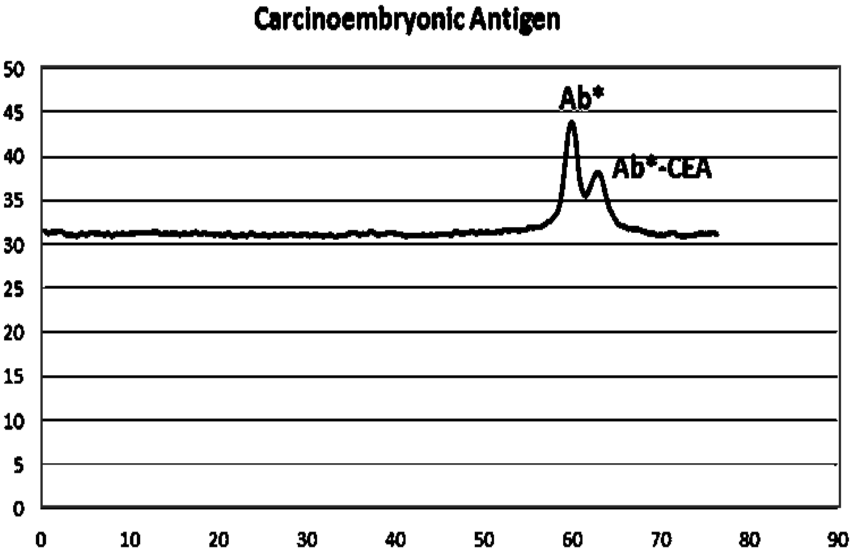

1.6 Snap-25 Separation

BoNT-A activity in vivo incorporates 4 main steps; binding of toxin to protein receptors, internalisation by endocytosis, translocation of light chain into the cytosol and cleavage of SNAP-25, inhibiting the release of acetylcholine. The mouse LD50 is currently used to determine potency before batch release; an in vitro alternative is encouraged to reduce animals used in research. Human induced pluripotent stem cells (hiPSCs)-derived neurons, sensitive to BoNT-A, are used to trial detection methods; Western Blot, Mass Spectrometry and Microchip Electrophoresis (MCE). Cells were grown for 7 days and incubated with 30 U/mL toxin for 48 hours at Southampton General hospital. The toxin activity is then measured by detecting relative amounts of cleaved SNAP-25 and full length SNAP-25. Our collaborators for Southampton General Hospital demonstrated that the incubation of hiPSCs-derived neurons with toxin for 48 hours at a concentration of 30 U/mL yields SNAP-25 cleavage and demonstrates results comparable to those of the mouse LD50. However, the repeatability and robustness of the Western Blot method is not suitable for a GMP validated assay. Mass Spectrometry accurately identifies synthetic SNAP-25 peptides, but our results indicate that quantifying in vitro SNAP-25 cleavage from cell samples is inconclusive. Microchip Electrophoresis (MCE) separates proteins allowing fluorescent detection of proteins in nanolitre sized droplets; a method designed for high throughput analysis. This method looks promising in quantifying the SNAP-25 cleavage by Gelchip. The main steps involved in the study are

Antibody-Antigen Reaction:

Pathway 1

Heat the samples to 95◦C in dry bath. Incubate with antibody at 4°C for 3-10 hours (need to optimise the reaction time). At different times of incubation, the separation can be performed and fluorescent can be studied. Need to optimise the dilution of antibody. Add LDS sample buffer to the samples (1:2 ratio). Heat the samples to 95◦C in dry bath.

Pathway 2

Heat the samples to 95◦C in dry bath. Add LDS sample buffer to the samples (1:2 ratio). Heat the samples to 95◦C in dry bath. After separation in Polyacrylamide gel, open the microchip and incubate with antibody at 4°C for overnight. Need to optimise the dilution of antibody. And also find out the way to transfer bands to membrane if required.

Step 2: Gel Preparation

Cure the polyacrylamide gel inside the microchannels (15%- optimisation required) using separation buffer (Tris-Glycine-SDS). Or Load the polyethylene oxide (2.5%) gel in the channels. The gel can be prepared with Tris-Glycine-SDS buffer.

Step 3: Separation and Band Detection

Load the samples to the sampling reservoirs, generate droplets, inject them into separation channels and start separation. Visualise the separation of bands, record images and analyse by imageJ to quantify the separation. Once successful in separation and protocol is defined, then quantitative studies can be done by changing the toxin concentrations and/or time for toxin exposure to cells.

Initial results indicate the size difference in two different channels for uncleaved and cleaved snap-25.

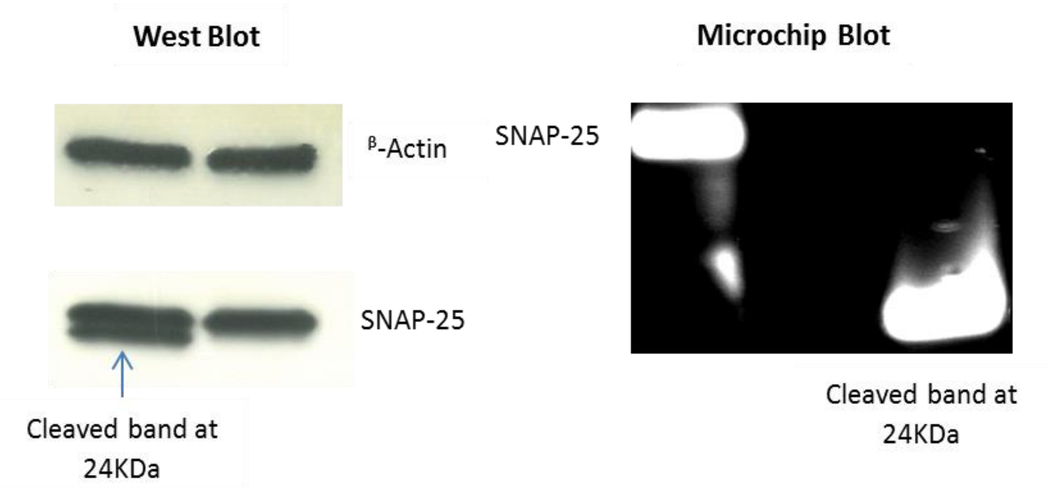

1.7 Droplet Gel Chip

Droplet gel chip consists of two plates of PMMA as shown below (a). Bottom plate acts as a base for curing gel and channel (0.4 mm) inside gel to inject droplets. It also has the channel for attaching tubing inlets and outlets. Top plate acts as the cover of the droplet gel chip which holds the gel in place and has cut through reservoirs to add buffer to the gel. After joining layers, the device was clamped with clips and/or magnets as shown in part b. The gel was cured in the device with 1 mm thickness of the layer A. the channel formed was 0.4 mm in the gel. After peeling off the tubing, the channel was flushed with duxback and then FC-40 with surfactant (1.8%). The droplets were generated in another tubing and loaded in the gel as shown in part c.

Appendix

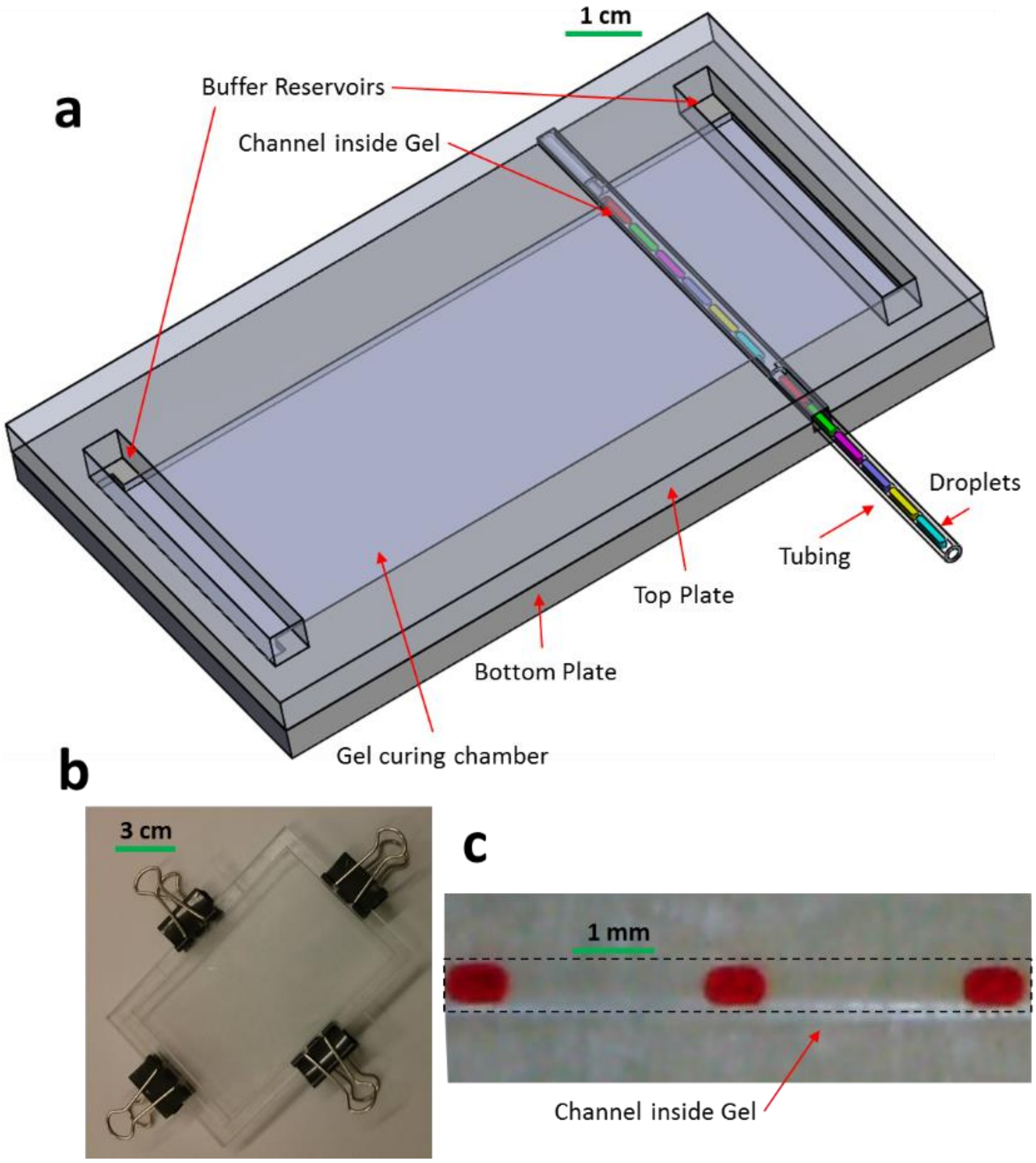

In 1mm thick gel and 0.4 mm channel, the dye droplet was observed while entering into the gel channel (a) and it can be seen that droplets transfer from tubing to the channel without breakage or contamination (1-4 in part a). The food dye was also observed under the application of an electric field 6V/cm. As shown part b (1-4), the droplet merges with the gel and starts moving towards the opposite electrode upon application of an electric field (b). When the electric field is applied, the shape of the aqueous droplet changes as the surface of the droplet makes a contact with the gel and the oil shape changes to become a droplet as shown in part b.

Appendix

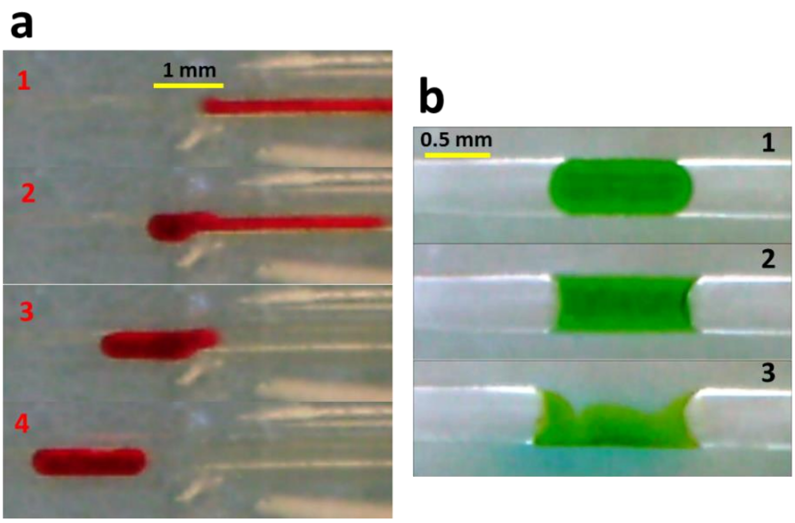

Figure below (a) shows Eosin Y droplets in the channel (0.4 um) and 1 mm thick gel. The droplets were generated using surfactant mixed oil and it was found that the droplets merged with the gel after application of an electric field and moved towards the opposite electrode. The dotted lines shows the direction of movement of fluorescent dyes. Part b shows the successful separation of Eosin Y and 5-Carboxyfluorescein droplets in gel chip.

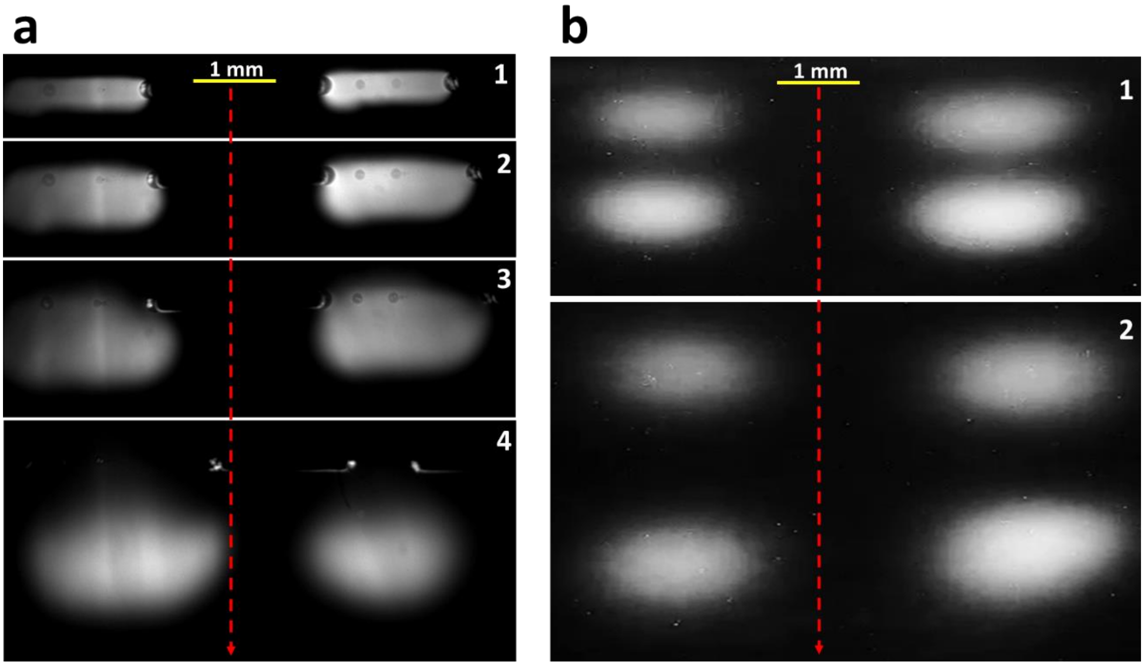

The gel chip has the potential to be studied for separation of biological molecules in real time and with very small amounts of the sample. 0.4 mm channels in 1 mm thick gel are made successfully and separation of two fluorescent molecules has been achieved so far. However, the gel thickness of 1mm limits the voltage applied and challenges the robustness of the device. Therefore, a much thinner gel (0.1-0.3mm) is required to increase the efficiency of the device and further reduce the sample size.

2. Continuous Chemical Sensor

2.1 LabView

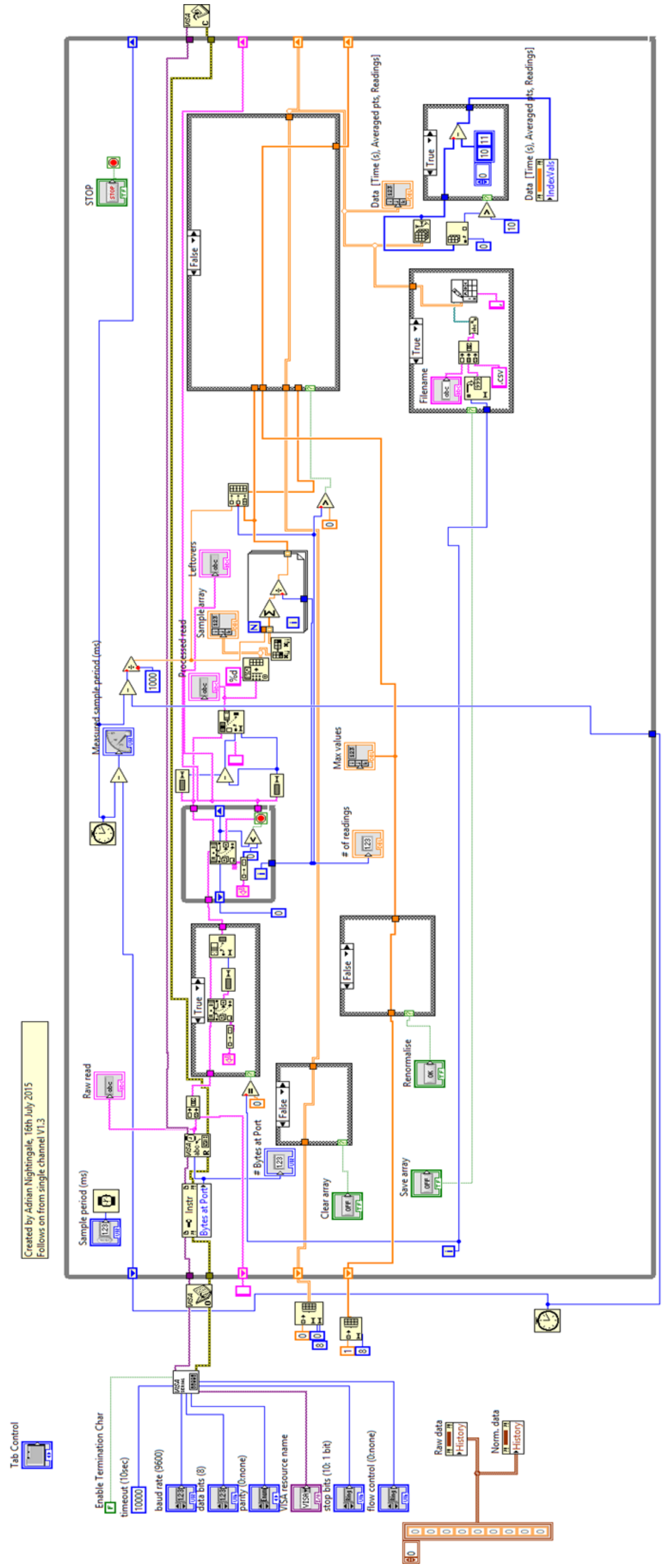

2.2 Matlab

2.2.1 To Load Data

```
a=[]';
subplot(7,1,1);
plot(a(1,:));grid;
subplot(7,1,2)
plot(a(2,:));grid;
subplot(7,1,3)
plot(a(3,:));grid;
subplot(7,1,4)
plot(a(4,:));grid;
subplot(7,1,5)
plot(a(5,:));grid;
subplot(7,1,6)
plot(a(6,:));grid;
subplot(7,1,7)
plot(a(7,:));grid;
% subplot(7,1,7)
% plot(a(7,:));grid;
```

2.2.2 Michaelis-menten Fit

```
function [x_fit,y_fit,f,g] =
michaelis_fit(S,y,fit_param1,fit_param2)

% INPUTS:
%
% 1) concentrations in uM
% 2) rates
% 3 & 4) [OPTIONAL] Starting guesses for fitting that correspond
to
%                a) Vmax * t.
%                b) Km.
%
% If there are no inputs, the function will run a demonstration
using
% generated data.
%
% OUTPUTS:
%
% 1) x co-ordinates of fit in uM
% 2) y co-ordinates of fit
% 3) the parameters of the fit - NB these are for concentrations
in M.
% 4) fit "goodness" parameters


if nargin == 0
    %% generate example data

    Km=0.001; %(units: M)
    Vmax= 10^-4; %(units: M/s)
```

```
    t=120;%(units: s)
    noise=10; %How much can "real" data deviate from ideality as
a %

    S=0:100:1000; %in uM
    S=S/10^6; %convert to SI
    y_ideal=t.*Vmax.*S./(Km+S);

    %generate noisy data
    y=ones(1,length(y_ideal));
    for i=1:length(y);
        y (i) =  y_ideal(i) * (1- (noise/100) * (rand-0.5) /
0.5);
    end

    %plot generated data
    figure(99)
    plot(S,y_ideal,'-',S,y,'ksq')
    hold on

else
    figure(99)
    plot(S,y,'ksq')
    hold on
end

if nargin < 4
    fit_param1 = 4*10^-3;
    fit_param2 = 7.5;
end

%% Analyse data

% First check data is in columns other the fitting program will
be upset!
q=size(S);
if q(1) == 1
    S = S';
end
q=size(y);
if q(1) == 1
    y = y';
end

g=fittype('a*x/(b+x)');
[f,g]=fit(S,y,g,'Start',[fit_param1;fit_param2]);
g
x_max=max(S)*1.2;
x_fit=0:x_max/100:x_max;
y_fit=f.a.*x_fit./(f.b+x_fit);
plot(x_fit,y_fit,'r--')
xlabel '[Substrate] / \muM'
ylabel 'Rate / A.U. s^-^1'
```

```
if nargin == 0
    legend('Ideal trend','Generated data','Fit','location','SE')
    legend 'boxoff'
else
%     legend('Data','Fit','location','SE')
%     legend 'boxoff'
end
title(['Michaelis-Menten fit, r^2 =',num2str(g.rsquare)])

% x_fit=x_fit *10^-6; %Convert to uM for output
```

2.3 Fluorescent Glucose Assay

Glucose (15 mM) was added from one inlet and Amplex Red (1mg/mL), peroxidase (24 U/mL) and glucose oxidase (24 U/mL) were added from other inlet. The reaction happened as the two layers merged even before the droplet generation. The intensity of the droplets increased. However, the chip had 400 and 600 um high channels so the intensity cannot be compared but the reaction can be seen happening.

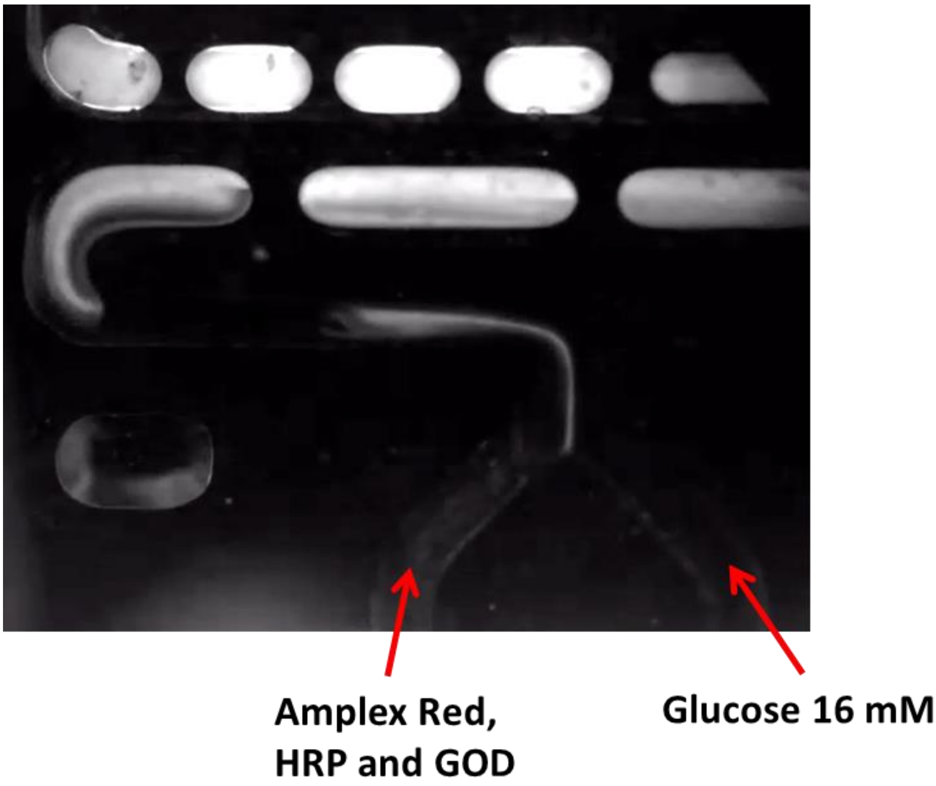

The reaction was performed under the microscope in a microchip, and the droplets were generated with micropump. Figure below shows the droplet generation and fluorescent signal from the reaction (1-6).

Appendix

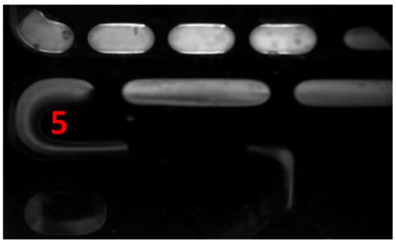

References

References

[1] G. M. Whitesides, “The origins and the future of microfluidics,” *Nature*, vol. 442, no. 7101, pp. 368–373, 2006.

[2] S. Y. Teh, R. Lin, L. H. Hung, and A. P. Lee, “Droplet microfluidics,” *Lab Chip*, vol. 8, no. 2, pp. 198–220, 2008.

[3] A. Huebner, S. Sharma, M. Srisa-Art, F. Hollfelder, J. B. Edel, and A. J. Demello, “Microdroplets: a sea of applications?,” *Lab Chip*, vol. 8, no. 8, pp. 1244–1254, 2008.

[4] R. Sista, Z. Hua, P. Thwar, A. Sudarsan, V. Srinivasan, A. Eckhardt, M. Pollack, and V. Pamula, “Development of a digital microfluidic platform for point of care testing.,” *Lab Chip*, vol. 8, no. 12, pp. 2091–104, 2008.

[5] A. Tiselius, “A new apparatus for electrophoretic analysis of colloidal mixtures,” *Trans. Faraday Soc*, vol. 33, p. 524−531, 1937.

[6] J. Ostergaard and H. Jensen, “Simultaneous evaluation of ligand binding properties and protein size by electrophoresis and Taylor dispersion in capillaries,” *Anal Chem*, vol. 81, no. 20, pp. 8644–8648, 2009.

[7] C. D. Isabelle Migneault Joëlle Vinh, “Two Glutaraldehyde- Immobilized Trypsin Preparations for Peptide Mapping by Capillary Zone Electrophoresis, Liquid Chromatography, and Mass Spectrometry,” *J. Liq. Chromatogr. Relat. Technol*, vol. 31, pp. 789–806, 2008.

[8] F. Pereira, S. Hassard, J. Hassard, and A. deMello, “CE of dsDNA in low-molecular-weight polyethylene oxide solutions,” *Electrophoresis*, vol. 30, no. 12, pp. 2100–2109, 2009.

[9] X. C. Huang, M. A. Quesada, and R. A. Mathies, “DNA sequencing using capillary array electrophoresis,” *Anal. Chem*, vol. 64, p. 2149−2154, 2002.

[10] S. Haeberle and R. Zengerle, “Microfluidic platforms for lab-on-a-chip applications,” *Lab Chip*, vol. 7, no. 9, pp. 1094–1110, 2007.

[11] L. B. Koutny, D. Schmalzing, T. A. Taylor, and M. Fuchs, “Microchip electrophoretic immunoassay for serum cortisol,” *Anal Chem*, vol. 68, no. 1, pp. 18–22, 1996.

[12] A. E. Herr, A. V Hatch, D. J. Throckmorton, H. M. Tran, J. S. Brennan, W. V Giannobile,

and A. K. Singh, "Microfluidic immunoassays as rapid saliva-based clinical diagnostics," *Proc Natl Acad Sci U S A*, vol. 104, no. 13, pp. 5268–5273, 2007.

[13] K. Karns and A. E. Herr, "Human tear protein analysis enabled by an alkaline microfluidic homogeneous immunoassay," *Anal Chem*, vol. 83, no. 21, pp. 8115–8122, 2011.

[14] M. Wang, G. T. Roman, M. L. Perry, and R. T. Kennedy, "Microfluidic chip for high efficiency electrophoretic analysis of segmented flow from a microdialysis probe and in vivo chemical monitoring," *Anal Chem*, vol. 81, no. 21, pp. 9072–9078, 2009.

[15] J. F. Dishinger, K. R. Reid, and R. T. Kennedy, "Quantitative monitoring of insulin secretion from single islets of Langerhans in parallel on a microfluidic chip," *Anal Chem*, vol. 81, no. 8, pp. 3119–3127, 2009.

[16] D. J. Harrison, A. Manz, Z. Fan, H. Luedi, and H. M. Widmer, "Capillary electrophoresis and sample injection systems integrated on a planar glass chip," *Anal. Chem.*, vol. 64, no. 20, pp. 1926–1932, 1992.

[17] S. V Ermakov, S. C. Jacobson, and J. M. Ramsey, "Computer simulations of electrokinetic injection techniques in microfluidic devices," *Anal Chem*, vol. 72, no. 15, pp. 3512–3517, 2000.

[18] M. Tabuchi, Y. Kuramitsu, K. Nakamura, and Y. Baba, "A 15-s protein separation employing hydrodynamic force on a microchip," *Anal Chem*, vol. 75, no. 15, pp. 3799–3805, 2003.

[19] A. T. Woolley and R. A. Mathies, "Ultra-High-Speed DNA Sequencing Using Capillary Electrophoresis Chips," *Anal. Chem.*, vol. 67, no. 20, pp. 3676–3680, 1995.

[20] J. H. Aborn, S. A. El-Difrawy, M. Novotny, E. A. Gismondi, R. Lam, P. Matsudaira, B. K. McKenna, T. O'Neil, P. Streechon, and D. J. Ehrlich, "A 768-lane microfabricated system for high-throughput DNA sequencing," *Lab Chip*, vol. 5, no. 6, pp. 669–674, 2005.

[21] S. Yang, J. Liu, C. S. Lee, and D. L. DeVoe, "Microfluidic 2-D PAGE using multifunctional in situ polyacrylamide gels and discontinuous buffers," *Lab Chip*, vol. 9, no. 4, pp. 592–599, 2009.

[22] C. A. Emrich, I. L. Medintz, W. K. Chu, and R. A. Mathies, “Microfabricated Two-Dimensional Electrophoresis Device for Differential Protein Expression Profiling,” *Anal. Chem.*, vol. 79, no. 19, pp. 7360–7366, 2007.

[23] L. Bousse, S. Mouradian, A. Minalla, H. Yee, K. Williams, and R. Dubrow, “Protein sizing on a microchip,” *Anal Chem*, vol. 73, no. 6, pp. 1207–1212, 2001.

[24] D. T. Chiu, “Micro- and nano-scale chemical analysis of individual sub-cellular compartments,” *TrAC Trends Anal. Chem.*, vol. 22, no. 8, pp. 528–536, 2003.

[25] X. Niu and A. J. deMello, “Building droplet-based microfluidic systems for biological analysis,” *Biochem. Soc. Trans.*, vol. 40, no. 4, pp. 615–623, 2012.

[26] A. S. Utada, E. Lorenceau, D. R. Link, P. D. Kaplan, H. A. Stone, and D. A. Weitz, “Monodisperse Double Emulsions Generated from a Microcapillary Device,” *Science*, vol. 308, no. 5721, pp. 537–541, 2005.

[27] H. Song, D. L. Chen, and R. F. Ismagilov, “Reactions in droplets in microfluidic channels,” *Angew Chem Int Ed Engl*, vol. 45, no. 44, pp. 7336–7356, 2006.

[28] X. Z. Niu, B. Zhang, R. T. Marszalek, O. Ces, J. B. Edel, D. R. Klug, and A. J. deMello, “Droplet-based compartmentalization of chemically separated components in two-dimensional separations,” *Chem Commun*, no. 41, pp. 6159–6161, 2009.

[29] M. C. Draper, X. Niu, S. Cho, D. I. James, and J. B. Edel, “Compartmentalization of Electrophoretically Separated Analytes in a Multiphase Microfluidic Platform,” *Anal. Chem.*, vol. 84, no. 13, pp. 5801–5808, 2012.

[30] J. S. Edgar, G. Milne, Y. Zhao, C. P. Pabbati, D. S. W. Lim, and D. T. Chiu, “Compartmentalization of Chemically Separated Components into Droplets,” *Angew. Chemie Int. Ed.*, vol. 48, no. 15, pp. 2719–2722, 2009.

[31] J. S. Edgar, C. P. Pabbati, R. M. Lorenz, M. He, G. S. Fiorini, and D. T. Chiu, “Capillary electrophoresis separation in the presence of an immiscible boundary for droplet analysis,” *Anal Chem*, vol. 78, no. 19, pp. 6948–6954, 2006.

[32] X. Niu, F. Pereira, J. B. Edel, and A. J. de Mello, “Droplet-interfaced microchip and capillary electrophoretic separations,” *Anal Chem*, vol. 85, no. 18, pp. 8654–8660, 2013.

References

[33] A. St John and C. P. Price, “Existing and Emerging Technologies for Point-of-Care Testing,” *Clin Biochem Rev*, vol. 35, no. 3, pp. 155–167, 2014.

[34] C. D. Chin, V. Linder, and S. K. Sia, “Commercialization of microfluidic point-of-care diagnostic devices,” *Lab Chip*, vol. 12, no. 12, pp. 2118–2134, 2012.

[35] M. L. Rogers and M. G. Boutelle, “Real-time clinical monitoring of biomolecules,” *Annu Rev Anal Chem (Palo Alto Calif)*, vol. 6, pp. 427–453, 2013.

[36] M. Montagnana, M. Caputo, D. Giavarina, and G. Lippi, “Overview on self-monitoring of blood glucose,” *Clin Chim Acta*, vol. 402, no. 1–2, pp. 7–13, 2009.

[37] S. Vaddiraju, D. J. Burgess, I. Tomazos, F. C. Jain, and F. Papadimitrakopoulos, “Technologies for continuous glucose monitoring: current problems and future promises,” *J Diabetes Sci Technol*, vol. 4, no. 6, pp. 1540–1562, 2010.

[38] P. Hashemi, R. Bhatia, H. Nakamura, J. P. Dreier, R. Graf, A. J. Strong, and M. G. Boutelle, “Persisting depletion of brain glucose following cortical spreading depression, despite apparent hyperaemia: evidence for risk of an adverse effect of Leao’s spreading depression,” *J Cereb Blood Flow Metab*, vol. 29, no. 1, pp. 166–175, 2009.

[39] M. L. Rogers, P. A. Brennan, C. L. Leong, S. A. N. Gowers, T. Aldridge, T. K. Mellor, and M. G. Boutelle, “Online rapid sampling microdialysis (rsMD) using enzyme-based electroanalysis for dynamic detection of ischaemia during free flap reconstructive surgery,” *Anal. Bioanal. Chem.*, vol. 405, no. 11, pp. 3881–3888, 2013.

[40] S. A. Gowers, V. F. Curto, C. A. Seneci, C. Wang, S. Anastasova, P. Vadgama, G. Z. Yang, and M. G. Boutelle, “3D Printed Microfluidic Device with Integrated Biosensors for Online Analysis of Subcutaneous Human Microdialysate,” *Anal Chem*, vol. 87, no. 15, pp. 7763–7770, 2015.

[41] H. Haugaa, E. B. Thorgersen, A. Pharo, K. M. Boberg, A. Foss, P. D. Line, T. Sanengen, R. Almaas, G. Grindheim, S. E. Pischke, T. E. Mollnes, and T. I. Tonnessen, “Early bedside detection of ischemia and rejection in liver transplants by microdialysis,” *Liver Transpl*, vol. 18, no. 7, pp. 839–849, 2012.

[42] A. Galvan, Y. Smith, and T. Wichmann, “Continuous monitoring of intracerebral glutamate levels in awake monkeys using microdialysis and enzyme fluorometric

detection," *J. Neurosci. Methods*, vol. 126, no. 2, pp. 175–185, 2003.

[43] W. Gao, S. Emaminejad, H. Y. Y. Nyein, S. Challa, K. Chen, A. Peck, H. M. Fahad, H. Ota, H. Shiraki, D. Kiriya, D.-H. Lien, G. A. Brooks, R. W. Davis, and A. Javey, "Fully integrated wearable sensor arrays for multiplexed in situ perspiration analysis," *Nature*, vol. 529, no. 7587, pp. 509–514, 2016.

[44] J. Wang, "Electrochemical glucose biosensors," *Chem Rev*, vol. 108, no. 2, pp. 814–825, 2008.

[45] N. M. iguel M. Pires, T. Dong, U. Hanke, and N. Hoivik, "Recent developments in optical detection technologies in lab-on-a-chip devices for biosensing applications," *Sensors (Basel).*, vol. 14, no. 8, pp. 15458–15479, 2014.

[46] K. P. Mitton and J. R. Trevithick, "High-performance liquid chromatography-electrochemical detection of antioxidants in vertebrate lens: Glutathione, tocopherol, and ascorbate," *Methods Enzymol.*, vol. 233, pp. 523–539, 1994.

[47] N. Wongkaew, P. He, V. Kurth, W. Surareungchai, and A. J. Baeumner, "Multi-channel PMMA microfluidic biosensor with integrated IDUAs for electrochemical detection," in *Analytical and Bioanalytical Chemistry*, 2013, vol. 405, no. 18, pp. 5965–5974.

[48] C. Elbuken, T. Glawdel, D. Chan, and C. L. Ren, "Detection of microdroplet size and speed using capacitive sensors," *Sensors Actuators, A Phys.*, vol. 171, no. 2, pp. 55–62, 2011.

[49] A. K. Ellerbee, S. T. Phillips, A. C. Siegel, K. A. Mirica, A. W. Martinez, P. Striehl, N. Jain, M. Prentiss, and G. M. Whitesides, "Quantifying Colorimetric Assays in Paper-Based Microfluidic Devices by Measuring the Transmission of Light through Paper," *Anal. Chem.*, vol. 81, no. 20, pp. 8447–8452, 2009.

[50] V. J. Sieben, C. F. A. Floquet, I. R. G. Ogilvie, M. C. Mowlem, and H. Morgan, "Microfluidic colourimetric chemical analysis system: Application to nitrite detection," *Anal. Methods*, vol. 2, no. 5, pp. 484–491, 2010.

[51] C. M. Rushworth, G. Jones, M. Fischlechner, E. Walton, and H. Morgan, "On-chip cavity-enhanced absorption spectroscopy using a white light-emitting diode and polymer mirrors," *Lab Chip*, vol. 15, no. 3, pp. 711–717, 2015.

[52] N. W. Tietz, C. A. Burtis, E. R. Ashwood, and D. E. Bruns, *Tietz textbook of clinical chemistry and molecular diagnostics*, vol. 5. Elsevier Health Sciences, 2006.

[53] H. Song, J. D. Tice, and R. F. Ismagilov, "A Microfluidic System for Controlling Reaction Networks in Time," *Angew. Chemie Int. Ed.*, vol. 42, no. 7, pp. 768–772, 2003.

[54] D. R. Link, E. Grasland-Mongrain, A. Duri, F. Sarrazin, Z. Cheng, G. Cristobal, M. Marquez, and D. A. Weitz, "Electric control of droplets in microfluidic devices," *Angew Chem Int Ed Engl*, vol. 45, no. 16, pp. 2556–2560, 2006.

[55] F. Lyu, M. Xu, Y. Cheng, J. Xie, J. Rao, and S. K. Y. Tang, "Quantitative detection of cells expressing BlaC using droplet-based microfluidics for use in the diagnosis of tuberculosis," *Biomicrofluidics*, vol. 9, no. 4, 2015.

[56] M. M. Kiss, L. Ortoleva-Donnelly, N. Reginald Beer, J. Warner, C. G. Bailey, B. W. Colston, J. M. Rothberg, D. R. Link, and J. H. Leamon, "High-throughput quantitative polymerase chain reaction in picoliter droplets," *Anal. Chem.*, vol. 80, no. 23, pp. 8975–8981, 2008.

[57] V. Srinivasan, V. K. Pamula, and R. B. Fair, "An integrated digital microfluidic lab-on-a-chip for clinical diagnostics on human physiological fluids.," *Lab Chip*, vol. 4, no. 4, pp. 310–315, 2004.

[58] R. B. Bird, W. E. Stewart, and E. N. Lightfoot, "Transport Phenomena," *J. Wiley*, 2007. .

[59] K. Handique and M. A. Burns, "Mathematical modeling of drop mixing in a slit-type microchannel," *J. Micromechanics Microengineering*, vol. 11, pp. 548–554, 2001.

[60] P. Garstecki, M. J. Fuerstman, H. a Stone, and G. M. Whitesides, "Formation of droplets and bubbles in a microfluidic T-junction-scaling and mechanism of break-up.," *Lab Chip*, vol. 6, no. 3, pp. 437–446, 2006.

[61] L. Yobas, S. Martens, W.-L. Ong, and N. Ranganathan, "High-performance flow-focusing geometry for spontaneous generation of monodispersed droplets.," *Lab Chip*, vol. 6, no. 8, pp. 1073–1079, 2006.

[62] J. H. Xu, S. W. Li, J. Tan, and G. S. Luo, "Correlations of droplet formation in T-junction microfluidic devices: From squeezing to dripping," *Microfluid. Nanofluidics*, vol. 5, no. 6, pp. 711–717, 2008.

[63] Y. Zhao, G. Chen, and Q. Yuan, “Liquid-liquid two-phase flow patterns in a rectangular MicroChannel,” *AIChE J.*, vol. 52, no. 12, pp. 4052–4060, 2006.

[64] J. H. Xu, S. W. Li, J. Tan, Y. J. Wang, and G. S. Luo, “Controllable preparation of monodisperse O/W and W/O emulsions in the same microfluidic device,” *Langmuir*, vol. 22, no. 19, pp. 7943–7946, 2006.

[65] J.-C. Baret, “Surfactants in droplet-based microfluidics,” *Lab Chip*, vol. 12, no. 3, p. 422, 2012.

[66] R. Seemann, M. Brinkmann, T. Pfohl, and S. Herminghaus, “Droplet based microfluidics,” *Rep. Prog. Phys. Rep. Prog. Phys*, vol. 75, no. 75, pp. 16601–41, 2012.

[67] D. J. Holt, R. J. Payne, W. Y. Chow, and C. Abell, “Fluorosurfactants for microdroplets: Interfacial tension analysis,” *J. Colloid Interface Sci.*, vol. 350, no. 1, pp. 205–211, 2010.

[68] W. Du, L. Li, K. P. Nichols, and R. F. Ismagilov, “SlipChip,” *Lab Chip*, vol. 9, no. 16, p. 2286, 2009.

[69] F. Shen, W. Du, J. E. Kreutz, A. Fok, and R. F. Ismagilov, “Digital PCR on a SlipChip.,” *Lab Chip*, vol. 10, no. 20, pp. 2666–72, 2010.

[70] S. Wang, S. Chen, J. Wang, P. Xu, Y. Luo, Z. Nie, and W. Du, “Interface solution isoelectric focusing with in situ MALDI-TOF mass spectrometry,” *Electrophoresis*, vol. 35, no. 17, pp. 2528–2533, 2014.

[71] L. Li, M. A. Karymov, K. P. Nichols, and R. F. Ismagilov, “Dead-end filling of slipchip evaluated theoretically and experimentally as a function of the surface chemistry and the gap size between the plates for lubricated and dry slipchips,” *Langmuir*, vol. 26, no. 14, pp. 12465–12471, 2010.

[72] F. Shen, E. K. Davydova, W. Du, J. E. Kreutz, O. Piepenburg, and R. F. Ismagilov, “Digital isothermal quantification of nucleic acids via simultaneous chemical initiation of recombinase polymerase amplification reactions on SlipChip,” *Anal. Chem.*, vol. 83, no. 9, pp. 3533–3540, 2011.

[73] F. Shen, B. Sun, J. E. Kreutz, E. K. Davydova, W. Du, P. L. Reddy, L. J. Joseph, and R. F. Ismagilov, “Multiplexed quantification of nucleic acids with large dynamic range using multivolume digital RT-PCR on a rotational SlipChip tested with HIV and

hepatitis C viral load," *J. Am. Chem. Soc.*, vol. 133, no. 44, pp. 17705–17712, 2011.

[74] R. R. Pompano, C. E. Platt, M. A. Karymov, and R. F. Ismagilov, "Control of initiation, rate, and routing of spontaneous capillary-driven flow of liquid droplets through microfluidic channels on slipchip," *Langmuir*, vol. 28, no. 3, pp. 1931–1941, 2012.

[75] L. Li, W. Du, and R. Ismagilov, "User-loaded SlipChip for equipment-free multiplexed nanoliter-scale experiments," *J. Am. Chem. Soc.*, vol. 132, no. 1, pp. 106–111, 2010.

[76] T. Schneider, J. Kreutz, and D. T. Chiu, "The potential impact of droplet microfluidics in biology," *Analytical Chemistry*, vol. 85, no. 7. pp. 3476–3482, 2013.

[77] Y. Zhao, F. Pereira, A. J. deMello, H. Morgan, and X. Niu, "Droplet-based in situ compartmentalization of chemically separated components after isoelectric focusing in a Slipchip.," *Lab Chip*, vol. 14, pp. 555–61, 2014.

[78] M. R. Bringer, C. J. Gerdts, H. Song, J. D. Tice, and R. F. Ismagilov, "Microfluidic systems for chemical kinetics that rely on chaotic mixing in droplets.," *Philos. Trans. A. Math. Phys. Eng. Sci.*, vol. 362, no. 1818, pp. 1087–1104, 2004.

[79] F. Sarrazin, L. Prat, N. Di Miceli, G. Cristobal, D. R. Link, and D. A. Weitz, "Mixing characterization inside microdroplets engineered on a microcoalescer," *Chem. Eng. Sci.*, vol. 62, no. 4, pp. 1042–1048, 2007.

[80] A. Liau, R. Kamik, A. Majumdar, and J. H. D. Cate, "Mixing crowded biological solutions in milliseconds," *Anal. Chem.*, vol. 77, no. 23, pp. 7618–7625, 2005.

[81] A. J. Szeri, S. Verguet, C. H. Duan, A. Liau, V. Berk, J. H. D. Cate, and A. Majumdar, "Mechanics of liquid-liquid interfaces and mixing enhancement in microscale flows," *J. Fluid Mech.*, vol. 652, pp. 207–240, 2010.

[82] Y.-C. Tan, J. S. Fisher, A. I. Lee, V. Cristini, and A. P. Lee, "Design of microfluidic channel geometries for the control of droplet volume, chemical concentration, and sorting.," *Lab Chip*, vol. 4, no. 4, pp. 292–298, 2004.

[83] L. Kan, D. Huijiang, C. Yong, and Z. Xing-Zhong, "Droplet based synthetic method using microflow focusing and droplet fusion.pdf," *Microfluid Nanofluid*, no. 3, pp. 239–243, 2007.

[84] X. Niu, S. Gulati, J. B. Edel, and A. J. deMello, “Pillar-induced droplet merging in microfluidic circuits.,” *Lab Chip*, vol. 8, no. 11, pp. 1837–1841, 2008.

[85] X. Niu, F. Gielen, A. J. DeMello, and J. B. Edel, “Electro-coalescence of digitally controlled droplets,” *Anal. Chem.*, vol. 81, no. 17, pp. 7321–7325, 2009.

[86] D. R. Link, S. L. Anna, D. a Weitz, and H. a Stone, “Geometrically mediated breakup of drops in microfluidic devices.,” *Phys. Rev. Lett.*, vol. 92, no. 5, p. 054503, 2004.

[87] Y.-C. Tan and A. P. Lee, “Microfluidic separation of satellite droplets as the basis of a monodispersed micron and submicron emulsification system.,” *Lab Chip*, vol. 5, no. 10, pp. 1178–83, 2005.

[88] B. Zheng and R. F. Ismagilov, “A microfluidic approach for screening submicroliter volumes against multiple reagents by using preformed arrays of nanoliter plugs in a three-phase liquid/liquid/gas flow,” *Angew. Chemie - Int. Ed.*, vol. 44, no. 17, pp. 2520–2523, 2005.

[89] H. Song, H. W. Li, M. S. Munson, T. G. Van Ha, and R. F. Ismagilov, “On-chip titration of an anticoagulant argatroban and determination of the clotting time within whole blood or plasma using a plug-based microfluidic system,” *Anal. Chem.*, vol. 78, no. 14, pp. 4839–4849, 2006.

[90] Z. T. Cygan, J. T. Cabral, K. L. Beers, and E. J. Amis, “Microfluidic platform for the generation of organic-phase microreactors,” *Langmuir*, vol. 21, no. 8, pp. 3629–3634, 2005.

[91] B. Ahmed, D. Barrow, and T. Wirth, “Enhancement of reaction rates by segmented fluid flow in capillary scale reactors,” *Adv. Synth. Catal.*, vol. 348, no. 9, pp. 1043–1048, 2006.

[92] A. M. Huebner, C. Abell, W. T. S. Huck, C. N. Baroud, and F. Hollfelder, “Monitoring a reaction at submillisecond resolution in picoliter volumes,” *Anal. Chem.*, vol. 83, no. 4, pp. 1462–1468, 2011.

[93] S.-H. Kim, J. W. Shim, and S.-M. Yang, “Microfluidic multicolor encoding of microspheres with nanoscopic surface complexity for multiplex immunoassays.,” *Angew. Chem. Int. Ed. Engl.*, vol. 50, no. 5, pp. 1171–4, Feb. 2011.

[94] B. Zheng, L. S. Roach, and R. F. Ismagilov, “Screening of protein crystallization conditions on a microfluidic chip using nanoliter-size droplets,” *J. Am. Chem. Soc.*, vol. 125, no. 37, pp. 11170–11171, 2003.

[95] Y. Zhu and Q. Fang, “Analytical detection techniques for droplet microfluidics-A review,” *Analytica Chimica Acta*, vol. 787. pp. 24–35, 2013.

[96] J.-U. Shim, G. Cristobal, D. R. Link, T. Thorsen, Y. Jia, K. Piattelli, and S. Fraden, “Control and measurement of the phase behavior of aqueous solutions using microfluidics.,” *J. Am. Chem. Soc.*, vol. 129, no. 28, pp. 8825–35, 2007.

[97] A. Townshen, “Principles of Instrumental Analysis,” *Anal. Chim. Acta*, vol. 152, p. 314, 2006.

[98] P. Riechel, T. Weiss, M. Weiss, R. Ulber, Heinrich Buchholz, and T. Scheper, “Determination of the minor whey protein bovine lactoferrin in cheese whey concentrates with capillary electrophoresis,” *J. Chromatogr. A*, vol. 817, no. 1–2, pp. 187–193, 1998.

[99] N. Siri, M. Lacroix, J. C. Garrigues, V. Poinsot, and F. Couderc, “HPLC-fluorescence detection and MEKC-LIF detection for the study of amino acids and catecholamines labelled with naphthalene-2,3-dicarboxyaldehyde,” *Electrophoresis*, vol. 27, no. 22, pp. 4446–4455, 2006.

[100] Y. Liu, R. S. Foote, S. C. Jacobson, R. S. Ramsey, and J. M. Ramsey, “Electrophoretic separation of proteins on a microchip with noncovalent, postcolumn labeling.,” *Anal. Chem.*, vol. 72, no. 19, pp. 4608–4613, 2000.

[101] R. Sjöback, J. Nygren, and M. Kubista, “Absorption and fluorescence properties of fluorescein,” *Spectrochimica Acta Part A: Molecular and Biomolecular Spectroscopy*, vol. 51, no. 6. pp. L7–L21, 1995.

[102] F. C. Huang, C. S. Liao, and G. Bin Lee, “An integrated microfluidic chip for DNA/RNA amplification, electrophoresis separation and on-line optical detection,” *Electrophoresis*, vol. 27, no. 16, pp. 3297–3305, 2006.

[103] O. O. Dada, D. C. Essaka, O. Hindsgaul, M. M. Palcic, J. Prendergast, R. L. Schnaar, and N. J. Dovichi, “Nine orders of magnitude dynamic range: Picomolar to millimolar

concentration measurement in capillary electrophoresis with laser induced fluorescence detection employing cascaded avalanche photodiode photon counters," *Anal. Chem.*, vol. 83, no. 7, pp. 2748–2753, 2011.

[104] S. M. Gruner, M. W. Tate, and E. F. Eikenberry, "Charge-coupled device area x-ray detectors," *Rev. Sci. Instrum.*, vol. 73, no. 8, p. 2815, 2002.

[105] M. He, J. S. Edgar, G. D. M. Jeffries, R. M. Lorenz, J. P. Shelby, and D. T. Chiu, "Selective encapsulation of single cells and subcellular organelles into picoliter- and femtoliter-volume droplets," *Anal. Chem.*, vol. 77, no. 6, pp. 1539–1544, 2005.

[106] L. S. Roach, H. Song, and R. F. Ismagilov, "Controlling nonspecific protein adsorption in a plug-based microfluidic system by controlling interfacial chemistry using fluorous-phase surfactants," *Anal. Chem.*, vol. 77, no. 3, pp. 785–796, 2005.

[107] H. Song and R. F. Ismagilov, "Millisecond Kinetics on a Microfluidic Chip Using Nanoliters of Reagents," *J. Am. Chem. Soc.*, vol. 125, no. 47, pp. 14613–14619, 2003.

[108] X. Xu, L. Li, and S. G. Weber, "Electrochemical and optical detectors for capillary and chip separations," *TrAC - Trends Anal. Chem.*, vol. 26, no. 1, pp. 68–79, 2007.

[109] X. Yang, W. Yan, H. Bai, H. Lv, and Z. Liu, "A scanning laser induced fluorescence detection system for capillary electrophoresis microchip based on optical fiber," *Opt. - Int. J. Light Electron Opt.*, vol. 123, no. 23, pp. 2126–2130, Dec. 2012.

[110] W. P. Ambrose, P. M. Goodwin, J. H. Jett, A. Van Orden, J. H. Werner, and R. A. Keller, "Single Molecule Fluorescence Spectroscopy at Ambient Temperature," *Chem. Rev.*, vol. 99, no. 10, pp. 2929–2956, Oct. 1999.

[111] M. Srisa-Art, A. J. deMello, and J. B. Edel, "High-throughput confinement and detection of single DNA molecules in aqueous microdroplets.," *Chem. Commun. (Camb).*, vol. 44, no. 43, pp. 6548–6550, 2009.

[112] J. C. Fister, S. C. Jacobson, L. M. Davis, and J. M. Ramsey, "Counting single chromophore molecules for ultrasensitive analysis and separations on microchip devices.," *Anal. Chem.*, vol. 70, no. 3, pp. 431–437, 1998.

[113] M. L. Chabinyc, D. T. Chiu, J. C. McDonald, A. D. Stroock, J. F. Christian, A. M. Karger, and G. M. Whitesides, "An integrated fluorescence detection system in

poly(dimethylsiloxane) for microfluidic applications," *Anal. Chem.*, vol. 73, no. 18, pp. 4491–4498, 2001.

[114] H. Ji, M. Li, L. Guo, H. Yuan, C. Wang, and D. Xiao, "Design and evaluation of capillary coupled with optical fiber light-emitting diode induced fluorescence detection for capillary electrophoresis.," *Electrophoresis*, vol. 34, pp. 2546–2552, 2013.

[115] A. Rodat-Boutonnet, P. Naccache, A. Morin, J. Fabre, B. Feurer, and F. Couderc, "A comparative study of LED-induced fluorescence and laser-induced fluorescence in SDS-CGE: Application to the analysis of antibodies," *Electrophoresis,* vol. 33, no. 12, pp. 1709–1714, 2012.

[116] M. T. Guo, A. Rotem, J. a. Heyman, and D. a. Weitz, "Droplet microfluidics for high-throughput biological assays," *Lab Chip*, vol. 12, no. 12, p. 2146, 2012.

[117] R. S. Sista, A. E. Eckhardt, V. Srinivasan, M. G. Pollack, S. Palanki, and V. K. Pamula, "Heterogeneous immunoassays using magnetic beads on a digital microfluidic platform.," *Lab Chip*, vol. 8, no. 12, pp. 2188–96, 2008.

[118] W. Liu, D. Chen, W. Du, K. P. Nichols, and R. F. Ismagilov, "SlipChip for immunoassays in nanoliter volumes," *Anal. Chem.*, vol. 82, no. 8, pp. 3276–3282, 2010.

[119] Y. Zhu and Q. Fang, "Integrated droplet analysis system with electrospray ionization-mass spectrometry using a hydrophilic tongue-based droplet extraction interface," *Anal. Chem.*, vol. 82, no. 19, pp. 8361–8366, 2010.

[120] J. Pei, Q. Li, M. S. Lee, G. A. Valaskovic, and R. T. Kennedy, "Analysis of samples stored as individual plugs in a capillary by electrospray ionization mass spectrometry," *Anal. Chem.*, vol. 81, no. 15, pp. 6558–6561, 2009.

[121] F. Pereira, X. Niu, and A. J. deMello, "A Nano LC-MALDI Mass Spectrometry Droplet Interface for the Analysis of Complex Protein Samples," *PLoS One*, vol. 8, no. 5, 2013.

[122] M. Geiger, A. L. Hogerton, and M. T. Bowser, "Capillary electrophoresis," *Analytical Chemistry*, vol. 84, no. 2. pp. 577–596, 2012.

[123] H. Whatley, "Basic principles and modes of capillary electrophoresis," *Clin. Forensic Appl. Capill. Electrophor.*, pp. 21– 58, 2001.

[124] E. T. T. Tay, W. S. Law, S. F. Y. Li, and L. J. Kricka, “Microchip capillary electrophoresis.,” *Methods in molecular biology (Clifton, N.J.)*, vol. 509. pp. 159–168, 2009.

[125] S. Magdeldin, *Gel Electrophoresis–Principles and Basics*. 2012.

[126] *Gel Electrophoresis: Nucleic Acids (Essential Techniques)*. Wiley-Blackwell, 1995.

[127] E. Stellwagen and N. C. Stellwagen, “Determining the electrophoretic mobility and translational diffusion coefficients of DNA molecules in free solution,” *Electrophoresis*, vol. 23, no. 16, pp. 2794–2803, 2002.

[128] S.-K. Lin, “Physical Biochemistry: Principles and Applications. By David Sheehan,” *Molecules*, vol. 5, no. 12. p. 1517, 2000.

[129] J. P. Landers, *Handbook of Capillary and Microchip Electrophoresis and Associated Microtechniques, Third Edition*. CRC Press, 2007.

[130] V. Dolník, “Wall coating for capillary electrophoresis on microchips,” *Electrophoresis*, vol. 25, no. 21–22. pp. 3589–3601, 2004.

[131] V. Dolnik, S. Liu, and S. Jovanovich, “Capillary electrophoresis on microchip,” *Electrophoresis*, vol. 21, no. 1. pp. 41–54, 2000.

[132] S. L. Llopis, J. Osiri, and S. A. Soper, “Surface modification of poly(methyl methacrylate) microfluidic devices for high-resolution separations of single-stranded DNA,” *Electrophoresis*, vol. 28, no. 6, pp. 984–993, 2007.

[133] H. Qu, H. Wang, Y. Huang, W. Zhong, H. Lu, J. Kong, P. Yang, and B. Liu, “Stable microstructured network for protein patterning on a plastic microfluidic channel: Strategy and characterization of on-chip enzyme microreactors,” *Anal. Chem.*, vol. 76, no. 21, pp. 6426–6433, 2004.

[134] H. Okada, N. Kaji, M. Tokeshi, and Y. Baba, “Rinse and evaporation coating of poly(methyl methacrylate) microchip for separation of sodium dodecyl sulfate-protein complex,” *J. Chromatogr. A*, vol. 1192, no. 2, pp. 289–293, 2008.

[135] C. A. Currie, J. S. Shim, S. H. Lee, C. Ahn, P. A. Limbach, H. B. Halsall, and W. R. Heineman, “Comparing polyelectrolyte multilayer-coated PMMA microfluidic devices

and glass microchips for electrophoretic separations," *Electrophoresis*, vol. 30, no. 24, pp. 4245–4250, 2009.

[136] S. Hardt and F. Schönfeld, *Microfluidic technologies for miniaturized analysis systems*. 2007.

[137] Giddings JC., " Unified Separation Science," *John Wiley sons New York*, p. 97–101, 1991.

[138] V. Dolnik and S. Liu, "Applications of capillary electrophoresis on microchip," *Journal of Separation Science*, vol. 28, no. 15. pp. 1994–2009, 2005.

[139] M. Novotny, S. R. Springston, P. A. Peaden, J. C. Fjeldsted, and M. L. Lee, "Capillary supercritical fluid chromatography," *Anal. Chem.*, vol. 53, no. 3, p. 407A–414A, Mar. 1981.

[140] H. H. Lauer and D. McManigill, "Capillary zone electrophoresis of proteins in untreated fused silica tubing," *Anal. Chem.*, vol. 58, pp. 166–170, 1986.

[141] Y. Li, M. M. Champion, L. Sun, P. A. D. Champion, R. Wojcik, and N. J. Dovichi, "Capillary Zone Electrophoresis-Electrospray Ionization-Tandem Mass Spectrometry as an Alternative Proteomics Platform to Ultraperformance Liquid Chromatography-Electrospray Ionization-Tandem Mass Spectrometry for Samples of Intermediate Complexity," *Anal. Chem.*, vol. 84, no. 3, pp. 1617–1622, Feb. 2012.

[142] D. T. R. Stewart, M. D. Celiz, G. Vicente, L. A. Col??n, and D. S. Aga, "Potential use of capillary zone electrophoresis in size characterization of quantum dots for environmental studies," *TrAC - Trends in Analytical Chemistry*, vol. 30, no. 1. pp. 113–122, 2011.

[143] J. Joneli, U. Wanzenried, J. Schiess, C. Lanz, J. Caslavska, and W. Thormann, "Determination of carbohydrate-deficient transferrin in human serum by capillary zone electrophoresis: Evaluation of assay performance and quality assurance over a 10-year period in the routine arena," *Electrophoresis*, vol. 34, no. 11, pp. 1563–1571, 2013.

[144] C. L. Colyer, S. D. Mangru, and D. J. Harrison, "Microchip-based capillary electrophoresis of human serum proteins.," *J. Chromatogr. A*, vol. 781, no. 1–2, pp. 271–276, 1997.

[145] M. A. Hayes, I. Kheterpal, and A. G. Ewing, “Electroosmotic flow control and surface conductance in capillary zone electrophoresis.,” *Anal. Chem.*, vol. 65, no. 15, pp. 2010–3, 1993.

[146] I. Mitra, S. P. Marczak, and S. C. Jacobson, “Microchip electrophoresis at elevated temperatures and high separation field strengths,” *Electrophoresis*, vol. 35, no. 2–3, pp. 374–378, 2014.

[147] F. Ye, M. Shi, Y. Huang, and S. Zhao, “Noncompetitive immunoassay for carcinoembryonic antigen in human serum by microchip electrophoresis for cancer diagnosis.,” *Clin. Chim. acta Int. J. Clin. Chem.*, vol. 411, no. 15–16, pp. 1058–1062, 2010.

[148] C. Cianciulli, T. Hahne, and H. Wätzig, “Capillary gel electrophoresis for precise protein quantitation,” *Electrophoresis*, vol. 33, no. 22, pp. 3276–3280, 2012.

[149] B. E. Root, B. Zhang, and A. E. Barron, “Size-based protein separations by microchip electrophoresis using an acid-labile surfactant as a replacement for SDS,” *Electrophoresis*, vol. 30, no. 12, pp. 2117–2122, 2009.

[150] H. Shadpour and S. A. Soper, “Two-dimensional electrophoretic separation of proteins using poly(methyl methacrylate) microchips,” *Anal. Chem.*, vol. 78, no. 11, pp. 3519–3527, 2006.

[151] Z. Shen, X. Liu, Z. Long, D. Liu, N. Ye, J. Qin, Z. Dai, and B. Lin, “Parallel analysis of biomolecules on a microfabricated capillary array chip,” *Electrophoresis*, vol. 27, no. 5–6, pp. 1084–1092, 2006.

[152] P. Y. Lee, J. Costumbrado, C.-Y. Hsu, and Y. H. Kim, “Agarose gel electrophoresis for the separation of DNA fragments.,” *J. Vis. Exp.*, no. 62, p. e3923, 2012.

[153] B. T. Kurien and R. H. Scofield, “Western blotting.,” *Methods*, vol. 38, no. 4, pp. 283–93, 2006.

[154] A. E. Herr and A. K. Singh, “Photopolymerized cross-linked polycrylamide gels for on-chip protein sizing,” *Anal. Chem.*, vol. 76, no. 16, pp. 4727–4733, 2004.

[155] B. J. Kirby, A. R. Wheeler, R. N. Zare, J. a Fruetel, and T. J. Shepodd, “Programmable modification of cell adhesion and zeta potential in silica microchips.,” *Lab Chip*, vol. 3,

no. 1, pp. 5–10, 2003.

[156] A. J. Hughes, R. K. C. Lin, D. M. Peehl, and A. E. Herr, “Microfluidic integration for automated targeted proteomic assays,” *Proc. Natl. Acad. Sci.*, vol. 109, no. 16, pp. 5972–5977, 2012.

[157] T. a Duncombe and A. E. Herr, “Photopatterned free-standing polyacrylamide gels for microfluidic protein electrophoresis.,” *Lab Chip*, vol. 13, no. 11, pp. 2115–23, 2013.

[158] J. Han and A. K. Singh, “Rapid protein separations in ultra-short microchannels: Microchip sodium dodecyl sulfate-polyacrylamide gel electrophoresis and isoelectric focusing,” *J. Chromatogr. A*, vol. 1049, no. 1–2, pp. 205–209, 2004.

[159] C. T. Lo, D. J. Throckmorton, A. K. Singh, and A. E. Herr, “Photopolymerized diffusion-defined polyacrylamide gradient gels for on-chip protein sizing.,” *Lab Chip*, vol. 8, no. 8, pp. 1273–1279, 2008.

[160] C. Hou and A. E. Herr, “Ultrashort separation length homogeneous electrophoretic immunoassays using on-chip discontinuous polyacrylamide gels,” *Anal. Chem.*, vol. 82, no. 8, pp. 3343–3351, 2010.

[161] H. Nan, D. J. Yoo, and S. H. Kang, “Fast parallel detection of feline panleukopenia virus DNA by multi-channel microchip electrophoresis with programmed step electric field strength.,” *J. Sep. Sci.*, vol. 36, no. 2, pp. 350–5, Jan. 2013.

[162] B. D. Hames, *An introduction to polyacrylamide gel electrophoresis. Gel electrophoresis of proteins: A practical approach*, 3rd ed. Oxford University Press: NY, USA, 1988.

[163] W. Pan, W. Chen, and X. Jiang, “Microfluidic western blot,” *Anal. Chem.*, vol. 82, no. 10, pp. 3974–3976, 2010.

[164] S. Jin, G. J. Anderson, and R. T. Kennedy, “Western blotting using microchip electrophoresis interfaced to a protein capture membrane,” *Anal. Chem.*, vol. 85, no. 12, pp. 6073–6079, 2013.

[165] S. Q. Tia, M. He, D. Kim, and A. E. Herr, “Multianalyte on-chip native western blotting,” *Anal. Chem.*, vol. 83, no. 9, pp. 3581–3588, 2011.

[166] R. Rodriguez-Diaz, T. Wehr, and M. Zhu, "Capillary isoelectric focusing.," *Electrophoresis*, vol. 18, pp. 2134–2144, 1997.

[167] E. R. Castro and A. Manz, "Present state of microchip electrophoresis: State of the art and routine applications," *Journal of Chromatography A*, vol. 1382. pp. 66–85, 2015.

[168] Q. Mao and J. Pawliszyn, "Demonstration of isoelectric focusing on an etched quartz chip with UV absorption imaging detection†," *Analyst*, vol. 124, no. 5, pp. 637–641, 1999.

[169] S. M. Shameli, C. Elbuken, J. Ou, C. L. Ren, and J. Pawliszyn, "Fully integrated PDMS/SU-8/quartz microfluidic chip with a novel macroporous poly dimethylsiloxane (PDMS) membrane for isoelectric focusing of proteins using whole-channel imaging detection," *Electrophoresis*, vol. 32, no. 3–4, pp. 333–339, 2011.

[170] B. Walowski, W. Hüttner, and H. Wackerbarth, "Generation of a miniaturized free-flow electrophoresis chip based on a multi-lamination technique-isoelectric focusing of proteins and a single-stranded DNA fragment," *Anal. Bioanal. Chem.*, vol. 401, no. 8, pp. 2465–2471, 2011.

[171] R. Ishibashi, T. Kitamori, and K. Shimura, "Two-step perpendicular free-solution isoelectric focusing in a microchamber array chip.," *Lab Chip*, vol. 10, no. 19, pp. 2628–31, 2010.

[172] P. H. O'Farrell, "High resolution two-dimensional electrophoresis of proteins.," *J. Biol. Chem.*, vol. 250, no. 10, pp. 4007–21, 1975.

[173] J. A. Mackintosh, H. Y. Choi, S. H. Bae, D. A. Veal, P. J. Bell, B. C. Ferrari, D. D. Van Dyk, N. M. Verrills, Y. K. Paik, and P. Karuso, "A fluorescent natural product for ultra sensitive detection of proteins in one-dimensional and two-dimensional gel electrophoresis," in *Proteomics*, 2003, vol. 3, no. 12, pp. 2273–2288.

[174] C. Cid, L. Garcia-Descalzo, V. Casado-Lafuente, R. Amils, and A. Aguilera, "Proteomic analysis of the response of an acidophilic strain of Chlamydomonas sp. (Chlorophyta) to natural metal-rich water," *Proteomics*, vol. 10, no. 10, pp. 2026–2036, 2010.

[175] P. Gu, K. Liu, H. Chen, T. Nishida, and Z. H. Fan, "Chemical-Assisted Bonding of Thermoplastics/Elastomer for Fabricating Microfluidic Valves," *Anal. Chem.*, vol. 83,

no. 1, pp. 446–452, Jan. 2011.

[176] S. C. Jacobson, R. Hergenroder, L. B. Koutny, R. J. Warmack, and J. M. Ramsey, “Effects of Injection Schemes and Column Geometry on the Performance of Microchip Electrophoresis Devices,” *Anal. Chem.*, vol. 66, no. 123, pp. 1107–1113, 1994.

[177] G. T. Roman, M. Wang, K. N. Shultz, C. Jennings, and R. T. Kennedy, “Sampling and electrophoretic analysis of segmented flow streams using virtual walls in a microfluidic device,” *Anal. Chem.*, vol. 80, no. 21, pp. 8231–8238, 2008.

[178] W. R. Vandaveer IV, S. A. Pasas-Farmer, D. J. Fischer, C. N. Frankenfeld, and S. M. Lunte, “Recent developments in electrochemical detection for microchip capillary electrophoresis,” *Electrophoresis*, vol. 25, no. 21–22. pp. 3528–3549, 2004.

[179] M. A. Roberts, J. S. Rossier, P. Bercier, and H. Girault, “UV laser machined polymer substrates for the development of microdiagnostic systems,” *Anal. Chem.*, vol. 69, no. 11, pp. 2035–2042, 1997.

[180] D. C. Duffy, J. C. McDonald, O. J. A. Schueller, and G. M. Whitesides, “Rapid prototyping of microfluidic systems in poly(dimethylsiloxane),” *Anal. Chem.*, vol. 70, no. 23, pp. 4974–4984, 1998.

[181] M. Abdelgawad, M. W. L. Watson, and A. R. Wheeler, “Hybrid microfluidics: a digital-to-channel interface for in-line sample processing and chemical separations.,” *Lab Chip*, vol. 9, no. 8, pp. 1046–1051, 2009.

[182] C. M. Wurster, W. P. Patterson, and M. M. Cheatham, “Advances in micromilling techniques: A new apparatus for acquiring high-resolution oxygen and carbon stable isotope values and major/minor elemental ratios from accretionary carbonate,” *Comput. Geosci.*, vol. 25, no. 10, pp. 1159–1166, 1999.

[183] H. Niino and A. Yabe, “Excimer laser polymer ablation: formation of positively charged surfaces and its application into the metallization of polymer films,” *Appl. Surf. Sci.*, vol. 69, no. 1–4, pp. 1–6, 1993.

[184] L. Peng, Y. Deng, P. Yi, and X. Lai, “Micro hot embossing of thermoplastic polymers: a review,” *J. Micromechanics Microengineering*, vol. 24, no. 1, p. 013001, 2014.

[185] I. R. G. Ogilvie, C. F. a. Floquet, R. Zmijan, M. C. Mowlem, and H. Morgan, “Reduction

of surface roughness for optical quality microfluidic devices in PMMA and COC," *J. Micromechanics Microengineering*, vol. 20, no. 6, p. 065016, 2010.

[186] Y. Miura, H. Wake, and T. Kato, "TBE, or not TBE, that is the question: Beneficial usage of tris-borate for obtaining a higher resolution of small DNA fragments by agarose gel electrophoresis," *Nagoya Med. J*, pp. 9–11, 1999.

[187] H. Schägger, "Tricine-SDS-PAGE.," *Nat. Protoc.*, vol. 1, no. 1, pp. 16–22, 2006.

[188] Sino Biological Inc., "Sds-Page," *Assay-Protocol.com*, pp. 10–13, 2013.

[189] Z. Zhu, J. J. Lu, and S. Liu, "Protein separation by capillary gel electrophoresis: A review," *Analytica Chimica Acta*, vol. 709. pp. 21–31, 2012.

[190] W. L. Tseng and H. T. Chang, "A new strategy for optimizing sensitivity, speed, and resolution in capillary electrophoretic separation of DNA," *Electrophoresis*, vol. 22, no. 4, pp. 763–770, 2001.

[191] C. Kang, K. B. Seung, I. Song, B. Choi, J. Chang, K. Cho, and Y. Kim, "DNA separation using cellulose derivatives and PEO by PDMS microchip," *Bull. Korean Chem. Soc.*, vol. 27, no. 4, pp. 519–523, 2006.

[192] V. Srinivasan, V. K. Pamula, and R. B. Fair, "Droplet-based microfluidic lab-on-a-chip for glucose detection," *Anal. Chim. Acta*, vol. 507, no. 1, pp. 145–150, 2004.

[193] M. H. Wu, H. Cai, X. Xu, J. P. G. Urban, Z. F. Cui, and Z. Cui, "A SU-8/PDMS hybrid microfluidic device with integrated optical fibers for online monitoring of lactate.," *Biomed. Microdevices*, vol. 7, no. 4, pp. 323–329, 2005.

[194] D. L. Nelson and M. M. Cox, "Lehninger Principles of Biochemistry 5th ed.," *Book*. pp. 1–1294, 2008.

[195] M. Sugiura and K. Hirano, "A new colorimetric method for determination of serum glucose.," *Clin. Chim. Acta.*, vol. 75, no. 3, pp. 387–391, Mar. 1977.

[196] E. Fradet, C. Bayer, F. Hollfelder, and C. N. Baroud, "Measuring Fast and Slow Enzyme Kinetics in Stationary Droplets," *Anal. Chem.*, vol. 87, no. 23, pp. 11915–11922, 2015.

[197] F. Gielen, T. Buryska, L. Van Vliet, M. Butz, J. Damborsky, Z. Prokop, and F. Hollfelder, "Interfacing microwells with nanoliter compartments: A sampler generating

high-resolution concentration gradients for quantitative biochemical analyses in droplets," *Anal. Chem.*, vol. 87, no. 1, pp. 624–632, 2015.

[198] F. Gielen, L. Van Vliet, B. T. Koprowski, S. R. A. Devenish, M. Fischlechner, J. B. Edel, X. Niu, A. J. Demello, and F. Hollfelder, "A fully unsupervised compartment-on-demand platform for precise nanoliter assays of time-dependent steady-state enzyme kinetics and inhibition," *Anal. Chem.*, vol. 85, no. 9, pp. 4761–4769, 2013.

[199] H. Gu, M. H. G. Duits, and F. Mugele, "Droplets formation and merging in two-phase flow microfluidics," *International journal of molecular sciences*, vol. 12, no. 4. pp. 2572–2597, 2011.

[200] P. Trinder, "Determination of Glucose in Blood Using Glucose Oxidase with an Alternative Oxygen Acceptor," *Ann. Clin. Biochem. An Int. J. Biochem. Med.* , vol. 6 , no. 1 , pp. 24–27, Jan. 1969.

[201] C.-Y. Lin, S.-H. Chen, G.-H. Kou, and C.-M. Kuo, "An enzymatic microassay for lactate concentration in blood and hemolymph," *Acta Zool. taiwanica*, vol. 10, no. 2, pp. 91–101, 1999.

[202] Y. Xia and G. M. Whitesides, "Soft Lithography," *Annu. Rev. Mater. Sci.*, vol. 28, pp. 153–184, 1998.

[203] A. D. Beaton, C. L. Cardwell, R. S. Thomas, V. J. Sieben, F.-E. Legiret, E. M. Waugh, P. J. Statham, M. C. Mowlem, and H. Morgan, "Lab-on-Chip Measurement of Nitrate and Nitrite for In Situ Analysis of Natural Waters," *Environ. Sci. Technol.*, vol. 46, no. 17, pp. 9548–9556, Sep. 2012.

[204] I. R. G. Ogilvie, V. J. Sieben, M. C. Mowlem, and H. Morgan, "Temporal optimization of microfluidic colorimetric sensors by use of multiplexed stop-flow architecture," *Anal. Chem.*, vol. 83, no. 12, pp. 4814–4821, 2011.

[205] Y. S. Lee, S. Shin, T. Shigihara, E. Hahm, M. J. Liu, J. Han, J. W. Yoon, and H. S. Jun, "Glucagon-like peptide-1 gene therapy in obese diabetic mice results in long-term cure of diabetes by improving insulin sensitivity and reducing hepatic gluconeogenesis," *Diabetes*, vol. 56, no. 6, pp. 1671–1679, 2007.

[206] P. Abrahamsson and O. Winsö, "An assessment of calibration and performance of the

microdialysis system," *J. Pharm. Biomed. Anal.*, vol. 39, no. 3–4, pp. 730–734, 2005.

[207] T. Laurell, J. Drott, and L. Rosengren, "Silicon wafer integrated enzyme reactors," *Biosens. Bioelectron.*, vol. 10, no. 3–4, pp. 289–299, 1995.

[208] J. Wang, "On-chip enzymatic assays," *Electrophoresis*, vol. 23, no. 5. pp. 713–718, 2002.

[209] H. Li, C. Y. Guo, and C. L. Xu, "A highly sensitive non-enzymatic glucose sensor based on bimetallic Cu-Ag superstructures," *Biosens. Bioelectron.*, vol. 63, pp. 339–346, 2015.

[210] K.-Y. Cheng, J.-C. Wang, C.-Y. Lin, W.-R. Lin, Y.-A. Chen, F.-J. Tsai, Y.-C. Chuang, G.-Y. Lin, C.-W. Ni, Y.-T. Zeng, and M.-L. Ho, "Electrochemical synthesis, characterization of Ir-Zn containing coordination polymer, and application in oxygen and glucose sensing.," *Dalton Trans.*, vol. 43, no. 17, pp. 6536–6547, 2014.

[211] M. L. Ho, J. C. Wang, T. Y. Wang, C. Y. Lin, J. F. Zhu, Y. A. Chen, and T. C. Chen, "The construction of glucose biosensor based on crystalline iridium(III)-containing coordination polymers with fiber-optic detection," *Sensors Actuators, B Chem.*, vol. 190, pp. 479–485, 2014.

[212] J. A. Bourne, "Intracerebral microdialysis: 30 Years as a tool for the neuroscientist," *Clinical and Experimental Pharmacology and Physiology*, vol. 30, no. 1–2. pp. 16–24, 2003.

[213] K. Lanckmans, R. Clinckers, A. Van Eeckhaut, S. Sarre, I. Smolders, and Y. Michotte, "Use of microbore LC-MS/MS for the quantification of oxcarbazepine and its active metabolite in rat brain microdialysis samples," *J. Chromatogr. B Anal. Technol. Biomed. Life Sci.*, vol. 831, no. 1–2, pp. 205–212, 2006.

[214] R. K. Benjamin, F. H. Hochberg, E. Fox, P. M. Bungay, W. F. Elmquist, C. F. Stewart, J. M. Gallo, J. M. Collins, R. P. Pelletier, J. F. de Groot, R. C. Hickner, I. Cavus, S. a Grossman, and O. M. Colvin, "Review of microdialysis in brain tumors, from concept to application: first annual Carolyn Frye-Halloran symposium.," *Neuro. Oncol.*, vol. 6, no. 1, pp. 65–74, 2004.

[215] E. Guihen and W. T. O'Connor, "Capillary and microchip electrophoresis in microdialysis: recent applications.," *Electrophoresis*, vol. 31, no. 1, pp. 55–64, Jan. 2010.

[216] M. Markus, “Microdialysis,” *BMJ*, vol. 324, 2002.

[217] N. Plock and C. Kloft, “Microdialysis - Theoretical background and recent implementation in applied life-sciences,” *European Journal of Pharmaceutical Sciences*, vol. 25, no. 1. pp. 1–24, 2005.

[218] V. I. Chefer, A. C. Thompson, A. Zapata, and T. S. Shippenberg, “Overview of brain microdialysis,” *Current Protocols in Neuroscience*, no. SUPPL. 47. 2009.

[219] B. U. Moon, M. G. De Vries, C. A. Cordeiro, B. H. C. Westerink, and E. Verpoorte, “Microdialysis-coupled enzymatic microreactor for in vivo glucose monitoring in rats,” *Anal. Chem.*, vol. 85, no. 22, pp. 10949–10955, 2013.

[220] S. Naredi, M. Olivecrona, C. Lindgren, a L. Ostlund, P. O. Grände, and L. O. Koskinen, “An outcome study of severe traumatic head injury using the ‘Lund therapy’ with low-dose prostacyclin.,” *Acta Anaesthesiol. Scand.*, vol. 45, no. 4, pp. 402–6, 2001.

[221] A. Helmy, K. L. Carpenter, and P. J. Hutchinson, “Microdialysis in the human brain and its potential role in the development and clinical assessment of drugs,” *Curr. Med. Chem.*, vol. 14, no. 14, pp. 1525–1537, 2007.

[222] B. M. Bellander, E. Cantais, P. Enblad, P. Hutchinson, C. H. Nordström, C. Robertson, J. Sahuquillo, M. Smith, N. Stocchetti, U. Ungerstedt, A. Unterberg, and N. V. Olsen, “Consensus meeting on microdialysis in neurointensive care,” in *Intensive Care Medicine*, 2004, vol. 30, no. 12, pp. 2166–2169.

[223] O. G. Nilsson, L. Brandt, U. Ungerstedt, and H. Säveland, “Bedside detection of brain ischemia using intracerebral microdialysis: Subarachnoid hemorrhage and delayed ischemic deterioration,” *Neurosurgery*, vol. 45, no. 5, pp. 1176–1185, 1999.

[224] M. M. Parkin, S. S. Hopwood, D. A. D. A. Jones, P. P. Hashemi, H. H. Landolt, M. M. Fabricius, M. M. Lauritzen, M. G. M. G. Boutelle, and A. J. A. J. Strong, “Dynamic changes in brain glucose and lactate in pericontusional areas of the human cerebral cortex, monitored with rapid sampling on-line microdialysis: relationship with depolarisation-like events.,” *J. Cereb. Blood Flow Metab.*, vol. 25, no. 3, pp. 402–413, 2005.

[225] D. A. Jones, M. C. Parkin, H. Langemann, H. Landolt, S. E. Hopwood, A. J. Strong, and

M. G. Boutelle, "On-line monitoring in neurointensive care: Enzyme-based electrochemical assay for simultaneous, continuous monitoring of glucose and lactate from critical care patients," *J. Electroanal. Chem.*, vol. 538–539, pp. 243–252, 2002.

[226] D. Feuerstein, A. Manning, P. Hashemi, R. Bhatia, M. Fabricius, C. Tolias, C. Pahl, M. Ervine, A. J. Strong, and M. G. Boutelle, "Dynamic metabolic response to multiple spreading depolarizations in patients with acute brain injury: an online microdialysis study.," *J. Cereb. Blood Flow Metab.*, vol. 30, no. 7, pp. 1343–55, 2010.

[227] C. J. Watson, B. J. Venton, and R. T. Kennedy, "In vivo measurements of neurotransmitters by microdialysis sampling," *Anal. Chem.*, vol. 78, no. 5, pp. 1391–1399, 2006.

[228] P. Nandi and S. M. Lunte, "Recent trends in microdialysis sampling integrated with conventional and microanalytical systems for monitoring biological events: A review," *Analytica Chimica Acta*, vol. 651, no. 1. pp. 1–14, 2009.

[229] M. Wang, G. T. Roman, K. Schultz, C. Jennings, and R. T. Kenned Y, "Improved temporal resolution for in vivo microdialysis by using segmented flow," *Anal. Chem.*, vol. 80, no. 14, pp. 5607–5615, 2008.

[230] T. R. Slaney, J. Nie, N. D. Hershey, P. K. Thwar, J. Linderman, M. A. Burns, and R. T. Kennedy, "Push-pull perfusion sampling with segmented flow for high temporal and spatial resolution in vivo chemical monitoring," *Anal. Chem.*, vol. 83, no. 13, pp. 5207–5213, 2011.

[231] T. Neff, J. Fischer, S. Fehr, O. Baenziger, and M. Weiss, "Start-up delays of infusion syringe pumps," *Paediatr. Anaesth.*, vol. 11, no. 5, pp. 561–565, 2001.

[232] H. Thimbleby, "Problems with a syringe pump," *YouTube*, 2008.

[233] L. Stern, A. Bakal, M. Tzur, M. Veinguer, N. Mazurski, N. Cohen, and U. Levy, "Doppler-based flow rate sensing in microfluidic channels," *Sensors (Switzerland)*, vol. 14, no. 9, pp. 16799–16807, 2014.

[234] S. L. Sjostrom, H. N. Joensson, and H. A. Svahn, "Multiplex analysis of enzyme kinetics and inhibition by droplet microfluidics using picoinjectors.," *Lab Chip*, vol. 13, no. 9, pp. 1754–61, 2013.

[235] S. Hassan, A. Nightingale, and X. Niu, “Continuous measurement of enzymatic kinetics in droplet flow for point-of-care monitoring,” *Analyst*, vol. 141, no. 11, pp. 3266–3273, 2016.

[236] T. Dong and C. Barbosa, “Capacitance variation induced by microfluidic two-phase flow across insulated interdigital electrodes in lab-on-chip devices,” *Sensors (Switzerland)*, vol. 15, no. 2, pp. 2694–2708, 2015.

[237] X. Niu, M. Zhang, S. Peng, W. Wen, and P. Sheng, “Real-time detection, control, and sorting of microfluidic droplets,” *Biomicrofluidics*, vol. 1, no. 4, 2007.

[238] J. Z. Chen, A. A. Darhuber, S. M. Troian, and S. Wagner, “Capacitive sensing of droplets for microfluidic devices based on thermocapillary actuation,” *Lab Chip*, vol. 4, no. 5, pp. 473–480, 2004.

[239] M. Demori, V. Ferrari, D. Strazza, and P. Poesio, “A capacitive sensor system for the analysis of two-phase flows of oil and conductive water,” *Sensors Actuators, A Phys.*, vol. 163, no. 1, pp. 172–179, 2010.

[240] A. Ernst, W. Streule, N. Schmitt, R. Zengerle, and P. Koltay, “A capacitive sensor for non-contact nanoliter droplet detection,” *Sensors Actuators, A Phys.*, vol. 153, no. 1, pp. 57–63, 2009.

[241] M. R. De Saint Vincent, S. Cassagnre, J. Plantard, and J. P. Delville, “Real-time droplet caliper for digital microfluidics,” *Microfluid. Nanofluidics*, vol. 13, no. 2, pp. 261–271, 2012.

[242] S. Jakiela, S. Makulska, P. M. Korczyk, and P. Garstecki, “Speed of flow of individual droplets in microfluidic channels as a function of the capillary number, volume of droplets and contrast of viscosities,” *Lab a Chip - Miniaturisation Chem. Biol.*, vol. 11, no. 21, pp. 3603–3608, 2011.

[243] R. Revellin, V. Dupont, T. Ursenbacher, J. R. Thome, and I. Zun, “Characterization of diabatic two-phase flows in microchannels: Flow parameter results for R-134a in a 0.5 mm channel,” *Int. J. Multiph. Flow*, vol. 32, no. 7, pp. 755–774, 2006.

[244] N. Damean, L. F. Olguin, F. Hollfelder, C. Abell, and W. T. S. Huck, “Simultaneous measurement of reactions in microdroplets filled by concentration gradients,” *Lab Chip*,

vol. 9, no. 12, pp. 1707–1713, 2009.

[245] S. Jambovane, D. J. Kim, E. C. Duin, S. K. Kim, and J. W. Hong, “Creation of stepwise concentration gradient in picoliter droplets for parallel reactions of matrix metalloproteinase II and IX,” *Anal. Chem.*, vol. 83, no. 9, pp. 3358–3364, 2011.

[246] D. Hess, A. Rane, A. J. Demello, and S. Stavrakis, “High-throughput, quantitative enzyme kinetic analysis in microdroplets using stroboscopic epifluorescence imaging,” *Anal. Chem.*, vol. 87, no. 9, pp. 4965–4972, 2015.

[247] M. W. Lada, T. W. Vickroy, and R. T. Kennedy, “High temporal resolution monitoring of glutamate and aspartate in vivo using microdialysis on-line with capillary electrophoresis with laser-induced fluorescence detection.,” *Anal. Chem.*, vol. 69, no. 22, pp. 4560–4565, 1997.